Capsules, secondary interactions and unusual multi-metallic complexes

John S. Hart

University of Edinburgh

Submitted for the degree of Doctor of Philosophy

21-05-2012

Declaration

The work described in this thesis is entirely my own, except where I have either acknowledged help from a named person or given reference to a published source. Text taken from another source will be enclosed in quotation mark and a reference given. This thesis has not been submitted, in whole or in part, for any other degree.

Signature: Date:

This thesis is dedicated to the memory of James W. Hart, my father, passed away the 14th of February 2006 whom I miss greatly everyday and I could only wish he was here to read the following work.

Acknowledgements

Abbreviations

General

°	degree	J	joule(s)
°C	degree Celsius	*m*	meta
Å	Ångstrom	M	mols.dm^{-3}
adps	anisotropic displacement parameters	Me	methyl
^{t}Bu	*tert*-butyl	MeCN	acetonitrile
CH_2Cl_2	dichloromethane	Mes	mesityl, 2,4,6-Me-C_6H_2
Cp	cyclopentadienyl, C_5H_5	$MgSO_4$	magnesium sulphate
CV	cyclic voltammogram	mol	mole(s)
Cy	cyclohexyl	mL	millilitres
Cyh	cyclohexyl hydrogen	mmol	millimole(s)
dm^3	decimeter(s) cubed	MS	Mass Spectrometry
DNA	deoxyribonucleic acid	ms	milliseconds
en	ethylenediamine	mV	millivolt(s)
EtOH	ethanol	NEt$_3$	triethylamine
Et$_2$O	diethyl ether	nm	nanometres
Fc	ferrocene, Cp$_2$Fe	*p*	para
g	grams	pyr	pyridine
h	hours	TBA	tetrabutylammonium

| K | Kelvin | THF | tetrahydrofuran |
| L | litres | V | Volt(s) |

Nuclear Magnetic Resonance Spectroscopic data

δ	chemical shift in ppm	MHz	megahertz
br	broad	NMR	Nuclear Magnetic Resonance
$^{13}C\{^1H\}$	proton decoupled ^{13}C NMR spectroscopy	ppm	parts per million
d	doublet	q	quaternary carbon
dd	doublet of doublets	s	singlet
dt	doublet of triplets	sep	septet
J	coupling constant	t	triplet
Hz	Hertz	td	triplet of doublets
m	multiplet	tt	triplet of triplets

Mass spectroscopic data

+ve	positive	m/z	mass to charge ratio
ESI	electrospray ionisation	M^+	molecular ion
ESMS	ElectroSpray Mass Spectrometry		

Infrared spectroscopic data

| cm^{-1} | wavenumber | IR | infrared |

Abstract

Research into inorganic supramolecular chemistry is burgeoning, in particular that which focuses on the formation of capsular molecules and the effects that these unique environments have on catalytic reactions. With the aim of producing new ligand designs that could not only support reactive metals, but also partake in supramolecular aggregation to provide a capsular microenvironment, new tripodal ligands and wide span imines and amines have been synthesised. Furthermore, the exploitation of hydrogen-bonding motifs formed through pyrrole-imine tautomerisation upon metallation of these ligands has been explored, with the aim of enhancing reactivity and stabilising reactive intermediates.

In Chapter one, the concept of covalent and non-covalent capsules is introduced, and includes the different aspects affecting the encapsulation of molecules and their use as nanoreactors. The use of secondary interactions, e.g. hydrogen-bonding in metal complexes of tetrapodal and tripodal ligands is discussed.

Chapter two describes the synthesis of a tripodal pyrrole-imine ligand and the formation of its multi-metallic complexes of Group one metals, transition metal and the f-block elements. The complete and partial tautomerisation of this ligand upon metal complexation is also examined.

In Chapter three, the formation of hangman complexes of the tripodal pyrrole-imine ligand is described and is extrapolated to the chemistry of a new pyrrole-amide ligand. The synthesis of this latter ligand and its properties with regards to anion binding are also explored.

Chapter four describes the formation of wide span diamine and diimine ligands and their propensity to form adducts with cobalt and zinc chlorometallates and unusual multimetallic palladium complexes.

The final conclusions of the work presented in this thesis are drawn in Chapter five.

Chapter six presents experimental details and characterising data for all of the new compounds presented in this thesis.

Table of contents

Appendix:

Chapter 1: Introduction

1.1 Supramolecular chemistry and the forces at our disposal

Supramolecular chemistry, described as "chemistry beyond the molecule", has been a burgeoning area in recent years and consists of the investigation of molecular systems held by intermolecular forces instead of covalent bonds.[1] Encompassing all major areas of chemistry, the inspiration behind the synthesis of these systems is usually based on biological systems, especially enzymes, due to the drive to mimic their catalytic properties.[2] This has led to the observance of the primordial concept of complementarity, also known as the "lock and key" principle as postulated by Fisher in 1894,[3] between the host molecule (lock) and its guest (key) which is best illustrated by the base pairing in the DNA double helix. A single DNA strand is made of purine and pyrimide bases linked together by a backbone of alternating phosphates and sugars. The DNA double helix is constituted of two antiparallel strands held together by complementary hydrogen bonds between each base pair.[4] Adenine interacts with thymine through two hydrogen bonds whilst cytosine and guanine use three (Figure 1).
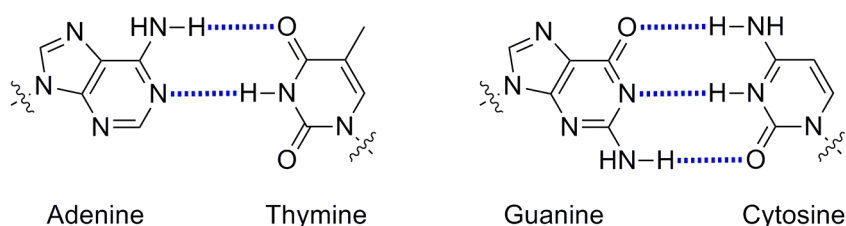
Figure 1: Complementary hydrogen bonded base pairs in DNA.

Although the "key" needs to have a certain shape to fit the "lock" in sterical terms, the electronic interactions between the two also need to be matched to maximise the complementarity. These need to be reversible so

that enzymes can act as catalysts. The architecture of supramolecular entities is therefore based on non-covalent interactions such as electrostatic interactions, hydrogen bonding, π–π stacking, van der Waals forces and hydrophobic effects.

Raymond and co-workers have studied the formation of host guest complexes driven by electrostatic interactions such as ionic interactions.[5] The formation of the tetrahedral host from four Ga^{III} cations representing the corners (Ga1···Ga2, 12.63 Å) and six deprotonated di-catechol ligands representing the edges resulted in the highly negatively charged complex $[Ga(L)]^{12-}$ shown in Figure 2.[6] This high negative charge and the hydrophobicity of the cavity provided by the multiple arenes of the capsule make the host the ideal vessel to encapsulate aromatic cations. This attraction has been shown by adding 4-methoxybenzenediazonium chloride to an NMR sample containing $[Ga_4L_6]^{12-}$ and 2,4-pentanedione. The diazonium cation is encapsulated faster than the spontaneous reaction with the diketone can occur. Although the encapsulation of related azonium cations was attempted, it was shown that those without hydrophobic aliphatic groups were not encapsulated within the tetrahedral host. This is the result of greater hydrophobic interactions between the two ethyl groups of 4-(diethylamino)benzenediazonium chloride and the hydrophobic walls of the capsules compared to the smaller interactions developed by a single methyl in 4-methoxybenzenediazonium chloride.
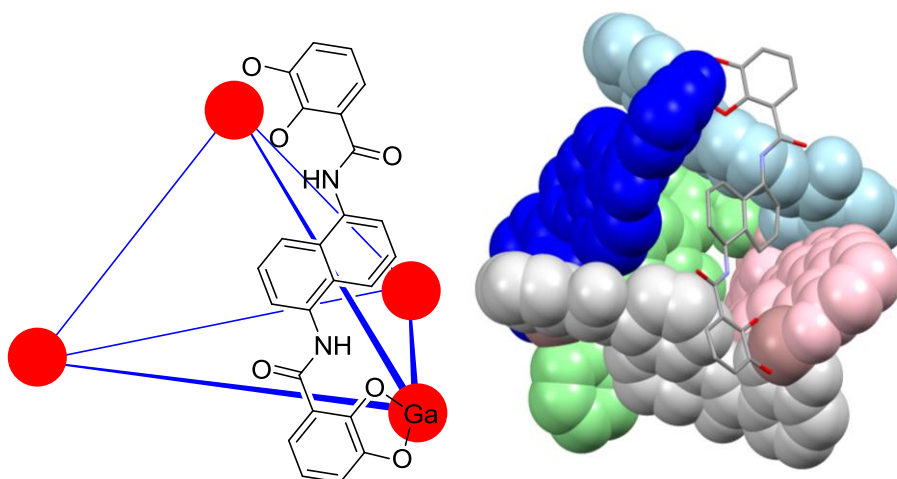
Figure 2: Schematic drawing of the [Ga$_4$L$_6$]$^{12-}$ tetrahedron showing the structure of the catechol ligand; lines represent the additional ligand molecules and the circles represent gallium cations. Hydrogen atoms omitted for clarity.[6]

Since its first synthesis, this Ga-based tetrahedron has been studied towards numerous applications such as a vessel for the protection of solvent sensitive species,[7] the stabilisation of reactive intermediates[8], a vessel for catalyst[9] and as a catalyst in its own right.[10] These possibilities are the result of the formation of a special environment within the hydrophobic cavity protected by the catechol ligands.

The directionality of hydrogen bonds makes them one of the most widely used types of non-covalent interactions. They allow chemists to predict the architecture that larger entities will display. Atwood and co-workers have demonstrated their use by the development of large calix[4]arene derivatives held together by hydrogen bonds derived from water molecules.[11] The first example of this effect was the self-assembly of six calix[4]resorcinarenes and eight water molecules through sixty hydrogen bonds in a snub cube structure akin to viral capsids (Figure 3). Alternating hydroxide groups of the individual resorcinarene hydrogen bond to a water molecule whereas the others are binding with other resorcinarene molecules (both 2.73(1) Å). Further hydrogen bonds are observed within each unit with

neighbouring hydroxides interacting with each other (2.64(1) Å). The capsule formed has an internal volume of 1.374 Å^3 which at the time was 4.5 times larger than any other reported.
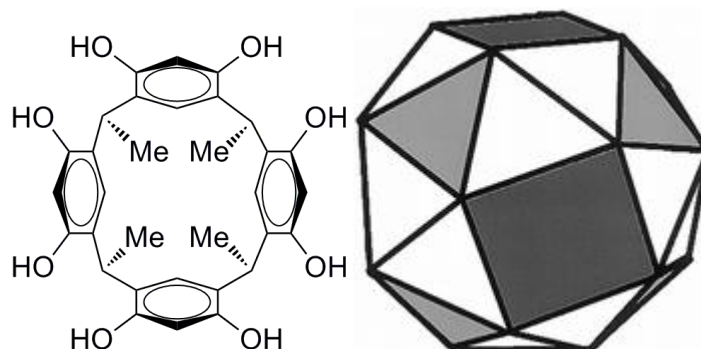
Figure 3: Calix[4]resorcinarene used in the capsule observed by Atwood and co-workers (left) represented as squares in the snub cube (right) with triangle occupied by water molecules in grey.[11]

Hydrogen bonds cannot only be used to form capsules but also to stabilise guest molecules within a host as has been observed by Beer and co-workers during the synthesis of the pyrrole-imine cryptands shown in Figure 4.[12] The Schiff base condensation reaction between two equivalents of 5, 5′, 5′′-triformyl-2,2′,2′′tripyrrylethane and three equivalents of diaminoalkanes led to the formation of the cryptand, templated around a single diamine molecule and resulting in a host-guest complex.
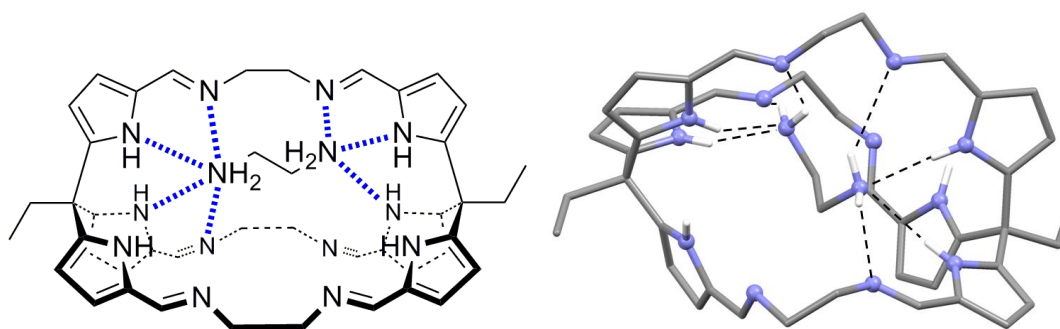
Figure 4: Encapsulation of 1,2-ethylenediamine by a pyrrole-imine cryptand observed by Beer and co-workers. Hydrogen atoms not involved in hydrogen bonding omitted for clarity.[12]

Seven hydrogen bonds were observed in the solid state between the two elements of the complex. At each end of the guest, two out of the three pyrrole NH groups orientate themselves towards the guest molecule and interact with the amine nitrogen with bond distances ranging from 3.04 to 3.06 Å ($N_{host} \cdots N_{guest}$) . The other interactions arising from guest amine donors towards the host's imine nitrogens with bond distances ranging from 3.17 to 3.20 Å ($N_{host} \cdots N_{guest}$). Although the host/guest binding constant is 1500(140) M^{-1}, the diamine-free cryptand can be obtained by stirring the complex in methanol overnight. New guests such as ethane-1,2-diol can then be introduced within the host's cavity (K = 1060(29) M^{-1}).

Face-to-face π–π stacking is well known for its role in the stacking adopted by carbon nanosheets and also well illustrated by the stacking of *bis*(η^6-benzene)chromium with molecules of hexafluorobenzene reported by Perutz and co-workers.[13] The X-Ray crystal structure of this self-assembled compound depicts an infinite stacking of alternating units of C_6F_6 and chromium complex as displayed in Figure 5. With the centre of each unit slightly offset from one another, the column is best thought of as a staircase with a step height of 3.48 Å. This offset is the result of the π orbital of neighbouring units interlocking with each other. Edge-to-face π-stacking, also known as t-shaped π-interactions, has also been exploited in interactions between quinone guests and macrocyclic hosts by Hunter with a view to better understand the binding domain of bacterial photosynthetic reaction centres.[14] Hunter used a macrocycle containing four hydrogen-bonding sites and six arenes for π–π interactions and observed that *p*-benzoquinone formed only four edge-to-face π–π interactions instead of forming the remaining two, four hydrogen bonds formed between its oxygens and the amido nitrogen of the host (Figure 5 right). This allows a maximisation of

interactions and provides a stable complex even in the presence of competing solvents.
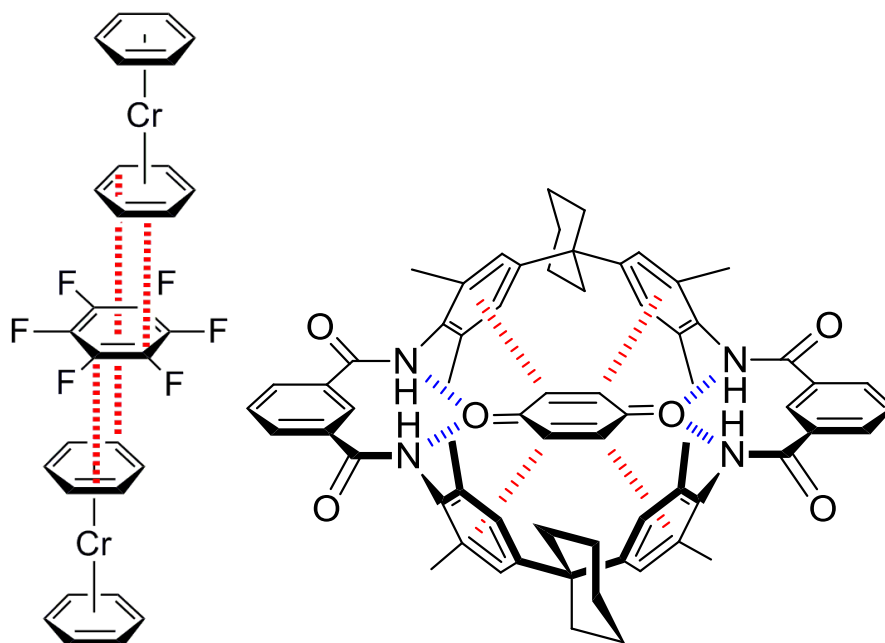
Figure 5: Face to face π stacking described by Perutz and co-workers between C_6F_6 and bis(η^6-benzene)chromium (left) and the edge to face π interactions described in the host guest complex described by Hunter (right) with π interactions in blue and hydrogen bonds in red.[13-14]

Van der Waals attraction forces are the result of the random motion of electrons around an atom's nucleus. At any one point, there can be more electrons on one side of the nucleus than on the other forming an instantaneous dipole. The atom will have on one side a partial negative dipole and on the other a partial positive dipole. If a second atom comes in proximity of this negative dipole, its electrons are repelled forming a positive dipole on this new atom. An attractive charge is therefore formed between the atoms. The nature of van der Waals forces makes it difficult to design capsules taking full advantage of them. Capsules of this type would also show stability difficulties as in solution solvation forces might exceed van der Waals forces. Ananchenko and co-workers have reported the formation of such a capsule formed by the arrangement of two tail-to-tail *para-*

hexanoylcalix[4]arenes as displayed in Figure 6.[15] Although the capsule is unstable, whether it is the result of van der Waals forces holding the capsule together or the polar chloroform guests doing so is debatable.
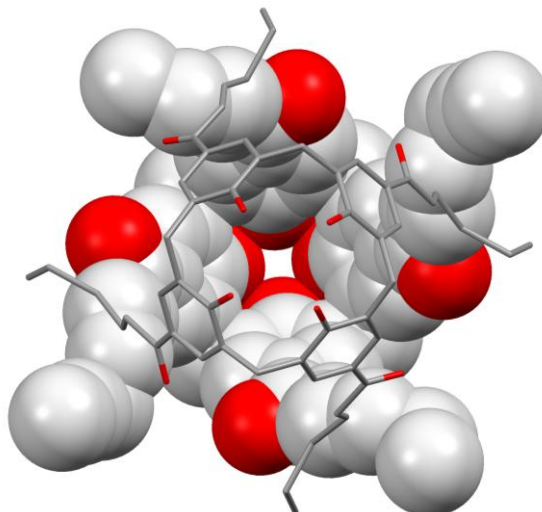
Figure 6: Capsule formed by two molecules of *para*-hexanoylcalix[4]arene held together through van der Waals forces reported by Ananchanko and co-workers.[15]

Sometimes mistaken as a force, the hydrophobic effect is the driving force behind the binding of two apolar molecules within an aqueous medium. Water molecules around an apolar host will form a highly ordered network through hydrogen bonding leading to the encapsulation of the host by water molecules. Upon guest complexation, the hydrogen bond network is broken, releasing disordered water molecules into the reaction medium which increases the entropy of the reaction. A clustering of apolar molecules such as oil molecules in water is therefore favourable and leads to guest encapsulation.

The ability to form capsules and provide an environment protecting guest molecules from the surrounding media has been intensively studied. Harnessing nature's ability to selectively promote reactions and protect guest molecules through encapsulation can lead to advances in enzyme mimics

and drug delivery systems. Host molecules are differentiated by the type of bonding by which the capsule is held together, either covalently or non-covalently.

1.2 Covalent Capsules

Early covalent nanoreactors involved low molecular weight catalysts containing a substrate binding site capable of recognising the substrate adjacent to an active site. The catalytic properties of cyclodextrin derivatives were extensively studied by Breslow and co-workers who developed and studied a ribonuclease A mimic consisting of two imidazoles joined covalently to the binding cavity shown in Figure 7.[16] This nanoreactor, which combines a hydrophobic binding site with two acid-base catalytic groups, has been seen to catalyse numerous reactions such as the hydrolysis of cyclic phophodiesters at rates a hundred fold faster than compared to the uncatalysed reaction.[17] Larger capsules including multiple cyclodextrins or a mixture of cyclodextrin cavities and transition metals have also been studied and have been shown to catalyse the hydrolysis of esters that all show varying catalytic accelerations.[18] The Zn[II] derivative shown in Figure 7 has been found to accelerate the hydrolysis of esters 1 400 000 fold.[19]
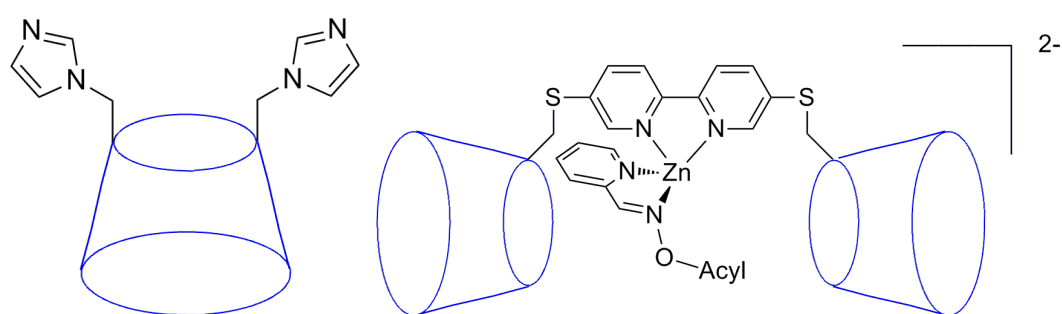
Figure 7: Ribonuclease A mimic capable of catalysing a wide range of reactions (left); cyclodextrin zinc derivative capable of catalysing the hydrolysis of esters 1 400 000 fold.[16, 19] Cyclodextrin units highlighted in blue.

This type of small catalyst has one major drawback in that being relatively small; they can only catalyse unimolecular reactions. In order to circumvent this difficulty, larger receptors have been designed.[20] Most of these catalysts have been constructed in such a way that the receptor's reaction chamber encapsulates the guest molecule(s) shielding it from its gross environment. However, other setbacks have been observed in this new type of nano-reactor, in particular, they are not truly catalytic, but merely arrange the molecules in the correct orientation for the reaction to proceed. By doing so, the product generally becomes strongly bound to the capsule and the turnover hence becomes non-existent. The cucurbit[6]uril capsule (shown in Figure 8) formed by the addition of formaldehyde to glycouril under acidic conditions, designed by Mock and co-workers, was seen to accelerate 1,3-dipolar cycloaddition reactions and illustrates this issue.[21]
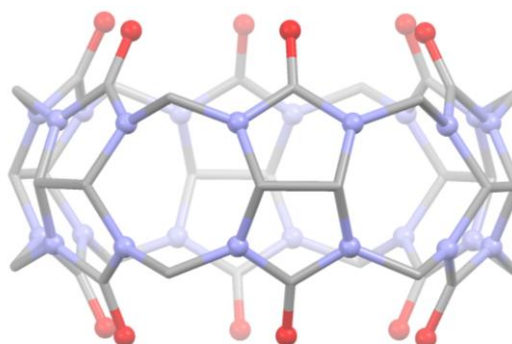
Figure 8: X-Ray crystal structure of cucurbit[6]uril. Hydrogen atoms omitted for clarity.

The cycloaddition reaction between propargyl ammonium and azidoethyl ammonium, shown in Scheme 1, is accelerated 55000 times in the presence of cucurbit[6]uril.
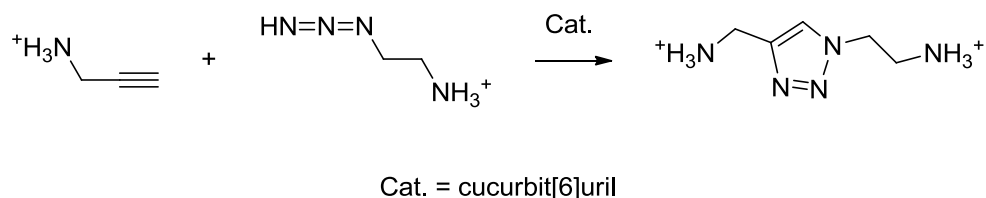
Cat. = cucurbit[6]uril

Scheme 1: Reaction scheme for the regioselective cycloaddition catalysed by cucurbit[6]uril.

Although the uncatalysed reaction produces the 1,2 and 1,3 diazole isomers in equal amounts, the catalysed reaction is regiospecific and only forms the 1,3 isomer as shown in Scheme 1. However, the product has a greater affinity for the cavity of the capsule than any of the starting materials, making the release of the product the rate determining step of the catalytic cycle. Since this early success, glycourils of different sizes have been synthesised and have been used in a wide variety of applications including molecular switches,[22] drug delivery, and catalysis.[23]

A further example of the problems associated with the non-lability of the product has been observed in the cyclic zinc porphyrin host designed by Sanders and co-workers consisting of three zinc porphyrins held together by alkyl groups (shown in Figure 9).[24] This proximity and the convergent geometry of the binding sites allow substrate molecules to bind as ligands to the metal centres and react with each other.[25]

R = CH$_2$CH$_2$CO$_2$CH$_3$
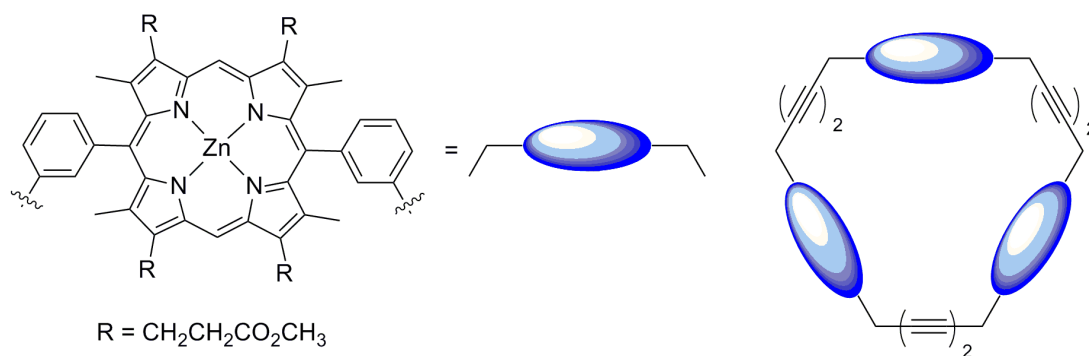
Figure 9: Monomer unit of the zinc prophyrin dimer (left) and the trimer macrocycle representation (right).[24]

In the presence of the zinc porphyrin macrocycle, the Diels-Alder reaction between the furan and the maleimide derivatives shown in Scheme 2, is accelerated two hundred fold.
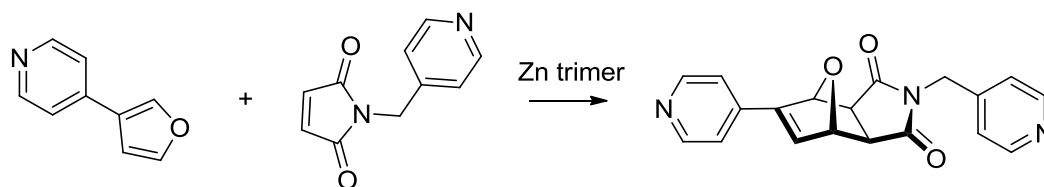
Scheme 2: Reaction scheme for the accelerated Diels-Alder reaction using the zinc trimer designed by Sanders and co-workers.[25]

Control reactions showed that the reaction was not accelerated in the sole presence of zinc porphyrin monomers and that the presence of tripyritriazine, which binds extremely strongly within the cavity of the macrocycle, has the same result. From these results it can be concluded that the simultaneous binding of the starting materials added to their proximity within the cavity of the host is the leading factor for the faster reactivity. The capsule is shown to be regioselective as only the *exo*-product is formed at any stage of the reaction and is hence acting as a template, forcing the starting materials in the correct arrangement to form this product. The high affinity between the product and the cavity, demonstrated by the high binding constant (4×10^5 dm^{3}mol^{-1}), is a hundred fold higher that of the starting material and makes the rate determining step of the catalytic cycle the ejection of the product from the nanoreactor. In this case, the problem arose from the product binding with two metal centres whereas each starting material molecule only binds to one. Indeed, using alternative starting materials and looking at forming products able to bind to a single zinc atom, showed that the capsules was catalysing, albeit moderately, the acyl transfer between 4-pyridinylmethanol and 1-acetylimidazole as shown in Scheme 3.[26]
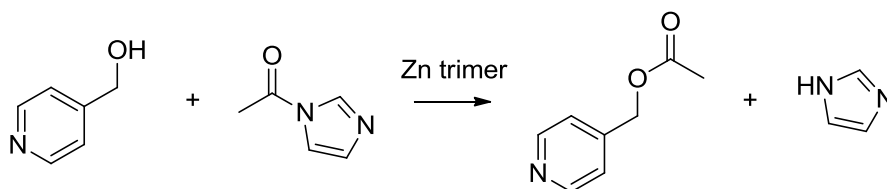
Scheme 3: Reaction scheme for the catalytic acyl transfer reaction unsing the zinc trimer designed by Sanders and co-workers.[26]

Two different approaches have been taken to solve the problem of product-capsule separation. The first is to redesign the capsule binding site so that they (a) bind more weakly to the products than the reactants or (b) target products that are either too small or large to fit in the guest molecule. The second approach is to completely redesign the ligand so that the guest can reversibly associate and disassociate itself. This has given rise to the construction of non-covalent capsules.

1.3 Non-covalent capsules

Non-covalent capsules can be defined as receptors with enclosed cavities that are formed by reversible non-covalent interactions (primarily hydrogen-bonding) between two or more complimentary molecules. Numerous different, relatively small molecules, such as calixarenes and resorcinarenes have been used to form larger capsules. However, the "soft-ball" capsule, held together by sixteen hydrogen bonds designed by Rebek and co-workers is one that has shown the most interest.[27] Consisting of two "U" shaped molecules made of a linear arrangement of aliphatic and aromatic rings ended by glycouril units, the seam of each molecule is lined with hydrogen bond donors and acceptors (Figure 10). The glycouril carbonyls are the complementary hydrogen-bonding sites for the four phenolic donors.

R = 4-n-heptylphenyl
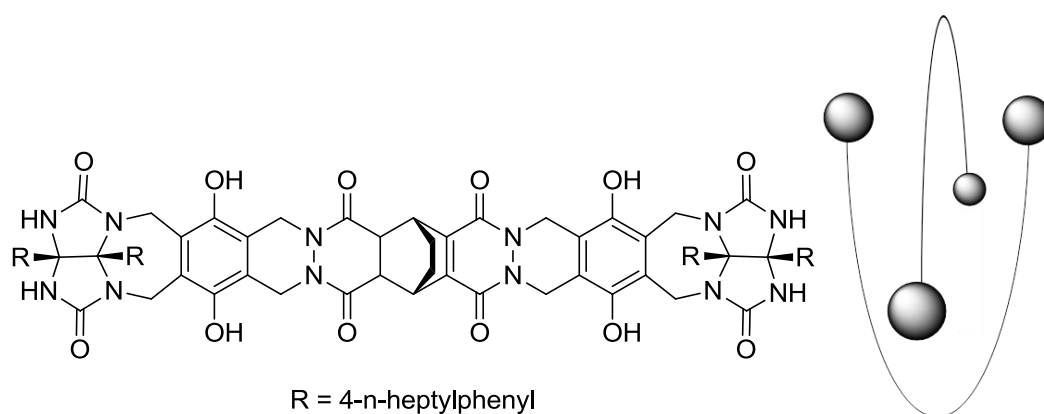
Figure 10: Structure of the self-complementary units designed by Rebek and co-workers (left) and a schematic rendering of their self-assembly (right) with the glycouril units represented as balls.[27]

Importantly, the guest encapsulation increases with temperature suggesting that the process is favoured entropically,[28] a characteristic rarely observed as it is usually disfavoured.[29] The large host cavity allows for the encapsulation of multiple solvent molecules (in this case $CDCl_3$) which would be required for a maximisation of van der Waals interactions between the capsule and its guests. By encapsulating a single guest large enough to fill the cavity (e.g. ferrocene), multiple solvent molecules are released within the reaction media, so increasing the entropy.

The possibility of encapsulating more than one guest makes the capsule a potential nano-reactor. Indeed, the capsule has later been shown to accelerate the Diels-Alder reaction between *para*-quinone and cyclohexadiene (shown in Scheme 4).[30] Although the reaction is accelerated two hundred-fold at room temperature, several days are required prior to product being observed outside the capsule, showing that again product inhibition is a problem and prevents turn-over. Replacing cyclohexadiene with 2,5-dimethylthiophene, however, afforded a product with poorer affinity to the capsule and resulted in a catalytic cycle with modest (ten-fold) rate enhancement compared to the uncatalysed reaction.[31]
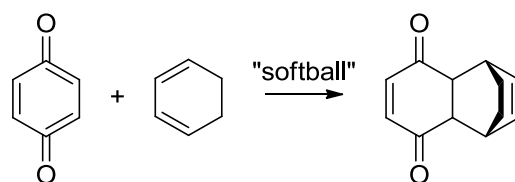
Scheme 4: Diels-Alder reaction promoted by the "softball" designed by Rebek and co-workers.[30]

Although hydrogen-bonded capsules are predominant in non-covalent capsules, metallo-organic capsules have been synthesised. Hydrogen bonds are linear and curvature is needed somewhere in the building block to promote capsule formation, whereas the angles between metal and ligands can be used to form the curvature required. Fujita and co-workers have been the pioneers of metal-organic polyhedra, boxes and cages. They reported the self-assembly of four *tris*(4-pyridyl)triazine ligands and six palladium complexes, regardless of the ratio of the starting material used, into an octahedron (shown in Scheme 5).[32]

Pd = Pd(en)
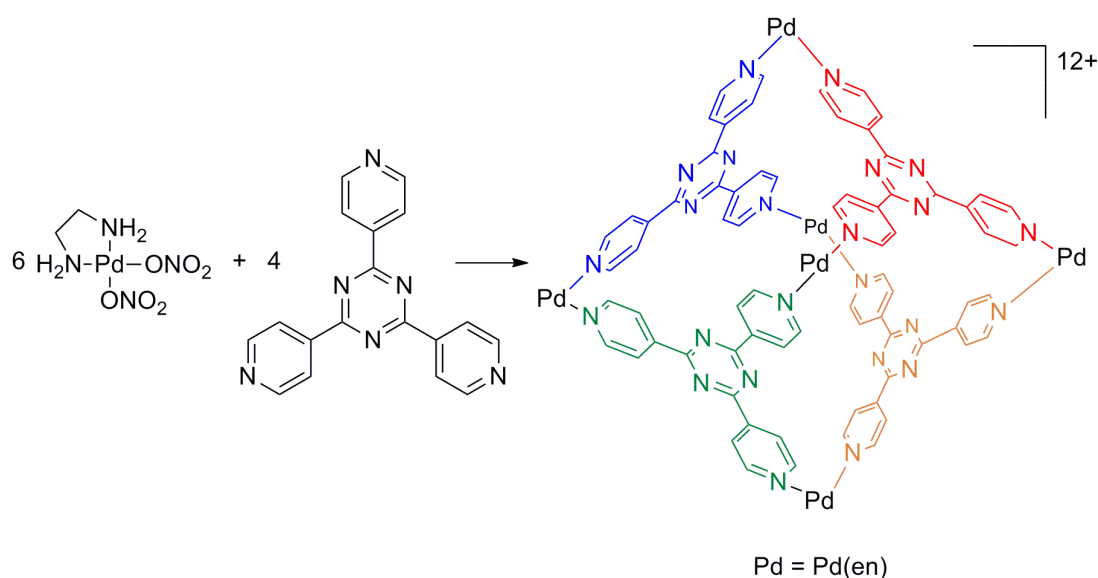
Scheme 5: Formation of an octahedral metallo-capsule with six Pd[II] corners and four *tris*(4-pyridyl)triazine faces.[32]

Each corner consists of a Pd[II] metal centre bound by two pyridyl units in a *cis* configuration whilst the other two coordination sites are occupied by

a single bidentate ethylenediamine molecule. Due to its solubility in water as well as its ability to bind to large neutral organic species,[33] it was first developed as a reverse phase-transfer catalyst,[34] bringing organic substrates into the aqueous phase and taking out the product away from the same phase. In conjunction with $Pd(en)(NO_3)_2$ acting as the oxidation catalyst, the capsule was found to promote the oxidation of styrene to acetophenone in a fashion not dissimilar to that described in the Wacker process (as shown in Scheme 6).[35] In this case however, the oxidation of the substrate takes place within the capsule by the action of the Pd^{II} catalyst, reoxidation of which is aerobic. The difference in hydrophobicity between styrene and acetophenone promotes the substitution of the product by new substrate molecules illustrating that the capsule acts as a nano-reactor.
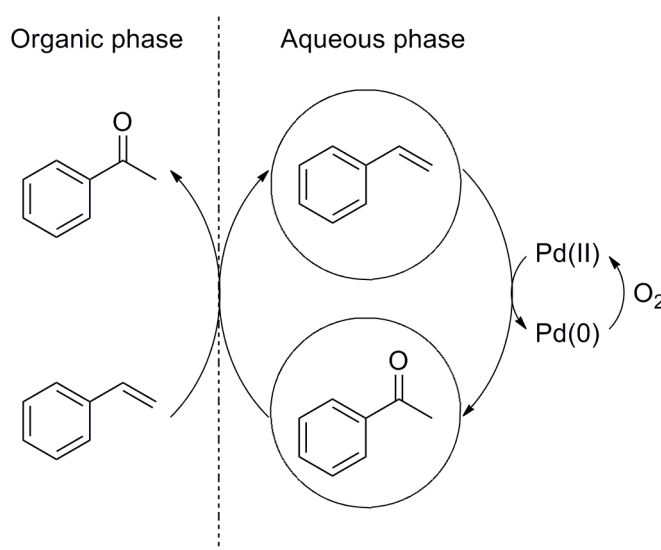
Scheme 6: Schematic representation of the reverse phase transfer catalysis for the Wacker oxidation of styrene by the metallo-capsule developed by Fujita and co-workers (represented by circles).[34]

The ability of this type of capsules to act as a transport agent and protect substrate molecules from the reaction medium has been used to form similar receptacles with a view to create cancer drug delivery systems,[36] catalysts, and to provide safe ways to transfer highly reactive molecules.[37]

Although complete encapsulation is not always necessary, shielding the catalytic site from its environment and providing high substrate reactivity is paramount. Reek and co-workers have designed what can be pictured as a giant tripodal molecule where each side consists of zinc porphyrins attached by their metal centre to the pyridyl group of a binding site, in this case *tris*(*m*-pyridyl)phosphine (Figure 11).[38] The phosphorus atom is free to coordinate to catalytically active transition metals, whilst the bulkiness of the porphyrin groups prevents the metal centre binding to multiple ligands.
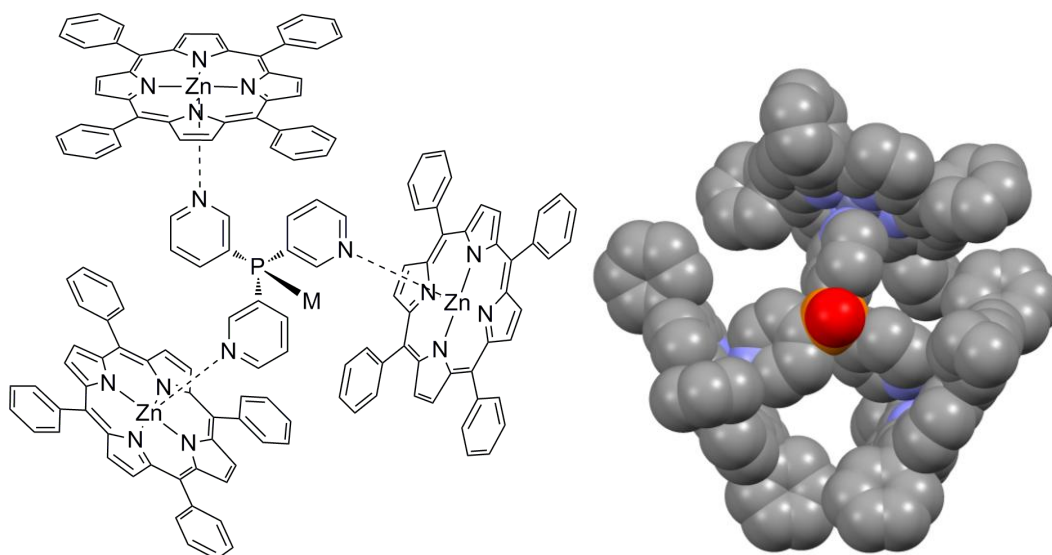
Figure 11: Schematic rendering of the tripodal nano-reactor synthesised by Reek and co-workers (left) and its X-Ray crystal structure (right) in which the hydrogen have been omitted for clarity.[38]

With the phosphine bound to a rhodium metal centre, the complex was tested as a catalyst in the hydroformylation of 1-octene (Scheme 7 top). At room temperature, the protected metal centre showed a ten-fold increase of turnover frequency, favoured the branched product, and showed a lower isomer ratio compared to the rhodium phosphine that was not bound to porphyrins. The formation of a special environment protecting the active metal centre is clearly the driving force behind the increased catalytic activity

and the regioselectivity of the reaction. With the metal centre replaced by palladium, the potential to catalyse the Heck reaction between iodobenzene and styrene was investigated (Scheme 7 bottom). Adding Pd^{II} to the phosphine unit in the absence of zinc porphyrin resulted in the formation of a phosphine tetramer which had no catalytic impact on the reaction. In contrast, the addition of zinc porphyrins formed a monophosphane palladium complex which accelerated the reaction forty-fold.

P = trisporphyrin(*m*-pyridyl)phosphane
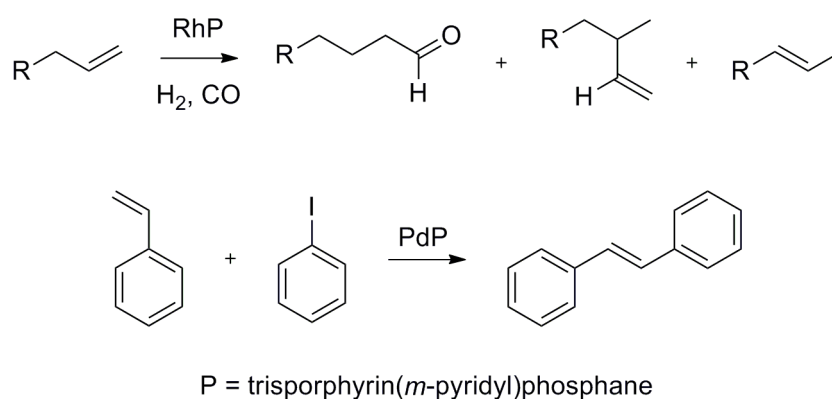
Scheme 7: Hydroformylation of 1-octene (top) and Heck reaction of iodobenzene and styrene (bottom) catalysed by rhodium and palladium nano-reactors designed by Reek and co-workers.[38]

Reek and co-workers have developed many more confined-metal-centre catalysts in which large planar ligands are used to protect highly active metal centres of various geometries.[39] Nano-reactors in which the reaction is promoted by an active metal centre such as the aforementioned example have shown far less product inhibition issues than their organic covalent counterpart.

1.4 Tripodal capsules

Many tripodal ligands are known. However not all of them are large enough to form capsules. When considering tripodal capsules, two different concepts can be imagined; (i) a metal centre is linked by the tripodal branch

of two different tripods. (ii) the tripod is large enough to accommodate the metal centre so that it can shield the substrate from the environment.

Trinuclear capsules are still in their early development and very few have been synthesised. Their study arises from a scientific effort to form predetermined structures by using a suitable metal ion. The vast majority of these capsules involve the use of Ag[I], Pd[II] or Pt[II] with *tris*(pyridyl) related ligands,[40] and can be illustrated by the recently formed capsule by Lindoy and co-workers in which two 1,3,5-*tris*((pyridine-4-ylthiol)methyl)benzene molecules are held together by three silver ions acting as bridges between the pyridyl units of different ligands as shown in Figure 12.[41]
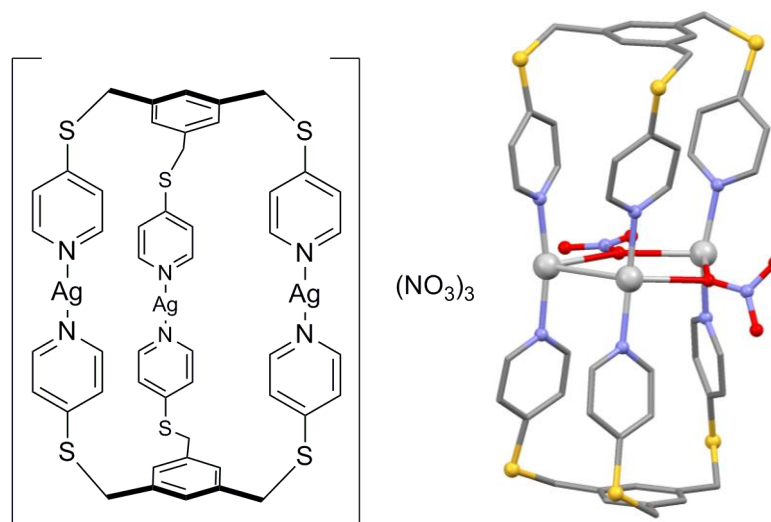
Figure 12: Solution state structure representation (left) and solid state X-Ray crystal structure of the tri-silver metallo-capsule designed by Lindoy and co-workers. The third nitrato ion and hydrogen atoms were omitted for clarity.[41]

Although a symmetrical structure is observed in solution by ^{1}H NMR experiments, the crystal structure shows only two equivalent silver cations interacting with each other at 3.16 Å which is smaller than the van der Waals diameter (3.44 Å) which is not uncommon.[42] Both equivalent silver atoms are connected to the third metal centre through a single nitrato group. Although a single metal centre was originally intended to coordinate to the

three sulphurs donors, steric effects between the aromatic rings prevent this coordination mode. Additionally, the strong coordination of pyridyl ligands to Ag[I] has been reported before.[43] Indeed the use of a very similar ligand where the central benzyl was replaced by a nitrogen and the pyridyl arms were replaced with benzyl groups, resulted in the formation of a complex where the metal centre is located within the ligand between the three sulphur atoms as displayed in Figure 13. This could also be the result of the sulphur donors residing closer to the centre of the cavity, increasing their interactions with the metal centre.[44]
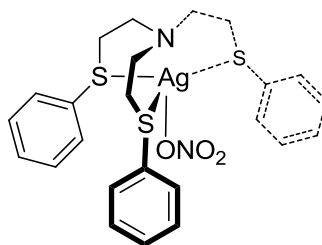
Figure 13: Silver complex developed by Lindoy and co-workers showing a different binding motif to the metallo-casule displayed in Figure 12 owing to minor ligand alterations.

Using a similar ligand to that described above, Gloe and Lindoy synthesised a trinuclear metallo-capsule using three Cu[II] centres. Although copper is in the same triad as silver and gold, it has not been as widely employed in the formation of metallo-capsules.[45] Each square planar metal centre is bound to the diketone derivative of a single branch of each ligand which are all bound to a central 1,3,5-triazine unit through sulphur bridges as seen in Scheme 8. Metal-β-diketone binding is of great interest to the area of metallo-cryptands and more generally to capsules due to the pH dependent nature of ligand which could be used for selective guest inclusion and release by pH control.
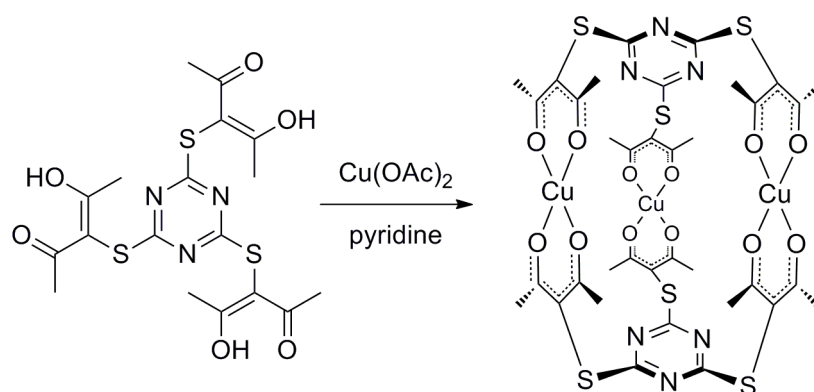
Scheme 8: Synthesis of the tris-copper metallocapsule designed by Gloe and co-workers.[45]

Although metallo-cryptands are of great interest due to the directionality of the metal/ligand binding, organic cryptands are also a popular research area in organometallic and catalytic chemistry. Their design, in the latter case, is usually driven by the possibility of binding a highly reactive metal centre at both ends of the molecule, encapsulating a substrate molecule and promoting a reaction within the newly formed nano-reactor. Nocera and co-workers have recently developed a tetrapodal cryptand consisting of two *tris*(2-aminoethyl)amine (TREN) metal binding sites linked through three aryl dicarbonyl groups as displayed in Figure 14.[46]
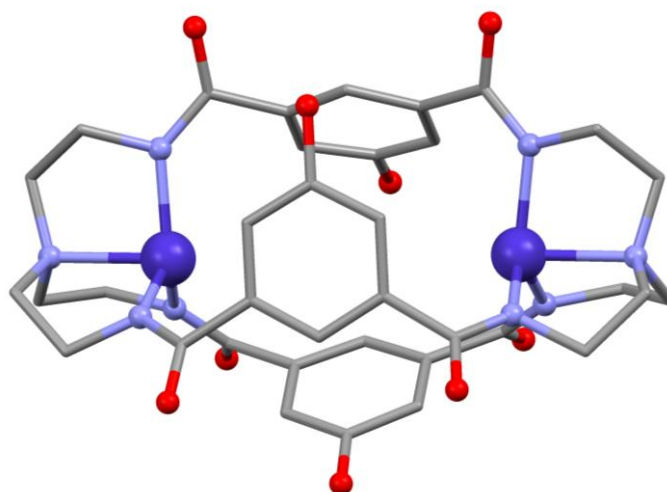
Figure 14: Crystal structure of the dicobalt cryptand prepared by Nocera and co-workers. Solvent molecules of crystallisation, K⁺ counterions, dipropoxyphenoxyl groups and hydrogen atoms are omitted for clarity.[46]

Upon metallation with two equivalents of Co^{II}, the complex did not show substrate molecules within the capsule. The addition of cyanide at 75 °C over two days leads to the binding of the small molecule between the two metal centres. The insertion of cyanide within the complex results in the Co^{II} cations being pulled towards the guest (Co⋯Co, 6.41 Å; MeCN bridged Co⋯Co, 5.33 Å) showing that the complex has the potential to activate small molecules. This is also supported by the change of electrochemical properties of the complex in the absence and presence of cyanide, which display an irreversible oxidation at 1090 mV for the former and irreversible reduction and oxidation at -1200 mV and -225 mV (vs Fc/Fc^+) respectively for the latter.

Further investigation revealed that a range of first row transition metals could be accommodated within the ligand to form dimetallic complexes (Mn^{II}, Fe^{II}, Ni^{II} and Zn^{II}).[47] Although it has not unambiguously been proven that the aforementioned complex can be used as a nano-reactor, the unmetallated ligand itself can reduce O_2 to O_2^{2-} which is found as a host/guest complex within the cryptand.[48] The three step reversible mechanism proposed for this chemistry consists of (i) reduction of O_2 to the superoxide (O_2^-), (ii) superoxide encapsulation and (iii) reduction of the encapsulated O_2^- to the peroxide (O_2^{2-}) (shown in Scheme 9).
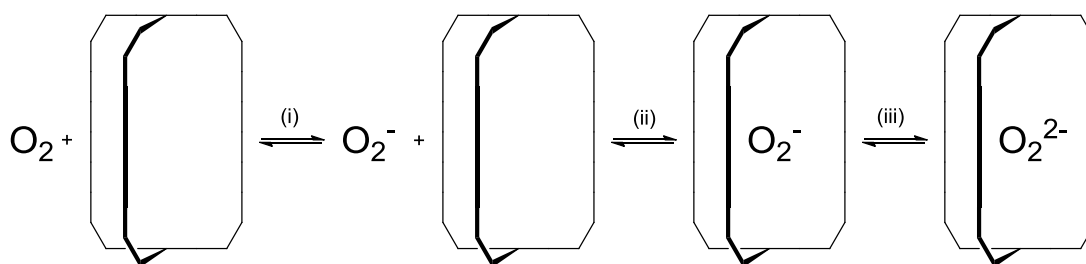
Scheme 9: Proposed mechanism of the reversible O_2 reduction to encapsulated O_2^{2-}.[48]

The formation of encapsulated O_2^{2-} was confirmed by X-Ray diffraction studies with O-O bond distances of 1.504(2) Å which is

comparable to those found for Na_2O_2 (1.49 Å) and its 1,6-anhydro-β-maltose adduct (1.50 Å).[49] The stabilisation of this active species within the capsule can be explained by the six hydrogen bonds formed between the TREN NHs and O_2^{2-}.

1.5 Pyrrolic tripods and tetrapods

The lower π-donation of pyrrole N donors compared to amides, as well as the possibility to functionalise the fifth position of pyrrole make it an attractive unit for transition metal co-ordination. A TREN derivative where all primary amines have been replaced by mesityl-substituted pyrroles was synthesised by Chang and co-workers in a single step through the Mannich reaction between 2-mesitylpyrrole, formaldehyde, and ammonium chloride.[50] Addition of Fe^{II} to the ligand resulted in a highly symmetric complex where the metal centre is bound in a trigonal pyramidal geometry to three deprotonated pyrroles in the equatorial position and the tertiary amine, linking the three branches of the ligand together, in the axial site. Exposure of this complex to an atmosphere of nitrous oxide (N_2O) resulted in the co-ordination of a terminal oxo ligand on the last axial site of the now trigonal bipyramidal Fe^{IV} metal centre. This intermediate abstracts a hydrogen atom from the surrounding media to form an Fe^{III} hydroxide complex (as shown in Scheme 10).
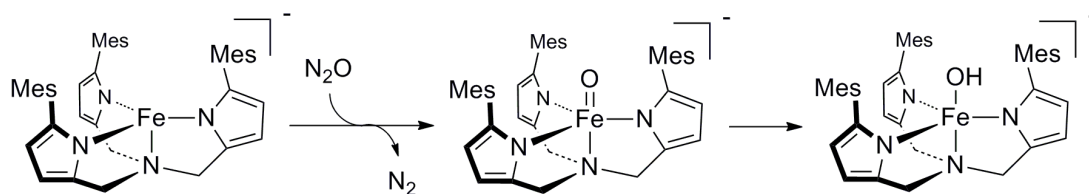
Scheme 10: Activation of N_2O with the non-heme iron tris-pyrrole complex synthesised by Chang and co-workers to form an Fe^{IV} oxo complex followed by hydrogen abstraction leading to an Fe^{III} hydroxide complex.[50]

This ability to activate N_2O is the result of accessing a metal geometry different from the four-fold symmetry commonly observed in nature and which has profound effects on the reactivity of the metal centre. Indeed Nocera and co-workers have commented on the effect the metal centre geometry can have on the activation of small molecules, in particular the oxo ligand.[51]
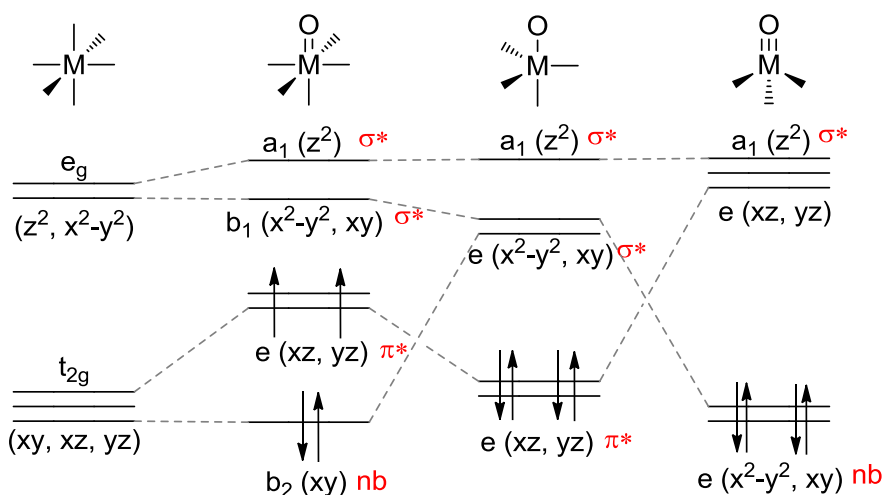
Figure 15: Molecular orbital splitting diagrams for a metal – oxo group in tetragonal, trigonal bipyramidal, and tetrahedral ligand fields compared to the octahedral ligand field. The d electron count and respective bond order shown represent a possible configuration for a d^4 metal centre.[51]

The substitution of an axial ligand of an octahedral metal centre by an oxo group leads to the destabilisation of the bonding d_{xz} and d_{yz} orbitals, as well as the anti-bonding d_{z^2} orbitals (Figure 15). This results in the metal oxo triple bond to be observed only with metal centres of d electron counts of four or less. The first two electrons populate the non-bonding d_{xy} orbital before the next electrons start occupying the d_{xz} and d_{yz} orbitals, which are now anti-bonding. As a result, an elongation of the triple bond will be observed with d^3 and d^4 metal and adding further d electrons will lead to a M=O double bond. For a trigonal bipyramidal complex, such as that described in the non-heme iron *tris*-pyrrole complex described above, the

two lowest orbitals (d_{xy} and d_{yz}) are anti-bonding. A metal oxo triple bond will only be obtained with d^0 metals, with double bond character being retained for metals with a d electron count of two and single bonds observed above this. The presence of two non-bonding orbitals ($d_{x^2-y^2}$ and d_{xy}) in the tetrahedral geometry allows for metals with larger d electron count (up to d^4) to retain a metal oxo triple bond with no destabilisation of the σ or π bonding.

Recently, efforts have been made to access highly reactive metal ions derived from the tetrahedral binding geometries using pyrrolic ligands. Betley and co-workers have demonstrated that a range of late first row transition metal (Mn^{II}, Fe^{II}, Co^{II}, Ni^{II} and Zn^{II}) complexes of *tris*(pyrrolyl)ethane ligands adopt *pseudo*-tetrahedral geometries through the axial coordination of a pyridine ligand (Scheme 11).[52] Electrochemical investigations showed that although oxidations are observed, these are ligand driven with the metal shifting the oxidation wave by up to 1.1 V compared to that of the free ligand (E_P = 375 mV vs. Fc/Fc$^+$). Only the Fe^{II} complex displays an extra quasi-reversible redox event at -750 mV (vs Fc/Fc$^+$).
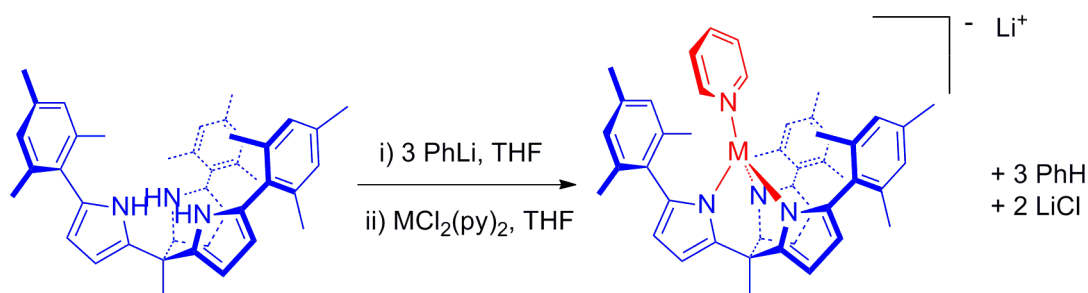
Scheme 11: Transition metal complexes of the tripodal pyrrole ligand developed by the Betley group.[52]

The chemical oxidation of the Li[(^{Mes}tpe)Fe(THF)] by Fc$^+$PF$_6^-$ led to a different solid state structure in which only two arms of the ligand are bound to the metal centre whilst the remaining branch is pendant. The two residual co-ordination sites on the metal are occupied by solvent molecules (pyridine)

and the pendant arm's pyrrole has regained its hydrogen atom through H-atom abstraction from the reaction medium as shown in Figure 16.
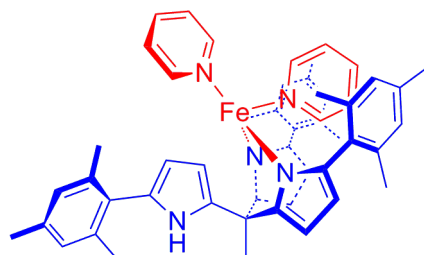
Figure 16: [(k^2-^{Mes}tpeH)Fe(Py)$_2$] synthesised from the chemical oxidation of Li[(^{Mes}tpe)Fe(THF)] by Fc$^+$PF$_6^-$ by Betley and co-workers.

The reactivity of the tripodal iron complex THF adduct was further probed by the addition *tert*-butylisocyanide which resulted in the co-ordinated solvent being substituted by three cyano groups as well as the tautomerisation of a single pyrrolide unit (N-C: 1.333(3) Å) which is rotated away from the metal centre and interacting with the lithium cation.[53] The X-Ray crystal structure of this complex, shown in Figure 17 , depicts the iron metal centre in an octahedral geometry with the additional co-ordination sites occupied by the nitrogen atom of two pyrrolide units in addition to a carbon donor from the tautomerised arm. It was suggested that this arrangement arises from the steric pressure encountered whilst trying to accommodate the three isocyanide ligands as this change in binding provides a greater volume better able to fit the additional ligands. Another concurrent driving force for this reorganisation is the change in spin state observed between the high spin tetrahedral and the low spin octahedral Fe^{II} centre.
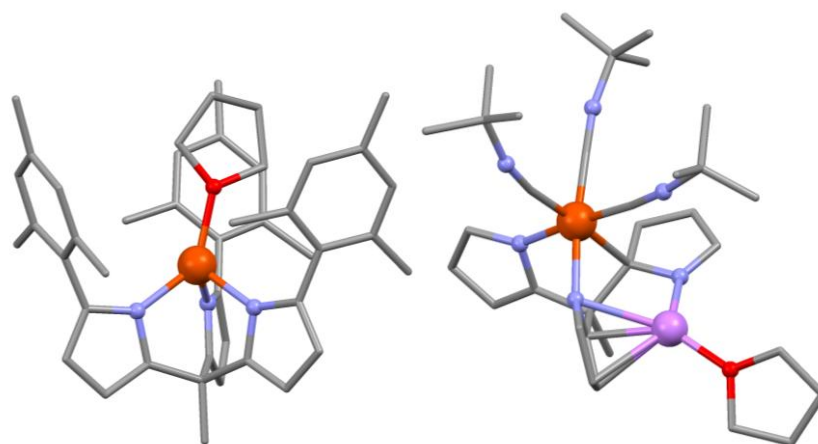
Figure 17: Solid state structure of Li[(^{Mes}tpe)Fe(THF)] (left) and its product, [*N,N,C*-^{Mes}tpe)Fe-(CN^{t}Bu)$_3$]Li(THF) (right), after addition of *tert*-butylisocyanide. Hydrogen atoms and mesityl groups for [*N,N,C*-^{Mes}tpe)Fe-(CN^{t}Bu)$_3$]Li(THF) are omitted for clarity.[53]

1.6 Outlook

In conclusion, catalytic properties are greatly enhanced by the encapsulation of substrate molecules within a large host molecule shielding it from the reaction media. Covalent and organic capsules have shown their limitation with issues surrounding not only host guest dissociation but also the rate of reaction. Non-covalent inorganic capsules have been seen to form catalysts of high turnover number and frequency. These could, however, be improved through the use of metal centres that adopt highly reactive tetrahedral geometries. Capsular complexes can concurrently provide a host environment in which to protect the substrate molecule and a metal in a highly reactive geometry capable of promoting catalytic reactions.

This thesis first describes the synthesis and characterisation of tripodal ligands, investigates their metal chemistry and the development of a substrate binding pocket proximate to the metal binding site. In a second part, the development of wide-span ligands is discussed and their metal chemistry assessed. The ultimate aim of this research is the formation of capsular complexes that are able to encapsulate substrate molecules in the vicinity of a highly reactive metal to induce small molecule activation such as the reduction of dinitrogen to ammonia.

1.7 References

[1]   S. J. Dalgarno, *Annu. Rep. Prog. Chem., Sect. B: Org. Chem.* **2011**, *107*, 182-198; J.-M. Lehn, *Chem. Soc. Rev.* **2007**, *36*, 151-160; B. G. Malmstrom,

Nobel Lectures, Chemistry 1981-1990, World Scientific, London, **1992**; J. W. Steed, J. L. Atwood, *Supramolecular Chemistry*, 2 ed., Wiley, Chichester, **2009**.

[2]   M. J. Wiester, P. A. Ulmann, C. A. Mirkin, *Angew. Chem. Int. Ed.* **2011**, *50*, 114-137; D. Wischang, O. Brücher, J. Hartung, *Coord. Chem. Rev.* **2011**, *255*, 2204-2217; R. G. E. Coumans, J. A. A. W. Elemans, R. J. M. Nolte, A. E. Rowan, *Proc. Natl. Acad. Sci.* **2006**, *103*, 19647-19651; Z. Dong, W. Yongguo, Y. Yin, J. Liu, *Curr. Opin. Colloid Interface Sci.* **2011**, *16*, 451-458.

[3]   E. Fischer, *Ber. Dtsch. Chem. Ges.* **1894**, *27*, 2985-2993.

[4]   H. Lodish, A. Berk, C. A. Kaiser, M. Krieger, M. P. Scott, A. Bretscher, H. Ploegh, P. Matsudaira, *Molecular cell biology* Basingstoke : Palgrave Macmillan,6th ed., 2007.

[5]   T. N. Parac, M. Scherer, K. N. Raymond, *Angew. Chem. Int. Ed.* **2000**, *39*, 1239-1242; B. E. F. Tiedemann, K. N. Raymond, *Angew. Chem. Int. Ed.* **2006**, *45*, 83-86; Julia L. Brumaghim, M. Michels, D. Pagliero, Kenneth N. Raymond, *Eur. J. Org. Chem.* **2004**, *2004*, 5115-5118.

[6]   D. L. Caulder, R. E. Powers, T. N. Parac, K. N. Raymond, *Angew. Chem. Int. Ed.* **1998**, *37*, 1840-1843.

[7]   D. Fiedler, D. Pagliero, J. L. Brumaghim, R. G. Bergman, K. N. Raymond, *Inorg. Chem.* **2004**, *43*, 846-848.

[8]   V. M. Dong, D. Fiedler, B. Carl, R. G. Bergman, K. N. Raymond, *J. Am. Chem. Soc.* **2006**, *128*, 14464-14465.

[9]   Z. J. Wang, C. J. Brown, R. G. Bergman, K. N. Raymond, F. D. Toste, *J. Am. Chem. Soc.* **2011**, *133*, 7358-7360; D. H. Leung, R. G. Bergman, K. N. Raymond, *J. Am. Chem. Soc.* **2007**, *129*, 2746-2747.

[10]   D. Fiedler, R. G. Bergman, K. N. Raymond, *Angew. Chem. Int. Ed.* **2004**, *43*, 6748-6751; C. J. Hastings, D. Fiedler, R. G. Bergman, K. N. Raymond, *J. Am. Chem. Soc.* **2008**, *130*, 10977-10983.

[11]   L. R. MacGillivray, J. L. Atwood, *Nature* **1997**, *389*, 469-472.

[12]   O. D. Fox, T. D. Rolls, M. G. B. Drew, P. D. Beer, *Chem. Commun.* **2001**, 1632-1633.

[13]   C. J. Aspley, C. Boxwell, M. L. Buil, C. L. Higgitt, R. N. Perutz, C. Long, *Chem. Commun.* **1999**, 1027-1028.

[14]   C. A. Hunter, *J. Chem. Soc., Chem. Commun.* **1991**, 749-751.

[15]   G. S. Ananchenko, K. A. Udachin, A. Dubes, J. A. Ripmeester, T. Perrier, A. W. Coleman, *Angew. Chem. Int. Ed.* **2006**, *45*, 1585-1588.

[16]   E. Anslyn, R. Breslow, *J. Am. Chem. Soc.* **1989**, *111*, 8931-8932.

[17]   R. Breslow, A. Graff, *J. Am. Chem. Soc.* **1993**, *115*, 10988-10989; J. M. Desper, R. Breslow, *J. Am. Chem. Soc.* **1994**, *116*, 12081-12082.

[18]   R. Breslow, P. J. Duggan, J. P. Light, *J. Am. Chem. Soc.* **1992**, *114*, 3982-3983; J. Yang, B. Gabriele, S. Belvedere, Y. Huang, R. Breslow, *J. Org. Chem.* **2002**, *67*, 5057-5067; J. Yan, R. Breslow, *Tet. Lett.* **2000**, *41*, 2059-2062; S. D. Dong, R. Breslow, *Tet. Lett.* **1998**, *39*, 9343-9346.

[19]   B. Zhang, R. Breslow, *J. Am. Chem. Soc.* **1997**, *119*, 1676-1681.

[20]   E. S. Barrett, J. L. Irwin, A. J. Edwards, M. S. Sherburn, *J. Am. Chem. Soc.* **2004**, *126*, 16747-16749; D. A. Makeiff, J. C. Sherman, *J. Am. Chem. Soc.*

2005, *127*, 12363-12367; X. Liu, R. Warmuth, *J. Am. Chem. Soc.* **2006**, *128*, 14120-14127.

[21] W. A. Freeman, W. L. Mock, N. Y. Shih, *J. Am. Chem. Soc.* **1981**, *103*, 7367-7368.

[22] D. Tuncel, M. Katterle, *Chem. Eur. J.* **2008**, *14*, 4110-4116; D. Sobransingh, A. E. Kaifer, *Org. Lett.* **2006**, *8*, 3247-3250.

[23] P. Montes-Navajas, M. Gonzalez-Bejar, J. C. Scaiano, H. Garcia, *Photochem. Photobiol. Sci.* **2009**, *8*, 1743-1747; Y. Zhao, D. P. Buck, D. L. Morris, M. H. Pourgholami, A. I. Day, J. G. Collins, *Org. Biomol. Chem.* **2008**, *6*, 4509-4515; C. Klöck, R. N. Dsouza, W. M. Nau, *Org. Lett.* **2009**, *11*, 2595-2598; J. W. Lee, S. Samal, N. Selvapalam, H.-J. Kim, K. Kim, *Acc. Chem. Res.* **2003**, *36*, 621-630; J. Lagona, P. Mukhopadhyay, S. Chakrabarti, L. Isaacs, *Angew. Chem. Int. Ed.* **2005**, *44*, 4844-4870.

[24] H. L. Anderson, J. K. M. Sanders, *J. Chem. Soc., Chem. Commun.* **1989**, 1714-1715.

[25] C. J. Walter, H. L. Anderson, J. K. M. Sanders, *J. Chem. Soc., Chem. Commun.* **1993**, 458-460.

[26] L. G. Mackay, R. S. Wylie, J. K. M. Sanders, *J. Am. Chem. Soc.* **1994**, *116*, 3141-3142.

[27] R. S. Meissner, J. Rebek, J. d. Mendoza, *Science* **1995**, *270*, 1485-1488.

[28] J. Kang, J. Rebek, *Nature* **1996**, *382*, 239-241.

[29] J. D. Dunitz, *Chem. Biol.* **1995**, *2*, 709-712; B. R. Peterson, P. Wallimann, D. R. Carcanague, F. Diederich, *Tetrahedron* **1995**, *51*, 401-421.

[30] J. Kang, J. Rebek, *Nature* **1997**, *385*, 50-52.

[31] J. Kang, J. Santamaría, G. Hilmersson, J. Rebek, *J. Am. Chem. Soc.* **1998**, *120*, 7389-7390.

[32] M. Fujita, D. Oguro, M. Miyazawa, H. Oka, K. Yamaguchi, K. Ogura, *Nature* **1995**, *378*, 469 - 471.

[33] T. Kusukawa, M. Fujita, *Angew. Chem. Int. Ed.* **1998**, *37*, 3142-3144.

[34] H. Ito, T. Kusukawa, M. Fujita, *Chem. Lett.* **2000**, *29*, 598-599.

[35] J. Smidt, W. Hafner, R. Jira, R. Sieber, J. Sedlmeier, A. Sabel, *Angew. Chem. Int. Ed.* **1962**, *1*, 80-88.

[36] N. P. E. Barry, O. Zava, P. J. Dyson, B. Therrien, *J. Organomet. Chem.* **2012**, *705*, 1-6; N. P. E. Barry, O. Zava, W. Wu, J. Zhao, B. Therrien, *Inorg. Chem. Commun.* **2012**, *18*, 25-28.

[37] M. D. Pluth, R. G. Bergman, K. N. Raymond, *J. Org. Chem.* **2008**, *74*, 58-63; P. Mal, B. Breiner, K. Rissanen, J. R. Nitschke, *Science* **2009**, *324*, 1697-1699.

[38] V. F. Slagt, J. N. H. Reek, P. C. J. Kamer, P. W. N. M. van Leeuwen, *Angew. Chem. Int. Ed.* **2001**, *40*, 4271-4274.

[39] T. Gadzikwa, R. Bellini, H. L. Dekker, J. N. H. Reek, *J. Am. Chem. Soc.* **2012**, *134*, 2860-2863; R. Bellini, S. H. Chikkali, G. Berthon-Gelloz, J. N. H. Reek, *Angew. Chem. Int. Ed.* **2011**, *50*, 7342-7345; V. F. Slagt, P. W. N. M. van Leeuwen, J. N. H. Reek, *Angew. Chem. Int. Ed.* **2003**, *42*, 5619-5623.

[40] J. PrakashaReddy, V. R. Pedireddi, *Eur. J. Inorg. Chem.* **2007**, *2007*, 1150-1158.

[41] D. J. Bray, L.-L. Liao, B. Antonioli, K. Gloe, L. F. Lindoy, J. C. McMurtrie, G. Wei, X.-Y. Zhang, *Dalton Trans.* **2005**, 2082-2083.

[42]   V. McKee, J. Nelson, D. J. Speed, R. M. Town, *J. Chem. Soc., Dalton Trans.* **2001**, 3641-3646; bR.-F. Song, Y.-B. Xie, J.-R. Li, X.-H. Bu, *Dalton Trans.* **2003**, 4742-4748.

[43]   L. Pan, E. B. Woodlock, X. Wang, K.-C. Lam, A. L. Rheingold, *Chem. Commun.* **2001**, 1762-1763; A. N. Khlobystov, A. J. Blake, N. R. Champness, D. A. Lemenovskii, A. G. Majouga, N. V. Zyk, M. Schröder, *Coord. Chem. Rev.* **2001**, *222*, 155-192.

[44]   S. S. Lee, I. Yoon, K.-M. Park, J. H. Jung, L. F. Lindoy, A. Nezhadali, G. Rounaghi, *J. Chem. Soc., Dalton Trans.* **2002**, 2180-2184.

[45]   D. J. Bray, B. Antonioli, J. K. Clegg, K. Gloe, K. Gloe, K. A. Jolliffe, L. F. Lindoy, G. Wei, M. Wenzel, *Dalton Trans.* **2008**, 1683-1685.

[46]   G. E. Alliger, P. Müller, C. C. Cummins, D. G. Nocera, *Inorg. Chem.* **2010**, *49*, 3697-3699.

[47]   G. E. Alliger, P. Müller, L. H. Do, C. C. Cummins, D. G. Nocera, *Inorg. Chem.* **2011**, *50*, 4107-4115.

[48]   N. Lopez, D. J. Graham, R. McGuire, G. E. Alliger, Y. Shao-Horn, C. C. Cummins, D. G. Nocera, *Science* **2012**, *335*, 450-453.

[49]   T. Kato, T. Fujimoto, A. Tsutsui, M. Tashiro, Y. Mitsutsuka, T. Machinami, *Chem. Lett.* **2010**, *39*, 136-137; T. Fujimoto, T. Kato, Y. Usui, O. Kamo, K. Furihata, K. Tsubono, T. Kato, T. Machinami, M. Tashiro, *Carbohydr. Res.* **2011**, *346*, 1991-1996.

[50]   W. H. Harman, C. J. Chang, *J. Am. Chem. Soc.* **2007**, *129*, 15128-15129.

[51]   T. A. Betley, Q. Wu, T. Van Voorhis, D. G. Nocera, *Inorg. Chem.* **2008**, *47*, 1849-1861; T. A. Betley, Y. Surendranath, M. V. Childress, G. E. Alliger, R. Fu, C. C. Cummins, D. G. Nocera, *Philos. Trans. R. Soc. Ser. B* **2008**, *363*, 1293-1303.

[52]   G. T. Sazama, T. A. Betley, *Inorg. Chem.* **2010**, *49*, 2512-2524.

[53]   G. T. Sazama, T. A. Betley, *Organometallics* **2011**, *30*, 4315-4319.

Chapter 2: Tripodal ligand and unexpected multimetallic complexes.

2.1 Introduction

Numerous tripodal pyrollyl host molecules have been designed by Beer and co-workers including the pyrrole dithiocarbamate cryptands which have been investigated for their anion binding properties.[1] Developed through the reaction of a pyrrolyl-amine tripod, carbon disulphide and a metal precursor under high dilution condition the metallo-cryptand, shown in Figure 1, is able to co-ordinate to metals favouring either a tetrahedral or a square planar geometry.

if R = benzyl: M = Ni, Cu, Zn-pyr
if R = cyclohexil: M = Ni
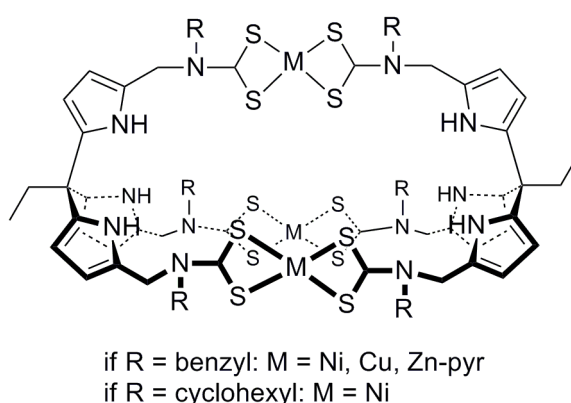
Figure 1: Metallo-cryptand developed by Beer and co-workers.

Although the anion binding studies of the tri-nickel complexes is not reported as they were deemed unsuitable due to the broadness of their ^{1}H NMR spectrum resonances, the copper metallo-cryptand properties were studied and showed the formation of a 1:1 host/guest complex with chloride, benzoate and dihydrogen anions. Only the cryptand benzoate binding constant could be calculated ($\log_{10}K$ = 5.73 (0.18) as it was the only one producing a significant shift in the UV-Vis absorption spectrum suggesting that the host preferentially binds benzoate anions.

The cyclohexane functionalised tris(pyrrolyl)ethane, shown in Figure 2 and precursor to the aforementioned metallo-cryptand, is potentially better suited for guest encapsulation than the pro-ligand developed by Betley and co-workers described in Chapter 1. Indeed the rotation of one arm away from the metal centre upon binding as well as the size and the angle of the mesityl cavity in the latter does not allow for the formation of a fully encapsulated space in which a small molecule could be activated.
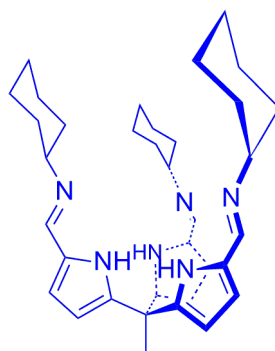
Figure 2: Tris(pyrrolyl)ethane functionalised with cyclohexyl imine.

Hydrogen bonding interactions between the guest and the three imine nitrogens promotes a *trans*-configuration, forcing the arms of the ligand to remain proximate to the cavity. Furthermore, the imine nitrogen can engage in secondary interactions with metal ions or small molecules. Last but not least, the size of the cyclohexyl substituents and their spatial flexibility could provide a fully isolated, hydrophobic cavity. While the anion binding properties and some cryptand derivatives of this tripyrrole imine have been studied, its metal binding potential has been overlooked.

2.2 Synthesis of H$_3$L

The tripodal pyrrole H$_3$L is straightforwardly prepared by reacting an excess of pyrrole with triethyl orthoacetate under acidic conditions following a preparation developed by Lindsey and co-workers and modified by Wang and Bruce.[2] The identity of the resulting tripod (H$_3$L^a) was confirmed by its

^{1}H NMR spectrum which showed a distinctive desymmetrisation of the pyrrolic resonances (6.06, 6.19 and 6.65 ppm). H_3L^a was then formylated under Vilsmeier-Haack conditions affording the triformylpyrrole (H_3L^{co}) in good yield. The presence of a singlet at 9.43 ppm in the ^{1}H NMR spectrum was indicative of successful formylation. Further functionalisation was achieved by the addition of a primary amine to the trialdehyde affording the imine derivative H_3L as delineated in Scheme 1.

3a R = [t]Bu
3b R = cyclohexane
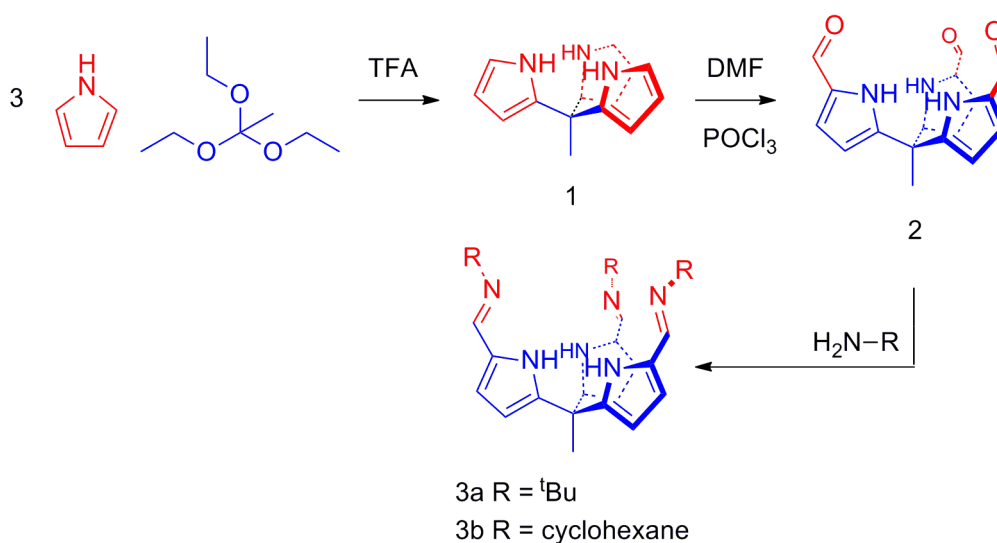
Scheme 1: Synthesis of H_3L.

The absence of aldehyde resonance at 9.43 ppm and the presence of a single imine resonance at 7.62 ppm in the ^{1}H NMR spectrum of H_3L displayed in Figure 3 clearly show the absence of any starting material. This is supported by the presence of a single set of two pyrrole doublets at 6.26 and 6.02 ppm as well as the presence of a lone cyclohexyl CH multiplet at 2.84 ppm.
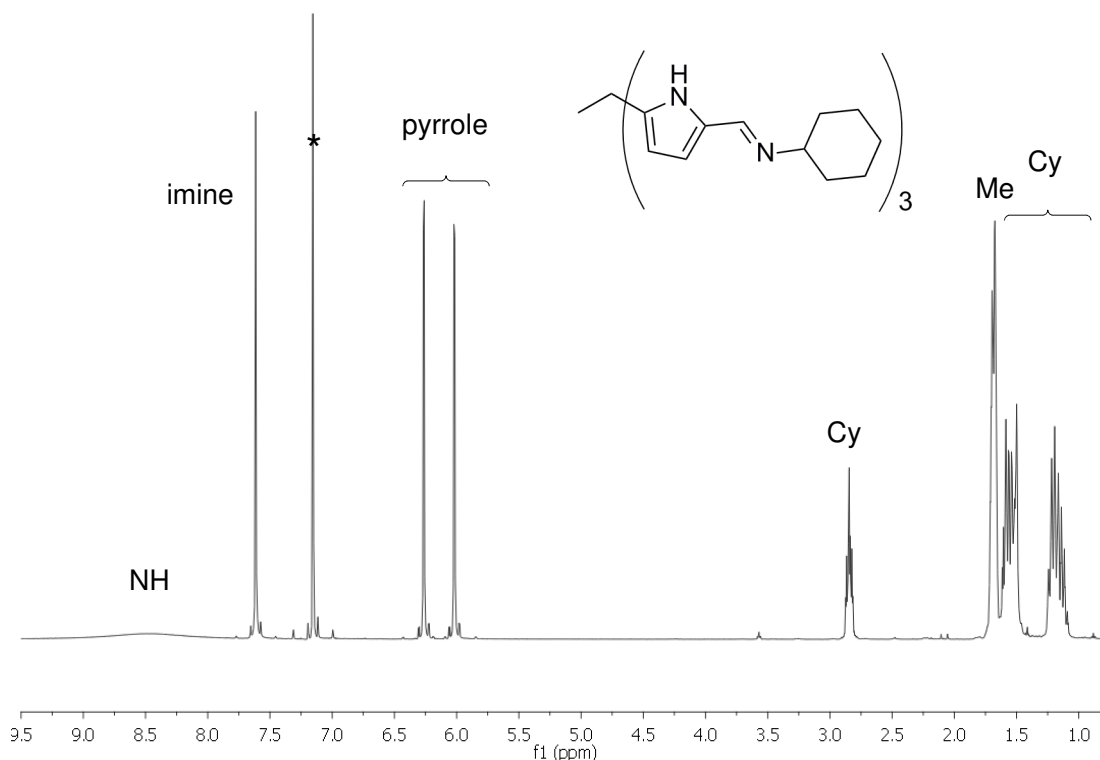
Figure 3: NMR of H_3L in $CDCl_3$, '*' denotes residual protio solvent.

Re-crystallisation of H_3L from a hot saturated solution of MeCN afforded crystals of the monohydrate $H_3L.H_2O$ suitable for X-ray crystallography. The solid state structure was determined and is shown in Figure 4, with selected bond lengths and angles detailed in Table 1 and crystal data in Table Ch1 Tab1. In the solid state structure of $H_3L.H_2O$ a single water molecule is found to be encapsulated by the tripodal ligand, with the oxygen atom O1 situated in the plane P_1 of the imine nitrogens N2, N4 and N6. This feature demonstrates the propensity of the pyrrole and imine groups to act as hydrogen bond donors (N1⋯O1: 3.12(2) Å) and acceptors (N2⋯O2: 2.87(2) Å), respectively. With an imine bond length indicative of double bonding (N2-C7: 1.24(2) Å) not to mention the pyrrole bond lengths and angles common to those observed in the literature,[3] it is reasonable to assume that the imine-pyrrole tautomer is retained upon water

binding. The structure holds a crystallographically-enforced C_{3v} symmetry. The interplanar distance between the planes P_1 and P_2 (the latter defined by the pyrrolo nitrogens N1, N3 and N5) of 2.60 Å supports the idea that the cavity could fit most transition metals and still have space to accommodate other guest molecules. This cavity could potentially be used to encapsulate a small molecule stabilised by interactions with the imine nitrogens.
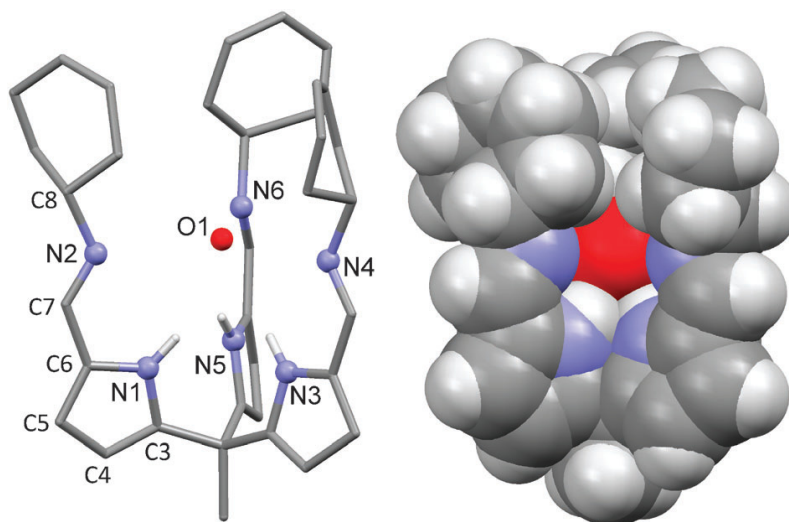
Figure 4: Ball and stick (left) and space-filled representations (right) of the solid state crystal structure of $H_3L \cdot H_2O$. For clarity, disorder components and all hydrogen atoms except on N1, N3, and N5 are omitted.

N1-C3	1.35(2)	N1⋯O1	3.12(2)
C3-C4	1.31(3)	N2⋯O1	2.87(8)
C4-C5	1.41(3)	N1⋯N3	2.84(4)
C5-C6	1.34(3)	N2⋯N4	5.01(2)
C6-N1	1.33(3)	P_1⋯O1	0.064
C6-C7	1.48(3)	P_1⋯P_2	2.60
C7-N2	1.24(2)	P_2⋯O1	2.67
C8-N2	1.51(2)	$P_{N1O1N2}{>}P_{N3O1N4}$	120

Table 1: Selected bond lengths (Å) and angles (°) of $H_3L \cdot H_2O$.

The directionality of hydrogen bonding has resulted in the three arms of the proligand H_3L to be oriented around the water molecule thus forming a sterically-protected hydrophilic pocket. This characteristic of hydrogen bonding has allowed for the use of water as a design element in molecular engineering.[4] Water has been found to act as a host that can encapsulate guest molecules such as fullerene through hydrogen bonding between the water molecules and the π system of the fullerene as well as hydrogen bonding between water molecules.[5] It has been observed as an integral part of the structure by Atwood and co-workers in a chiral molecular assembly where six calix[4]resorcinarenes and eight water molecules self assemble into a sphere held through sixty hydrogen bonds.[6] As observed with $H_3L.H_2O$, it can also act as a guest molecule.

A large proportion of capsules, calixarenes and cucurbiturils for example, are achiral and offer hydrophobic cavities to their guests, limiting their selectivity and activity. Host molecules incorporating internal polar or hydrogen bonding sites are much less common owing to difficulties encountered in their construction. However, recently, Szumna and co-workers have developed a non-covalent inverted capsule, shown in Figure 5, comprising numerous polar and non-polar functionalities shielded from the environment by hydrophobic phenylalanine chains.[7] The internal walls of the capsule $(L-1)_2$ are made of hydrogen bond donors as well as hydrogen bond acceptors, amino and carboxyl groups respectively, which in this case encapsulate two nitromethane molecules in addition to four water molecules as described in Figure 6.
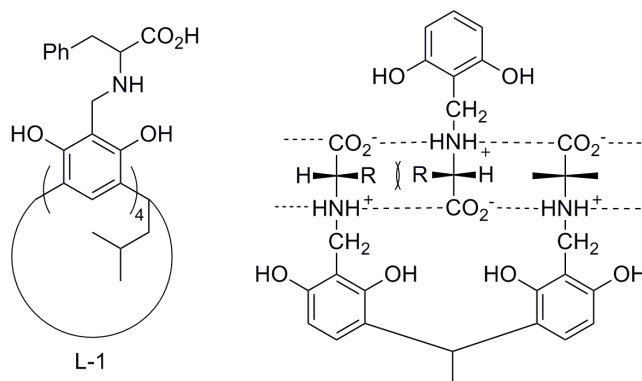
Figure 5: (a) molecular structure of the ligand reported by Szumna and co-workers; (b) binding motif with marked possible steric repulsions for the self-assembled capsule.[7]
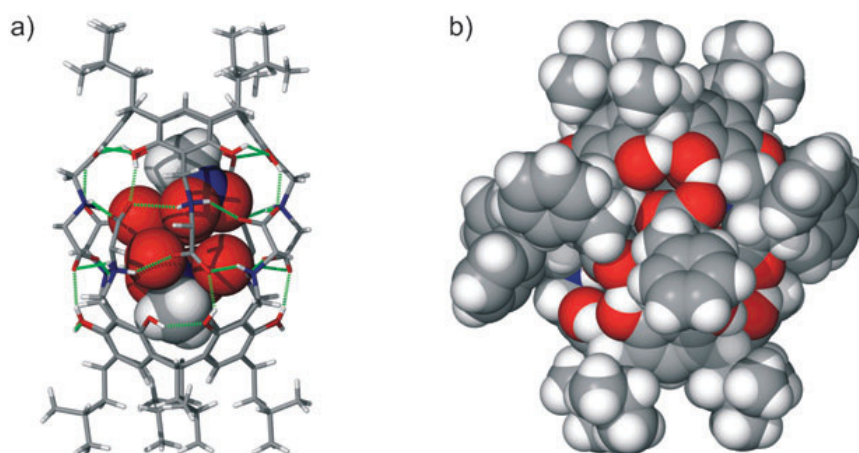
Figure 6: X-ray structure of (L-1)$_2$: (a) capsule with encapsulated (MeNO$_2$)$_2$(H$_2$O)$_4$; (b) space fill representation.[7]

2.3 Group 1 complexes of H$_3$L

Group 1 dipyrromethane complexes have been previously reported by the Love group.[8] Although potassium complexes are observed as polymeric chains of alternating ligand and metal cations, the lithium deprotonation of the ligand on the pyrrole and imines nitrogens leads to the formation of {LiN}$_3$ chains which interlock to form a twelve-rung lithium amide circular ladder (Figure 7 left). This core, represented in Figure 7 right, is surrounded by a helical arrangement of the three ligand anions.
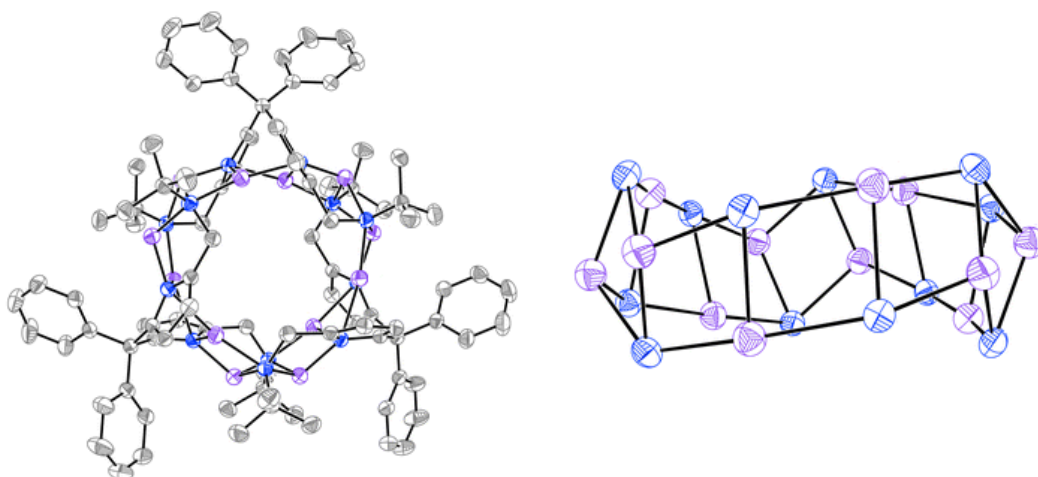
Figure 7: ORTEP representation of the solid state structure of $[Li_4(L)]_4$ (left) and its $\{LiN\}_{12}$ core with carbon, nitrogen and lithium atoms represented in grey, blue and purple respectively. For clarity, all hydrogen atoms are omitted.

Although lithium amide circular ladders derived from singly deprotonated amines are the result of edge to edge LiN ring combination, the nature of the ligand precludes the formation of this repeating unit. Instead, the formation mechanism for the structure previously displayed, consist of the association of three laterally-shifted chains coordinated with the cyclisation of the motif, as described in Figure 8.
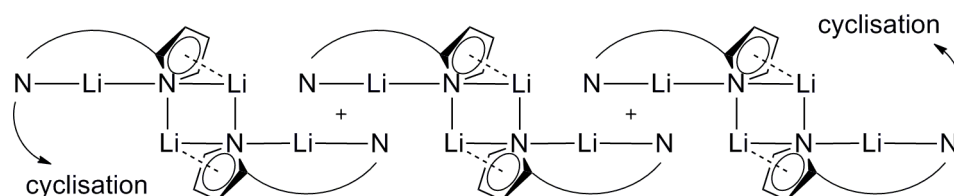
Figure 8: Possible mechanism for the formation of the dipyrromethane LiN ladder.

Deprotonation of H_3L with strong bases was attempted with a view to prepare the Group 1 metal salts required for the formation of transition metal complexes through salt elimination reactions as displayed in Scheme 2.
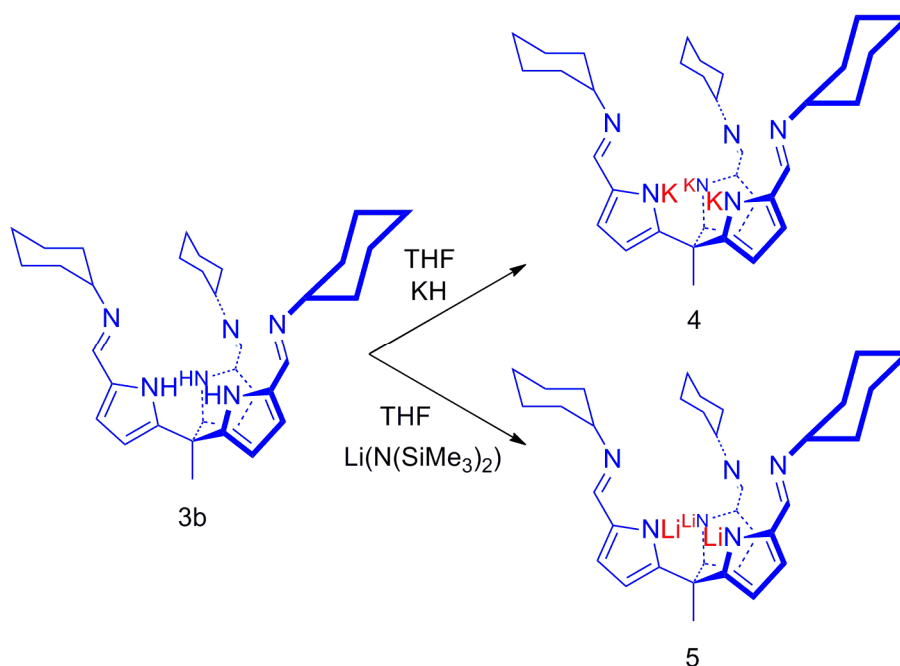
Scheme 2: Synthesis of K_3L and Li_3L.

The reaction between H_3L and a large excess of KH under anaerobic conditions resulted in the deprotonation of the ligand and the formation of the potassium salt K_3L in quantitative yields. Full deprotonation of H_3L was supported by the absence of the NH resonance in the ^1H NMR spectrum (a broad singlet at 8.47 ppm for the proligand spectrum) as well as the lack of NH stretch in the IR spectrum (υ 3288 cm^{-1} for the proligand). Attempts to crystallise K_3L were unsuccessful.

The reaction between H_3L and three equivalents of $LiN(SiMe_3)_2$ under anaerobic conditions resulted in the formation of the lithium salt Li_3L in good yield. As for K_3L, full deprotonation was supported by the lack of NH resonance in the ^1H NMR spectrum and the absence of NH stretch in the IR spectrum.

Crystallisation of a sample of [Li_3L] by the diffusion of hexane into a saturated solution of THF afforded crystals of the new lithium hydroxide cluster, [$Li_3(THF)_3(LiOH)_3(L)$]$_2$ suitable for X-ray crystallography. The

formation of this hydroxide cluster is likely the result of either an adventitious amount of water inside the N_2 atmosphere of the glovebox or a result of the strong coordination of the water molecule inside the pyrrole-imine cavity, with the ligand remaining hydrated even after drying under high vacuum. The solid state structure was determined and is shown in Figure 9, with selected bond lengths and angles detailed in Table 2 and crystal data in Table Ch1 Tab1. In the structure of $[Li_3(THF)_3(LiOH)_3(L)]_2$ two ligands are found in a staggered conformation linked by six {Li-O-Li} bridges. The six cyclohexyl substituents adopt chair-conformations and fully encapsulate a Li-OH core. This core is best described as two superimposed Li_3O_3 six-membered rings that adopt chair conformations, as shown in Figure 10. Two lithium environments are observed in the structure, designated as edge (Li1, Li2 and Li3) and core (Li4, Li5 and Li6) lithium atoms. The edge lithium atoms are bound in a tetrahedral geometry by the nitrogen atoms of two pyrrolides (Li1-N1: 2.069(6) Å and Li1-N3: 2.076(6) Å), to a hydroxide group (Li1-O6: 1.920(5) Å) and the oxygen atom of a THF adduct molecule (Li1-O1: 2.058(6) Å). The core lithium atoms are bound in a tetrahedral geometry by two intra (Li4-O5 and Li4-O6, 1.928(6) and 1.915(6) Å respectively) and one inter-ring (Li4-O4': 2.063(5) Å) hydroxide groups as well as the nitrogen atom (Li4-N4: 2.078(6) Å) of an imine group.
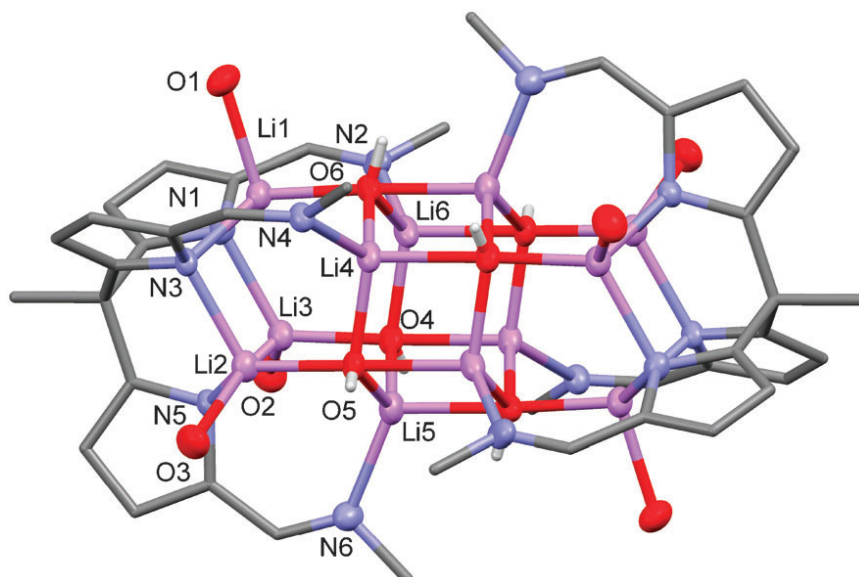
Figure 9: X-ray crystal structure of [Li$_3$(THF)$_3$(LiOH)$_3$(L)]$_2$. For clarity, cyclohexyl carbon atoms, disorder components, and all hydrogen atoms except those on O4, O5, and O6 are omitted (50% probability displacement ellipsoids where drawn).

Li1-N1	2.069(6)	N2⋯N4	6.535
Li1-N4	2.072(6)	N1-Li1-N3	100.9(2)
Li1-O1	2.058(6)	Li4-O6-Li6	117.9(3)
Li1-O6	1.920(5)	Li4-O6-Li2′	80.9(2)
Li4-N4	2.078(6)	Li1-N1-Li3	99.0(2)
Li4-O4′	2.063(5)	O5-Li4-O6	116.7(3)
Li4-O5	1.928(6)	O1-Li1-O6	102.4(2)
Li4-O6	1.915(6)	P$_1$⋯P$_2$	8.143

Table 2: Selected bond lengths (Å) and angles (°) of [Li$_3$(THF)$_3$(LiOH)$_3$(L)]$_2$
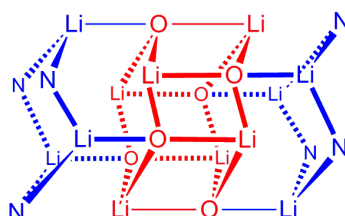
Figure 10: Representation of the Li hydroxide core from the structure of [Li$_3$(THF)$_3$(LiOH)$_3$(L)]$_2$

With a C_3 axis of rotation, three vertical planes, and six C_2 axes perpendicular to the main axis of rotation, the structure possesses a D_{3d} point group with the inversion centre located at the centre of the $\{Li_6O_6\}$ core in the solid state. The two pyrrolide nitrogen planes, P_1 and P_2, are separated by 8.143 Å. Although the arms of the tripod are long enough to encapsulate the core of $[Li_3(THF)_3(LiOH)_3(L)]_2$, they do not protect the capping lithiums atoms; coordination sphere of which is therefore completed by the binding of THF solvent molecules. The area between the imine nitrogens (N2, N4 and N6) of 21.35 Å^2, extrapolated from the distance separating N2 and N4 (6.535 Å) compared to that of H_3L (12.6 Å^2 extrapolated from N2···N4 = 5.01 Å) shows that the ligand is highly flexible. Added to the possibility that multiple ligands can come together to interact with a single larger molecular entity shows that the ligand can encapsulate molecules of varying sizes, 19.93 Å^3 in this case (extrapolated from the hexagonal prism defined by $\{LiOH\}_6$). Comparatively, the softball developed by the Rebek group can encapsulate guest of size ranging from 145 to 226 Å^3, a selection of which is displayed in Figure 11.[9]

| 145 Å^3 | 164 Å^3 | 205 Å^3 | 226 Å^3 |
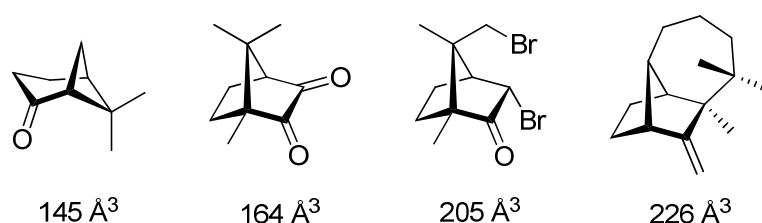
Figure 11: Sample of the guests and their corresponding volume encapsulated by the softball developed by Rebek and co-workers. Molecular modelling of assemblies and guest was carried out using MacroModel 6.5

Li(OR) compounds assemble into a variety of motifs, the most common being ladders and $Li_3(OR)_3$ rings. More unusual structures include distorted prisms and step-form structures.[10] Increasing the number of Li(OR) units can lead to more complex architectures such as octameric structures and octahedral cages ($Li_{12}O_{12}$) which can be regarded as two

parallel $Li_3(OR)_3$ single rings linked by six Li(OR) units.[11] {LiOH}$_6$ structural motifs have been observed in various forms, with examples including octahedrons as observed by Shilov and co-workers as well as the "S" shaped twelve-membered rings described by Scott and Dinger and displayed in Figure 11.[12] Possible intermediate structures between these include $Li_3(OR)_3$ single rings that stacked on top of one another of which the {LiOH}$_6$ structure described above is an example.[13]
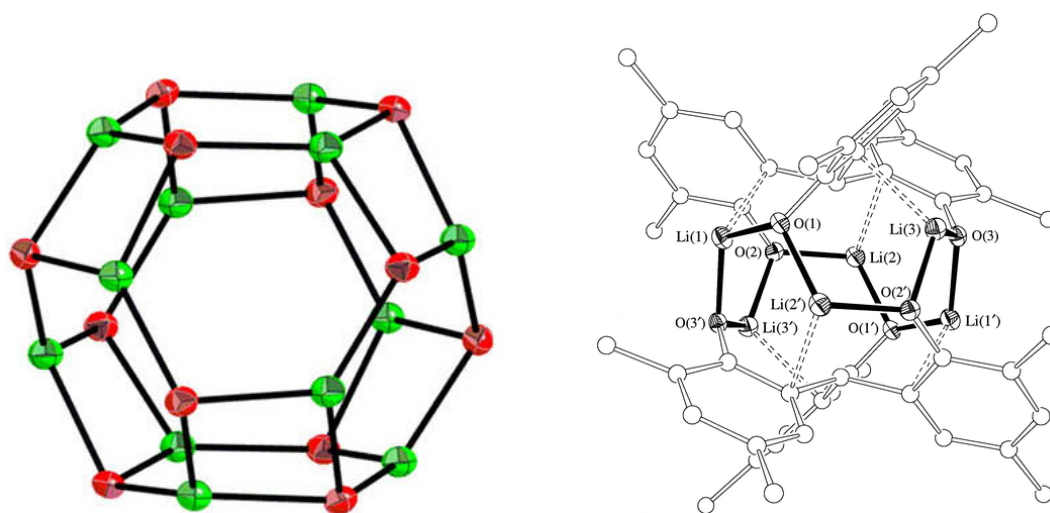
Figure 11: {LiOR}$_{12}$ octahedron observed by Shilov and co-workers with oxygen atoms in red and lithium atoms in green (left); {Li(OR)}$_6$ 12 membered ring described by Scott and Dinger.[12]

Examples of the {LiOH}$_6$ motif are displayed in Figure 12. It has been observed monocapped on a single side (left) of the hexagonal faces as part of an aggregate formed by 1-methyl-(*S*)-2-(hydroxymethyl)pyrrolidines by the Strohmann group a or capped on both sides (centre) and acting as a countercation to a tetra-tellurium complex formed by the Davies group.[14] In these structures, the capping lithium atom is bound to all three hydroxo groups from the closest ring. On the other hand, the bi-capped {LiOH}$_6$ motif observed by Girolami and co-workers displayed in Figure 12 (right), shows that the core is capped on both sides by a lithium cation bound to a single hydroxyl oxygen and a second lithium cation bound to the two remaining

hydroxo groups of the $Li_3(OR)_3$ hexagon.[15] It is noteworthy that this last motif possesses an inversion centre as the lithium atoms that are terminally-bound to a single hydroxyl oxygen are on opposite sides of the core. In contrast, the structure of $[Li_3(THF)_3(LiOH)_3L]_2$ represents the first $\{LiOH\}_6$ stacked rings motif that is triply-capped by lithium cations on both of its hexagonal faces. The complete encapsulation of this core by the two tripodal pyrrole imine ligands presumably stabilises this motif.
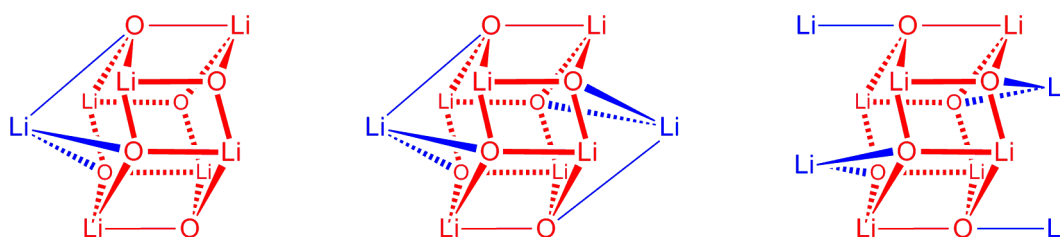
Figure 12: Representation of $\{LiOH\}_6$ mono-capped on 1 side (left), mono-capped on both sides (centre), bi-capped on both sides (right).

Synthetic pathways have been formulated to synthesise some of these aggregates.[16] It is thought that the choice of solvent influence the type of structure observed. Only species containing dimeric Li(OR) units are produced when using pyridine as a solvent, whereas the use of tetrahydrofuran leads to the formation of four or six membered rings of Li-O atoms of various shape and size including square, cube, hexagon and hexagonal prisms. The formation of $[Li_3(THF)_3(LiOH)_3(L)]_2$ in which one $\{LiOH\}_6$ ring has formed within each ligand as a THF adduct supports these conclusions.

2.4 Synthesis of the cobalt complex $[Co(H_3L)_2][Cl]_3$

With an aim to form a cobalt complex with a ligand to metal ratio of 1:1, H_3L was reacted with $CoCl_2$ under aerobic conditions. The intended result was the promotion of the tautomerisation of the pyrrole-imine ligand

into its azafulvene-amine form by complexation of the metal centre to the pyrrole-nitrogens. This was expected to result in the formation of a hydrogen-bonding pocket able to partake in anion binding. Instead, as described in Scheme 3, the reaction led to the formation of the new Co^{III} complex $[Co(H_3L)_2][Cl]_3$ in 88 % yield after workup as a green solid.

Cyclohexyls and
Chloride anions
omitted for clarity
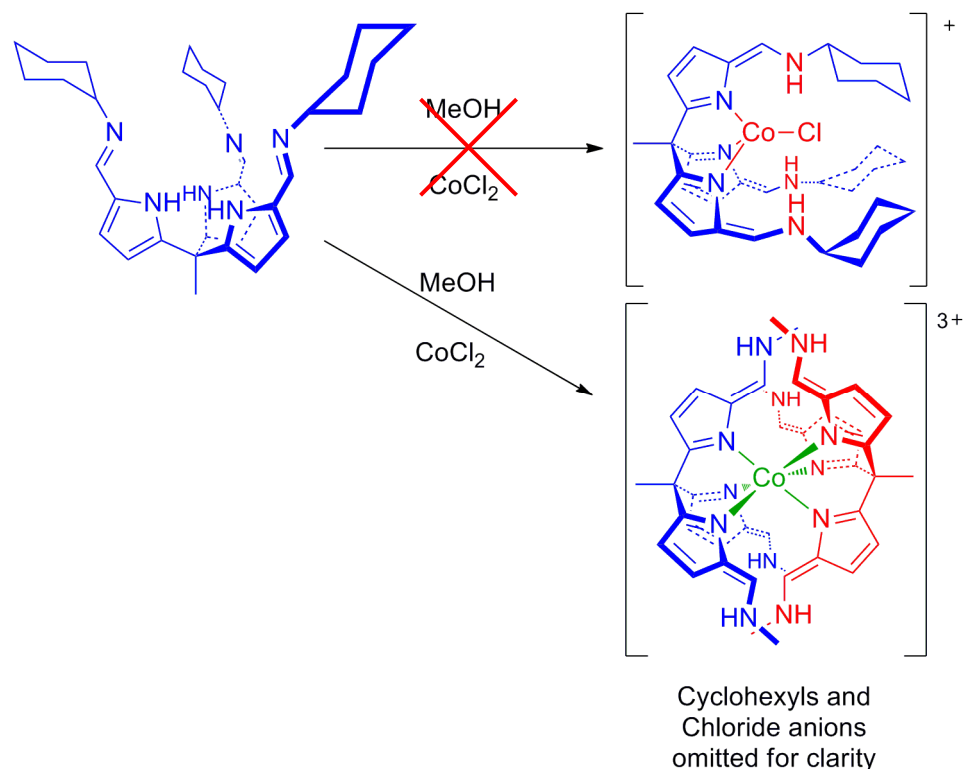
Scheme 3: Synthesis of $[Co(H_3L)_2][Cl]_3$.

The diamagnetism of the ^{1}H NMR spectrum displayed in Figure 13, is concordant with oxidation of Co^{II} to Co^{III}. Tautomerisation of the ligand from the pyrole-imine into the azafulvene upon metallation is indicated by the appearance of new doublet resonances at 7.45 and 6.89 ppm as well as the imine CH proton shifting from 8.47 to 5.60 ppm and appearing now as a doublet. This coupling pattern was confirmed by ^{1}H-^{1}H COSY experiment.
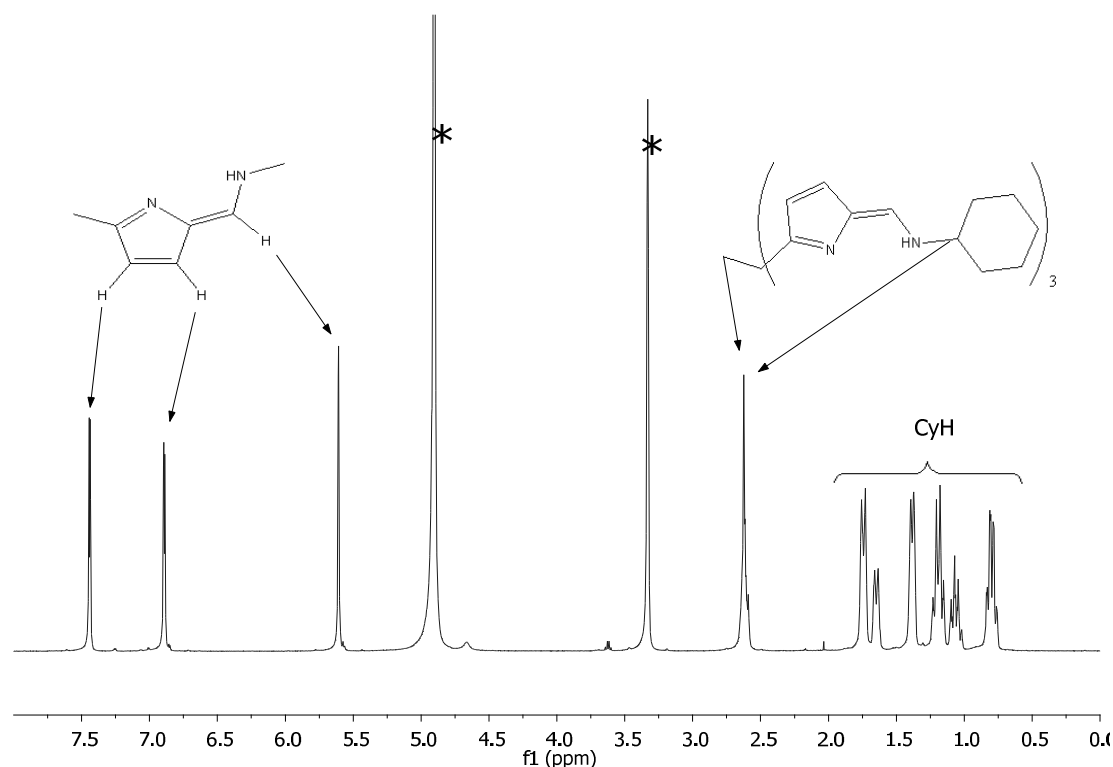
Figure 13: ^{1}H NMR spectrum of [Co(H$_3$L)$_2$][Cl]$_3$ in MeOD, '*' denotes residual protio solvent.

Crystallisation of [Co(H$_3$L)$_2$][Cl]$_3$ by the diffusion of Et$_2$O into a MeOH solution of the complex afforded crystals suitable for X-ray crystallographic studies. The solid state structure was determined and is shown in Figure 14, with selected bond lengths and angles detailed in Table 3 and crystal data in Table Ch1 Tab1. In the solid state structure of [Co(H$_3$L)$_2$][Cl]$_3$, two ligands are found to bind to the single metal cation in a manner similar to *tris*(pyrazolyl)borates, with the three pyrrole nitrogens of each ligand binding to the Co^{III} centre that adopts an octahedral geometry. A shortening of C6-C7 and C4-C5 bonds from 1.48(3) and 1.41(3) to 1.395(7) and 1.380(7) Å respectively as well as an elongation of N2-C7 and C5-C6 from 1.24(2) and 1.34(3) to 1.290(6) and 1.416(6) respectively is observed. These differences are concordant with the ^{1}H NMR spectrum in that they support the tautomerisation of the ligand into the azafulvene. The imine bonds are

clearly shown in an E conformation, pointing outwards with hydrogen bonding interactions observed between the azafulvene NH and the surrounding chloride anions (N2···Cl2, 3.167(6) Å).
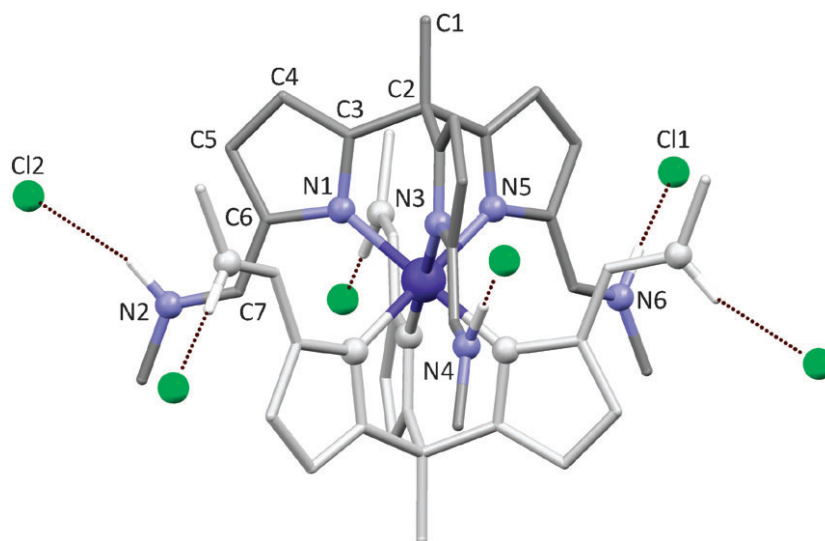
Figure 14: Ball and stick representation of the X-ray crystal structure of $[Co(H_3L)_2][Cl]_3$. For clarity, all hydrogen atoms, cyclohexyl carbons and disorder components are omitted.

The structure has a D_{3d} point group in its solid state. Due to the small splitting of the alkene CH in the ^{1}H NMR spectrum, it is unclear whether this is retained in solution. As in the X-ray structure of H₃L, each vertical plane cuts the other two at an angle of 120°, bisecting the metal centre which is also the structure's inversion centre. The interplanar distance between the pyrrolide planes of each ligand P_1 and P_2 is 2.325 Å with the cobalt metal centre equidistant to the two planes (1.162 Å). Each chloride anion is hydrogen bonded to imine nitrogens of two different complexes, forming an extended supramolecular network.

Co1-N1	1.953(3)	C6-C7	1.395(7)
Co1-N3	1.956(3)	C7-N2	1.290(6)
Co1-N5	1.945(3)	N2⋯Cl2	3.167(6)
N1-C3	1.344(5)	N4⋯Cl2	3.149(5)
C3-C4	1.380(6)	N6⋯Cl1	3.167(6)
C4-C5	1.380(7)	N1-Co1-N3	88.44(14)
C5-C6	1.416(6)	P_1⋯P_2	2.325
C6-N1	1.405(6)	P_1⋯Co1	1.162

Table 3: Selected bond lengths (Å) and angles (°) of $[Co(H_3L)_2][Cl]_3$.

It was hoped that H_3L would bind to the metal centre in a fashion not dissimilar to that observed in tris(pyrazolyl)borate complexes. A particular example of this was reported by Wolowiec and co-workers and displayed in Figure 15 left,[17] in which a single tris(pyrazolyl)borate ligand binds to the metal centre through the equivalent of the pyrrole nitrogens of H_3L in a trigonal pyramidal geometry. The coordination sphere of the cobalt is then completed by a thiocyanate anion and a THF molecule resulting in a distorted trigonal bipyramidal geometry. It is important to note in this case that when only two arms of the tripodal ligand are equivalent, and the third arm support less sterically demanding groups than the others, the THF adduct was not formed. Indeed, the ligand binds more tightly to the metal centre preventing the formation of the adduct. Another anticipated binding mode of H_3L is that shown in Figure 15 right, observed by Ward and co-workers who obtained a six coordinate cobalt metal centre bound to their hexadentate ligand hydrotris[3-(2-pyridyl)pyrazol-1-yl]borate.[18] The metal is bound to the six ligand nitrogens, three from the tris(pyrazolyl)borate part of the ligand and one from each of the pyridyl groups. Although six

coordinated metal centres favour an octahedral geometry for Ligand Field Stabilisation Energy (LFSE) and steric reasons,[19] the rigidity of the ligand's arms enforces a rare trigonal prismatic geometry onto the Co[II] cation.[20] The two ligands:one metal motif observed in $[Co(H_3L)_2][Cl]_3$ is well known and complexes in which two ligands bind to an octahedral metal centre in a staggered arrangement have been observed by Trofimenko and Reglinski.[21]
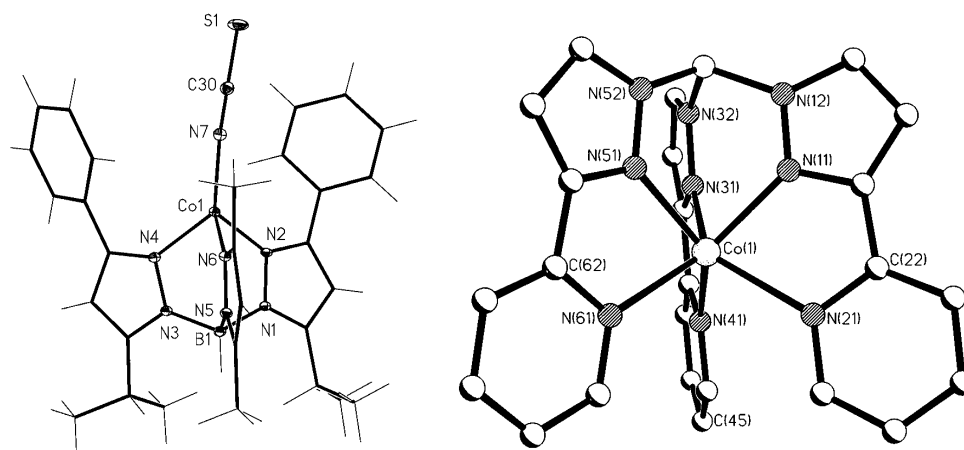
Figure 15: Wolowiec's *tris*(pyrazolyl)borate binding to the metal centre *via* three nitrogen atoms (left); Ward's octahedral cobalt complex (right).

The tautomerisation of pyrrole imine upon metallation has been observed previously by the Love group.[22] This is achieved by reacting imine-functionalised dipyrromethanes with metal halides as depicted in Scheme 4. Contrary to $[Co(H_3L)_2][Cl]_3$, the chloride ions are still bound to the metal centre which maintains a tetrahedral arrangement. A more stable octahedral arrangement with three ligands probably involves too many steric constraints to be feasible. The X-ray crystal structure therefore shows that only one arm of the ligand partakes in intramolecular secondary interactions between the azafulvene NH and the chloride ion. The second branch participates in intermolecular H-bonding with the chloride ions of a second molecule.
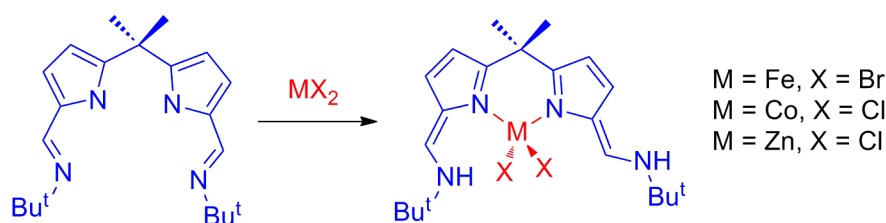
Scheme 4: Pyrrole imine tautomerisation upon metallation.[22b]

This behaviour is likely driven by a maximisation of the covalent and non-covalent number of bonds with metal cations upon metallation as observed by Sessler and co-workers with the imine-amine tautomerisation of a Schiff-base expanded prophyrin and Tasker and co-workers with the H-migration from the phenol oxygen to the amine nitrogen of a salicylaldoximine ligand.[23]

2.5 Synthesis of the zinc complex [Zn$_2$(H$_2$L)$_2$][Cl]$_2$

The use of ZnCl$_2$ was directed by the desire to enforce a tripodal geometry whilst preventing the motif previously observed in [Co(H$_3$L)$_2$][Cl]$_3$. Unfortunately, the reaction of ZnCl$_2$ with H$_3$L under neutral conditions produced multiple products that could not be isolated. However, the addition of a ZnCl$_2$ solution in EtOH to a solution of H$_3$L in EtOH under basic conditions led to the formation of the new binuclear complex, [Zn$_2$(H$_2$L)$_2$][Cl]$_2$ as a colourless solid in 26 % yield as described in Scheme 5.
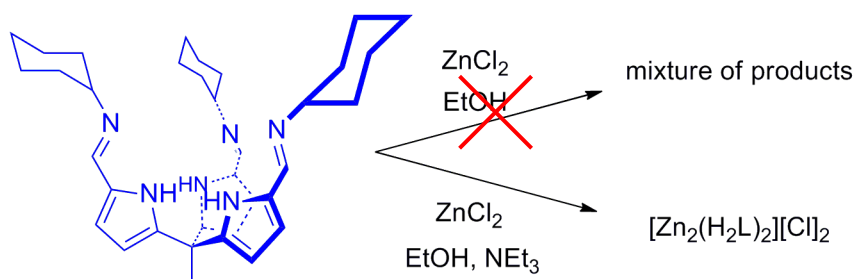
Scheme 5: Synthesis of [Zn$_2$(H$_2$L)$_2$][Cl]$_2$.

Crystallisation of [Zn$_2$(H$_2$L)$_2$][Cl]$_2$ by the diffusion of Et$_2$O in a saturated MeOH solution of the complex afforded crystals suitable for X-ray

diffraction studies. The solid state structure was determined and is shown in Figure 16, with selected bond lengths and angles detailed in Table 4 and crystal data in Table Ch1 Tab2. In the solid state structure of $[Zn_2(H_2L)_2][Cl]_2$, two tetrahedral Zn^{II} cations are found to be separated by 4.2448(8) Å, coordinated to the pyrrolide and imine nitrogens of one ligand and to two pyrrole nitrogens of the other. This is the result of one arm of each ligand being deprotonated whilst the other two are tautomerised into the azafulvene-amine. This is supported by the elongation of the imine bonds N2-C7 (1.327(6) Å) and N4-C18 (1.312(6) Å) compared to N6-C29 (1.291(6) Å) and the shortening of C6-C7 (1.395(7) Å) and C17-C18 (1.381(7) Å) compared to C28-C29 (1.424(8) Å). The proximity of the amine nitrogens and chloride anions that are present in the superstructure, with N4···Cl1 and N2···Cl1' of 3.173(4) and 3.198(5) Å respectively, suggest the presence of hydrogen–bonding interactions between the two.

The structure has a C_{2v} point group passing through an inversion centre located between the two zinc atoms. The planes P_1 defined by Zn1, N1 and N3 (double pyrrolide binding) and P_2 delineated by Zn1, N5 and N6 (imine pyrrole binding) bisect each other at right angles. The relatively small interplanar distance between P_1 and P_3, the latter defined by Zn2, N7 and N9, of 3.547 Å can be interpreted as π-π stacking between the different pyrrole and imine bonds of the two ligands. This could very well be the driving factor for the formation of this bimetallic bis(ligand) complex.
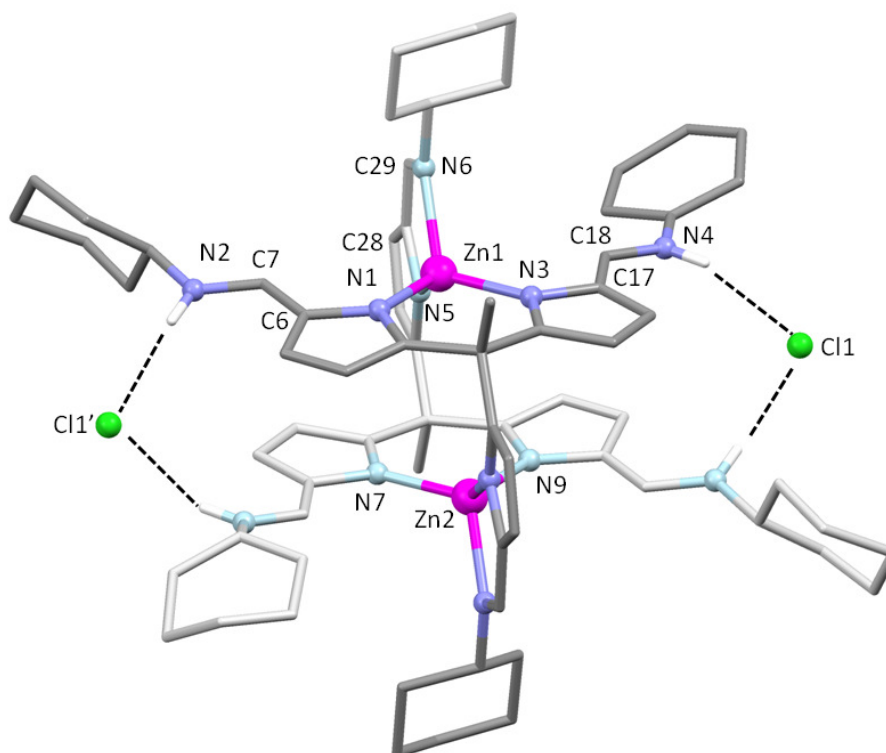
Figure 16: Ball and stick representation of the crystal structure of $[Zn_2(H_2L)_2][Cl]_2$. For clarity, disorder components and all hydrogen atoms except those on N2 and N4 are omitted.

Zn1-N1	1.977(4)	C17-C18	1.381(7)
Zn1-N3	1.963(4)	N6-C29	1.291(6)
Zn1-N5	2.006(4)	C28-C29	1.424(8)
Zn1-N6	2.063(4)	N1-Zn1-N3	96.0(2)
Zn1⋯Zn2	4.2488(8)	N1-Zn1-N5	122.5(2)
N2⋯Cl1	3.173(4)	N1-Zn1-N6	116.1(2)
N4⋯Cl1	3.198(5)	N5-Zn1-N6	83.8(2)
N2-C7	1.327(6)	$P_1 \cdots P_3$	3.547
C6-C7	1.395(7)	$P_1 P_2$	89.5
N4-C18	1.318 (6)		

Table 4: Selected bond lengths (Å) and angles (°) of $[Zn_2(H_2L)_2][Cl]_2$.

The ^{1}H NMR spectrum of [Zn$_2$(H$_2$L)$_2$][Cl]$_2$, depicted in Figure 17, shows that the solid state structure is retained in solution as two sets of resonances are observed in a 2:1 ratio. A set of pyrrole resonances is seen at 7.65 and 5.98 ppm and correlate to the alkene CH shifted to 6.50 ppm appearing as a doublet that is associated to a doublet at 10.2 ppm for the NH protons with the coupling constant $^3J_{HH}$ = 15.1 Hz. This is consistent with the tautomerisation of the pyrrole-imine into an azafulvene-amine. The size of the CH-NH coupling suggests an anti-configuration (180 °) which is in agreement with the X-ray crystal structure. The resonances of the singly-deprotonated imine-pyrrolide are all shifted downfield compared to the resonances of H$_3$L (8.10 ppm for the imine resonance and 6.80 and 6.67 ppm for the pyrrolic resonances).
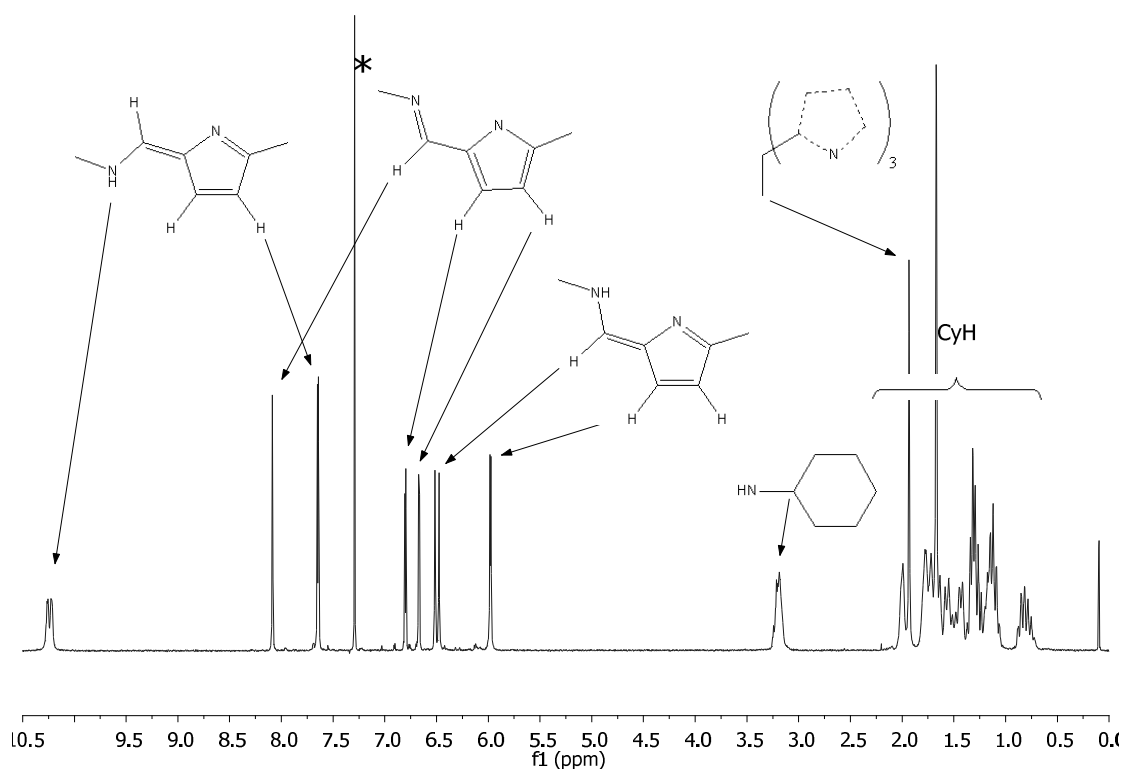
Figure 173: ^{1}H NMR spectrum of [Zn$_2$(H$_2$L)$_2$][Cl]$_2$ in CDCl$_3$, '*' denotes residual protio solvent.

Linked iminopyrroles have been reported by the Love group to form binuclear zinc complexes bridged by two ligands, the vast majority forming helical structures. The introduction of a chiral imine substituents such as (*R*)-CH(Me)^{t}Bu results in the formation of chiral mesocates instead of diastereomers of helicates, though chirality does not seem to be the main reason behind the geometry adopted by the complex.[24] Indeed, the addition of (*R*)-CH(Me)Ph leads to the formation of a racemic mixture of diasteromeric helicates. It should be noted that the chain length of the imine is not a deciding factor either as both long and short chains lead to the formation of the helical structure as shown in Scheme 6.
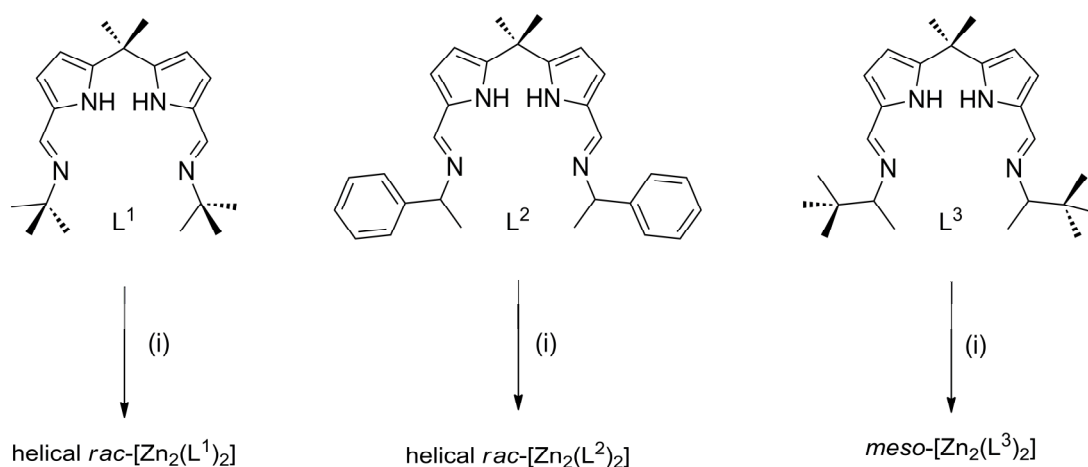
Scheme 6: Synthesis of dinuclear, double-stranded helicates and mesocates $[M_2(L_2)]$. Reagents and conditions: (i) $ZnMe_2$, toluene, Δ.

The energy difference between the two geometries was determined using molecular mechanics calculations and even though the difference in global minimum energy is marginal (<10 kcal mol^{-1}), it does correlate to the products observed. For L^1 and L^2, the helicate structure displayed in Figure 18 is of lower energy; $\Delta E = 6.51$ and 4.75 kcal mol^{-1} respectively whereas in the case of L^3, the mesocate form is favoured ($\Delta E = -1.26$ kcal mol^{-1}).
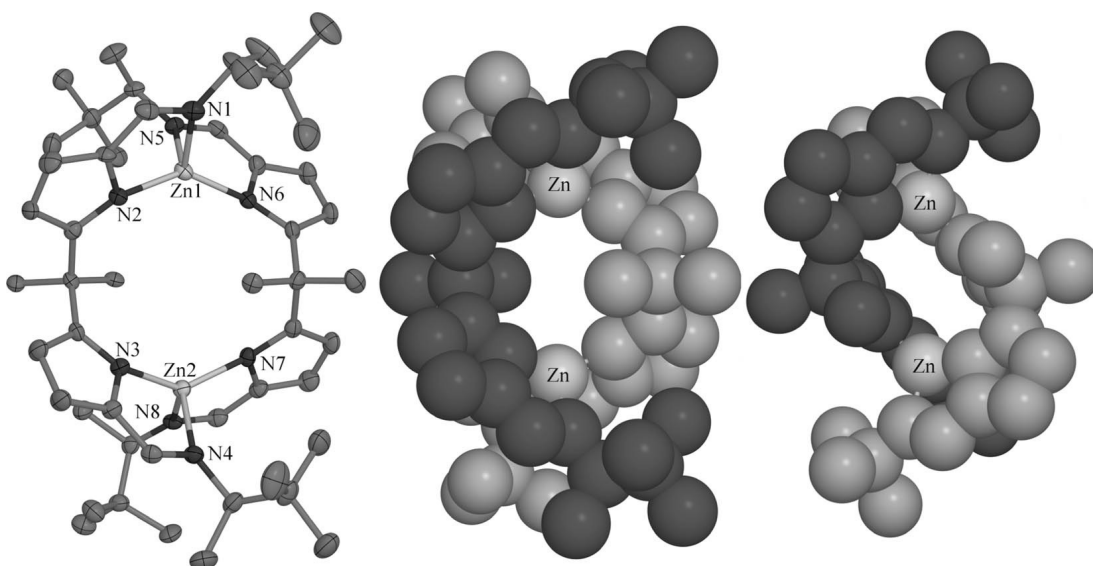
Figure 18: Solid-state structure of the mesocate $[Zn_2(L_2)]$ (left). For clarity, only one molecule per asymmetric unit is shown, all hydrogen atoms are omitted, and the thermal displacement ellipsoids are drawn at 50% probability; spaced-filled diagrams of *meso*-[Zn-$_2(L_2)$] (centre) and *rac*-[Zn$_2(L_2)$] (right) are included for comparison.

The reasons behind the formation of mesocates rather than helicates is still unclear and although this type of geometry would be difficult to observe in the case of H₃L, it shows that Zn^{II} preferentially binds to two different ligands rather than a single one in a tetrahedral geometry. The partial tautomerisation of the ligand in [Zn$_2$(H$_2$L)$_2$][Cl]$_2$ which allows the complex to partake in secondary interactions sets this complex clearly apart from its dipyrromethane predecessors.

2.6 Synthesis of cerium complex [Ce$_2$(L)$_2$THF$_2$]

f-block elements have a propensity to form complexes of high coordination number due to their large covalent radii (Ce^{III}: between 115 and 128 pm compared to Ti^{III}: 81 pm),[25] the product of the addition of Ce^{III} to the ligand was expected to result, as in Scheme 7, in the cerium bound not only to the three pyrroles nitrogen, but also to the three imine nitrogens of a single ligand. The complex observed after X-ray analysis has, however structural traits similar to that of [Zn$_2$(H$_2$L)$_2$][Cl]$_2$ in which a two ligands:two metals motif is seen.
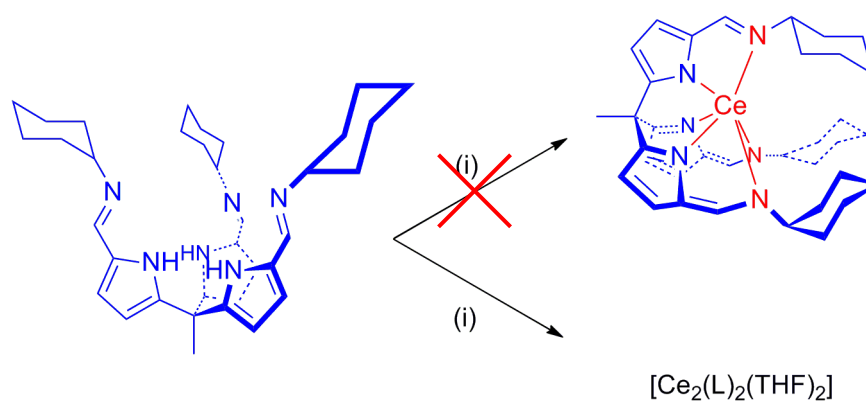
Scheme 7: Synthesis of [Ce$_2$(L)$_2$(THF)$_2$]; (i): Ce[N(SiMe$_3$)$_2$]$_3$

Crystallisation of [Ce$_2$(L)$_2$(THF)$_2$] by the diffusion of hexane into a saturated THF solution of the complex afforded crystals suitable for X-ray crystallography. The solid state structure was determined and is shown in

Figure 19, with selected bond lengths and angles detailed in Table 5 and crystal data in Table Ch1 Tab2. In the solid state structure of $[Ce_2(L)_2(THF)_2]$, two 7 coordinate Ce^{III} are held in distorted pentagonal bipyramidal geometries and are separated by 5.472(1) Å. The coordination sphere of each metal centre is made up of one pyrrolide and imine nitrogen of one ligand and two pyrrolide and imine nitrogens of the other. This is the result of the tripodal ligand being fully deprotonated. The seventh coordination site of the Ce centre is occupied by a solvent molecule (THF).

Overall the structure is similar to that of $[Zn_2(H_2L)_2][Cl]_2$ with the major difference observed in the metal to metal bond distance which has increased by 1.224 Å. The planes delineated by Ce1, N1 and N3 (P_1) and Ce2, N7 and N9 (P_2) are parallel with an interplane distance of 3.643 Å. This is only marginally longer than that observed with the zinc analogue (3.547 Å) and still in the range of π–π stacking. The last resemblance with the structure described previously is the co-planarity of the branches binding to a different cerium than the two other branches of the tripod. The interplanar angle between P_1 and the lone arm binding defined by Ce1, N5, N6 is distorted to 79.5° in this structure. One coordination site on the metal centres was disordered and was modelled as 60/40 occupancy of THF and H_2O. A second THF molecule was modelled with 40 % occupancy and was found to hydrogen-bond to the water molecule.
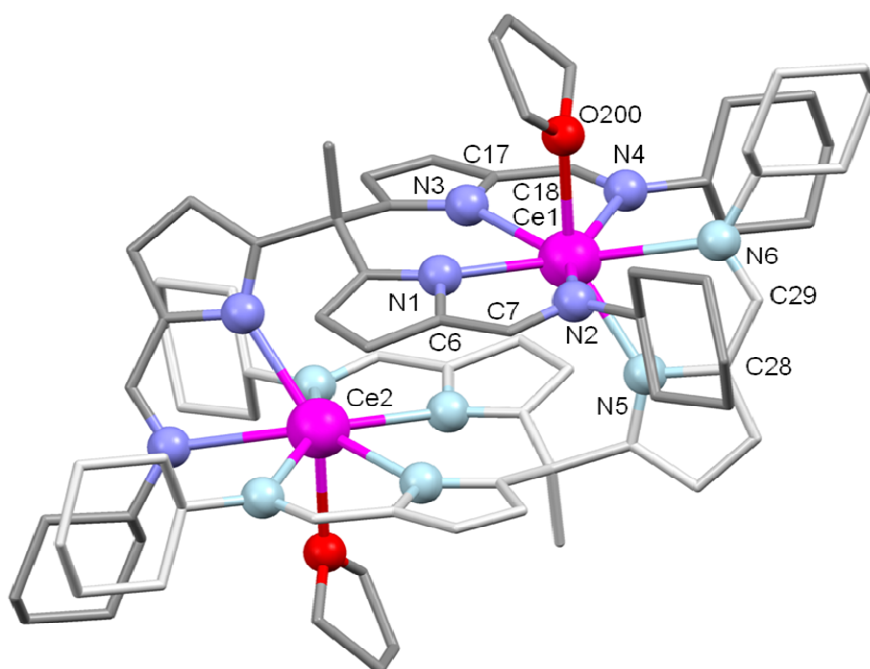
Figure 19: Ball and stick representation of the crystal structure of [Ce$_2$(L)$_2$(THF)$_2$]. For clarity, disorder components and all hydrogen atoms are omitted.

Ce1-N1	2.525(4)	C18-N4	1.297(6)
Ce1-N2	2.641(4)	C28-C29	1.430(6)
Ce1-N5	2.494(4)	C29-N6	1.292(6)
Ce1-N6	2.702(4)	N1-Ce1-N2	67.03(11)
Ce1-O200	2.510(13)	N5-Ce1-N6	65.69(12)
Ce1···Ce1′	5.472(1)	N1-Ce1-N5	137.23(13)
C6-C7	1.414(6)	N5-Ce1-O200	141.8(3)
C7-N2	1.301(6)	P$_1$···P$_2$	3.643
C17-C18	1.452(6)		

Table 5: Selected bond lengths (Å) and angles (°) of [Ce$_2$(L)$_2$(THF)$_2$].

Gambarotta has previously reported an example of two identical tripodal pyrrolide ligands bridging two lanthanides by binding through two arms of the first ligand and one arm of the second (Figure 20).[26] However, as

the basic tripod is unable to provide enough electrons to stabilise the low-valent niobium metal centres through η^1: η^1: η^1 coordination, the two ligands adopt a bridging motif between the two metal centres. Each tripod uses two arms to bind to both metal centres through σ bonds with the pyrrolide nitrogens. The last pyrrolyl ring forms a π bond with a first niobium and a σ bond with the second.
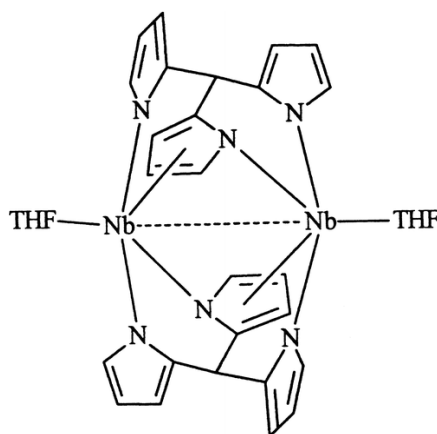
Figure 204: Gambarotta's di-niobium complex.[26]

However, the deprotonation of the ligand with KH or LiMe also afforded a minor product in which the niobium metal centres formed bonds with the three pyrrolo nitrogens of two ligands forming a structure not dissimilar to that previously observed in $[Co(H_3L)_2][Cl]_3$ (Figure 21 left). It is interesting to note that the lithium cation only partakes in charge balancing and binds to four THF molecules whereas the potassium cations binds to the ligand forming an infinite zig-zag shaped anionic polymer (Figure 21 right). The ionic complex is formed by two octahedral niobium complexes which are charge balanced by the $(TMEDA)_4Nb_4Cl_{11}K_2(THF)_4$ dication.
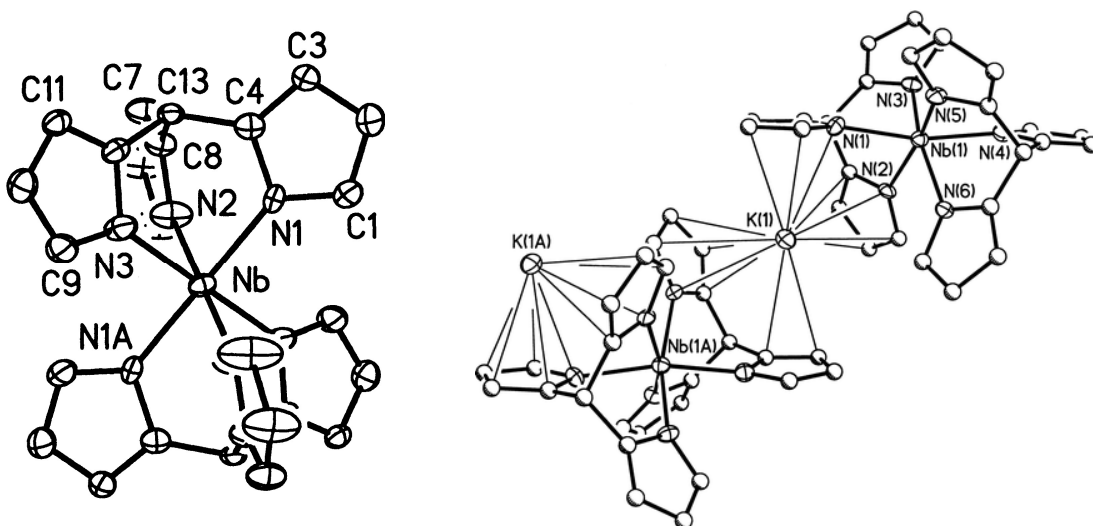
Figure 21: Partial ORTEP representation of $[Nb(L^A)_2]^{2-}$ from the lithium precursor (left) and $K[Nb(L^A)_2]^-$ from the potassium precursor (right). Thermal ellipsoids are drawn at the 30% probability level.[26]

The formation of the multinuclear complexes $[Zn_2(H_2L)_2][Cl]_2$ and $[Ce_2(L)_2(THF)_2]$ is not surprising. Indeed dipyrromethanes are well known within the Love and Gambarotta groups for their propensity to form multinuclear complexes with a range of transition metals as well as f-block elements.[27] Although Love and co-workers have reported the formation of binuclear complexes with early transition metals such as zirconium, a larger tetranuclear iron complex has also been observed and is displayed in Figure 22.[28]
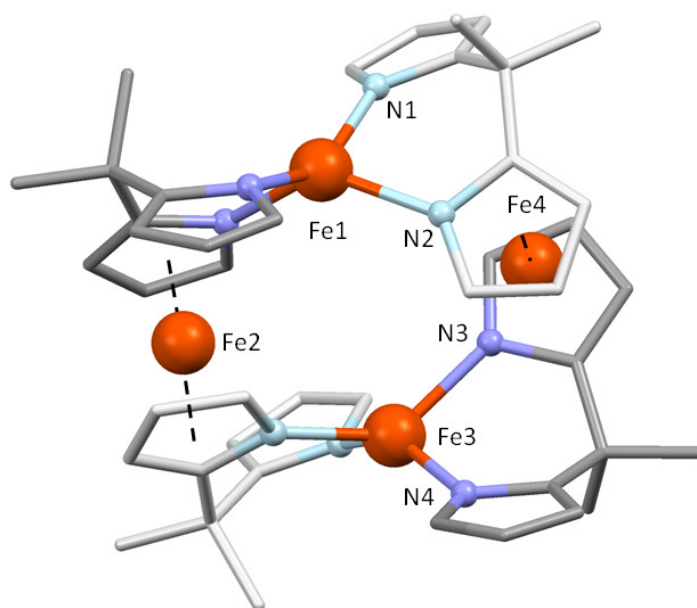
Figure 225: Tetranuclear Fe^{II} dipyrromethane complex observed by Love and co-workers. For clarity, all hydrogen atoms were omitted.

The iron metal centres present themselves in a diamond arrangement linked by four dipyrromethane ligands. The axial cations are bound to four pyrrolide nitrogens in a tetrahedral arrangement through four σ bonds whilst the remaining metal centres form diazaferrocene units by forming η^5 bonding with two pyrrolide rings. The mechanism behind the formation of this metallo-cycle is yet to be determined.

2.7 Conclusions

The H$_3$L pro-ligand developed by Beer and co-workers has been found to have a strong propensity to encapsulate small molecules such as water on a 1:1 ratio as well as larger entities such {LiOH}$_6$ stacked rings in a 2:1 ratio.

Reaction between H$_3$L and metals adopting octahedral or tetrahedral derived geometries result either in mono-metallic multi-ligand complexes such as [Co(H$_3$L)$_2$][Cl]$_3$ or multi-metallic multi-ligand complexes as seen with [Li$_3$(THF)$_3$(LiOH)$_3$(L)]$_2$, [Zn$_2$(H$_2$L)$_2$][Cl]$_2$ and [Ce$_2$(L)$_2$(THF)$_2$].

Although the reaction with $CoCl_2$ led to the complete and partial tautomerisation of the ligand into the aza-fulvene, this was only partial (two branches out of three) for the equivalent reaction with $ZnCl_2$. This shows the potential of H_3L to develop a substrate binding pocket upon metallation.

2.8 References

[1] O. D. Fox, T. D. Rolls, M. G. B. Drew, P. D. Beer, *Chem. Commun.* **2001**, 1632-1633; P. D. Beer, A. G. Cheetham, M. G. B. Drew, O. D. Fox, E. J. Hayes, T. D. Rolls, *Dalton Trans.* **2003**, 603-611.

[2] B. J. Littler, M. A. Miller, C.-H. Hung, R. W. Wagner, D. F. O'Shea, P. D. Boyle, J. S. Lindsey, *J. Org. Chem.* **1999**, *64*, 1391-1396; Q. M. Wang, D. W. Bruce, *Synlett* **1995**, 1267.

[3] R. Goddard, O. Heinemann, C. Kruger, *Acta Crystallogr., Sect. C* **1997**, *53*, 1846-1850; N. Arumugam, W.-Y. Chung, S.-W. Lee, C.-H. Lee, *Bull. Korean Chem. Soc.* **2001**, *22*, 932-934.

[4] S. Varughese, G. R. Desiraju, *Cryst. Growth Des. 10*, 4184-4196.

[5] J. Hernandez-Rojas, J. Breton, J. M. Gomez Llorente, D. J. Wales, *J. Phys. Chem. B* **2006**, *110*, 13357-13362.

[6] L. R. MacGillivray, J. L. Atwood, *Nature* **1997**, *389*, 469-472.

[7] B. Kuberski, A. Szumna, *Chem. Commun.* **2009**, 1959-1961.

[8] J. B. Love, A. J. Blake, C. Wilson, S. D. Reid, A. Novak, P. B. Hitchcock, *Chem. Commun.* **2003**, 1682-1683.

[9] J. M. Rivera, T. Martin, J. Rebek, *J. Am. Chem. Soc.* **2001**, *123*, 5213-5220.

[10] B. W. F. Gordon, M. J. Scott, *Inorg. Chim. Acta* **2000**, *297*, 206-216; C. D. Carmichael, M. D. Fryzuk, *Dalton Trans.* **2008**, 800-806.

[11] J. Randazzo, J. Jacob Morris, J. A. Rood, B. C. Noll, K. W. Henderson, *Inorg. Chem. Commun.* **2008**, *11*, 1270-1272; P. C. Andrews, J. G. MacLellan, R. E. Mulvey, P. J. Nichols, *J. Chem. Soc., Dalton Trans.* **2002**, 1651-1655.

[12] M. B. Dinger, M. J. Scott, *Inorg. Chem.* **2000**, *39*, 1238-1254; T. A. Bazhenova, R. M. Lobkovskaya, R. P. Shibaeva, A. E. Shilov, A. K. Shilova, *J. Organomet. Chem.* **1987**, *330*, 9-15.

[13] L. M. Jackman, D. Cizmeciyan, P. G. Williard, M. A. Nichols, *J. Am. Chem. Soc.* **1993**, *115*, 6262-6267.

[14] C. Strohmann, T. Seibel, D. Schildbach, *J. Am. Chem. Soc.* **2004**, *126*, 9876-9877; R. P. Davies, M. G. Martinelli, L. Patel, A. J. P. White, *Inorg. Chem.* **2010**, *49*, 4626-4631.

[15] R. J. Morris, G. S. Girolami, *Polyhedron* **1988**, *7*, 2001-2008.

[16] T. J. Boyle, D. M. Pedrotty, T. M. Alam, S. C. Vick, M. A. Rodriguez, *Inorg. Chem.* **2000**, *39*, 5133-5146.

[17] T. Ruman, Z. Ciunik, S. Wołowiec, *Eur. J. Inorg. Chem.* **2003**, *2003*, 2475-2485.

[18] R. L. Paul, A. J. Amoroso, P. L. Jones, S. M. Couchman, Z. R. Reeves, L. H. Rees, J. C. Jeffery, J. A. McCleverty, M. D. Ward, *J. Chem. Soc., Dalton Trans.* **1999**, 1563-1568.

[19] R. Hoffmann, J. M. Howell, A. R. Rossi, *J. Am. Chem. Soc.* **1976**, *98*, 2484-2492; W. O. Gillum, R. A. D. Wentworth, R. F. Childers, *Inorg. Chem.* **1970**, *9*, 1825-1832.

[20] A. A. Belal, P. Chaudhuri, I. Fallis, L. J. Farrugia, R. Hartung, N. M. MacDonald, B. Nuber, R. D. Peacock, J. Weiss, K. Weighardt, *Inorg. Chem.* **1991**, *30*, 4397-4402; C. Wendelstorf, R. Krämer, *Angew. Chem. Int. Ed.* **1997**, *36*, 2791-2793; H. Al-Sagher, I. Fallis, L. J. Farrugia, R. D. Peacock, *J. Chem. Soc., Chem. Commun.* **1993**, 1499-1500.

[21] S. Trofimenko, *J. Am. Chem. Soc.* **1966**, *88*, 1842-1844; C. A. Dodds, M.-A. Lehmann, J. F. Ojo, J. Reglinski, M. D. Spicer, *Inorg. Chem.* **2004**, *43*, 4927-4934; P. J. Bailey, M. Lanfranchi, L. Marchiò, S. Parsons, *Inorg. Chem.* **2001**, *40*, 5030-5035; J. Reglinski, M. D. Spicer, M. Garner, A. R. Kennedy, *J. Am. Chem. Soc.* **1999**, *121*, 2317-2318.

[22] J.-i. Setsune, A. Tanabe, J. Watanabe, S. Maeda, *Org. Biomol. Chem.* **2006**, *4*, 2247-2252; S. D. Reid, C. Wilson, A. J. Blake, J. B. Love, *Dalton Trans.* **2010**, *39*, 418-425.

[23] J. L. Sessler, E. Tomat, V. M. Lynch, *Chem. Commun.* **2006**, 4486-4488; R. S. Forgan, J. E. Davidson, S. G. Galbraith, D. K. Henderson, S. Parsons, P. A. Tasker, F. J. White, *Chem. Commun.* **2008**, 4049-4051.

[24] S. D. Reid, C. Wilson, C. I. De Matteis, J. B. Love, *Eur. J. Inorg. Chem.* **2007**, *2007*, 5286-5293; K. A. Ames, S. R. Collinson, A. J. Blake, C. Wilson, J. B. Love, D. W. Bruce, B. Donnio, D. Guillon, M. Schröder, *Eur. J. Inorg. Chem.* **2008**, *2008*, 5056-5066.

[25] P. L. Arnold, N. A. Potter, C. D. Carmichael, A. M. Z. Slawin, P. Roussel, J. B. Love, *Chem. Commun.* **2010**, *46*, 1833-1835; Y.-Y. Zhang, S.-X. Liu, *Acta Crystallogr. Sect. C* **2009**, *65*, m269-m272; M. Rafizadeh, V. Amani, E. Iravani, B. Neumüller, *Z. Anorg. Allg. Chem.* **2005**, *631*, 952-955.

[26] M. Tayebani, S. Conoci, K. Feghali, S. Gambarotta, G. P. A. Yap, *Organometallics* **2000**, *19*, 4568-4574.

[27] A. Novak, A. J. Blake, C. Wilson, J. B. Love, *Chem. Commun.* **2002**, 2796-2797; T. Dubé, S. Conoci, S. Gambarotta, G. P. A. Yap, G. Vasapollo, *Angew. Chem. Int. Ed.* **1999**, *38*, 3657-3659; M. Ganesan, S. Gambarotta, G. P. A. Yap, *Angew. Chem. Int. Ed.* **2001**, *40*, 766-769; D. M. M. Freckmann, T. Dubé, C. D. Bérubé, S. Gambarotta, G. P. A. Yap, *Organometallics* **2002**, *21*, 1240-1246; T. Dubé, S. Conoci, S. Gambarotta, G. P. A. Yap, *Organometallics* **2000**, *19*, 1182-1185.

[28] J. B. Love, P. A. Salyer, A. S. Bailey, C. Wilson, A. J. Blake, E. S. Davies, D. J. Evans, *Chem. Commun.* **2003**, 1390-1391.

Chapter 3: Hangman complexes of H₃L and a new tripodal amide ligand.

3.1: Introduction

Ligands that are capable of providing further, peripheral binding sites upon complexation with a transition metal to stabilise and direct reactivity have been of great interest to chemists looking to design new catalysts and enzyme mimics.[1] The majority of these complexes have been used in the multiproton-electron transfer reactions which are required for the activation of small molecules.[2] Nocera and co-workers have developed numerous "hangman" porphyrins and corroles that promote the four electron-four proton reduction of oxygen to water.[3] Cobalt corroles are known for reducing oxygen and producing hydrogen peroxide through a two proton/electron process despite efforts to achieve the formation of water.[4] The "hangman effect", however, in which the pendant arm can act as a proton channel (Figure 1), is shown to promote the formation of water over hydrogen peroxide.[5] In these systems, the lack of a proton on the pendant arm results in a drop of 25 % in the formation of water which shows its importance in the proton transfer mechanism that results in the O-O bond cleavage.
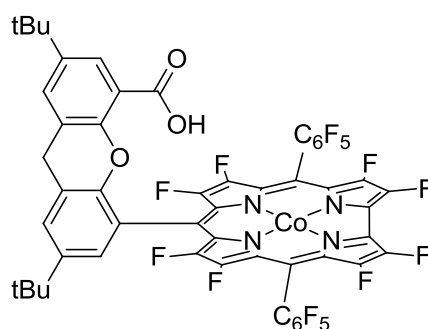
Figure 1: Hangman corrole designed by Nocera and co-workers and observed to preferentially reduce dioxygen to water.[5]

The use of metals preferentially adopting a tetrahedral or octahedral derived geometry with H_3L showed the development of substrate binding elements, such as hydrogen bond donors, through ligand tautomerisation. The multi-ligand/multi-metal complexes observed prevented the formation of a guest binding pocket proximate to the metal centre. Transition metal complexes favouring square planar or square planar derived geometry should provide not only a metal coordination site with two arms chelating to the ligand but also a substrate binding site with hydrogen bond donors and acceptors located on the pendant arm.

3.2: Synthesis of [Pd(HL)] and [Cu(HL)]

The formation of a hangman complex from the pro-ligand H_3L requires the use of transition metals that preferentially adopt a square planar or square planar derived geometry such as Pd^{II} and Cu^{II}. As such, it was discovered that the addition of $Pd(OAc)_2$ or $Cu(OAc)_2$ to a solution of H_3L under basic conditions led to the formation of hangman complexes in 62 and 60 % respectively, as shown in Scheme 1.
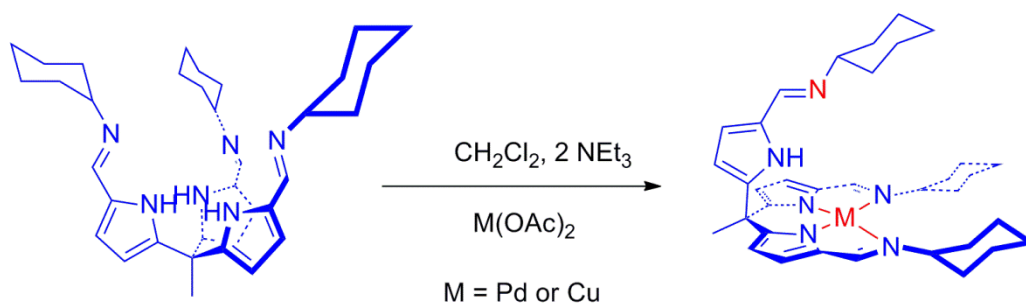
Scheme 1: Synthesis of hangman complexes [Pd(HL)] and [Cu(HL)]

The ^1H NMR spectrum of [Pd(HL)] (Figure 2) contains two different sets of resonances in a 2:1 ratio in the aromatic region. The pyrrolide-imine resonances are observed at 7.57, 6.65 and 6.16 ppm whilst the pendant pyrrole-imine resonances are observed at 7.59, 6.60 and 5.89 ppm. Although a single multiplet is observed for all three cyclohexyl methine CHs, the

complexity of the multiplet suggests that the expected two sets of signals are overlapping. This is supported by an integral worth three hydrogens for the resonance observed at 3.24 ppm. The ESI spectrum supports the coordination of the metal centre to the ligand with a molecular ion peak observed at 657.36 *m/z* for [Pd(HL)].
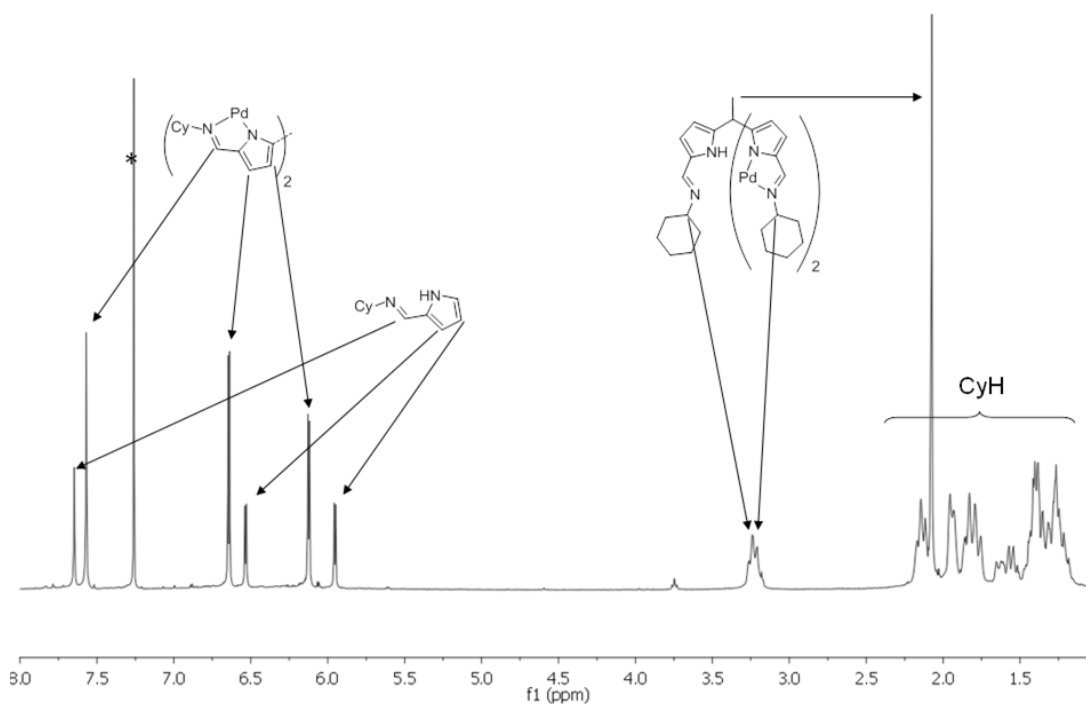
Figure 2: ^{1}H NMR spectrum of [Pd(HL)] in CDCl$_3$.

Re-crystallisation of [Pd(HL)] from hot acetonitrile afforded crystals suitable for X-ray diffraction studies. The solid state structure, which supports the structure in solution, was determined and is shown in Figure 3, with selected bond lengths and angles detailed in Table 1 and crystal data in Table Ch3 Tab1. The Pd^{II} cation is held in a distorted square planar geometry by two deprotonated pyrrole-imines of the tripodal ligand (Pd1- N1, 1.944(2) and Pd1-N2, 2.084(2) Å) with the metal centre residing slightly above the plane (P3) of the four chelating nitrogens (Pd···P3, 0.065 Å). This has resulted in an upward tilt of the two pyrrolyl-imines with their planes, defined by

65

their respective nitrogens and imine carbon, bisecting each other at an angle of 17°. The pendant imine bond distance of 1.263(3) Å shows that unlike [Co(H$_3$L)$_2$] and [Zn$_2$(HL)$_2$], the azafulvene-amine tautomer is not favoured in this case with the pyrrole-imine tautomer retained. The torsion angle defined by Pd1, C2, C25 and N5 of 5° shows that the pendant arm resides above the axial coordination site of the metal centre which leads to the formation of a hydrophobic cavity by the cyclohexyl substituents.
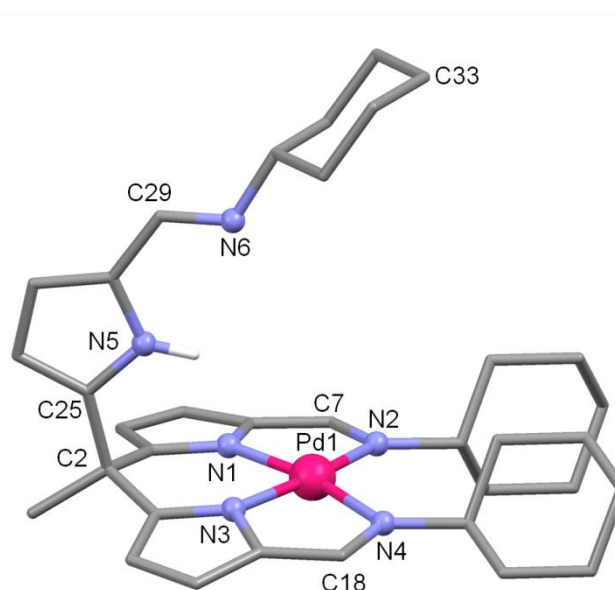
Figure 3: X-Ray crystal structure of [Pd(HL)]. For clarity, all hydrogens atoms except the pyrrolyl NH are omitted and the plane defined by the chelating nitrogens N1, N2, N3 and N4 is referred to as P3.

Pd1-N1	1.944(2)	Pd1···N6	5.240(4)
Pd1-N2	2.084(2)	Pd1···P3	0.065
N2-C7	1.301(3)	N1-Pd1-N2	80.43(7)
N4-C18	1.299(3)	N1-Pd1-N3	87.23(7)
N6-C29	1.263(3)	N1-Pd1-N4	167.34(7)
Pd1···N5	3.938(4)	Pd1···C2-C25-N5	4.91

Table 1: Selected bond lengths (Å) and angles (°) of [Pd(HL)]. For clarity, the plane defined by the four chelating nitrogens N1, N2, N3 and N4 is referred to as P3.

The extended structure shows numerous interactions between adjacent complexes. The bulky hydrophobic cyclohexyl substituents

interdigitate forming a dimeric structure similar to a stretched analogue of [$Zn_2(H_2L)_2$] in which the shortest C-C interaction is 3.74 Å and the two Pd^{II} atoms are separated by 10.89 Å (Figure 4). The pendant arm is also seen to interact with the vacant axial site of a third complex through its cyclohexyl CHs (C33···Pd1′, 3.73 Å).
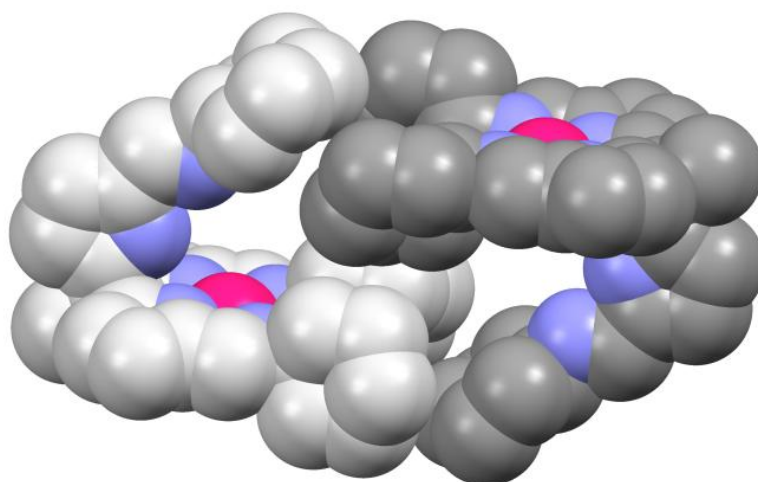
Figure 4: Extended structure of [Pd(HL)].

The addition of $Cu(OAc)_2$ to H_3L in MeCN led to the formation of a mixture of products. Pure [Cu(HL)] was obtained by redissolving the residual solids in THF and precipitating the product as a green powder by the addition of hexanes. Although no crystals of [Cu(HL)] could be obtained, the ESI spectrum displays a molecular ion peak at 614 *m/z* which confirms coordination of the ligand around the metal centre with all acetate ion displaced as acetic acid. The solution magnetic moment of 2.23 BM supports the presence of the d^9 metal centre which is concordant with a structure similar to that of [Pd(HL)]. Elemental analysis is concordant with the obtention of a pure material.

3.3 Synthesis of the ion pair receptors [Pd(H$_2$L)][Cl] and [CuCl(H$_2$L)].

The presence of hydrogen bond donors and acceptors in novel coordination compounds is significant and allows for the development of proton channels that could mimic enzymatic catalytic function. The protonation of the pendant arm in [M(HL)] complexes can be achieved by the use of an alternative metal precursor such as metal halides rather than metal acetates. As such, the addition of PdCl$_2$(MeCN)$_2$ or CuCl$_2$ to a solution of H$_3$L under basic conditions led to the formation of [Pd(H$_2$L)][Cl] in 60 % as a yellow solid and [CuCl(H$_2$L)] in 65 % as a green solid as described in Scheme 2.
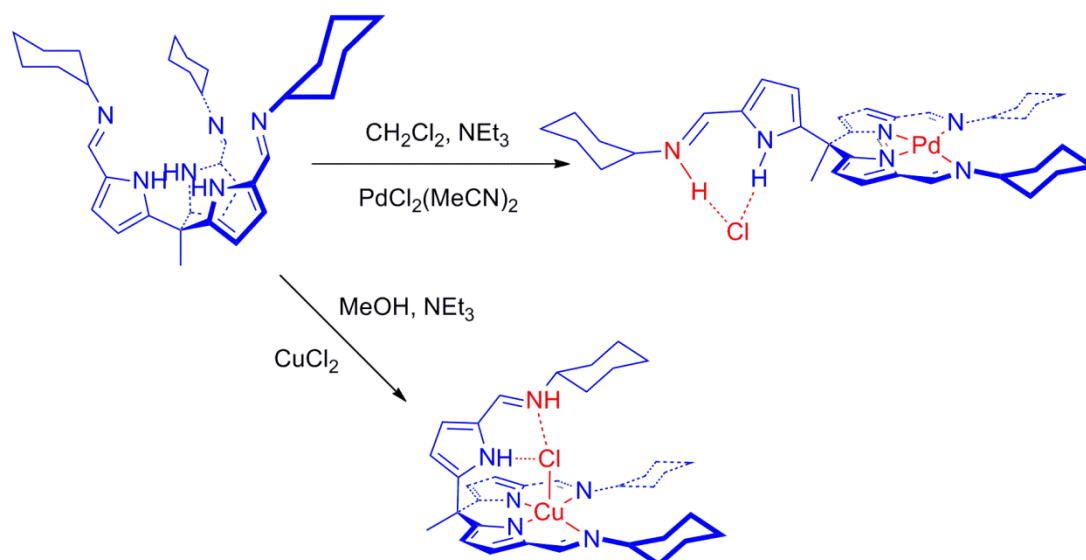
Scheme 2: Synthesis of the ion pair receptors [Pd(H$_2$L)][Cl] and [CuCl(H$_2$L)].

In solution, [Pd(H$_2$L)][Cl] shows similar characteristics to [Pd(HL)]. The ^{1}H NMR spectrum, displayed in Figure 5 and 6, contains two distinct pyrrole-imine environments in a 2:1 ratio. Two arms of the tripodal ligand are deprotonated (no pyrrolic NH resonance worth two hydrogens is seen) and can be observed at 7.57, 6.65 and 6.35 ppm. The pyrrolic resonances corresponding to the third arm are observed at 13.34 (unbound NH), 6.72 and 5.71 ppm. The imine resonances comprise a doublet at 7.38 ppm

correlating in the ^{1}H-^{1}H COSY spectrum to a multiplet at 12.86 ppm which supports the protonation of the imine nitrogen. The large splitting pattern of the resonance associated with the protonated imine (15.5 Hz) suggest that the imine and pyrrole protons adopt an *anti* configuration at the C=N bond. Furthermore, the cyclohexyl CHs can now be seen as two distinct resonances at 3.42 and 3.23 ppm, integrating for 1 and 2 protons, respectively.
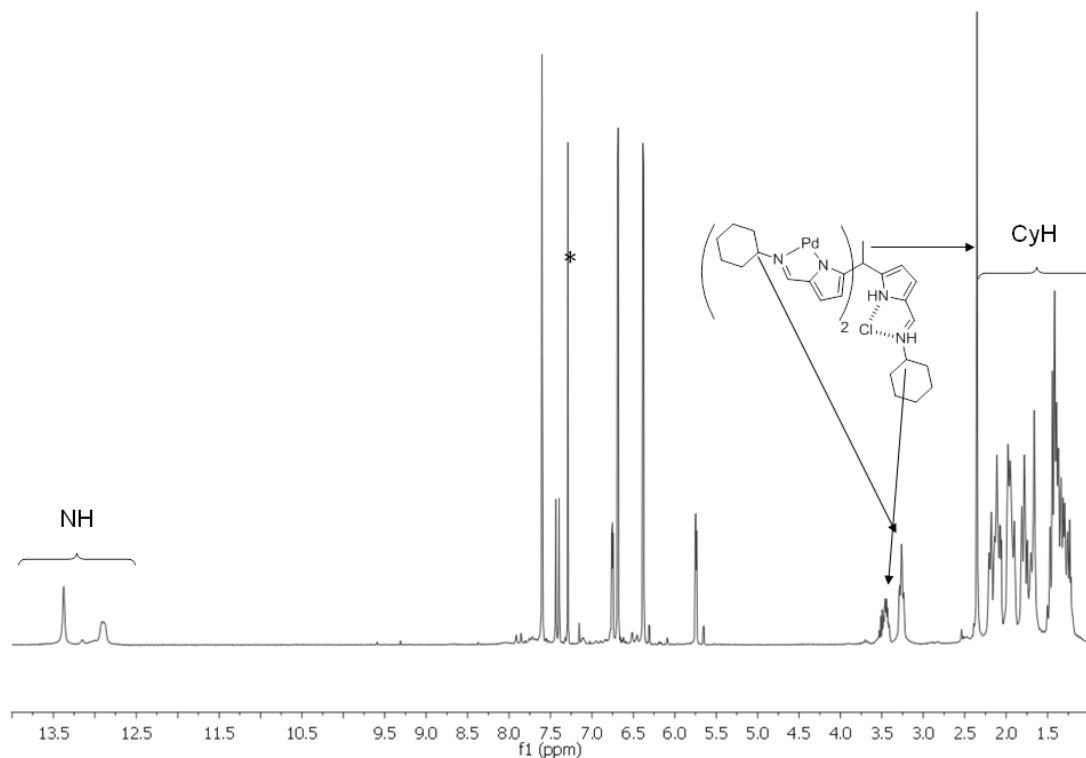
Figure 5: ^{1}H NMR spectrum of [Pd(H$_2$L)][Cl] in CDCl$_3$.
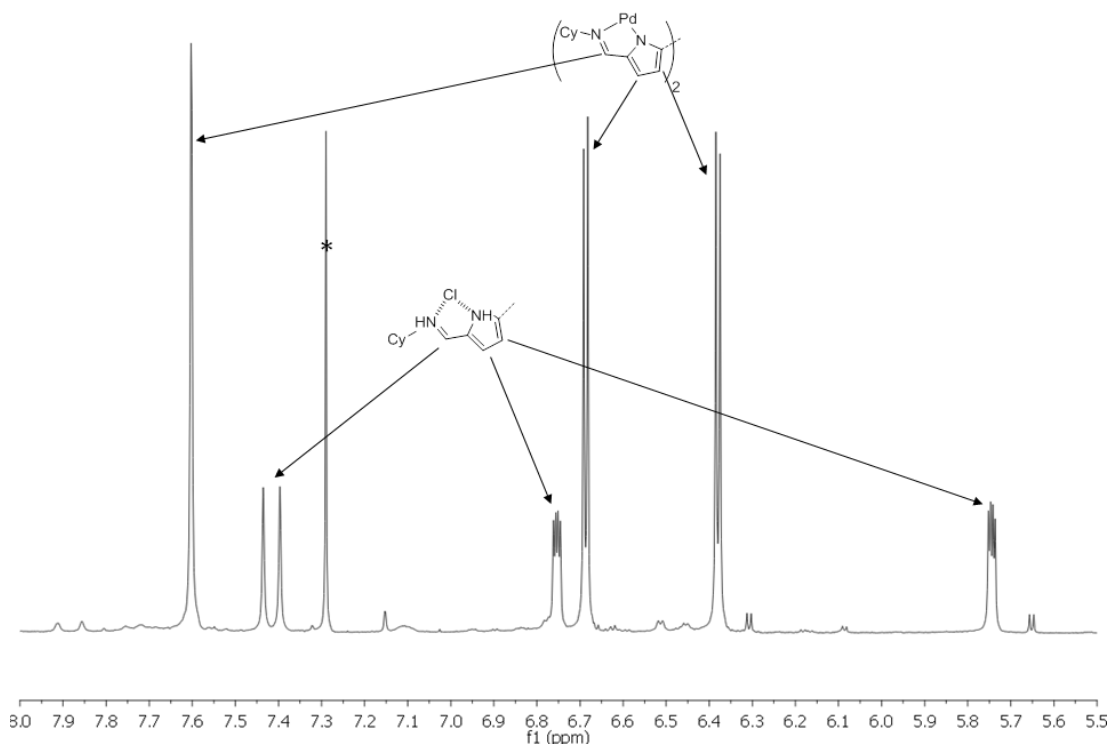
Figure 6: Expansion of the aromatic region of the ^{1}H NMR of [Pd(H$_2$L)][Cl] in CDCl$_3$.

Re-crystallisation of [Pd(H$_2$L)][Cl] from hot MeCN afforded yellow crystals suitable for X-ray diffraction studies. The solid state structure was determined and is shown in Figure 7, with selected bond lengths and angles detailed in Table 2 and crystal data in Table Ch3 Tab1. In the solid state structure of [Pd(H$_2$L)][Cl], the metal centre is held in a square planar geometry by the deprotonated pyrrole nitrogens (Pd1-N1, 1.952(4) Å and Pd1-N3, 1.955(4) Å) and imine nitrogens (Pd1-N2, 2.108(4) Å and Pd1-N4, 2.116(4) Å) of two branches of H$_3$L. Compared to [Pd(HL)] the palladium metal centre is contained within the plane (P1) of the four nitrogen atoms resulting in the co-planarity of both pyrrolide-imine arms making it a similar mode of bonding to porphyrins. The third arm is protonated by a molecule of HCl that is formed intrinsically during the course of the reaction and is rotated away from the metal binding site. The chloride counter anion is partaking in hydrogen bonding interactions with both the pyrrole and imine

NHs (3.175(4) and 3.138(3) Å respectively). Although the pendant arm imine bond has lengthened significantly on protonation compared to that of H_3L (1.305(6) and 1.24(2) Å respectively), the pyrrole-imine tautomeric structure is retained (C28-C29, 1.405(6) Å). The presence of a CH⋯Cl interaction between C1 and the anion (3.902(7) Å) prevents the third arm from being rotated 180° away from the metal centre and adds to the asymmetry of the molecule in the solid state. Instead, the torsion angle defined by Pd1, C2, C25 and N5 is of 137°. It is noteworthy that the overall structure also contains a molecule of chloroform hydrogen bonding to the chloride anion (C50⋯Cl1, 3.425(4)).
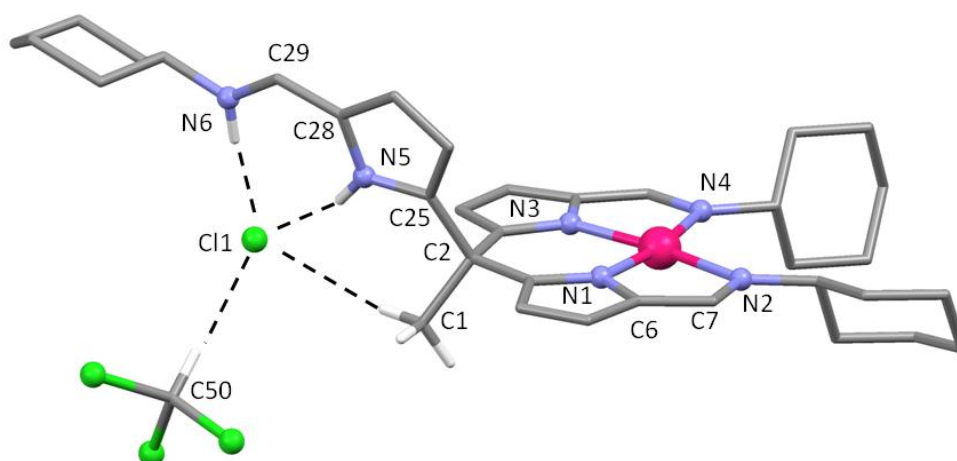
Figure 7: X-Ray crystal structure of [Pd(H$_2$L)][Cl]. P1 is the plane defined by the four chelating nitrogens (N1, N2, N3 and N4). For clarity, all hydrogens not partaking in H⋯Cl interactions are omitted.

Pd1-N1	1.952(4)	C6-C7	1.415(7)
Pd1-N2	2.108(4)	N6-C29	1.305(6)
N5⋯Cl1	3.175(4)	C28-C29	1.405(6)
N6⋯Cl1	3.138(3)	N1-Pd1-N2	80.12(16)
C50⋯Cl1	3.425(4)	N1-Pd1-N3	87.03(16)
C1⋯Cl1	3.902(7)	N1-Pd1-N4	167.10(16)
N2-C7	1.301(6)	N2-Pd1-N4	112.64(15)

Table 2: Selected bond lengths (Å) and angles (°) of [Pd(H$_2$L)][Cl].

Re-crystallisation of [CuCl(H$_2$L)] from hot MeCN afforded crystals suitable for X-ray diffraction studies. The solid state structure was determined and is shown in Figure 8, with selected bond lengths and angles detailed in Table 3 and crystal data in Table Ch3 Tab1. The solid state structure shows the metal centre held by the four nitrogen atoms of two deprotonated arms of the ligand in a *pseudo* square planar arrangement (N1-Cu1, 1.946(3) and N2-Cu1, 2.085(3) Å) in which similarly to [Pd(HL)], the metal centre sits above the plane of the four nitrogens P1 (P1···Cu1, 0.56 Å). This results in an upward tilt of the two pyrrole-imine arms the planes of which (P$_2$ defined by N1, N2 and Cu1 and P$_3$ defined by N3, N4 and Cu1) intersects each other at an angle of 33.6°. As in [Pd(H$_2$L)][Cl], the third arm takes no part in the coordination of the metal and has been protonated by a molecule of HCl (N6···Cl1, 3.099(3) Å) formed during the course of the reaction. However the propensity of Cu^{II} to form five coordinate complexes leads to the formation of a covalent bond with the Cl$^-$ anion (Cu1-Cl1, 2.583(1) Å) resulting in the square pyramidal geometry. As a consequence, the pendant arm resides above the metal centre, fully encapsulating the chloride ion in an overall structure similar to that of [Pd(HL)]. Furthermore, the anion also partakes in CH···Cl interactions with a cyclohexyl carbon (Cl1···C20, 3.711(5) Å) and a molecule of acetonitrile which was used as solvent for the crystallisation process (Cl1···C402, 3.810(10) Å).
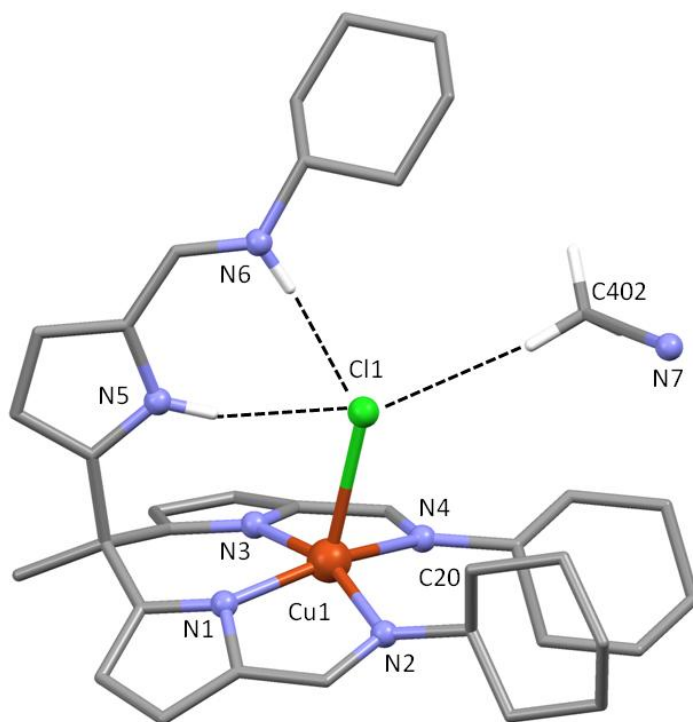
Figure 8: X-ray crystal structure of [CuCl(H₂L)]. For clarity, all hydrogens not partaking in H···Cl interactions are omitted.

Cu1-N1	1.946(3)	N1-Cu1-N2	80.87(11)
Cu1-N2	2.085(3)	N1-Cu1-N3	84.76(12)
Cu1-Cl1	2.583(1)	N2-Cu1-N4	108.15(12)
Cl1···N5	3.270(3)	N1-Cu1-N4	161.15(12)
Cl1···N6	3.099(3)	N1-Cu1-Cl1	99.91(9)
Cl1···C20	3.711(5)	N2-Cu1-Cl1	89.76(9)
Cl1···C402	3.810(10)	N5···Cl1···N6	56.46(8)

Table 3: Selected bond lengths (Å) and angles (°) of [CuCl(H₂L)].

The ESI mass spectrum displays a molecular ion peak at 650 *m/z* which confirms the coordination of the ligand around the metal as well as the presence of a chloride anion. The isotopic pattern is concordant with a complex containing both Cu and Cl ions with the presence of an ion peak at 652 *m/z* worth 9 % (3/4 of the [M+H⁺] ion peak) corresponding to the combination of ^{65}Cu and ^{37}Cl. The solution magnetic moment of 1.94 BM

supports the presence of the d^9 metal centre which is concordant with the solid state structure.

It is clear from the last two complexes that H_3L can act as an ion pair receptor. The metal cation, however, dictates the type of binding that will ensue. The use of the four coordinate Pd^{II} resulted in a "host-separated" ion pair (Figure 9 right) in which the anion and cation are separated by the host molecule (H_3L). In contrast, the use of Cu^{II}, due to its ability to form five coordinate complexes, favours the formation of a "contact" ion pair (Figure 9 left) in which the anion and cation are bound. In the case of metals favouring square planar derived geometry, H_3L can be seen as having two different binding sites: a porphyrin-like site consisting of two deprotonated pyrrole-imine arms of the tripodal ligand as well as a hydrogen donor/acceptor site constituted by the pendant arm.[6] A solvent-bridged ion pair has not been observed with H_3L thus far.
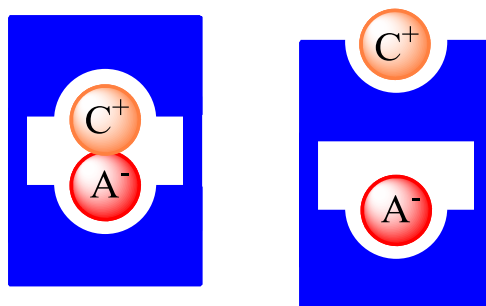
Figure 9: Types of ion-pair to receptor binding observed in H_3L with H_3L in blue, anion represented as A^- and cation as C^+. Contact ion pair (left) observed in [CuCl(H_2L)] and host-separated ion pair observed in [Pd(H_2L)][Cl] (right).[6]

3.4 Investigation into the redox chemistry of [Pd(HL)], [Pd(H₂L)][Cl], [Cu(HL)] and [CuCl(H₂L)].

The reduction/oxidation potential of the above complexes was investigated to ascertain their possible use in redox catalysis, in particular in proton-coupled-electron-transfer chemistry. All experiments were conducted

in dry THF with Bu_4NBF_4 electrolyte (0.2 molL^{-1}) and referenced to ferrocene (Fc/Fc$^+$ = 0 V). Scans were conducted at 500, 300 and 100 mVs^{-1}, and all features were scanned starting from the most positive vertex point.

As a reference, the CV of the ligand (H$_3$L) was investigated as shown below in Figure 10, and displays no electrochemical redox features between +0.33 and -2.66 V.
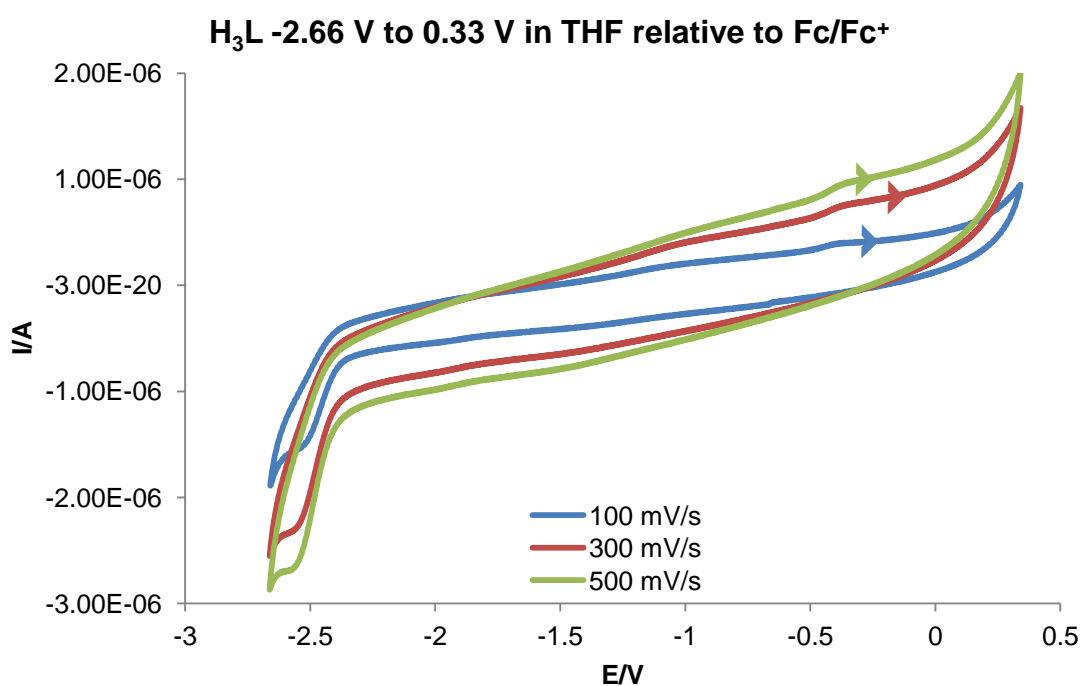
Figure 10: Cyclic voltammogramof H$_3$L in THF (Bu$_4$NBF$_4$, Fc/Fc$^+$).

Similarly, [Pd(HL)] showed no features within the THF window (*ca.* -2.66 to 0.33 V) (Figure 11).

[Pd(HL)] -2.66 V to 0.33 V in THF relative to Fc/Fc⁺
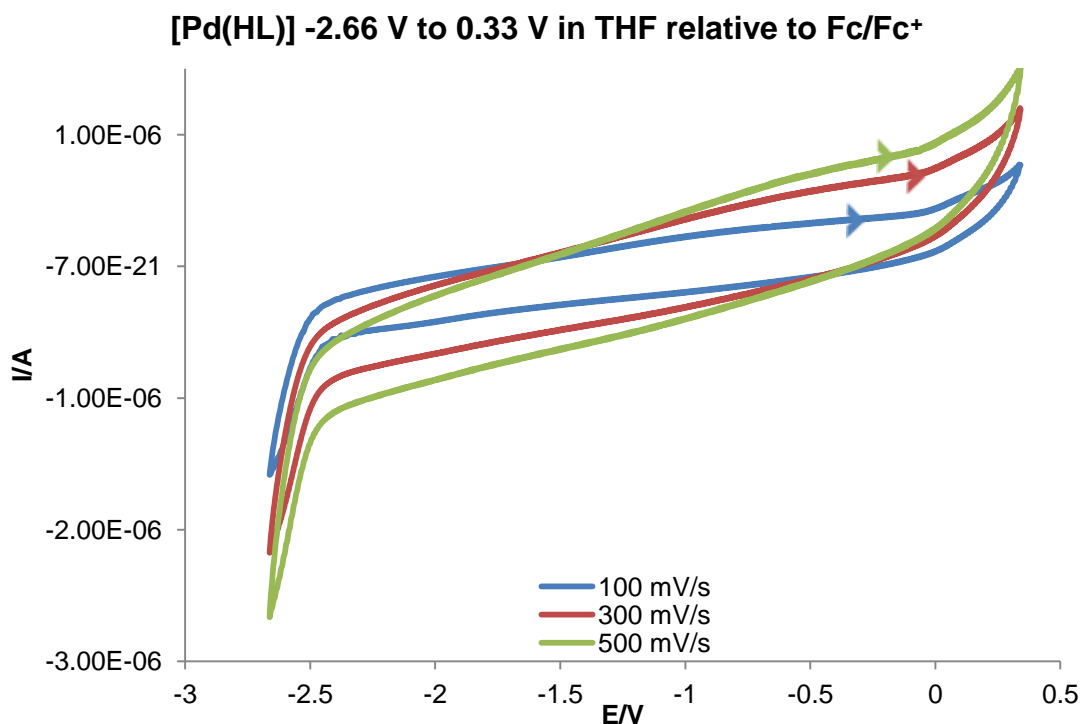
Figure 11: Cyclic voltammogram of [Pd(HL)] in THF (Bu$_4$NBF$_4$, Fc/Fc$^+$).

[Pd(H₂L)][Cl] shows three scan-rate dependent features including two oxidations that migrate from -0.82 to -0.68 V and 0.04 to 0.17 V and a single reduction -1.37 to -1.46 V (*vs* Fc/Fc⁺) as the scan rate was increased from 100 to 500 mV/s suggesting that these are irreversible (displayed in Figure 12). Undoubtedly, the differences observed between the cyclic voltammograms of [Pd(HL)] and [Pd(H₂L)][Cl] are due to the presence of HCl. Investigating each feature independently led to only the oxidation at -0.68 V being observed. This is most likely the oxidation of chloride anions into chlorine gas which afterwards allows the reduction at -1.46 V of hydrogen into dihydrogen gas through the deprotonation of the imine as shown in Scheme 3.

$$2\ [Pd(H_2L)][Cl] \longrightarrow 2\ [Pd(H_2L)]^+ + Cl_2 + 2\ e^-$$

$$2\ [Pd(H_2L)]^+ + 2\ e^- \longrightarrow 2\ [Pd(HL)] + H_2$$
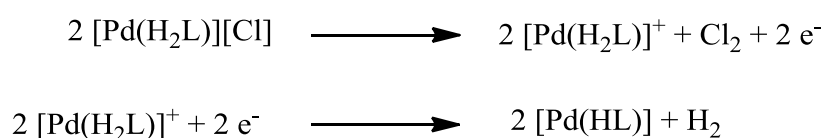
Scheme 3: Species formed during the electrochemical study of [Pd(H₂L)][Cl].

[Pd(H$_2$L)][Cl] -2.66 V to 0.33 V in THF relative to Fc/Fc$^+$
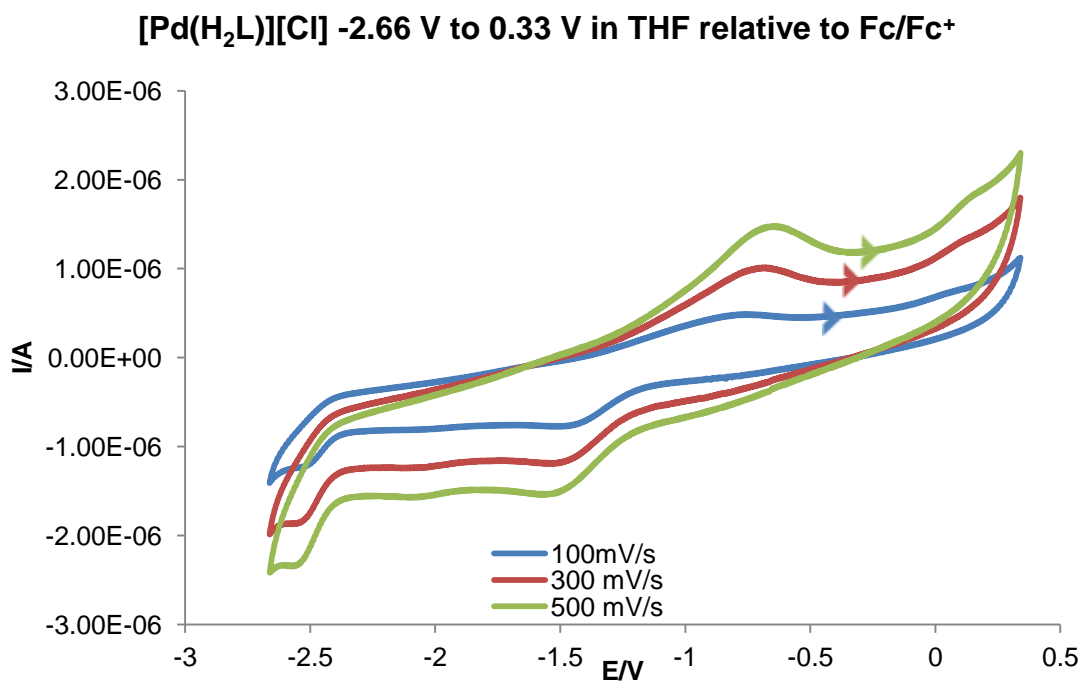
Figure 12: Cyclic Voltammogram of [Pd(H$_2$L)][Cl] in THF (Bu$_4$NBF$_4$, Fc/Fc$^+$)

The redox characteristics of [Pd(H$_2$L)][Cl] in the presence and absence of CO$_2$ were also investigated, but did not show any reactivity (Figure 13).

Comparison of [Pd(H$_2$L)][Cl] in the presence and absence of CO$_2$ -2.66 V to 0.33 V in THF relative to Fc/Fc$^+$
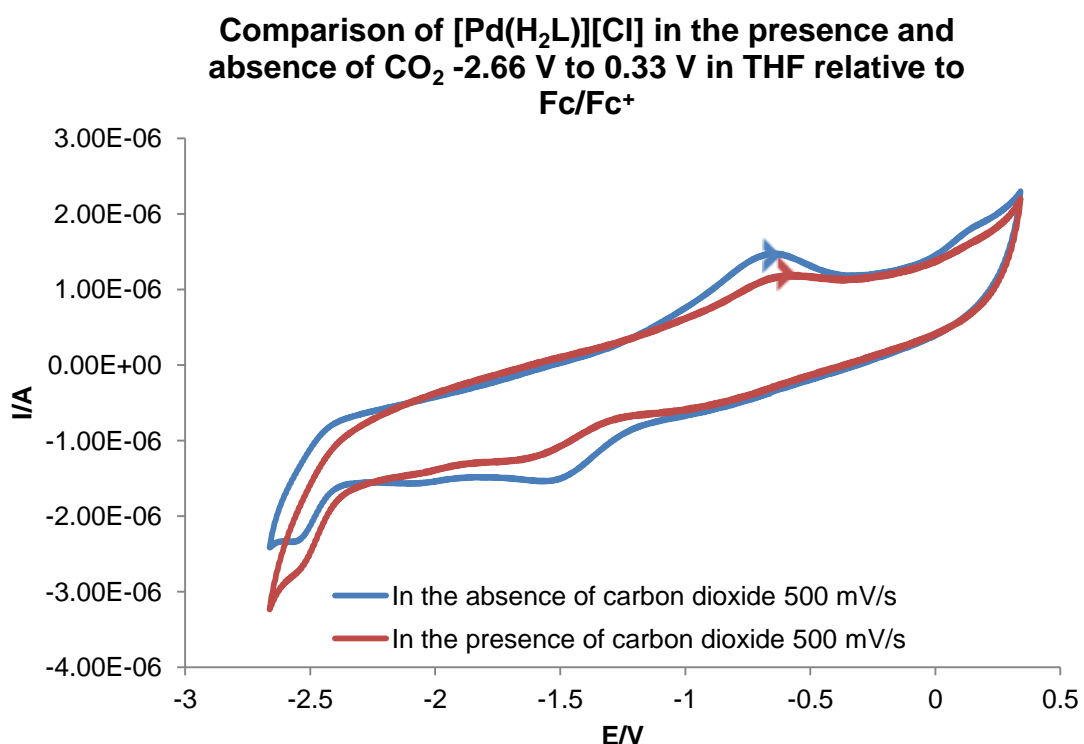
Figure 13: Cyclic Voltammogram of [Pd(H$_2$L)][Cl] in the absence and presence of CO$_2$ in THF (Bu$_4$NBF$_4$, Fc/Fc$^+$)

The cyclic voltammogram of [Cu(HL)] shows a single feature different from that of H_3L and [Pd(HL)] at -2.25 V (*vs* Fc/Fc⁺) which can therefore be attributed to the metal centre (Figure 14). Although this irreversible redox feature was not substantial enough to be fully analysed, it is highly likely to involve the reduction of Cu^{II} to Cu^{I}.
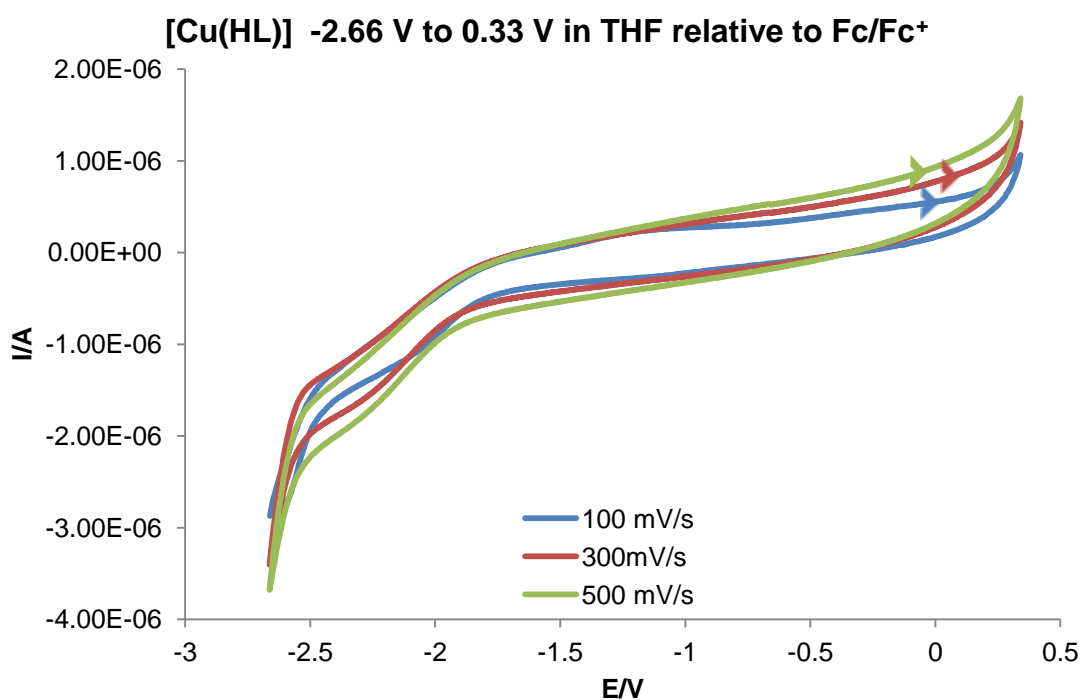
Figure 14: Cyclic Voltammogram of [Cu(HL)] in THF (Bu₄NBF₄, Fc/Fc⁺).

The cyclic voltammogram of [CuCl(H₂L)] (Figure 15) is similar if not identical to that of [Pd(H₂L)][Cl] confirming that the reduction/oxidation potentials observed are due to the protonation of the ligand with HCl and are not metal dependent. Once again, it can be inferred that the observed oxidation is the result of the formation of chlorine from chloride and that the reduction is the result of the formation of H_2 from the deprotonation of the pendant arm imine as shown in Scheme 4.

$$2\,[CuCl(H_2L)] \longrightarrow 2\,[Cu(H_2L)]^+ + Cl_2 + 2\,e^-$$

$$2\,[Cu(H_2L)]^+ + 2\,e^- \longrightarrow 2\,[Cu(HL)] + 2\,H_2$$
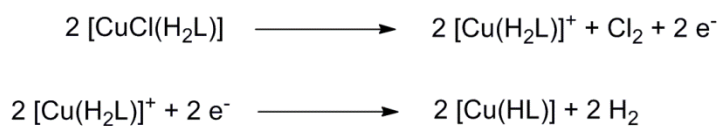
Scheme 4: Species formed during the electrochemical study of [CuCl(H$_2$L)].
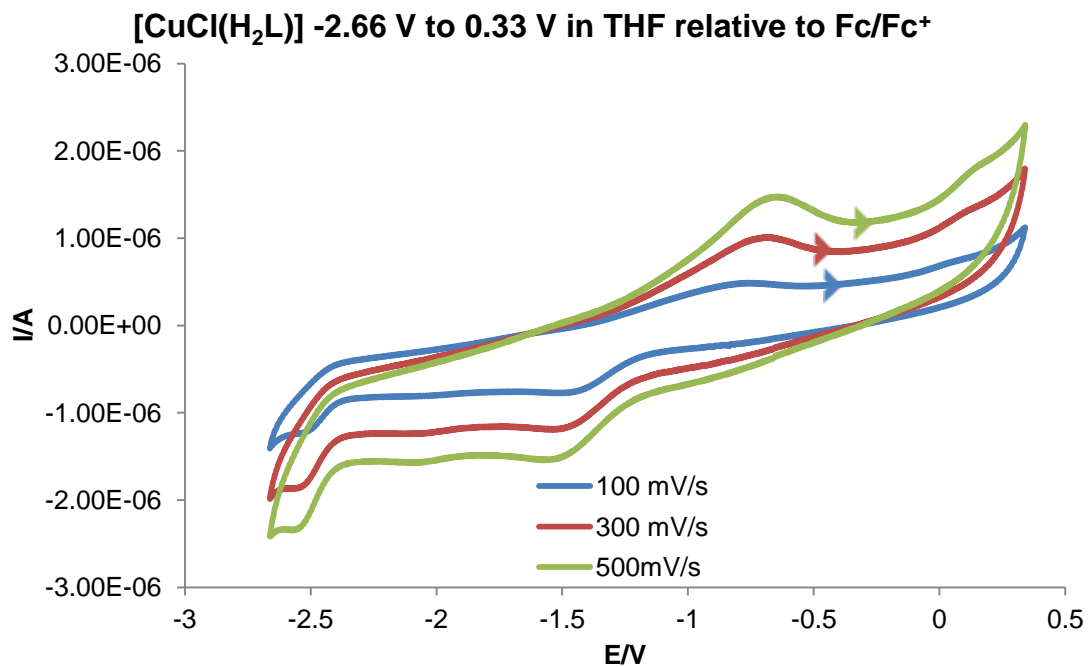
Figure 15: Cyclic Voltammogram of [CuCl(H$_2$L)] in THF (Bu$_4$NBF$_4$, Fc/Fc$^+$).

Comparison of the cyclic voltammogram of [CuCl(H₂L)] in the presence and absence of CO₂ again does not show any further reactivity (Figure 16).

[CuCl(H$_2$L)] in the presence and absence of CO$_2$ in THF relative to Fc/Fc$^+$
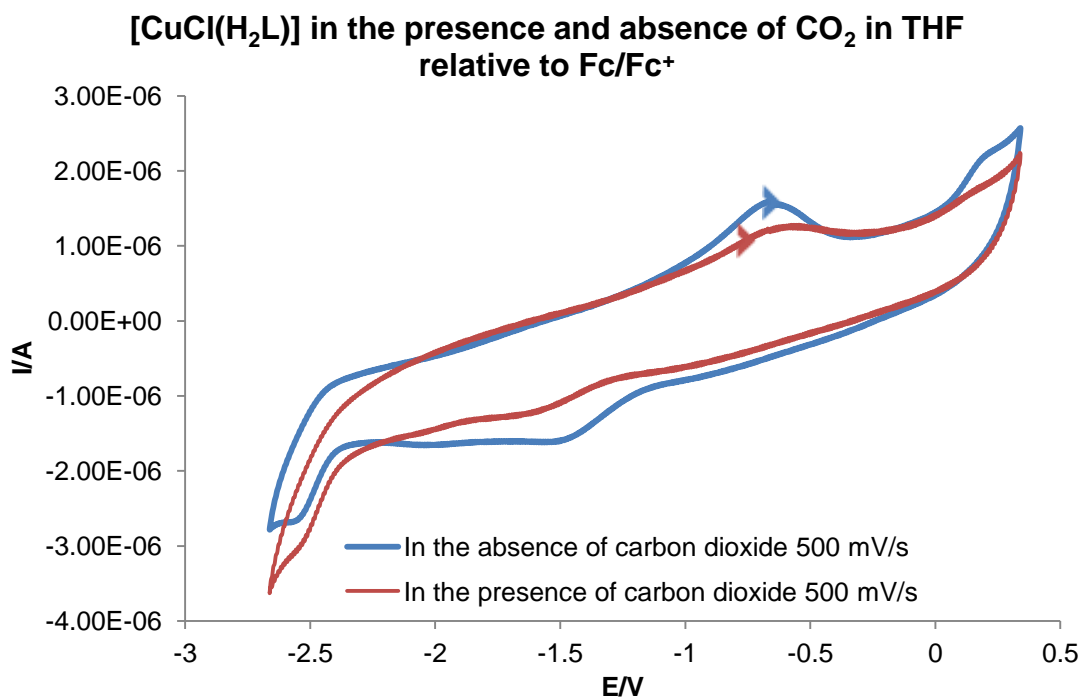
Figure 16: Cyclic Voltammogram of [Pd(H$_2$L)][Cl] in THF (Bu$_4$NBF$_4$, Fc/Fc$^+$).

3.5: Synthesis of the tripodal pyrrole-amide ligand H$_6$L.

Recently, Cohen and co-workers have demonstrated the binding versatility of dipyrrin ligands that incorporate the amide functionality.[7] Reactions involving the complexation of metal halides (CuCl$_2$ or NiCl$_2$) with a diamidodipyrrin ligand demonstrated that metals can choose whether to bind to the amide oxygen or to the deprotonated amide nitrogen as shown in Scheme 5.

For example, the reaction between CuCl$_2$ and the amide-dipyrrin H$_3$X formed the Cu complex [CuCl(H$_2$X)] which shows the coordination of the metal centre in a square pyramidal geometry with the two pyrrin nitrogens and the amide oxygens occupying the equatorial sites and a single chloride anion occupying the axial site. The ligand has been deprotonated a single time and the metal centre retains a d^9 electron count. On the other hand, reaction between H$_3$X and NiCl$_2$ results in the metal centre binding to the doubly deprotonated ligand through three nitrogens (two pyrroles and one

amide) and one amide oxygen with no chloride anion present and the metal has retained its d^8 electron count.
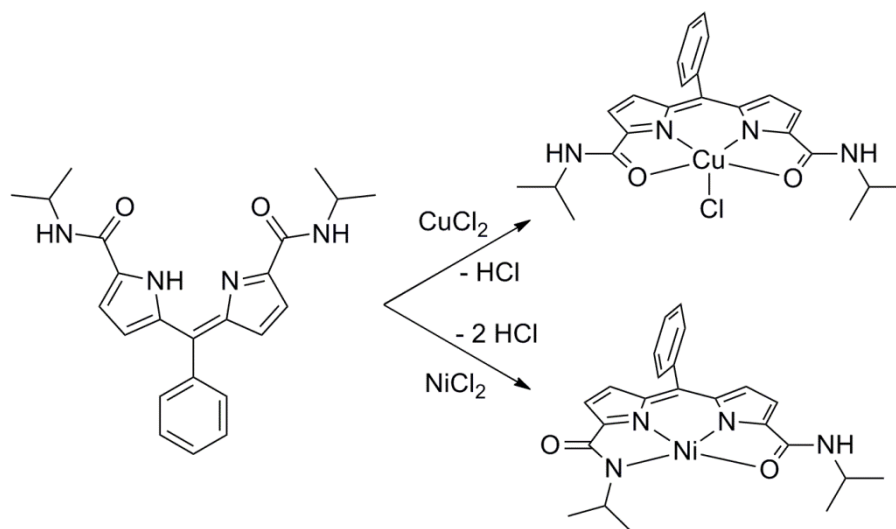
Scheme 5: Coordination of Ni[II] and Cu[II] metal salts with diamidopyrrins as observed by Cohen and co-workers.[7]

The potential of pyrrole-amides towards anion binding has been extensively studied.[8] Their coordination chemistry with transition metals has, however, been relatively overlooked despite the expectation that the amide functionality would alter the electronic and structural properties of complexes.[9] It is also well known that amide ligands are less sensitive to aqueous conditions and compared to H_3L, pyrrole-imine tautomerisation of the ligand into the aza-fulvene cannot be observed. The most likely ligand rearrangement would be the formation of an amino-alcohol through an H-migration from the amide nitrogen to the oxygen.

An amide variant of H_3L was synthesised by forming the trichloroacetyl derivative (H_3L^{CCl3}) of H_3L^a through a preparation adapted from Schmuck and co-workers as described in Scheme 6.[10] Three equivalents of trichloroacetyl chloride were added to H_3L^a at 0°C under a flow of N_2 resulting in the formation of the product as a dark pink powder in a 65 %

yield. The formation of H₃L^{CCl3} was confirmed by ESI-MS and IR spectroscopy by the presence of a molecular ion peak at 659.1 *m/z* and of a C=O stretch at 1642 cm^{-1} respectively. The ^{1}H NMR spectrum shows a broad singlet resonance corresponding to the pyrrole NH at 10.07 ppm as well as two doublet resonances at 7.37 and 6.27 ppm due to the pyrrolic CHs resonances, confirming that the reaction took place at the 5 position.
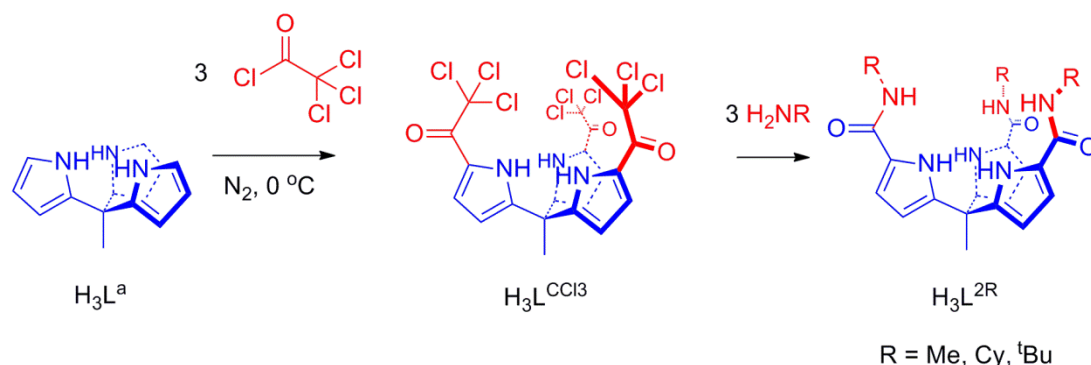
Scheme 6: Synthesis of H₆L^2.

The final step of the overall synthesis required the addition of three equivalents of neat amine to the tricholoroacetyl pyrrole precursor at 0 °C and resulted in the formation of the ligand H₆L^2 in 95 % yield. The formation of H₆L^2 was confirmed by IR spectroscopy with the presence of two separate NH stretches at 3436 and 3288 cm^{-1} for the amide and pyrrole NH and the C=O stretch shifted to 1633 cm^{-1}. The ESI-MS displays a molecular ion peak at 600.8 *m/z* and is concordant with the formation of the ligand.

3.6: Synthesis of titanium hangman complexes [Ti(O^{i}Pr)$_2$(H₄L^{2R})] (R = Me, Cy)

The complexation of Ti^{IV} by pyrrole-imine ligands has been well studied.[11] A recent example includes the synthesis of heterobimetallic Sm^{III}/Ti^{IV} complexes described by Li and co-workers.[12] Having previously reported the use of pyrrolo samarium complexes in polymerization reactions,[13] and knowing that titanium pyrrolo complexes have shown high

catalytic activity for the hydroamination of alkynes;[14] they designed and studied the polymerisation and hydroamination potential of the heterobinuclear complex shown in Scheme 7 (Compound 2).
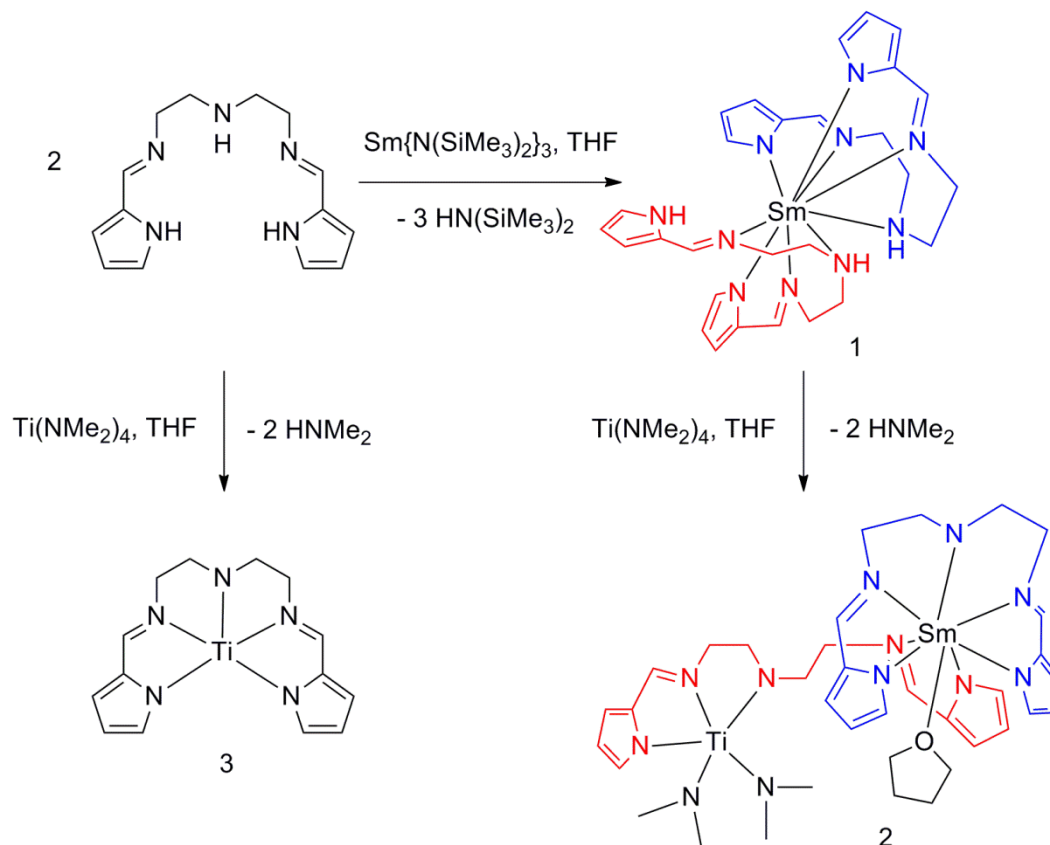
Scheme 7: Synthesis of a Ti-Sm heterobinuclear complex as reported by Li and co-workers.[13]

The hydroamination of phenylacetylene was observed to be catalysed by the binuclear complex (2) in good yield compared to Ti(NMe2)4 and to the titanium complex (3) shown in Scheme (7). Regioselectivity was also improved compared to Ti(NMe2)4 but similar or worse compared to 3 depending on the amine used. The polymerisations of ε-Caprolactone using 1 and 2 were compared and showed that whilst there is little difference between the polymers formed, 2 has higher activity than the mononuclear samarium complex, achieving nearly quantitative yields at much lower temperatures.

Pyrrole-amides can be highly versatile ligands as the oxophilicity of the metal will dictate whether the metal will interact with the carbonyl or the NH group. Despite this, complexation of titanium by pyrrole-amide ligands has not been reported and very few examples exist with other transition metals.[7, 15] As such, $[Ti(O^iPr)_2(H_4L^{2Me})]$ and $[Ti(O^iPr)_2(H_4L^{2Cy})]$ (see below) represent the first two pyrrolo-amido titanium complexes.

The addition of $Ti(O^iPr)_4$ to $H_6L^{2Me/Cy}$ in THF, under an atmosphere of N_2, led to the formation of $[Ti(O^iPr)_2(H_4L^{2Me/Cy})]$ and the elimination of two equivalents of HO^iPr, as shown in Scheme 8, in 66 and 62 % yield for H_6L^{2Me} and H_6L^{2Cy} respectively . Attempts to remove further HO^iPr and fully encapsulate the metal centre proved unsuccessful, even at elevated temperatures.
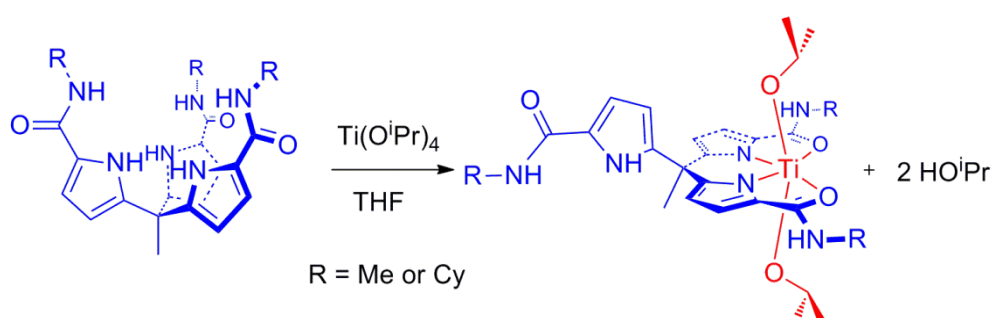
Scheme 8: Synthesis of $[Ti(O^iPr)_2(H_4L^2)]$.

The ^{1}H NMR spectra of both $[Ti(O^iPr)_2(H_4L^{2Me})]$ and $[Ti(O^iPr)_2(H_4L^{2Cy})]$ (Figure 17) confirm the formation of an asymmetric complex similar to that of $[Pd(HL)]$ and $[Pd(H_2L)][Cl]$, displaying two sets of resonances in a 2:1 ratio and supporting the coordination of two arms to the metal centre whilst the third tripodal arm remains pendant.
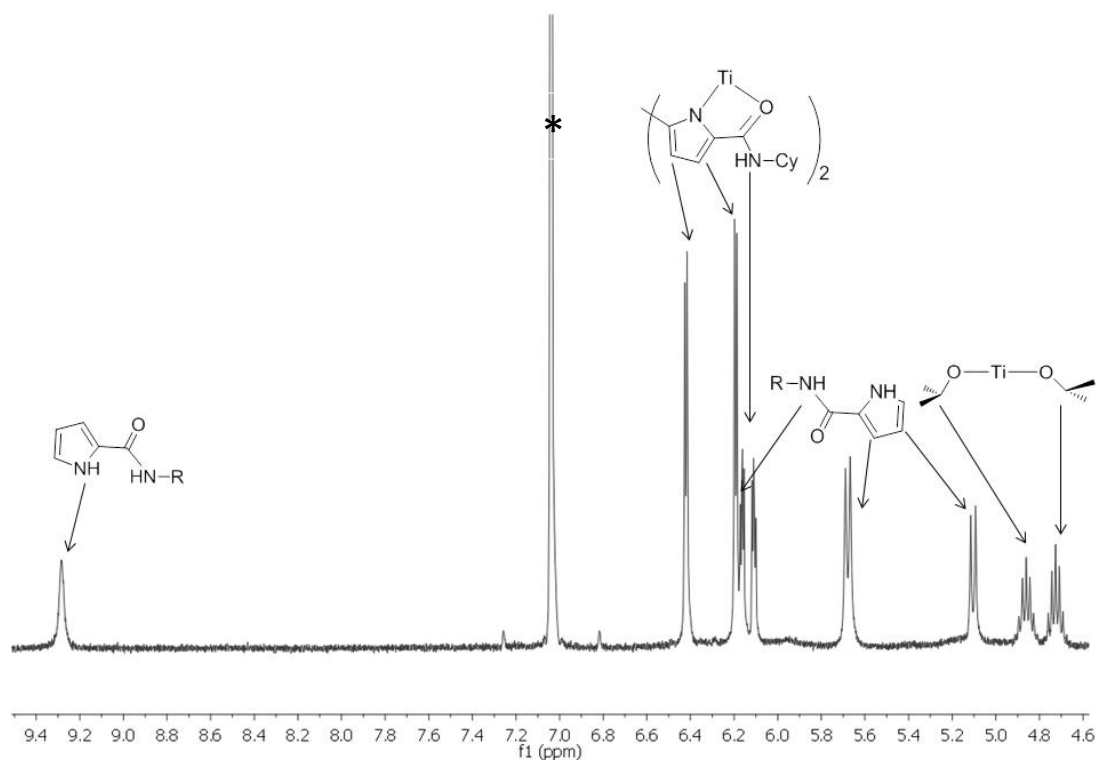
Figure 17: Expansion of the aromatic region of the ^{1}H NMR of [Ti(O^{i}Pr)$_2$(H$_4$L^{2Cy})] in C$_6$D$_6$.

The first set of resonances, corresponding to the two identically bound branches of the complex, contains two pyrroles and a single NH resonance at 6.57, 6.02 and 7.07 ppm and 6.65, 6.42 and 6.36 ppm for [Ti(O^{i}Pr)$_2$(H$_4$L^{2Me})] and [Ti(O^{i}Pr)$_2$(H$_4$L^{2Cy})] respectively. This latter resonance indicates that the pyrroles have been deprotonated and are now binding to the metal centre whilst the amide nitrogens are not partaking in ligand-metal interactions. The four ^{1}H NMR resonances corresponding to the pendant arm of the tripod are observed at 6.25 and 5.82 ppm for the pyrrolic resonances and 8.57 and 6.29 ppm for the two separate NHs in [Ti(O^{i}Pr)$_2$(H$_4$L^{2Me})] and 5.90, 5.33, 9.32 and 6.36 ppm for the corresponding resonances in [Ti(O^{i}Pr)$_2$(H$_4$L^{2Cy})]. The presence of both NHs in the spectrum confirms that this branch is not taking part in metal-ligand coordination. Additionally, two set of isopropyl resonances are observed in each complex at 4.65, 4.53, 1.16 and 1.00 ppm and

5.08, 4.95, 1.35 and 1.20 ppm in [Ti(O^{i}Pr)$_2$(H$_4$L^{2Me})] and [Ti(O^{i}Pr)$_2$(H$_4$L^{2Cy})] respectively. These multiple resonances arises, as in [Pd(H$_2$L)][Cl], from a de-symmetrisation of the complex by the pendant arm. The IR spectra show two separate C=O stretches at 1591 and 1540 cm^{-1} and 1600 and 1558 cm^{-1} in [Ti(O^{i}Pr)$_2$(H$_4$L^{2Me})] and [Ti(O^{i}Pr)$_2$(H$_4$L^{2Cy})] respectively. This does not necessarily indicate asymmetry and could also be caused by symmetric and asymmetric stretches of the bound carbonyls which could be overlapping with the pendant carbonyl stretch.

Slow cooling of a saturated solution of [Ti(O^{i}Pr)$_2$(H$_4$L^{2Me})] in MeCN resulted in the formation of crystalline material suitable of X-ray diffraction studies. The solid state structure was determined and is shown in Figure 18, with selected bond lengths and angles detailed in Table 4 and crystal data in Table Ch3 Tab2. The solid state structure of [Ti(O^{i}Pr)$_2$(H$_4$L^2)] shows that the metal centre adopts a distorted octahedral geometry. Two branches of H$_6$L^2 occupy the equatorial binding sites of the Ti^{IV} anion through the pyrrolide nitrogen (Ti1-N1 = 2.05(2) Å) and the amide oxygens (Ti1-O1 = 2.07(3) Å). This binding motif is preferred from one that would see a binding through the amide nitrogens due to the oxophilicity of titanium. The two axial binding sites are occupied by two isopropoxide ligands which have not been removed during the reaction (Ti-O4 = 1.78(2) Å).

The third branch of H$_6$L^{2Me} is turned away from the metal centre, but as with [Pd(HL)], it is not co-planar with the plane defined by Ti1, C1 and C2; instead, a torsion angle set by Ti1, C2, C15 and N5 is of 124.9 °. This can only be explained by steric interactions between the unbound pyrroles and the methyl constituting the base of the tripod.
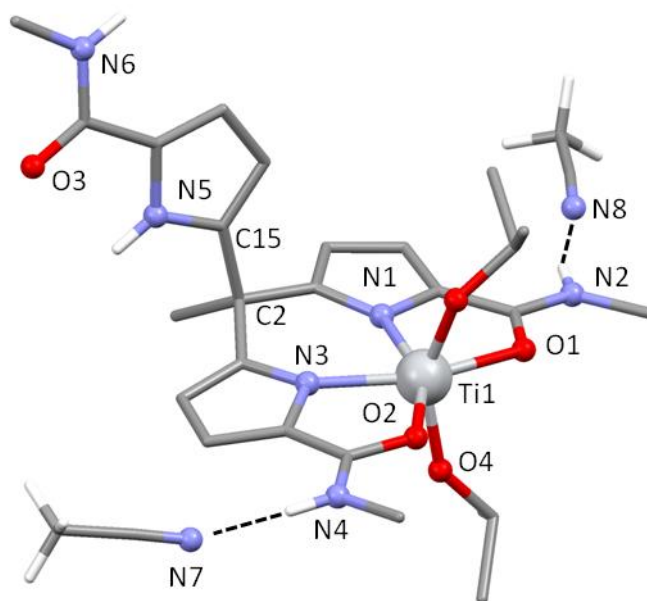
Figure 18: X-Ray crystal structure of [Ti(O^{i}Pr)$_2$(H$_4$L^{2Me})]. For clarity, all hydrogens not partaking in H···Cl interactions are omitted.

Ti1-N1	2.05(2)	O4-Ti1-O5	150.3(2)
Ti1-N3	2.06(2)	N1-Ti1-O2	155.7(1)
Ti1-O1	2.07(2)	N1-Ti1-O1	76.1(2)
Ti1-O2	2.11(2)	O1-Ti1-O2	128.1(1)
Ti1-O4	1.78(2)	N1-Ti1-O5	104.2(2)
Ti1-O5	1.81(2)	O1-Ti1-O5	84.4(2)
Ti1···C2-C15-N5	124.9	N1-Ti1-N3	79.3(2)

Table 4: Selected bond lengths (Å) and angles (°) of [Ti(O^{i}Pr)$_2$(H$_4$L^{2Me})].

In the extended structure, the amide NHs are partaking in hydrogen bonding interactions with the nitrogen atom of acetonitrile solvent molecules (N4···N8, 3.05(3) Å and N2···N7, 2.93(3) Å). The pendant arm of the ligand interacts through hydrogen bonding interactions with the unbound arm of two neighbouring complexes as shown in Figure 19. The carbonyl group (O3) and amide NHs (N6') of proximate molecules are separated by 2.79(5) Å.
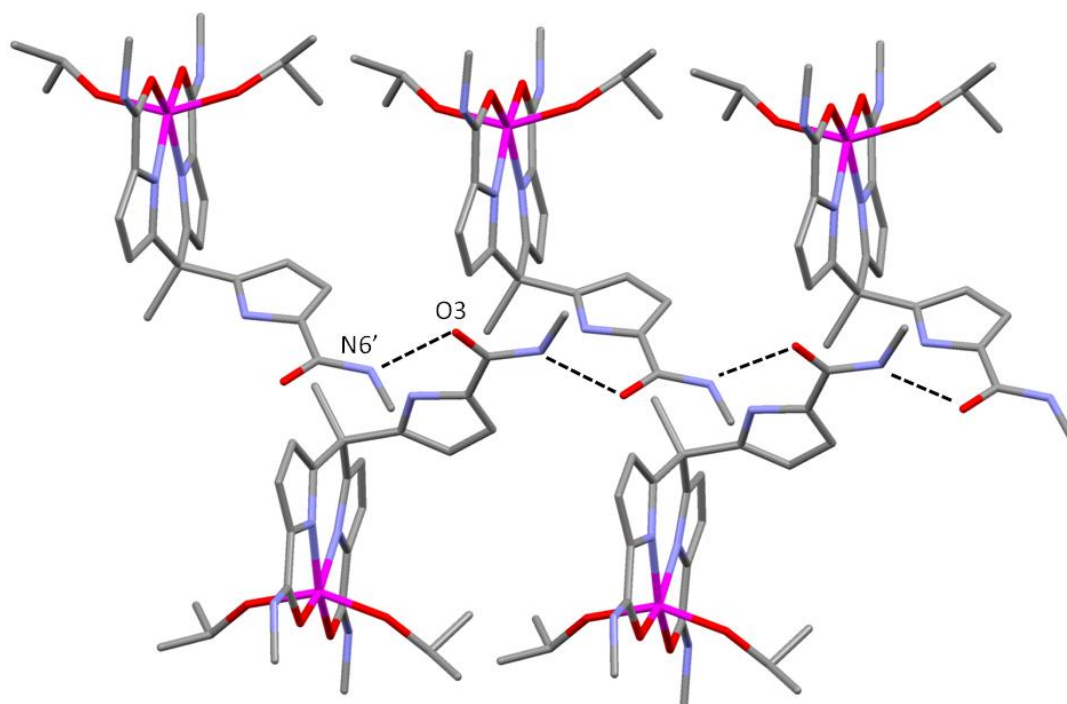
Figure 19: Extended X-ray crystal structure of [Ti(O^{i}Pr)$_2$(H$_4$L^{2Me}) showing the hydrogen bonding interactions between the amide groups of neighbouring complexes. MeCN molecules and hydrogen atoms omitted for clarity

3.7: Anion binding studies of H$_6$L^{2Cy}.

Anion binding receptors play a central role in many fields of chemistry from pollutant detection to transportation of anions through cell membranes.[16] Loeb and co-workers have studied the anion binding capabilities of a tetrapodal Pt^{II} complex.[17] Although addition of di-hydrogen phosphate and sulphate anion resulted in the expected encapsulation of the tetrahedral species in a 1:1 ratio, this is not the case with spherical halide anions. With spherical guests, the tetrapod forms a 2:1 guest host complex in which each halide coordinates, through hydrogen bonds to the urea groups of two separate arms of the host, on opposite sides of the metal centre as displayed in Figure 20. Although it shows a 1,3 alternate structure, the 1,2 alternate has also been observed.
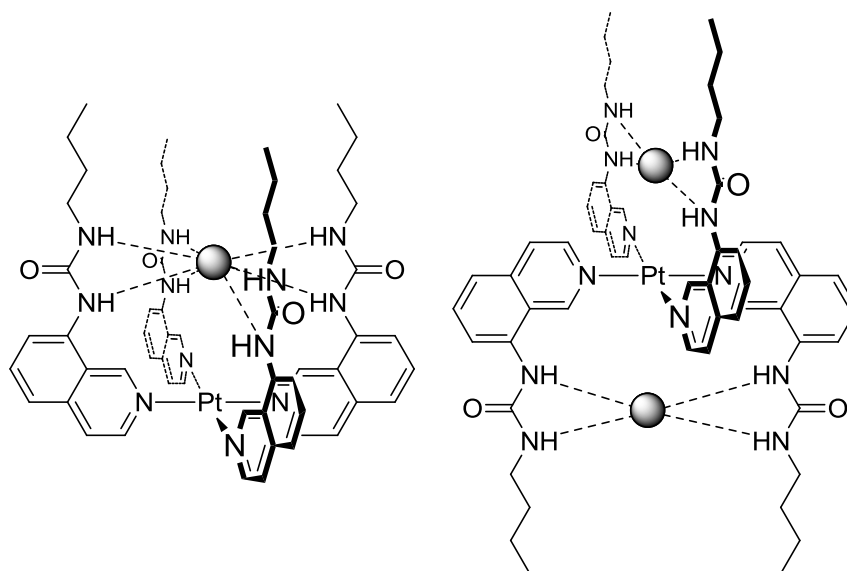
Figure 20: Full encapsulation and "two up, two down" binding motif adopted by the complex reported by Loeb and co-workers with tetrahedral (left) and spherical (right) anions respectively. All anions represented as spheres for clarity.[17]

The result of these difference in terms of encapsulation of guest as well as the number of donors interactions between the host and the guest result in a vast spread of stability constants. Unsurprisingly the 1,3 alternate complexes shows the lowest stability constant (as small as 52 M^{-1} for I^-) which can be explained by longer hydrogen bonds compare to those that would be expected in the 1,2 alternate. The full encapsulation of the tetrahedral anions results in values of K upwards from 10^5 which are the result of the host using all four arms to bind to a single anion.

The combined presence of numerous hydrogen bond acceptors and donors on the ligand as well as the propensity of H_3L to encapsulate small molecules such as water, lead to an investigation of the anion binding potential of H_6L^{2Cy}.

Determining the stoichiometry of the chemical equilibrium of reactions in solution can be done through a variety of techniques such as the slope ratio method and the mole ratio method.[18] Job's method of continuous

variations is, however, the most widely used due to its simplicity.[19] It involves determining the coefficients *a, b* and *c* in the following equation where H_6L^2 and A^- are the free ligand and anion and $(H_6L^2)_aA^-_b$ is the product formed by the complexation of H_6L^2 with the anion.[20]

$$a\ H_6L^2 + b\ A^- \rightleftharpoons c\ (H_6L^2)_aA^-_b$$
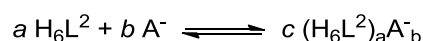
As the ratio of A^- for any one H_6L^2 is to be calculated, the previous equation can be written as:

$$H_6L^2 + k\ A^- \rightleftharpoons m\ (H_6L^2)_aA^-_b$$
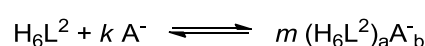
where k = b/a and m = c/a

If a series of solutions is prepared, each containing the same total number of moles of H_6L^2 and A^- but a different mole fraction *f* of H_6L^2 to A^-, the maximum amount of product $(H_6L^2)_aA^-_b$ is obtained in a solution in which *f* = *k* (stoichiometric ratio). Following the first part of this statement, then the mole fraction x of H_6L^2 and A^- can be written as below:

$$\text{moles of } H_6L^2 = a = x$$

$$\text{moles of } A^- = b = 1 - x$$

Therefore:

$$f = \frac{1 - x}{x}$$

After measurements, one plots the number of moles of product *c* against *f*. When *f* > *k*, H_6L^2 is limiting reagent; as *f* decreases, *c* increases until *f* = *k* with *c* given by the following relationship:

$$c = mx$$

Alternatively, when $f < k$, A⁻ is limiting reagent; as f increases, c decreases until $f = k$ and this time c can be expressed by the following equation:

$$c = m\frac{1-x}{k}$$

A plot of both equations over a series of sample should give two lines of which the intersection is the point where $f = k$. The intersection can be expressed in terms of x by solving the following equation:

$$mx = m\frac{1-x}{k}$$

$$\Leftrightarrow kx = 1 - x$$

$$\Leftrightarrow k = \frac{1}{x} - 1$$

$$\Leftrightarrow x(1+k) = 1$$

$$\Leftrightarrow x = \frac{1}{1+k}$$

Therefore:

$$f = \frac{1-x}{x} = \frac{1 - \frac{1}{1+k}}{\frac{1}{1+k}} = k$$

The concentration of the complex can be measured by any parameter proportional to the concentration such as UV/vis or an NMR integral if the system is under slow exchange conditions and two distinct chemical shifts can be observed for the starting material and the product. If the system exchanges rapidly, a single signal will be observed in the ¹H NMR spectrum at an averaged chemical shift[21]

$$\delta_{obs} = f_{sm}\delta_{sm} + f_p\delta_p$$

where f represents the mole fraction, *sm* is starting material and p is product.

Since $f_{sm} = 1 - f_p$, the previous equation can be rewritten as:

$$\delta_{obs} = f_{sm}\delta_{sm} + (1 - f_{sm})\delta_p = f_{sm}(\delta_{sm} - \delta_p) + \delta_p$$

$$f_{sm} = \frac{\delta_{obs} - \delta_p}{\delta_{sm} - \delta_p}$$

The concentration of product is therefore given by:

$$[host]f_{sm} = [host]\frac{\delta_{obs} - \delta_p}{\delta_{sm} - \delta_p}$$

The interactions between H_6L^2 and spherical anions such as halides and trigonal planar anions such as acetates have been studied. Unfortunately, tetrahedral anions could not be represented as the host-guest adduct formed during the reaction was insoluble and hence no data were available for the construction of a Job plot. Comparison between spherical and trigonal planar anions should establish whether the binding motif is geometry dependent. Size dependence was also investigated through the study of multiple halides (F^-, Cl^-, Br^- and I^-). The Job plot representation of the acetate anion (displayed in Figure 21) shows an apex at 0.5 mole fraction of ligand. This is translated as the formation of 1:1 anion to ligand complex. The lack of asymmetry in the ^1H NMR spectrum upon addition of TBAOAc to H_6L^2 suggests that the anion interacts with the ligand in a similar manner to $H_3L.H_2O$ and is fully encapsulated.
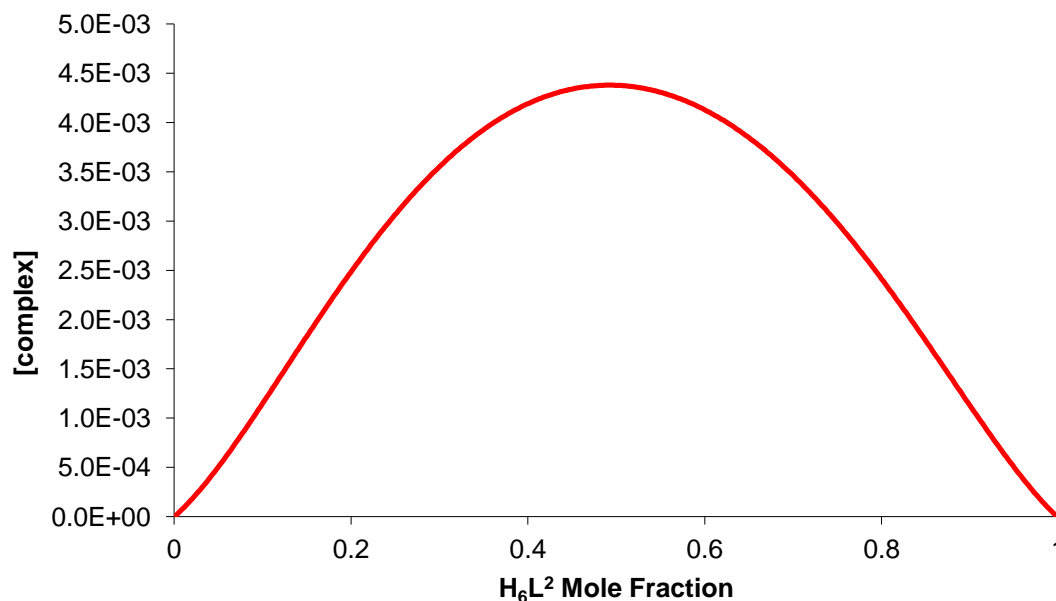
Figure 21: Job Plot of TBAOAc

The Job plot of the halide series, displayed in Figure 22, shows that in solution, the chloride, bromide and iodide anion all preferentially form 1:1 complexes with H_6L^{2Cy}. It is reasonable to assume that these complexes are of a form similar to that of $H_3L.H_2O$ and that the anion is fully encapsulated by the ligand. H_6L^{2Cy} shows an uptake of 1.5 fluoride anions per ligand. A potential structure for this uptake involves two hangman H_6L^{2Cy} fluoride complexes linked together through a hydrogen bonding interactions between the pendant arm of each complex and a third fluoride anion as displayed in Figure 23.
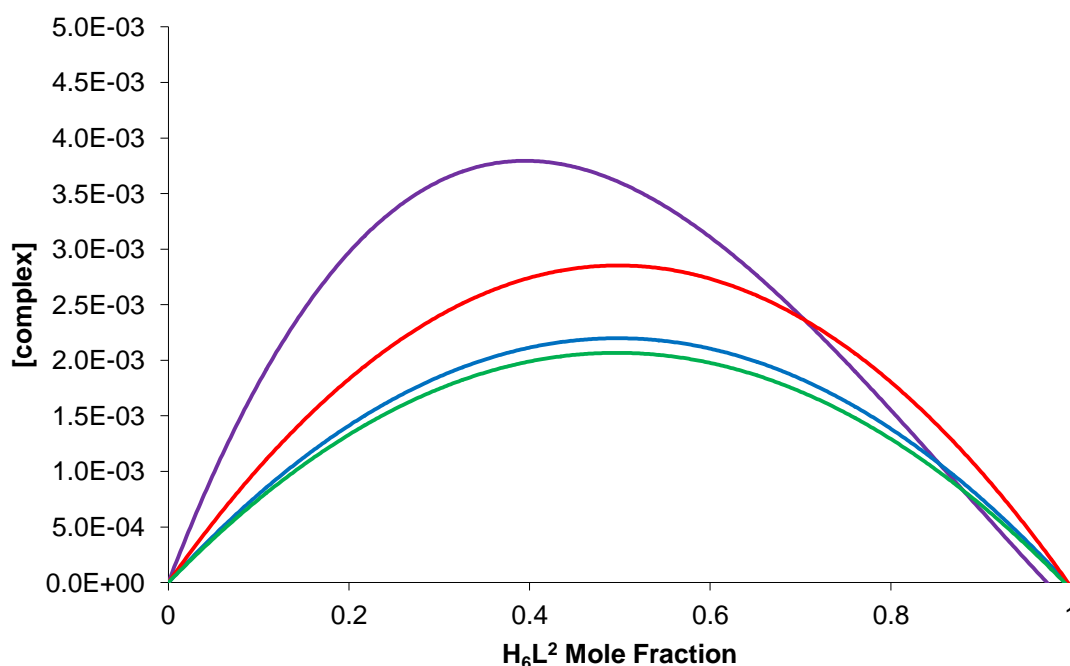
Figure 22: Job plot of the halide series (F⁻: purple; Cl⁻: blue; Br⁻: red; I⁻: green).
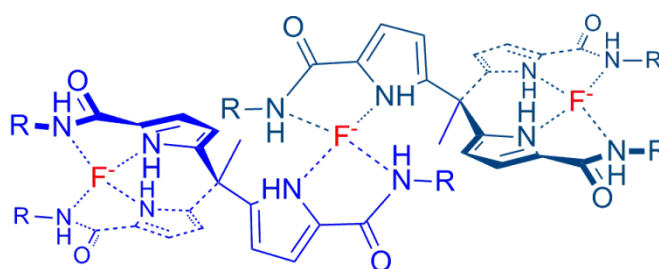
Figure 23: Plausible form for the 2:3 H_6L^{2Cy} to fluoride complex.

Slow diffusion of hexane into a saturated dioxane solution of 1:1 H_6L^{2Cy} and TBACl resulted in the formation of crystalline material suitable of X-ray diffraction studies. The solid state structure was determined and is shown in Figure 24, with selected bond lengths and angles detailed in Table 5 and crystal data in Table Ch3 Tab2. Although the above liquid state, anion-binding studies shows the propensity of 1:1 binding between spherical anions and H_6L^2, possibly encapsulated in the same manner as seen in $H_3L.H_2O$, the solid state structure shows the ligand partakes in hydrogen bonding interactions with three chloride anions. Each branch of the tripod

interacts with a single anion through both the pyrrole and amide NHs (3.285 and 3.221 Å respectively). This structure is surrounded by three tetrabutylamine counter anions. The molecule has a C_3 point group (C3-C2-C25, 111.2(2)°) in the solid state and each branch is angled such that the H_6L^2 takes a propeller-like shape (N1-C3···C14-N3, 99.43°).
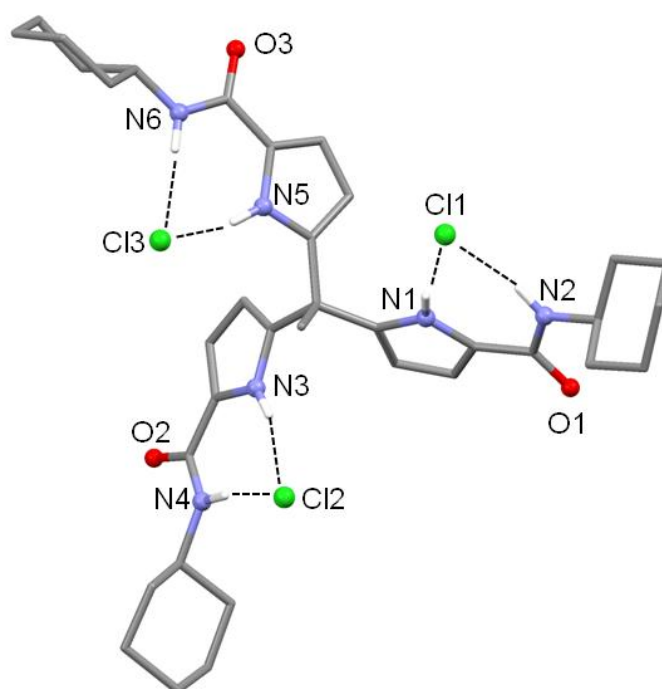
Figure 24: X-Ray crystal structure of $H_6L^{2Cy}(Cl)_3(TBA)_3$. TBA molecules omitted for clarity

N1···Cl1	3.285	C7-N2	1.350(4)
N2···Cl1	3.221	C3-C2-C25	111.2(2)
O1-C7	1.231(3)	N1-C3···C14-N3	99.43

Table 5: Selected bond lengths (Å) and angles (°) of $H_6L^{2Cy}(Cl)_3(TBA)_3$.

The anion binding properties of tripodal ligands has been investigated by numerous research groups.[22] Bowman-James and co-workers have developed acyclic TREN derived anion receptors (as shown in Figure 25 left) and studied their binding selectivity for different anions.[23] *N, N', N''*-Tris(2-benzylaminoethyl)amine (H₃Z), displayed in Figure 25 right, has shown similar anion binding properties to those displayed by H_6L^2.

R =

R' = alkyl or aromatic substituents
X = O, S
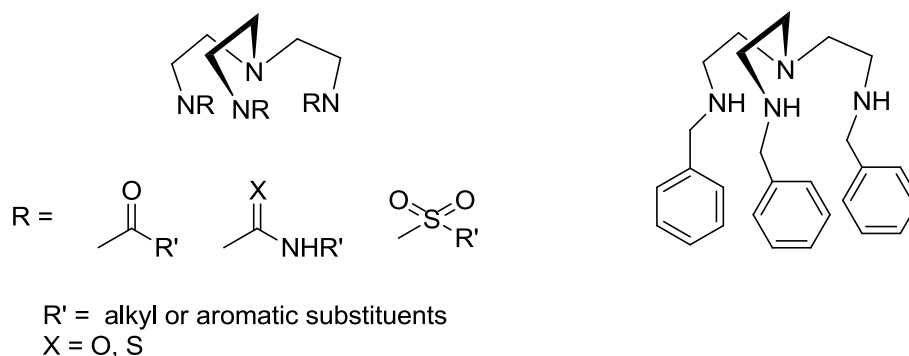
Figure 25: TREN derived ligands developed by Bowman-James and co-workers as anion receptors (left) and *N, N', N''*-Tris(2-benzylaminoethyl)amine (H$_3$Z) which displays similar properties to H$_6$L^2 (right).[23]

^{1}H NMR studies indicated a 1:1 host guest association with anions of various geometries such as spherical halides, tetrahedral phosphate and trigonal planar nitrate. However, in the solid state, the crystal structures of the phosphate and bromide salts showed the formation of 3:1 anion to ligand complexes. [H$_3$Z][Br]$_3$ (Figure26) displays a structure not dissimilar to that of [Pd(H$_2$L)][Cl].
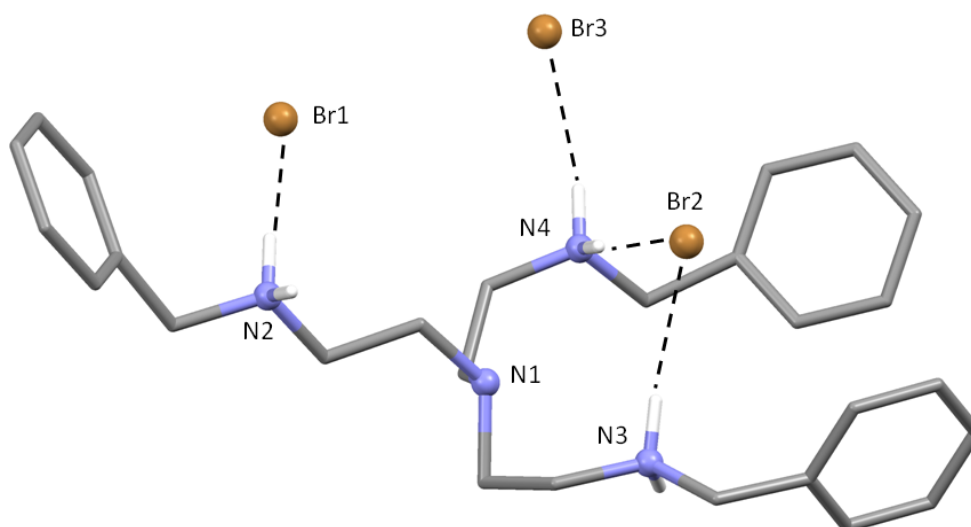
Figure 26: X-Ray crystal structure of [H$_3$Z][Br]$_3$ synthesised by Bowman-James and co-workers. All hydrogens not partaking in Hydrogen bonding interactions are omitted for clarity.

Two arms are partaking in hydrogen-bonding interactions with a central bromide anion whilst a second bromide is located on the outer side of

this pocket interacting with a single branch of the ligand. The third arm is rotated away from the central pocket and partakes in hydrogen-bonding interactions with the final anion.

The solid state crystal structure of the phosphate salt displayed in Figure 27 showed that not only each branch interacts with a single phosphate anion through a hydrogen-bond but also with a central phosphoric acid molecule formed by the presence of acid within the crystallisation medium. The latter prevents the formation of a hangman type structure in [H$_3$Z][H$_2$PO$_4$]$_3$.H$_3$PO$_4$.
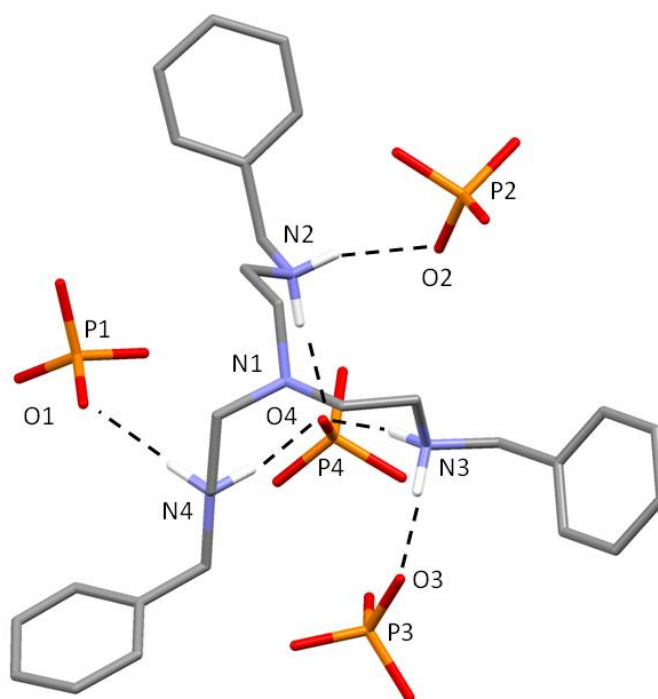
Figure 27: X-Ray crystal structure of [H$_3$Z][H$_2$PO$_4$]$_3$ observed by Bowman-James and co-workers. All hydrogens not partaking in Hydrogen bonding interactions are omitted for clarity.

3.8: Conclusion

The new mono-metallic, mono-ligand complexes [Cu(HL)] and [Pd[HL] have been synthesised by the addition of Group 10 and 11 transition metals (Pd^{II} and Cu^{II}) to the tripodal pyrrole-imine ligand H$_3$L.

Tautomerisation of the ligand into the aza-fulvene was not observed when using these metals, and square planar or square pyramidal geometries were favoured. The two arms of the ligand chelating to the metal centre are deprotonated whilst the third branch is pendant, resulting in a hangman structure. The type of metal precursor used also influenced the overall shape of the complex. The addition of $PdCl_2$ or $CuCl_2$ to H_3L resulted in the formation of the ion pairs $[CuCl(H_2L)]$ and $[Pd(H_2L)][Cl]$ due to the uptake of HCl formed during the reaction. In both cases, the pendant arm is protonated at the imine nitrogen and is hydrogen bonding with the chloride anion. $[CuCl(H_2L)]$ is observed as a contact ion pair in which the chloride anion binds to the metal centre whereas $[Pd(H_2L)][Cl]$ is seen as a host separated ion pair with the pendant arm rotated away from Pd^{II}. Although the redox chemistry of $[Cu(HL)]$, $[Pd[HL]$, $[CuCl(H_2L)]$ and $[Pd(H_2L)][Cl]$ was investigated, most significant observations involved the formation of Cl_2 and H_2 from the incorporated HCl within $[CuCl(H_2L)]$ and $[Pd(H_2L)][Cl]$.

New tripodal pyrrole-amide ligands (H_6L^2) were synthesised in good yields from readily available precursors. Reactions with Ti^{IV} resulted in the formation of hangman complexes with two arms of the ligand occupying the equatorial sites of the octahedral metal centre through the pyrrole nitrogen and amide oxygen donors. The axial sites have retained the isopropoxide groups present in the metal precursor. The anion binding potential of H_6L^{2Cy} was investigated and showed in solution the formation of 1:1 anion to ligand complexes for trigonal planar and spherical anions except fluoride which showed the formation of a 3:2 anion to ligand complex. In the solid state however, the formation of a 3:1 anion to ligand complex is observed with chloride anions.

3.9: References

[1]   R. L. Shook, A. S. Borovik, *Chem. Commun.* **2008**, *46*, 6095-6107; D. Natale, J. C. Mareque-Rivas, *Chem. Commun.* **2008**, *4*, 425-437; P. W. N. M. Van Leeuwen, Z. Freixa, in *Supramolecular Catalysis*, Wiley-VCH Verlag GmbH & Co. KGaA, **2008**, 255-299.

[2]   A. D. Wilson, R. K. Shoemaker, A. Miedaner, J. T. Muckerman, D. L. DuBois, M. R. DuBois, *PNAS* **2007**, *104*, 6951-6956; S. Fukuzumi, *Chem. Lett.* **2008**, *37*, 808-813; E. E. Benson, C. P. Kubiak, A. J. Sathrum, J. M. Smieja, *Chem. Soc. Rev.* **2009**, *38*, 89-99; C. Finn, S. Schnittger, L. J. Yellowlees, J. B. Love, *Chem. Commun.* **2012**, *48*, 1392-1399.

[3]   J. Stubbe, D. G. Nocera, C. S. Yee, M. C. Y. Chang, *Chem. Rev.* **2003**, *103*, 2167-2202; S.-Y. Liu, D. G. Nocera, *J. Am. Chem. Soc.* **2005**, *127*, 5278-5279; D. K. Dogutan, D. K. Bediako, T. S. Teets, M. Schwalbe, D. G. Nocera, *Org. Lett.* **2010**, *12*, 1036-1039; R. McGuire Jr, D. K. Dogutan, T. S. Teets, J. Suntivich, Y. Shao-Horn, D. G. Nocera, *Chem. Sci.* **2010**, *1*, 411-414; D. K. Dogutan, S. A. Stoian, R. McGuire, M. Schwalbe, T. S. Teets, D. G. Nocera, *J.Am.Chem. Soc.* **2010**, *133*, 131-140.

[4]   K. M. Kadish, L. Frémond, Z. Ou, J. Shao, C. Shi, F. C. Anson, F. Burdet, C. P. Gros, J.-M. Barbe, R. Guilard, *J. Am. Chem. Soc.* **2005**, *127*, 5625-5631; J. P. Collman, M. Kaplun, R. A. Decreau, *Dalton Trans.* **2006**, *4*, 554-559; G. Givaja, M. Volpe, M. A. Edwards, A. J. Blake, C. Wilson, M. Schröder, J. B. Love, *Angew. Chem. Int. Ed.* **2007**, *46*, 584-586; K. M. Kadish, J. Shen, L. Frémond, P. Chen, M. E. Ojaimi, M. Chkounda, C. P. Gros, J.-M. Barbe, K. Ohkubo, S. Fukuzumi, R. Guilard, *Inorg. Chem.* **2008**, *47*, 6726-6737.

[5]   D. K. Dogutan, R. McGuire, D. G. Nocera, *J. Am. Chem. Soc.* **2011**, *133*, 9178-9180.

[6]   S. K. Kim, J. L. Sessler, *Chem. Soc. Rev.* **2010**, *39*, 3784-3809.

[7]   V. S. Thoi, J. R. Stork, E. T. Niles, E. C. Depperman, D. L. Tierney, S. M. Cohen, *Inorg. Chem.* **2008**, *47*, 10533-10541.

[8]   P. A. Gale, *Chem. Commun.* **2005**, 3761-3772.

[9]   H. Golchoubian, O. Nazari, B. Kariuki, *Inorg. Chim. Acta* **2010**, *363*, 2673-2676; J. Singh, G. Hundal, R. Gupta, *Eur. J. Inorg. Chem.* **2009**, *2009*, 3259-3265.

[10]   C. Schmuck, V. Bickert, M. Merschky, L. Geiger, D. Rupprecht, J. Dudaczek, P. Wich, T. Rehm, U. Machon, *Eur. J. Org. Chem.* **2008**, *2008*, 324-329.

[11]   M. Volpe, S. D. Reid, A. J. Blake, C. Wilson, J. B. Love, *Inorg. Chim. Acta* **2007**, *360*, 273-280; J. B. Love, *Chem. Commun.* **2009**, 3154-3165; A. Novak, A. J. Blake, C. Wilson, J. B. Love, *Chem. Commun.* **2002**, 2796-2797; Y. Yoshida, S. Matsui, Y. Takagi, M. Mitani, T. Nakano, H. Tanaka, N. Kashiwa, T. Fujita, *Organometallics* **2001**, *20*, 4793-4799; eF. Zhang, H. Song, G. Zi, *J. Organomet. Chem.* **2010**, *695*, 1993-1999.

[12]   F. Zhou, M. Lin, L. Li, X. Zhang, Z. Chen, Y. Li, Y. Zhao, J. Wu, G. Qian, B. Hu, W. Li, *Organometallics* **2011**, *30*, 1283-1286.

[13]   L. Xiang, Q. Wang, H. Song, G. Zi, *Organometallics* **2007**, *26*, 5323-5329.

[14]   G. Zi, X. Liu, L. Xiang, H. Song, *Organometallics* **2009**, *28*, 1127-1137.

[15]   G. W. Bates, P. A. Gale, M. E. Light, M. I. Ogden, C. N. Warriner, *Dalton Trans.* **2008**, 4106-4112; bJ. Singh, G. Hundal, R. Gupta, *Eur. J. Inorg. Chem.* **2009**, *2009*, 3259-3265.

[16]   P. A. Gale, *Chem. Commun.* **2011**, *47*, 82-86; A. Ojida, I. Takashima, T. Kohira, H. Nonaka, I. Hamachi, *J. Am. Chem. Soc.* **2008**, *130*, 12095-12101; Y. Kim, F. o. P. Gabbaï, *J. Am. Chem. Soc.* **2009**, *131*, 3363-3369; A. P. Davis, D. N. Sheppard, B. D. Smith, *Chem. Soc. Rev.* **2007**, *36*, 348-357; T. M. Fyles, *Chem. Soc. Rev.* **2007**, *36*, 335-347; D.-W. Yoon, D. E. Gross, V. M. Lynch, C.-H. Lee, P. C. Bennett, J. L. Sessler, *Chem. Commun.* **2009**, 1109-1111; M. Arunachalam, P. Ghosh, *Org. Lett.* **2009**, *12*, 328-331; S. K. Kim, D. E. Gross, D.-G. Cho, V. M. Lynch, J. L. Sessler, *J. Org. Chem.* **2010**, *76*, 1005-1012.

[17]   C. R. Bondy, P. A. Gale, S. J. Loeb, *J. Am. Chem. Soc.* **2004**, *126*, 5030-5031.

[18]   A. E. Harvey, D. L. Manning, *J. Am. Chem. Soc.* **1950**, *72*, 4488-4493; J. H. Yoe, A. L. Jones, *Ind. Eng. Chem. Anal. Ed.* **1944**, *16*, 111-115.

[19]   W. C. Vosburgh, G. R. Cooper, *J. Am. Chem. Soc.* **1941**, *63*, 437-442; J. Jiang, M. J. MacLachlan, *Chem. Commun.* **2009**, 5695-5697; S. Upadhyay, G. Kumar, *Chem. Cent. J.* **2009**, *3*, 9-18; P. Job, *Ann. Chim.* **1928**, *9*, 113-134.

[20]   E. J. Olson, P. Bühlmann, *J. Org. Chem.* **2011**, *76*, 8406-8412; P. MacCarthy, *Anal. Chem.* **1978**, *50*, 2165-2165.

[21]   R. S. Macomber, *J. Chem. Educ.* **1992**, *69*, 375.

[22]   B. Kuswandi, N. N/a, W. Verboom, D. Reinhoudt, *Sens.* **2006**, *6*, 978-1017; W. A. Quinn, M. A. Saeed, D. R. Powell, M. A. Hossain, *Int. J. Environ. Res. Public Health* **2010**, *7*, 2057-2070; H. Ihm, S. Yun, H. G. Kim, J. K. Kim, K. S. Kim, *Org. Lett.* **2002**, *4*, 2897-2900; S. Valiyaveettil, J. F. J. Engbersen, W. Verboom, D. N. Reinhoudt, *Angew. Chem. Int. Ed.* **1993**, *32*, 900-901; P. D. Beer, Z. Chen, A. J. Goulden, A. Graydon, S. E. Stokes, T. Wear, *J. Chem. Soc., Chem. Commun.* **1993**, 1834-1836; P. D. Beer, P. K. Hopkins, J. D. McKinney, *Chem. Commun.* **1999**, 1253-1254.

[23]   M. A. Hossain, J. A. Liljegren, D. Powell, K. Bowman-James, *Inorg. Chem.* **2004**, *43*, 3751-3755.

Chapter 4: Chlorometallate and palladium cluster complexes of wide-span diimine and diamine ligands

4.1 Introduction

The formation of ligands capable of promoting the assembly of multiple metal cations into precise arrangements such as metallo-cycles, metallo-cryptands and metallo-capsules is of great interest. These motifs can have an impact on a wide range of chemical topics, including catalysis.[1] Mirkin and co-workers have demonstrated, with a metallo-cycle complex containing four binding sites, how these arrangements can lead to catalysts that can be switch on and off (Figure 1).[2] Two binding sites are used as structural domains and contain two Rh^I cations linking the two sides of the metallo-cycle. The other two binding sites are used as catalytic domains, each containing a Zn^{II} metal centre. This complex has been shown to have the capacity to catalyse the acyl transfer reaction between acetic anhydride and pyridyl carbinol to form 4-acetoxymethylpyridine and acetic acid.
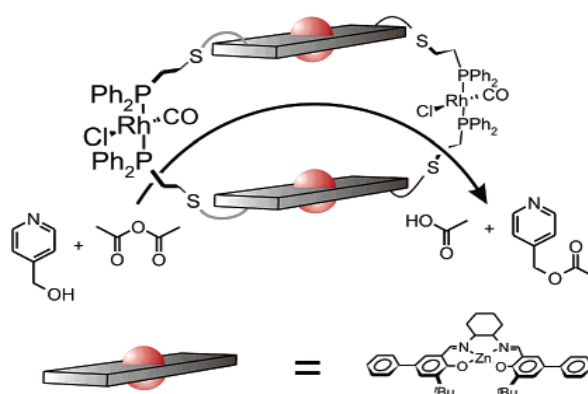
Figure 1: Multimetallic metallo-cycles catalyst designed by Mirkin and co-workers.[2]

Although in Figure 1, the catalyst is shown in a reactive form, it first presents in its "switched off" form where the sulphur donors replace the

carbonyl and chloride ligands on the rhodium cation. This brings the two catalytic domains closer and halts the catalytic cycle. Addition of CO gas in the presence of chloride anion breaks the sulphur metal bonds moving the zinc metal centres further apart, and switching the reaction on.

Other highly ordered complexes such as metallo-enzymes have been observed in the field of bio-inorganic chemistry.[3] Babcock and Wilkstrom described the transformation of O_2 into H_2O across the inner mitochondrial membrane, or the cell membrane in prokaryotes.[4] This reduction is achieved by the bimetallic haem iron-copper reaction centre within cytochrome oxidases, such as that displayed in Figure 2. Dioxygen is sandwiched between an octohedral haem iron, with its remaining axial site occupied by a histidine, and a tetrahedral copper metal centre ligated to three histidines and its last binding site free to interact with O_2. The introduction of electrons and protons into the binuclear centre results in the formation of two water molecules. The method employed by enzyme to carry such a reaction is still under investigation due to very rapid reduction of O_2 (<0.2 ms) which prevents the study of reaction intermediates with current technologies.
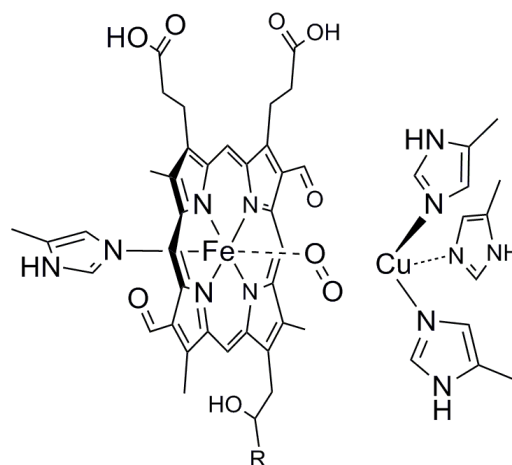
Figure 2: Bimetallic haem iron-copper reaction centre in cytochrome oxidases with O_2 bound.[4]

A vast array of arranged multimetallic complexes with application to medicine have been described by Therrien and co-workers.[5] These can have numerous uses ranging from diagnostic agents for MRI to chelation therapy. A particular example is that depicted by Vincent and co-workers in which the trinuclear complex $[Cr_3O(O_2CCH_2CH_3)_6(H_2O)_3]^+$ is formed from the self-assembly of three Cr^{III} cations and six propionate anions (Figure 3).[6] This complex, first synthesised by Earnshaw and co-workers for its magnetic properties, has been found to activate the tyrosine kinase activity of insulin receptor proteins.[7] It comprises of a planar triangular arrangement of chromium ions surrounding a central μ_3-oxide. The metal centres are linked to one another through two bridging carboxylate ligands and their coordination spheres are completed by water molecules. Investigation into the complex's activation of insulin receptors showed that the ligands play an important role. Indeed, if the ligands are acetates, the activation is inhibited whereas if they are propionate the activation is stimulated by 100 %. This clearly demonstrates the difficulties of the "lock and key principle" and the issues surrounding the release of substrate within the reaction medium. The acetate complex is a very good fit to the receptors, is preferentially bound and inhibits the reaction whereas the propionate complex which is not as good a fit, is released into the reaction medium.
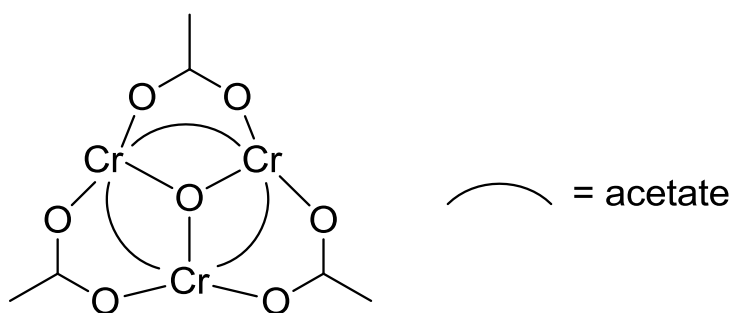
Figure 3: Earnshaw and co-workers chromium complex.[7]

Last but not least, ordered self-assembled multimetallic complexes have been widely used in the field of single molecule magnetism. These complexes, commonly referred to as SMMs, are generally rich in metal centres that can easily adopt different oxidation states.[8]. The first example of a SMM was the cluster $[Mn_{12}O_{12}(O_2CME)_{16}(H_2O)_4]$, also referred to as $Mn_{12}OAc$, discovered in the 1990's, and comprises an inner core of twelve μ_3-oxo ions assembling eight Mn^{III} and four Mn^{IV} ions, as shown in Figure 4.[9]
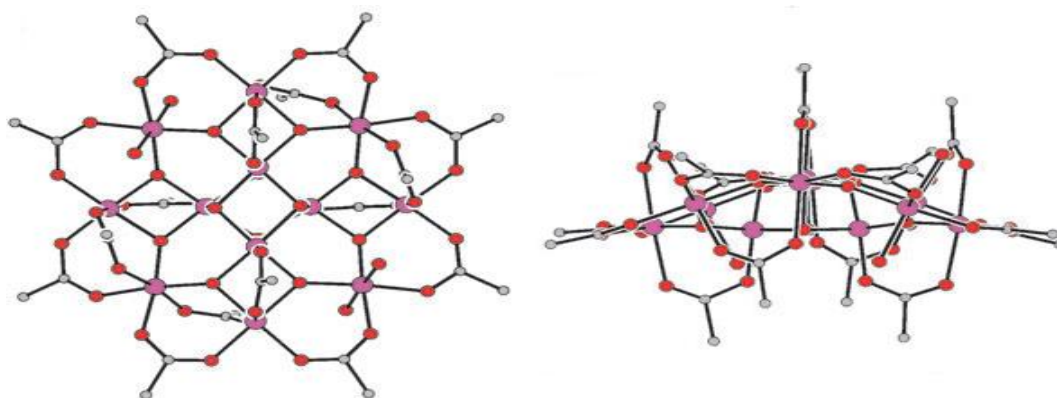
Figure 4: Representation of $[Mn_{12}O_{12}(O_2CMe)_{16}(H_2O)_4]$ from the top (left) and from the side (right). Hydrogen atoms are omitted for clarity. Code for atoms: purple, Mn; red, O; grey, C.[8a]

The core is encapsulated by sixteen bridging acetate anions and four water molecules. Exchange interactions between the metal centres leads to a total spin ground state S = 10 for the whole molecule. The appliance of an external magnetic field results in the Zeeman effect in which the previously degenerate electron configurations are split. Electron configurations with a positive spin quantum number (m_s) are destabilised whereas those with negative m_s are stabilized. Although most complexes regain their unperturbed energy states upon removal of the external magnetic field, and paramagnetic complexes do so rapidly, in $Mn_{12}OAc$ this is very slow. This is attributable to the presence of an energy barrier (ΔE) which completely blocks this return to degeneracy below a certain temperature, and is of

extreme importance as it suggests that SMMs should be capable of storing magnetic information. Since this discovery, numerous homo and hetero multi-metallic examples of various sizes have been observed.[10]

Recently, ligands such as acyclic imines and amines, macrocycles and cryptands containing 1,4-disusbstituted arenes have been under much scrutiny as they favour the formation of bi- and multinuclear complexes due to the inability of the two donor groups to chelate to a single metal cation.[11] This is exemplified by the dicopper complex developed by Brooker and co-workers in which 1,2-diazine moieties have been functionalised to form a (2 + 2) Schiff-base macrocycle upon metallation, shown in Figure 5.[12]
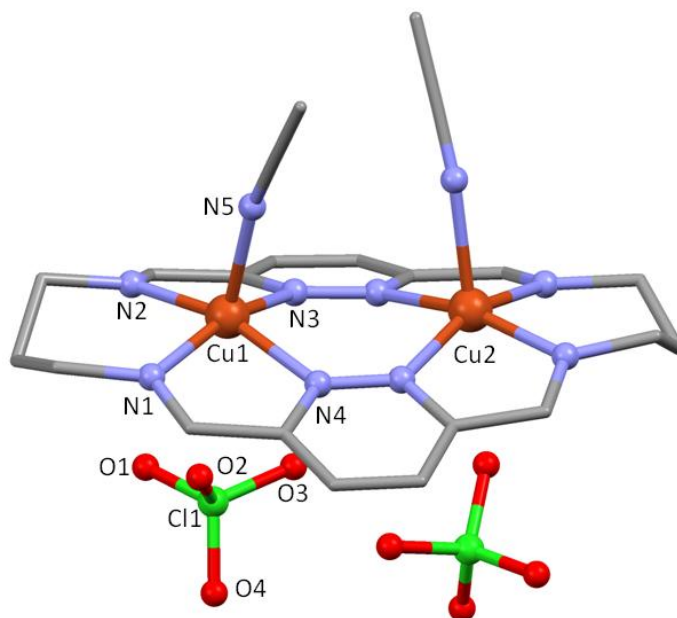
Figure 5: Crystal structure of the dicopper complex $[Cu_2L(MeCN)_2(ClO_4)_2][ClO_4]_2$ developed by Brooker and co-workers.[12]

The crystal structures of the dicopper complex shows both metal centres binding to two identical chelating sites on opposite sides of the diazine moieties in a square pyramidal geometry. Each Cu^{II} anion is held by two bridging pyridazine donors from opposite sides of the macrocycle and

two imine nitrogen donors; the final coordination site being occupied by the solvent of crystallisation (MeCN).

The acyclic Schiff-base reported by Puddephatt and co-workers is another noteworthy example.[13] In this ligand, the central 1,4-disusbstituted arene is functionalised by side chains containing both an imine and an amine group. The addition of dimethylplatinum to the complex resulted in the formation of a binuclear complex in which each platinum metal centre is held in a square planar arrangement through the chelating N-donor groups of a single arm of the ligand, as shown in Figure 6. It is important to note that this is the sole product and that no metallo-cycle is observed. The imines adopt a trans-configuration to alleviate steric interactions which would otherwise incur between the two extremities of the complex.
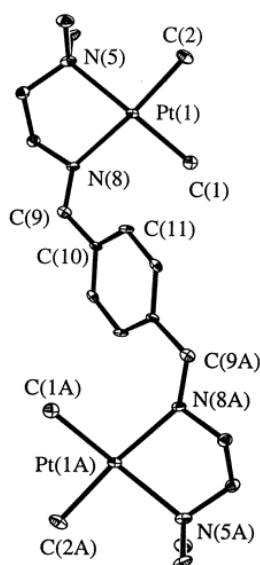
Figure 6: Ortep view of the diplatinum acyclic complex observed by Puddepphat and co-workers.[13]

Wide-span ligands similar to those developed by Puddepphat and co-workers can lead to the formation of metallo-macrocycles and metallo-cryptands under the right conditions. The metal centres can act both as a

structural domain, linking the sides of the capsule, and as a catalytic domain, binding to substrates and activate small molecules.

4.2 Synthesis of wide-span diimines and diamines
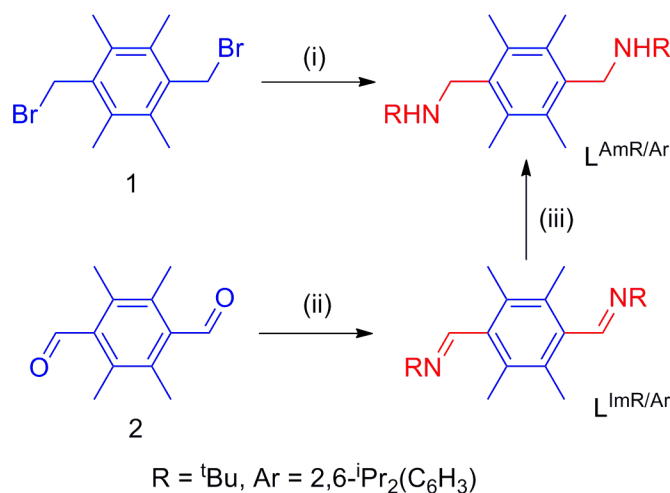
Scheme 1: Synthesis of wide-span diimine (L^{Im}) and diamine (L^{Am}) ligands. Reagents and conditions: (i) H_2NR/Ar, MeCN; (ii) H_2NR/Ar, MeCN; (iii) $NaBH_4$, MeOH, R = ^tBu.

The wide-span diimine and diamine pro-ligands L^{Im} and L^{Am} have been synthesised in high yielding reactions from the readily available precursors 1,4-dibromomethyl-2,3,5,6-tetramethylbenzene (1) and 2,3,5,6-tetramethylterephthalaldehyde (2) respectively (Scheme 1). Durene was used in the ligand design in order to ensure that cyclometallation reactions were minimised.

Both 2,6-diisopropylaniline (L^{ImAr}) and tert-butyl amine version of these ligands (L^{ImR}) were obtained through a Schiff-base condensation in high yield (86 and 70 % respectively). The formation of both compounds was supported by ^1H NMR spectroscopy in which imine resonances at 8.67 and 8.55 ppm for L^{ImAr} and L^{ImR} respectively were observed, as shown in Figure 7 for L^{ImAr}. The simplicity of the ^1H NMR spectrum is concordant with the formation of a highly symmetrical compound.
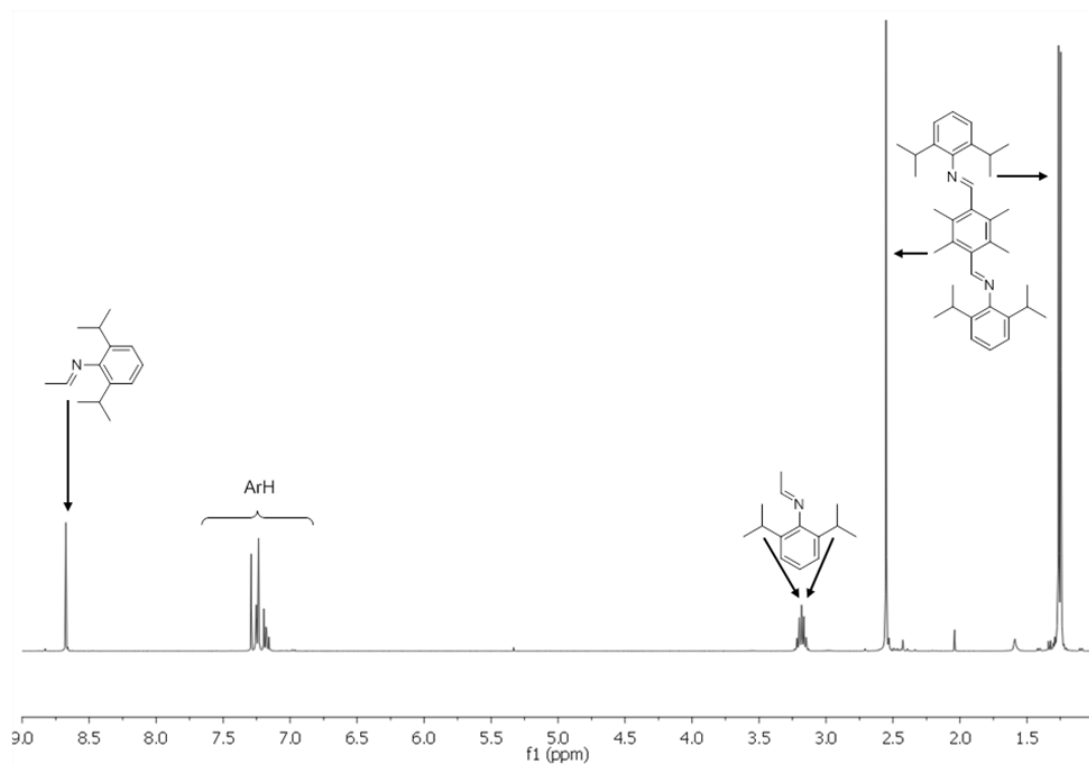
Figure 7: ^{1}H NMR spectrum of L^{ImAr}.

Although both equivalent secondary amine proligands can be synthesised through nucleophilic substitution of the bromide by either 2,6-diisopropylaniline (L^{AmAr}) and tert-butyl amine (L^{AmR}), they can also be obtained through borohydride reduction of the imines L^{ImAr} and L^{ImR}. While the most reproducible route to L^{AmAR} is through the bromide substitution route (53 % yield as opposed to 17 % over two steps), L^{AmR} is best obtained through the previously mentioned reduction (62 % over two steps compared to 40 %). This is most likely due to the lack of solubility of L^{ImAr} in MeOH, the solvent in which the best results for borohydride reduction were obtained. The use of a mixture of solvents and of a large excess of NaBH$_4$ did not improve yields. The synthesis of the amine proligands was supported, by the presence of CH$_2$ groups resonances 4.22 and 3.73 ppm in the ^{1}H NMR spectra of L^{AmAr} and L^{AmR} respectively, and showed the loss of the imine resonances of their respective precursors. An NH resonance at 3.07 ppm is also observed

in the ^{1}H NMR spectrum of L^{AmAr}. Although this is not observed in L^{AmR}, FT-IR analysis supports the formation of a secondary amine with an NH stretch at 3334 cm^{-1} which is similar to that observed in L^{ImAr} (3400 cm^{-1}).

Re-crystalisation of L^{ImAr}, L^{ImR} and L^{AmAr} from hot saturated solutions of MeCN afforded crystals suitable for X-ray crystallography studies. The solid state structures were determined and are shown in Figures 8 and 9, with selected bond lengths and angles detailed in Table 1, 2 and 3 as well as crystal data in Table Ch4 Tab1. All three compounds are found to crystallise in the solid state without any solvent present within the unit cell, and rely either on H-π or hydrogen bonding supramolecular interactions to aggregate.
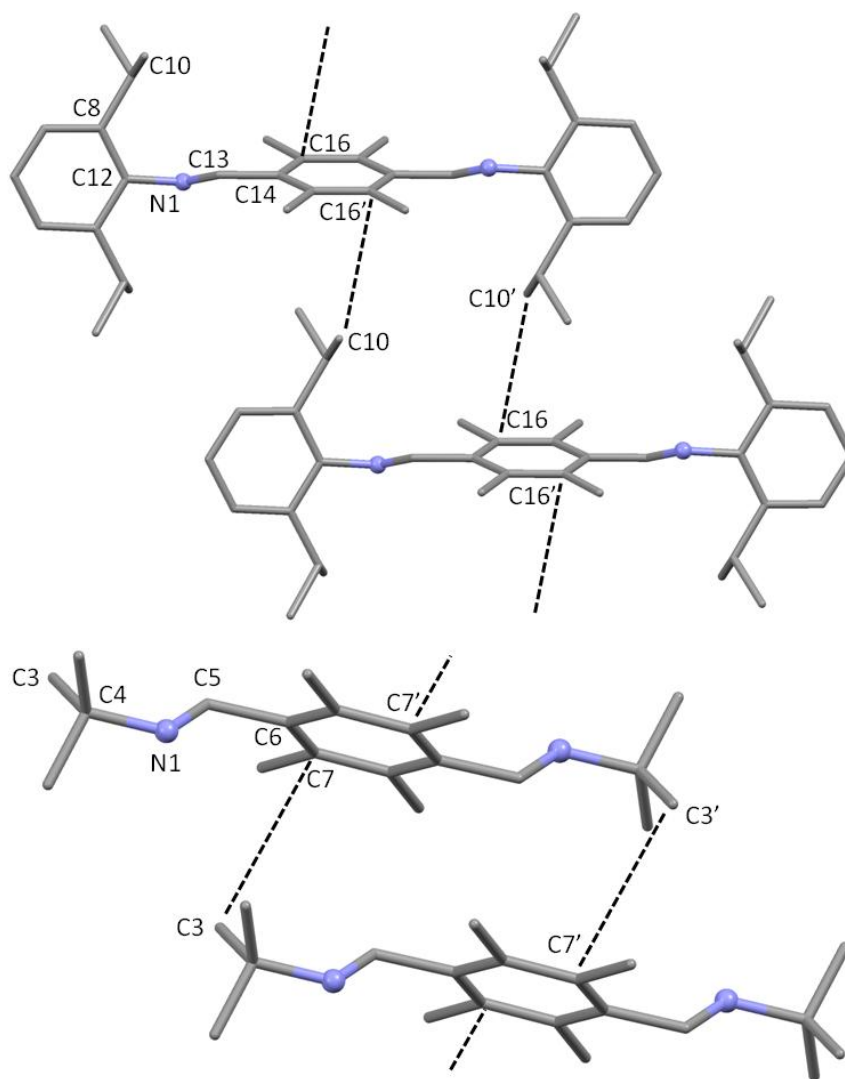
Figure 8: Ball and stick representation of the X-ray crystal structures of the imines L^{ImAr} (top) and L^{ImR} (bottom). For clarity, all hydrogen atoms are omitted.

The formation of imine bonds is supported by the bond lengths of N1-C13 (1.236(2)) and N1-C5 (1.237(5)) observed in the solid state structures of L^{ImAr} and L^{ImR} respectively which are concordant to those usually seen in the literature.[14] The crystal structures can be considered identical, but for the amine derivatives, with the imine bonds adopt an anti-conformation (178.0(2)° and 172.2(3)° for L^{ImAr} and L^{ImR} respectively). The torsion angle defined by N1, C13, C14 and C16 and N1, C5, C6 and C7 in L^{ImAr} and L^{ImR} respectively could have been expected to be of 90° to minimise steric interactions between the methyl groups of the durene and the imine group.

They are, however, offset by 29.8(3)° in L^{ImAr} and 57.3(5)° in L^{ImR}. These angles are likely to be related to the steric interactions between the terminal appendages present on the two different ligands and that of the durene methyl substituents of neighbouring molecules. It is noteworthy that in the case of L^{ImAr} the torsion angle between the imine and the isopropyl arene is of 72.7(2)°, which is much closer to the expected 90°, and that the planes defined by the end and central arene units (P2 and P1 respectively) bisect each other at 80.0° and can be considered orthogonal.

The extended structure does not show any π-π interactions which would have been expected between the multiple aryl units of adjacent molecules. Instead, H-π interactions are observed between C16′ and C10 in L^{ImAr} and C3 and C7 in L^{ImR} (C16′···C10 = 3.745 Å and C3···C7 = 3.850 Å in L^{ImAr} and L^{ImR} respectively). Although the distance between the H-π interaction is similar in both ligands, the distance between the planes of the central aryl units between adjacent neighbouring molecules is almost doubled when the tertiary-butyl appendages are replaced by 2,6-$^iPr_2(C_6H_3)$ (P1···P1′ = 6.772 Å and P2···P2′ = 3.666 Å for L^{ImAr} and L^{ImR} respectively).

N1-C12	1.427(2)	∠N1-C13-C14-C16	29.8(3)
N1-C13	1.236(2)	∠C8-C12-N1-C13	72.7(2)
C16···C10′	3.745	P1···P1′	6.772
∠C12-N1-C13-C14	178.0(2)		

Table 1: Selected bond lengths (Å) and angles (°) of L^{ImAr} (∠ denotes dihedral angle).

N1-C4	1.480(4)	∠C4-N1-C5-C6	172.2(3)
N1-C5	1.237(5)	∠ C7-C6-C5-N1	90.6(3)
C3···C7	3.850	P2···P2′	3.666

Table 2 Selected bond lengths (Å) and angles (°) of L^{ImR} (∠ denotes dihedral angle).

In the solid state, L^AmAr does not pack in the same neat arrangement observed with the two imine ligands; owing to the added flexibility of the amine bond (N1-C13 = 1.489(2) Å). The two amines adopt a *syn*-conformation with torsion angles of 79.9(2)° (N1-C13-C14-C19) and 84.0(2)° (N2-C24-C17-C18) with respect to the durene unit. This allows, in the extended structure, for the durene units of two adjacent molecules to interact with one another through π-π stacking. Other supramolecular interactions involving the opposing *syn*-side of the molecule (occupied by the amine appendages) can be observed in the extended network.
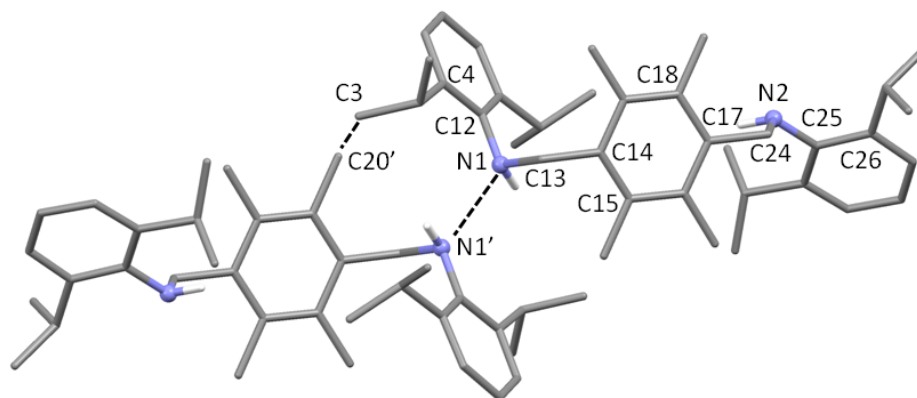
Figure 9: Ball and stick representation of the X-ray crystal structures of L^AmAr. For clarity, all hydrogen atoms and disordered components are omitted.

N1-C12	1.430(2)	∠N2-C24-C17-C18	84.0(2)
N1-C13	1.489(2)	∠N1-C13-C14-C15	79.9(2)
N1···N1'	3.264	∠C4-C12-N1-C13	76.1(2)
∠C12-N1-C13-C14	82.99(18)	∠C26-C25-N2-C24	68.3(2)

Table 3: Selected bond lengths (Å) and angles (°) of L^AmAr (∠ denotes dihedral angle).

As in L^ImAr, the steric demand of the C_6H_3-2,6-$^iPr_2$ substituent results in an approximately orthogonal orientation of the amines with regard to this group (76.1(2)° and 68.2(2)°). The added flexibility of the amine, however, allows for greater variety of position to minimise the interactions between these groups, which does not result in a 90° angle between the terminal arene

substituent, and the central arene. This geometrical freedom permits the amines of adjacent molecules to be proximate and interact through hydrogen bonding (N1···N1' = 3.264 Å). Last but not least, interactions between the CH_3 substituents of the central durene and the *iso*-propyl CH_3 groups of adjacent molecules are also observed (C3···C20' = 3.937 Å).

4.3 Synthesis of cobalt and zinc chlorometallates

The coordination chemistry of these wide span ligands was investigated (Scheme 2). Reactions between L^{Im} and L^{Am} and either $CoCl_2$ or $ZnCl_2$ in THF showed no change in the ligand resonances in the ^1H NMR spectrum. The use of bench $CDCl_3$ as the NMR solvent resulted in the formation of crystals of the chlorometallate salts $[H_2L^{AmR}][CoCl_4]$ and $[H_2L^{ImAr}][Zn_4Cl_{10}]$, most likely due to the presence of adventitious HCl.
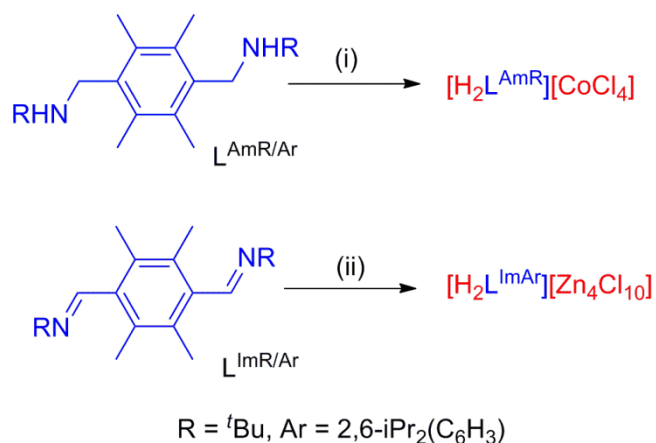
Scheme 2: Synthesis of L^{Im} and L^{Am} chlorometallates. Reagents and conditions: (i) 2 HCl, Et_2O, $CoCl_2$; (ii) 2 HCl, Et_2O, 4 $ZnCl_2$.

Scaled up reactions were carried out in which the ligands were protonated by two equivalents of HCl in Et_2O followed by the addition of one or four equivalents of $CoCl_2$ or $ZnCl_2$ in Et_2O, respectively. This resulted in the formation of analytically pure material according the C, H, N

elemental analysis. No NMR spectra of these chlorometallate compounds were recorded due to their insolubility.

The solid state structures of $[H_2L^{AmR}][CoCl_4](H_2O)(CDCl_3)$ and $[H_2L^{ImAr}][Zn_4Cl_{10}]$ were determined and are shown in Figures 10 and 12 respectively, with selected bond lengths and angles detailed in Tables 4 and 5 and crystal data in Table Ch4 Tab2. Both solid state structures show that the protonated ligand and the chlorometallate interact through numerous hydrogen bonding interactions; all hydrogens involved in hydrogen-bonding were located in the difference Fourier map and refined with riding thermal parameters and bond distance restraints.

In the solid state structure of $[H_2L^{AmR}][CoCl_4](H_2O)(CDCl_3)$, displayed in Figure 10, a water molecule was found to be hydrogen bonding between the protonated amine of one arm of the ligand (N1$\cdots$O1 = 2.817 Å) and the chlorometallate (O1$\cdots$Cl4 = 3.165 Å). The remaining N1 hydrogen as well as both N2 hydrogens partake in "direct" hydrogen-bonding interactions with $[CoCl_4]^{2-}$ (N1$\cdots$Cl2 = 3.357 Å, N2$\cdots$Cl1 = 3.215 Å and N2$\cdots$Cl4 = 3.255 Å). One C-H$\cdots$Cl interaction is also observed between one of the durene CH_3 hydrogens and Cl1 (C14$\cdots$Cl1 = 3.656 Å). As described above in the discussion about the solid state structures of the free ligands, other intra- and intermolecular contacts are present in the extended structure, especially with the solvent of crystallisation ($CHCl_3$). The chloro-metallate/ligand interactions result in the adoption of a *syn*-conformation of the ligand, resulting in both imine arms being orientated towards the single chlorometallate. This leads to the formation of a hydrogen-bonded cavity that appears to be preferentially suited for chlorometallate recognition over chloride.
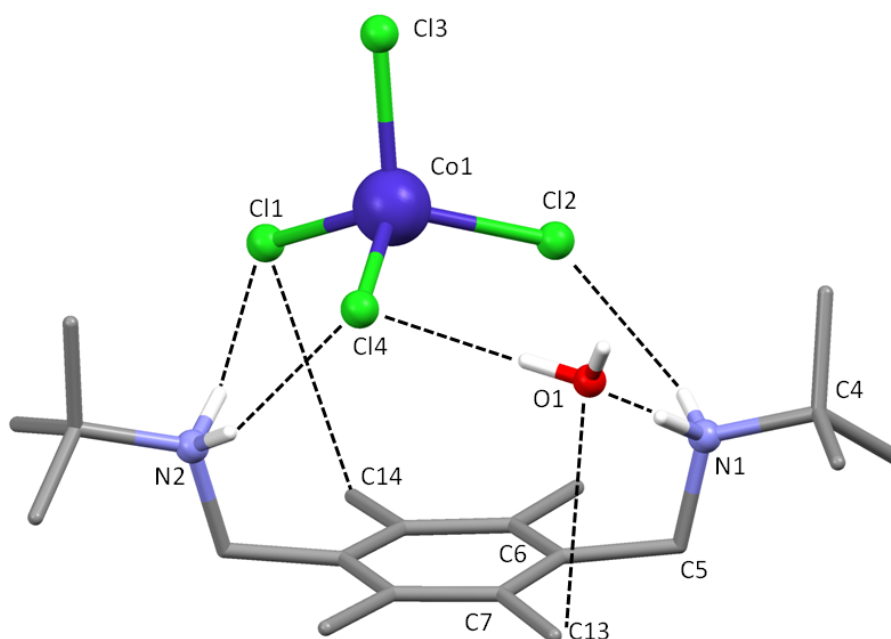
Figure 10: Ball and stick representation of the X-ray crystal structures of [H$_2$L^{AmR}][CoCl$_4$](H$_2$O)(CHCl$_3$). For clarity, CHCl$_3$ solvent of crystallisation and all hydrogen atoms except those involved in hydrogen bonding are omitted.

N1-C4	1.522(4)	O1···C2	3.363
N1-C5	1.517(4)	O1···C13	3.325
N1···O1	2.817	Co1- Cl1	2.2703(9)
N1···Cl2	3.357	N1···O1···Cl4	109.78
N2···Cl1	3.215	Cl1-Co1-Cl2	110.89(4)
N2···Cl4	3.255	∠C4-N1-C5-C6	172.2(3)
Cl1···C14	3.656	∠N1-C5-C6-C7	90.6(3)
O1···Cl4	3.165		

Table 4: Selected bond lengths (Å) and angles (°) of [H$_2$L^{AmR}][CoCl$_4$](H$_2$O)(CHCl$_3$) (∠ denotes dihedral angle).

CoCl$_4{}^{2-}$ ions are very well known and their properties have been extensively studied in a wide range of sciences such as in geochemistry in which its behaviour in hydrothermal solution has been established and electrochemistry where cobalt halides have been studied for their potential as electrolyte.[15] A noteworthy example of a use for this anion is the formation of a supramolecular network observed by Brammer and co-workers.[16] The propensity of metal halides to act as directional Lewis bases and organic halogens to behave as Lewis acids has previously been observed.[17]

Assembling these two characteristics is of interest to the field of crystal engineering due to its potential to form networks through reversible interactions.[15b, 18] Whether the formation of these networks is the result of weak attractive intermolecular interactions or the molecules are simply taking positions with the least repulsive forces has been the subject of debate.[15c, 16]
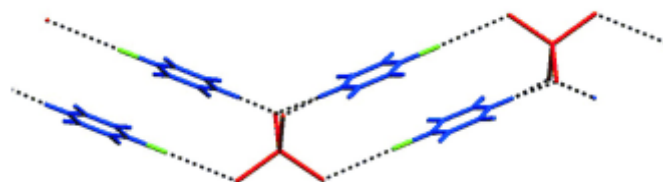
Figure 11: X-ray crystal structure of one of the networks observed by Brammer and co-workers.[16] In red: $CoCl_4^{2-}$; in green: organic halogen atom; in blue: all other atoms.

The network formed by Lee Brammer (Figure 11) is self-assembled through M-X and C-X′ interactions (X and X′ can be either Cl or Br). $CoCl_4^{2-}$ and $CoBr_4^{2-}$ were used as M-X and halo-pyridiniums were used as linkers. The networks formed are iso-structural but showed that C-X′···X interactions are linear whereas Co-X···X′ interactions are bent with an angle ranging from 120.3 and 123.7°. Hydrogen bonds have also been observed from the NH group and two chloride anions with H···X bond distances ranging between 2.300 and 2.825 Å. The metal cluster is clearly deformed with some of the X-M-X angles as low as 98° compared to 110° in the case of $[H_2L^{AmR}][CoCl_4](H_2O)(CHCl_3)$. This is the result of a local electric field formed by the surrounding ions which ultimately generates a dipole moment along the twofold axis of the anion. This conclusion was supported by computational analysis. Although the formation of a network is not seen in $[H_2L^{AmR}][CoCl_4](H_2O)(CHCl_3)$, it is clearly observed in the zincate example that follows.

In contrast with that of $[H_2L^{AmR}][CoCl_4](H_2O)(CHCl_3)$, the solid state structure of $[H_2L^{ImAr}][Zn_4Cl_{10}]$ shows that the protonated imine (N1-C13 = 1.274(3) Å) appendages of the ligand adopt an *anti*-configuration (torsion angle = 176.0(2)°). Each arm of the ligand interacts with a different chlorometallate through hydrogen bonding leading to the formation of a network of alternating protonated ligands and metallates in the extended structure.
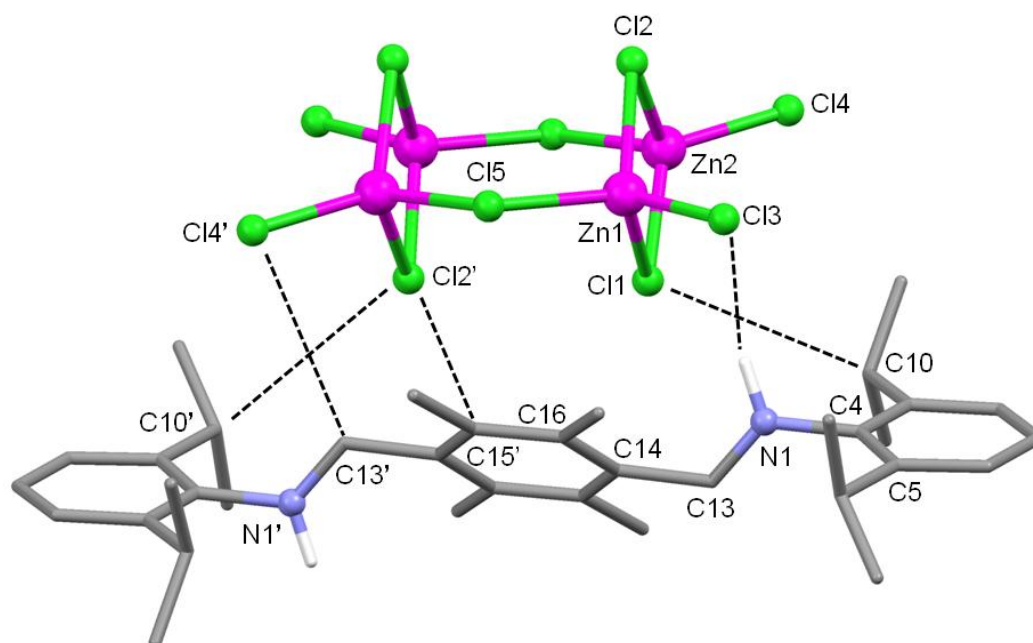
Figure 12: Ball and stick representation of the X-ray crystal structures of $[H_2L^{ImAr}][Zn_4Cl_{10}]$. For clarity, all hydrogen atoms except those involved in hydrogen bonding are omitted.

The torsion angle formed between the terminal arene rings and imine bond can, as with the pro-ligand, be consider as orthogonal (C5-C4-N1-C13 = 88.1(3)°). On the other hand, the torsion angle N1-C13-C14-C16 between the imine and the central durene unit has increased from 29.8(3)° in the pro-ligand to 53.3(4)°. This is attributable to the NH···Cl hydrogen bonds (N1···Cl3 = 3.152 Å) holding the two supramolecular components proximate, in addition to the multiple CH···Cl interactions observed that range from

3.446 to 3.759 Å. This latest set of interactions involves either the bridging chlorine atoms and the isopropyl CH units (Cl1···C10 = 3.759, Cl2'···C10' = 3.745 Å) or terminal chlorine atoms and the imine CH (Cl4'···C13' = 3.529 Å). It is also important to note that one anion-π interaction is seen between Cl2' and C15 (3.446 Å) of the central durene ring. As a result of a decrease in the angle between the central (P1) and the terminal (P2) arenes by half (down to 42.0°), interactions between the ligand and $[Zn_4Cl_{10}]^{2-}$ are maximised.

Zn1-Cl1	2.3074(8)	Cl3···N1	3.152
Zn1-Cl3	2.1996(7)	Cl2'···C15	3.745
Zn1-Cl5	2.2730(7)	Cl2'···C10'	3.842
N1-C13	1.274(3)	C13'···Cl4'	3.529
Cl1···C10	3.759	Zn1-Cl1-Zn2	85.30(2)
Cl1-Zn1-Cl2	94.69(3)	Cl3-Zn1-Cl5	109.65(3)

Table 5: Selected bond lengths (Å) and angles (°) of $[H_2L^{ImAr}][Zn_4Cl_{10}]$.

Contrary to previous examples, the chlorometallate $[Zn_4Cl_{10}]^{2-}$ is observed in a rectangular arrangement.[17a, 19] On its longest side (3.834 Å), the zinc cations are singly bridged by a chloride anion (Zn1-Cl5 = 2.2730(7) Å; Zn1-Cl5-Zn2 = 114.24(3)°), whereas on its shortest side (3.140 Å) the zinc atoms are bridged by two anions (Zn1-Cl1 = 2.3074(8) Å; Zn1-Cl1-Zn2 = 85.30(2)°). Each metal centre is coordinated to a fourth terminal chlorine anion (Zn1-Cl3 = 2.1996(7) Å).

The numerous $Zn_4Cl_{10}^{2-}$ clusters reported have always been shown to adopt either adamantane or open chain structures. This is, however, the first example of a rectangular arrangement of Zn cations.[19-20] One of the earliest adamantane $Zn_4Cl_{10}^{2-}$ clusters to be reported was that observed by Bottomley and co-workers illustrated in Figure 13.[21]
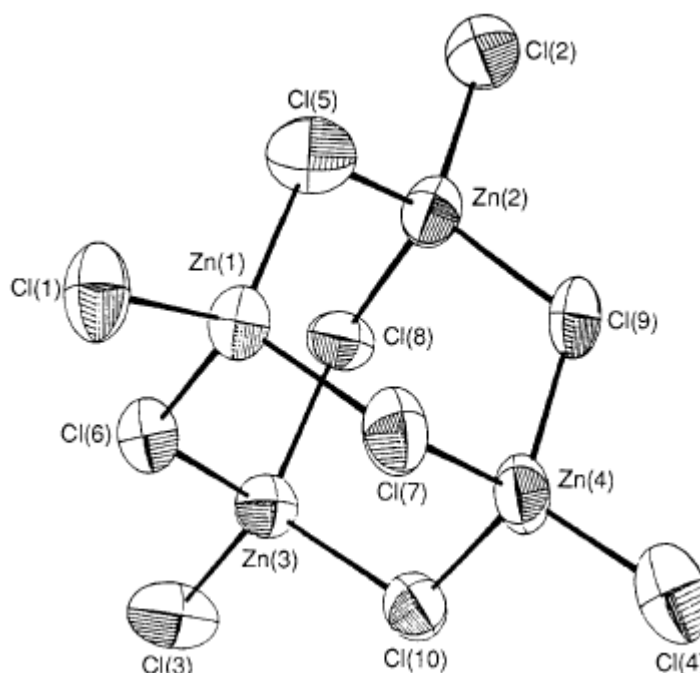
Figure 13: Example of $Zn_4Cl_{10}^{2-}$ adamantane observed by Bottomley and co-workers.[21]

In this example, the cluster anion is not the counter-anion of a protonated ligand, but of clusters of niobium chloride and oxide. The cluster can be better described as $[\{ZnCl\}_4(\mu\text{-}Cl)_6]^{2-}$ consisting of four tetrahedral zinc atoms each with a terminal chloride and bridged by three Cl anions to the three remaining metal centres. Although the Zn-Cl bond distances are similar to those of the rectangular cluster presented in this work, at 2.181(12) Å and 2.1996(7) Å respectively, in the former complex a single type of μ-Cl is observed with average Zn-Cl bond distance of 2.298(12) Å. This correlates to the Zn-μ–Cl bond distances involved in the bridging of the small side of the $Zn_4Cl_{10}^{2-}$ rectangle.

Seddon and co-workers have described synthetic methods to prepare chloro-zincate clusters ranging from $[ZnCl_3]^-$ to $[Zn_4Cl_{10}]^{2-}$.[22] In this example, the cluster exists as an open framework structure in which the building units bind to one another through bridging chlorides. This leads to the first example of a five co-ordinate zinc. A previous report claiming the existence of this anion was interpreted incorrectly and actually contained $[ZnCl_4]^{2-}$

with positional disorder.[18] A cut-out taken from the crystal structure of the $\{Zn_4Cl_{10}\}$ framework, displayed in Figure 14, clearly shows two trigonal bipyramidal zinc anions (Zn5 and Zn6) bridged by two Cl atoms instead of one for the other brindging chlorides. The Zn-(μ-Cl) bond distances for the tetrahedral zinc atoms range between 2.225(4) and 2.302(3) Å. Although these are similar to that of the equatorial Zn-Cl of the five coordinate metal centres (from 2.216(4) to 2.329(3) Å), a net elongation of the equatorial Zn-Cl is observed with bond distances ranging from 2.510(4) to 2.741(4) Å. Figure 15 clearly demonstrates the propensity of the building units to assemble around the imidazolium guest molecule through hydrogen bonding interactions, forming a cavity of diameter ranging from 9.9 to 10.5 Å.
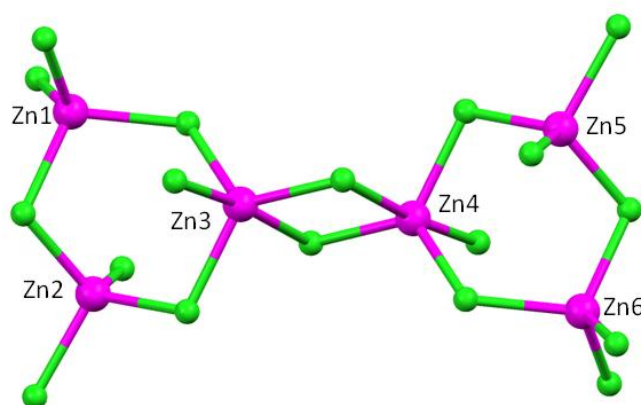
Figure 14: Cutout from the framework structure of [C$_2$mim]$_2${Zn$_4$Cl$_{10}$} showing the building units with corner-sharing tetrahedral and edge-sharing trigonal pyramids.[22]
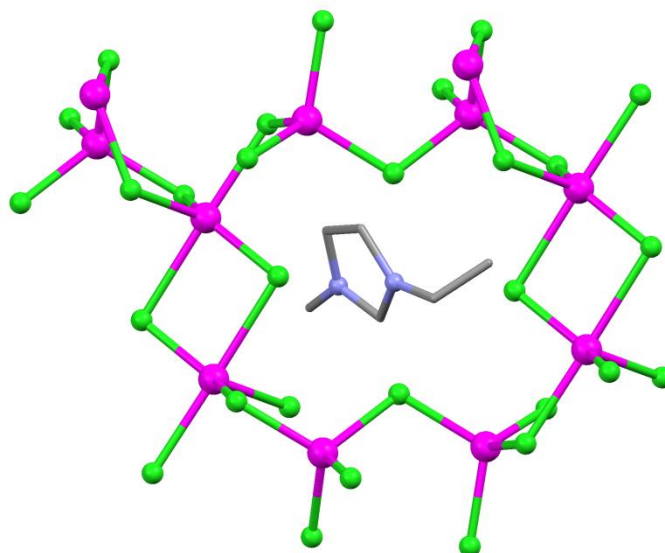
Figure 15: Framework structure of [C$_2$mim]$_2${Zn$_4$Cl$_{10}$} with an anion in the centre of the cavity.[22]

The propensity for L^{AmR} and L^{ImAr} to extract metals through supramolecular interactions is of particular interest within the field of hydrometallurgy and a study was carried out by Jennifer Turkinton of the Tasker group to evaluate their ability as zinc extractants. Unfortunately, in the case of L^{AmR}, the formation of a third phase at low acid concentration was observed and prevented further analysis. Furthermore, L^{ImAr} was only observed to extract relatively low amounts of cations (up to 0.36 ppm) before the formation of a third phase was observed. It is therefore clear that more organic soluble versions of these compounds need to be made in order to circumvent third phase formation.

4.4 Synthesis of palladium clusters

The planar geometry enforced by Pd^{II} onto its surrounding ligands can be exploited to form a metallo-macrocycle. Indeed the addition of equimolar amounts of Pd^{II} and to a bidentate ligand unable to chelate both binding sites to a single metal cation should lead to the formation of a [2+2] macrocycle. This was expected to lead to the formation of a complex of nature similar to

that observed by Steel and O'Keefe as well as many other examples reported in the literature.[23] The Steel group developed a ligand consisting of a central *para* substituted arene ring functionalised by four donor sites made of a sulphide and an imine on both sides. The addition of four Pd(OAc)$_2$ to two equivalents of ligand in acetic acid led to the double C,N-cyclopalladation of both ligands. Although one acetate ligand is displaced from the starting material, the four others bridge the two metal centres as shown in Scheme 3. It is thought that π-π stacking of the pro-ligand prior to metallation results in the formation of [Pd$_4$L$_2$(OAc)$_4$]. Although the ligand developed for the formation of this complex shares similarities with L^{ImAr} such as the distance between the two metal binding sites (one arene unit), the use of durene as a central unit will prevent the cyclopalladation.
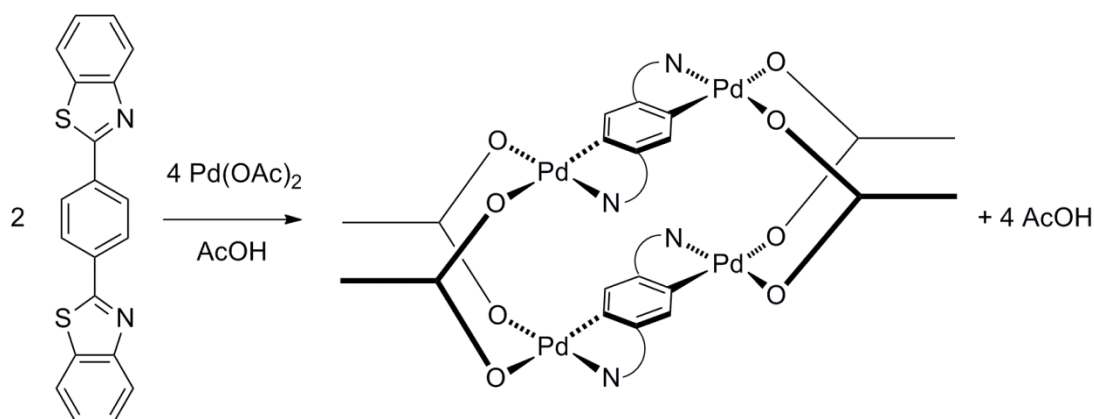
Scheme 3: Synthesis of [Pd$_4$L$_2$(OAc)$_4$].[23]

The reaction between three equivalents of PdCl$_2$(MeCN)$_2$ and either L^{ImAr} or L^{ImR} in CH$_2$Cl$_2$ as described in Scheme 4, led to the formation of the trinuclear palladium chloride cluster [Pd$_3$Cl$_6$(L)], the formulations of which are supported by elemental analysis. Addition of only one or two equivalents of the metal precursor was attempted, but resulted solely in a mixture of free ligand and the tripalladium product.

$R = {}^{t}Bu, Ar = 2,6\text{-}^{i}Pr_2(C_6H_3)$
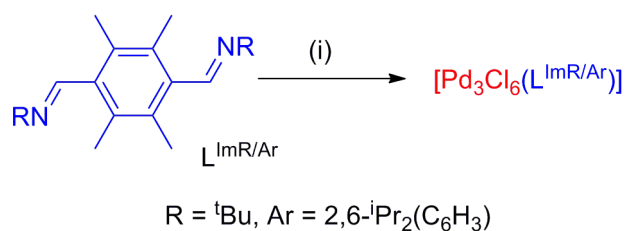
Scheme 4: Synthesis of L^{Im} palladium clusters. Reagents and conditions: (i) 3 $PdCl_2(MeCN)_2$, CH_2Cl_2.

Re-crystallisation of $[Pd_3Cl_6(L^{ImAr})]$ and $[Pd_3Cl_6(L^{ImR})]$ by the cooling of saturated CH_2Cl_2 solutions afforded crystals of the aforementioned complexes that were suitable for X-ray diffraction studies. The solid state structures of both compounds were determined and are shown in Figures 16 and 17, with selected bond lengths and angles detailed in Tables 6 and 7 and crystal data in Table Ch4 Tab2. The imine appendages adopt a synclinal conformation (torsion angle N1-C5···C16-N2 = 6° in $[Pd_3Cl_6(L^{ImR})]$) similar to that observed in $[H_2L^{AmR}][CoCl_4]$ that allows for the chelation of a single Pd_3Cl_6 cluster through the imine nitrogens N1 and N2. Even though each Pd cation is held in a square planar geometry in both complexes, the cluster itself is not linear due to the short distance between the chelating imines. This leads to the formation of a cradle-like arrangement in which the angle formed by Pd1, Pd2 and Pd3 is 128.0° with each Pd cation being bridged by Cl atoms through an angle of approximately 90° and Pd-μ–Cl bond lengths varying between 2.370(6) and 2.304(4) for $[Pd_3Cl_6(L^{ImAr})]$ and 2.350(1) and 2.2901(2) for $[Pd_3Cl_6(L^{ImR})]$.
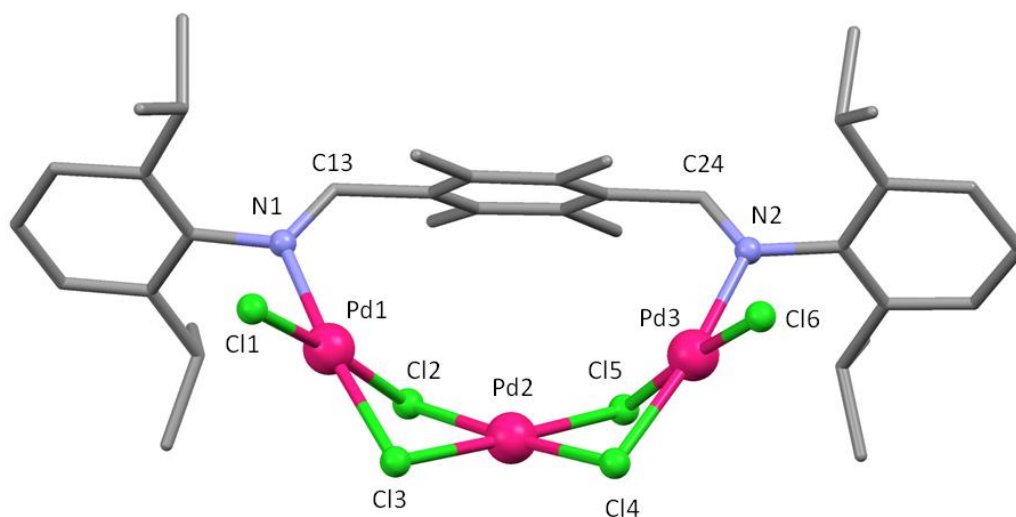
Figure 16: Ball and stick representation of the X-ray crystal structures of [Pd$_3$Cl$_6$(L^{ImAr})]. For clarity, all hydrogen atoms and disordered components are omitted.

N1-C13	1.219(9)	Pd2-Cl2	2.307(5)
N1-Pd1	2.023(14)	Pd1-Pd2-Pd3	127.98
Pd1-Cl1	2.279(6)	Pd2···P$_{durene}$	3.939
Pd1-Cl2	2.351(6)	Pd1-Cl3	2.343(6)

Table 6: Selected bond lengths (Å) and angles (°) of [Pd$_3$Cl$_6$(L^{ImAr})] ($\angle$ denotes dihedral angle).
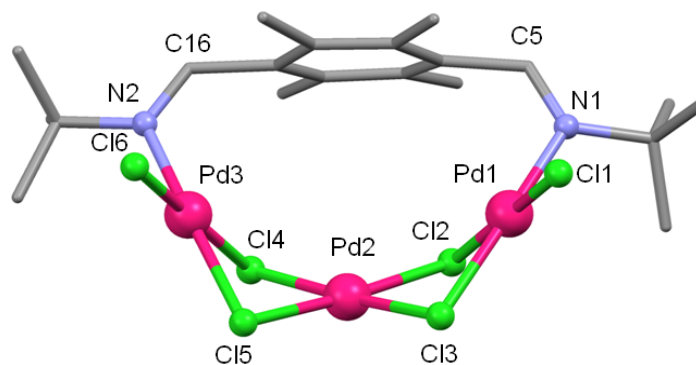
Figure 17: Ball and stick representation of the X-ray crystal structures of [Pd$_3$Cl$_6$(L^{ImR})]. For clarity, all hydrogen atoms and disordered components are omitted.

N1-C5	1.277(7)	Pd2-Cl2	2.301(1)
N1-Pd1	2.025(4)	Pd1···Pd2···Pd3	122.79
Pd1-Cl1	2.286(2)	Pd2···P$_{durene}$	4.126
Pd1-Cl2	2.341(1)	Pd1-Cl3	2.337(1)

Table 7: Selected bond lengths (Å) and angles (°) of [Pd$_3$Cl$_6$(L^{ImAr})]..

The ^{1}H NMR spectra of [Pd$_3$Cl$_6$(L^{ImAr})] and [Pd$_3$Cl$_6$(L^{ImR})] show that the structures are retained in solution (displayed in Figure 16 and 17 respectively). The two spectra and solid state structure being similar, for clarity purposes, only the ^{1}H NMR spectrum of [Pd$_3$Cl$_6$(L^{ImAr})] will be discussed. The asymmetry of the Pd$_3$Cl$_6$ cluster is reflected by the presence of a single imine resonance observed at 8.38 ppm as well as the presence of two distinct methyl resonances for the durene at 3.75 and 2.09 ppm. The asymmetry of the central aryl unit is further enhanced by a tilt of 73.4° relative to the imine bond resulting in one side of the durene being closer to the metal cluster. Additionally the ^{1}H NMR spectrum shows the presence of two isopropyl CH resonances at 3.56 and 3.49 ppm and four resonances for the methyl environments at 1.85, 1.48, 1.25 and 1.23 ppm. The bulkiness of the isopropyl groups and their proximity to the terminal Cl anion results in the hindrance of the free rotation around the N-C bond of the terminal groups. This feature is not observed in [Pd$_3$Cl$_6$(L^{ImR})] as a single resonance for the ^{t}Bu substituent is seen at 1.22 ppm as shown in Figure 17.
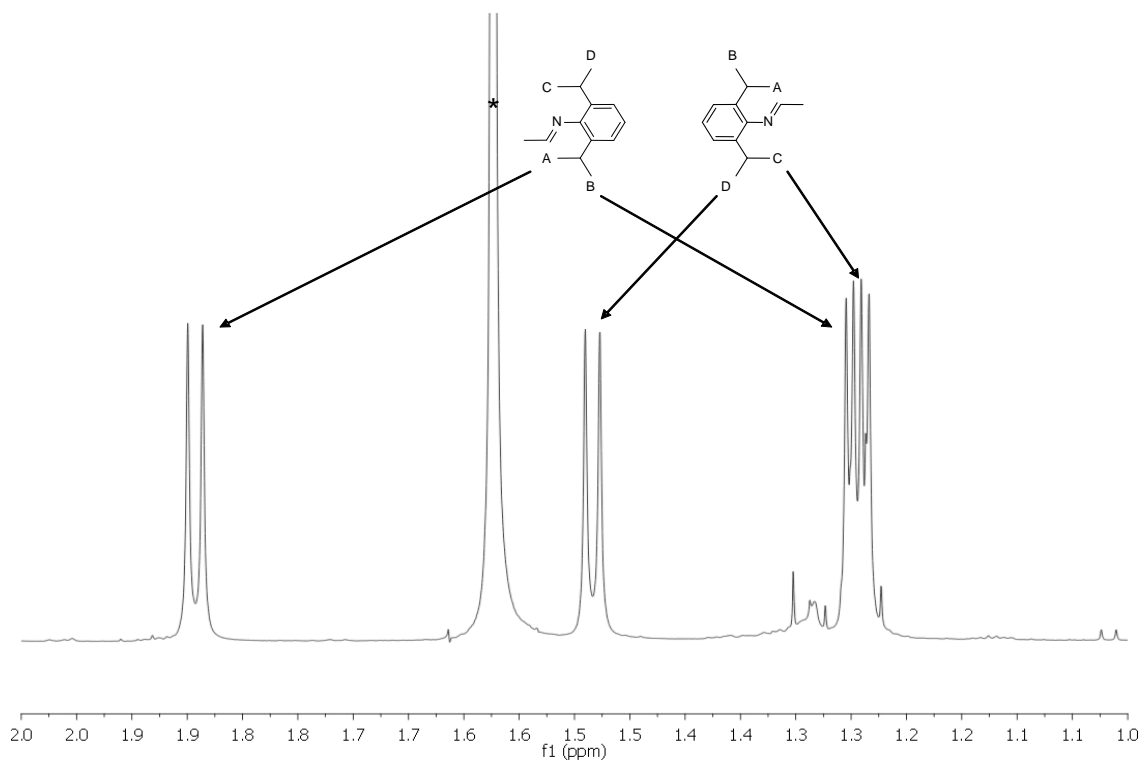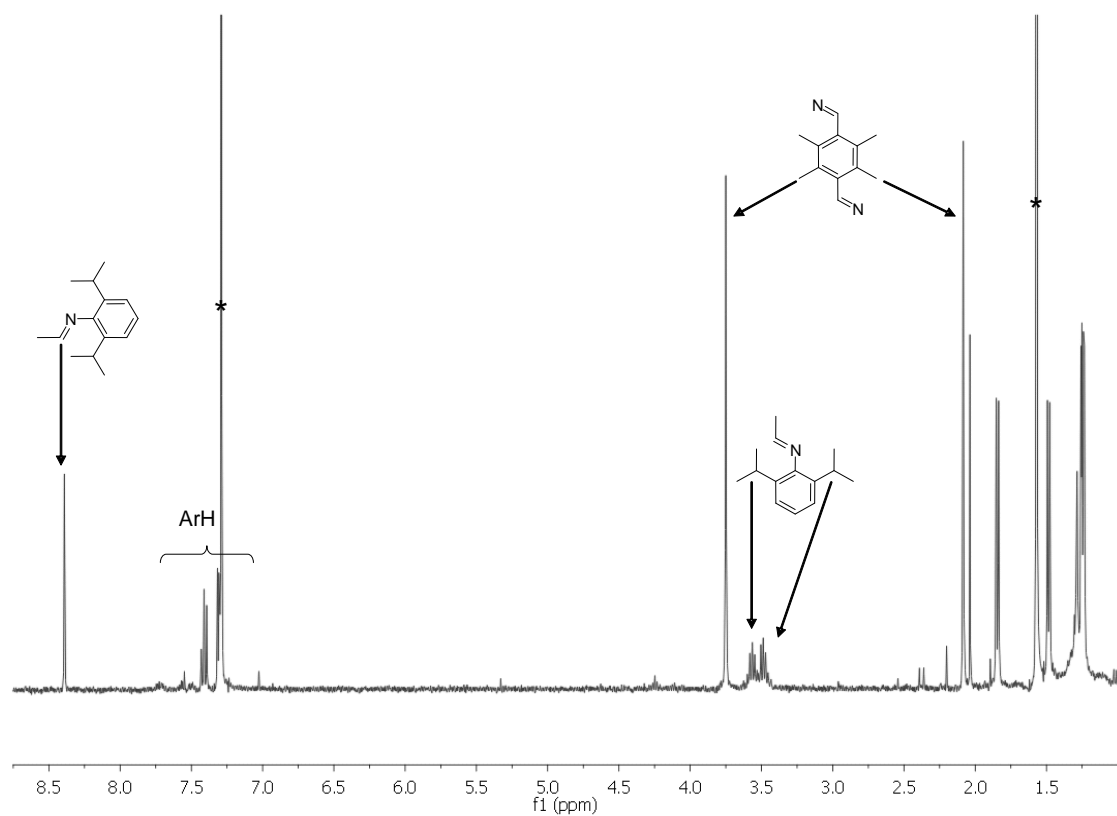
Figure 18: ^{1}H NMR spectra of [Pd$_3$Cl$_6$(L^{ImAr})] in CDCl$_3$ (* residual CHCl$_3$ and H$_2$O). Top: full spectrum; bottom: expansion of 2.0-1.0 ppm region.
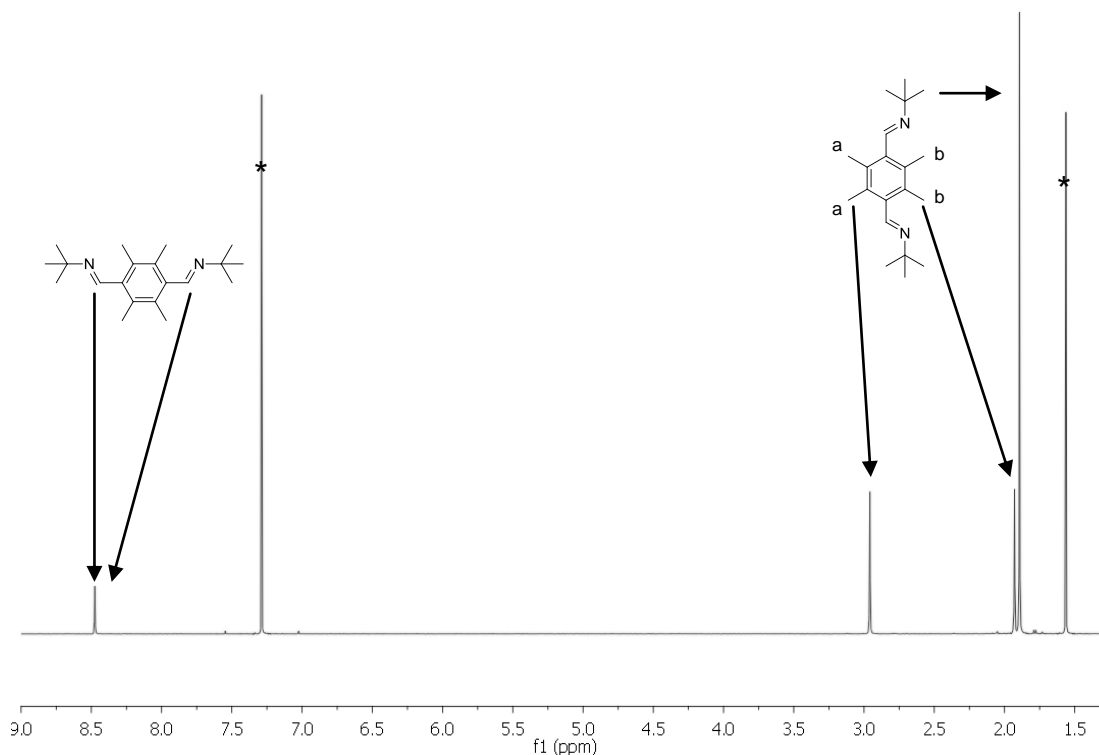
Figure 19: ^1H NMR spectrum of [Pd$_3$Cl$_6$(L^{ImR})] in CDCl$_3$ (* residual CHCl$_3$ and H$_2$O)

Although it is well known that PdCl$_2$ exists as a polymer, the Pd$_3$Cl$_6$ clusters such as that observed in [Pd$_3$Cl$_6$(L^{ImAr})] and [Pd$_3$Cl$_6$(L^{ImR})] are rare.[24] Even though they have been postulated a handful of times, structural evidence for this cluster formulation has been demonstrated only once prior to this investigation by Kawashima and co-workers.[25] When reacted with palladium (II) halides, tertiary phosphines usually produce the 2:1 complexes [PdX$_2$(PR$_3$)$_2$] or 2:2 complexes [(PdX$_2$)$_2$(PR$_3$)$_2$]. However, the addition of PdCl$_2$ to the tertiary phosphine ligands developed by the Kawashima group solely afforded the unprecedented 2:3 complex [(PdX$_2$)$_3$(PR$_3$)$_2$] shown in Figure 20.[25]
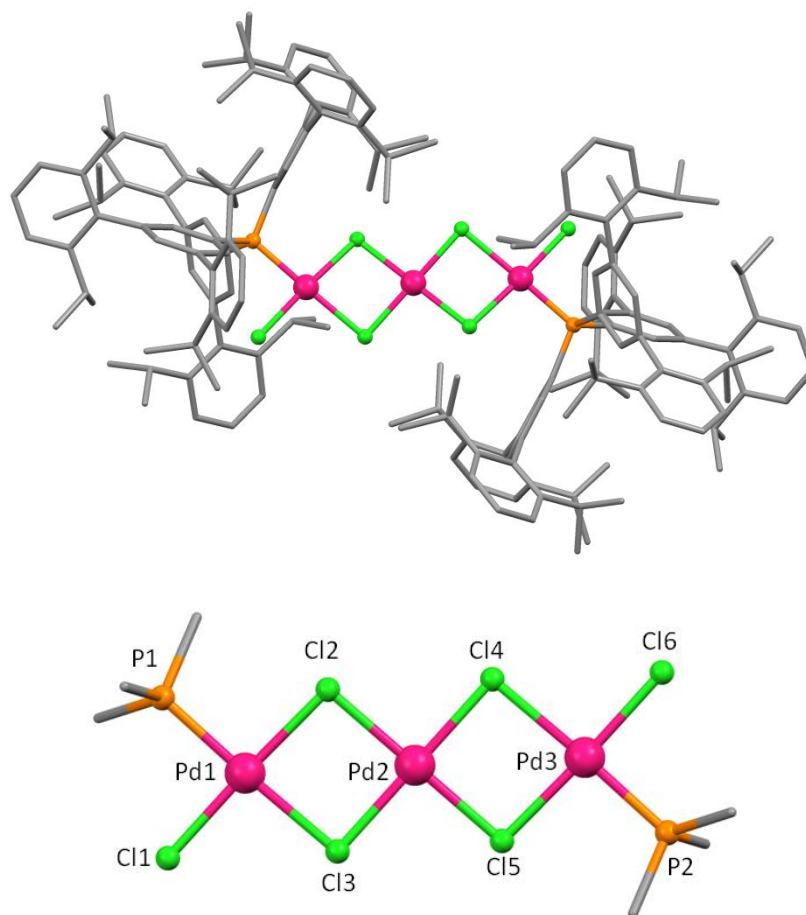
Figure 20: X-ray crystal structure of $[(PdCl_2)_3(PR_3)_2]$ (PR_3 = (2,2'',6,6''-tetraalkyl[1,1':3'1''-terphenyl]-5'-yl)phosphine (top) and its core (bottom) developed by Kawashima and co-workers.[25] For clarity, all hydrogen atoms and disordered components are omitted.

Three major differences can be observed in the Pd_3Cl_6 clusters of Kawashima and co-workers and that presented in this thesis. The terminal chloride anions in the former are in a *trans*-conformation which is due to the steric interaction which would otherwise arise if the ligands came into proximity. The clusters presented in this work afford a *cis* conformation which enables chelation to the two imine nitrogen appendages of a single ligand. This coordination mode also results in the cradle arrangement described above, whereas the phosphine ligand system provides a planar cluster. The sole discrepancy in Pd-Cl bonds between the two complexes is arising from the *trans* effect of the phosphorus which induces the

lengthening of the *trans* bridging Pd1-Cl3 bond to 2.421(5) Å compared to 2.343(6) and 2.337(1) Å in [Pd$_3$Cl$_6$(L^{ImAr})] and [Pd$_3$Cl$_6$(L^{ImR})], respectively. The terminal Pd-Cl bond and Pd-(μ-Cl) *cis* to a phosphorus are of similar lengths to those discussed in [Pd$_3$Cl$_6$(L^{ImAr}) and [Pd$_3$Cl$_6$(L^{ImR}).

Although the first Pd$_3$Cl$_6$ bridging clusters were structurally characterised by Kawashima, related clusters with varying amounts of palladium (II) cations and chloride anions have also been characterised. Hughes and co-workers have demonstrated the self-assembly of both bridging Pd$_2$Cl$_2$ and Pd$_3$Cl$_4$.[26] In this example, the ligand (1,2,3-tri-*tert*-butyl-3-vinyl-1-cyclopropene) is ring opened to form a dimeric η^3-cyclobutenyl complex resulting in two chlorides migrating onto the ligand as shown in Figure 21.
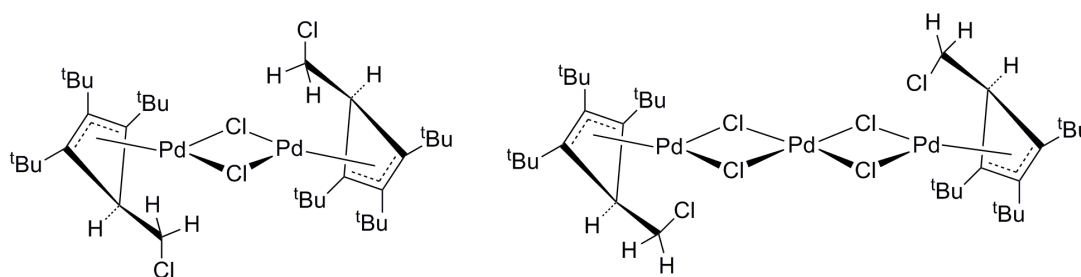
Figure 21: Hughes and co-workers bridging Pd$_2$Cl$_2$ cluster (left) and Pd$_3$Cl$_4$ cluster (right).[26]

Other examples of bridging Pd$_3$Cl$_4$ clusters include those observed by Maitlis and co-workers as well as Wing and co-workers, and which contain 2-methylallyl and *endo*-9-methylbicyclo[6.1.0]non-4-ene ligands respectively.[27] These ligands all bind to the Pd$_3$Cl$_4$ clusters through an η^3 coordination mode and as in the above Hughes and co-workers example, all the clusters are planar which sets them apart from the Pd$_3$Cl$_6$ cradle described here. This suggests that the latter can only be formed with binucleating ligands in which distances between the binding sites are short enough to enforce this motif.

4.5 Synthesis of H_2L^{Cp}

Cycloaromatic ligands such as cyclopentadienes make highly versatile ligands capable of interacting with most metals.[5, 28] An important example to the field of catalysis is that reported by Chirik and co-workers in which the binding preferences of N_2 with a variety of bis(cyclopentadienyl)titanium complexes was investigated (Figure 22).[29] Although the binding preference is dependent on the size of the ring substituent, in the presence of excess group four metals, such as titanium, N_2 will form binuclear complexes.
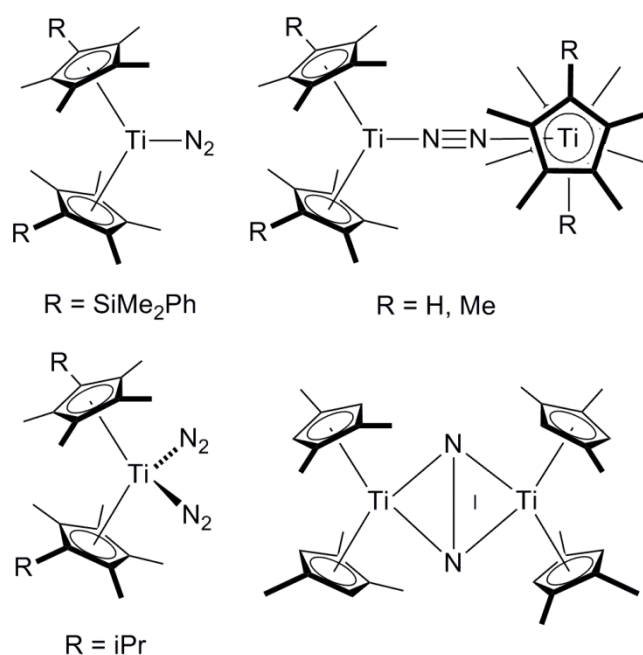
Figure 22: Some structurally characterised examples of disubstituted bis(cyclopentadienyl)titanium dinitrogen complexes.[29]

The N_2 binding mode was investigated by IR spectroscopy save for centrosymmetric, bridging end-on complexes for which cases, solid state characterisation was necessary. In order to assess the electron density of the multiple ligands and differentiate it from their steric contributions, the dicarbonyl derivatives of each titanocene complex were formed following a method developed by Parkin and co-workers as well as Chirik and co-

workers.[30] This showed that the relative electronic donation of the different cyclopentadienyl substituents increases with smaller electropositive substituents. Chirik and co-workers have also investigated the activation of N_2 with bis(cyclopentadienyl) complexes with metals such as zirconium and halfnium.[31]

In an effort to bind a wider variety of metals and help enforcing a binding motif leading to the formation of metallo-macrocyles, the imine and amine group that were previously used to functionalise 1,4-dibromomethyl-2,3,5,6-tetramethylbenzene were replaced by cyclopentadienes. This reaction was carried out under an atmosphere of dry nitrogen and involved the nucleophilic substitution of each bromide by a cyclopentadienyl and yielded H_2L^{Cp} as a colourless powder in over 93 % yield (shown in Scheme 5).
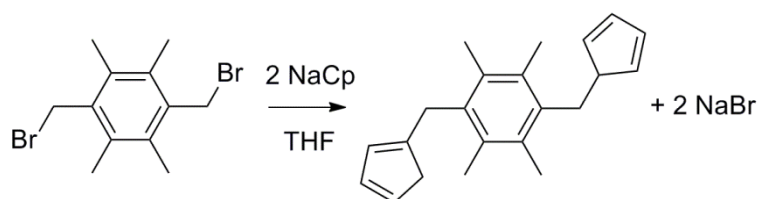
Scheme 5: Synthesis of H_2L^{Cp}.

The ^1H NMR spectrum shows a multitude of resonances between 6.55 and 5.69 ppm corresponding to the multiple diene isomers of H_2L^{Cp}. A single resonance is observed for the durene's CH_3 supporting the formation of a pure material. The purity of this pro-ligand was also corroborated by the elemental analysis.

4.6 Synthesis of [Li$_2$L^{Cp}]

The addition of Li[N(SiMe$_3$)$_2$] to H_2L^{Cp} under an atmosphere of dry nitrogen led to the formation of [Li$_2$L^{Cp}] as a colourless powder in 95 % yield (as seen in Scheme 6).
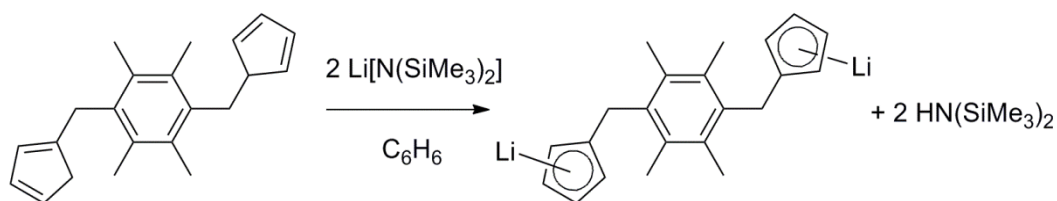
Scheme 6: Synthesis of [Li$_2$L^{Cp}]

The ^{1}H NMR spectrum confirms the formation of the complex with the presence of only two resonances corresponding to the cyclopentadienyl rings being once again aromatic. The singlet CH$_2$ resonance, as well as the lack of C**H**-CH$_2$ resonance is concordant with the deprotonation of both CpH rings.

(η^5-Cp)Li complexes are well known and used to synthesise a variety of sandwich and half-sandwich complexes through either trans-metallation or salt elimination reaction.[32] Although no crystals of Li$_2$L^{Cp} suitable for X-ray crystallography were obtained, most [LiCp$_2$] structures can be viewed as fragments of polymeric lithium cyclopentadienyl (Figure 23 a). These, recently described by Long include: the lithocene sandwich anion; the inverted sandwich cation (two lithium atoms binding to a single ring); and the piano chair monomeric 1:1 lithium cyclopentadienyl, displayed in Figure 23 b, c and d respectively.[33]
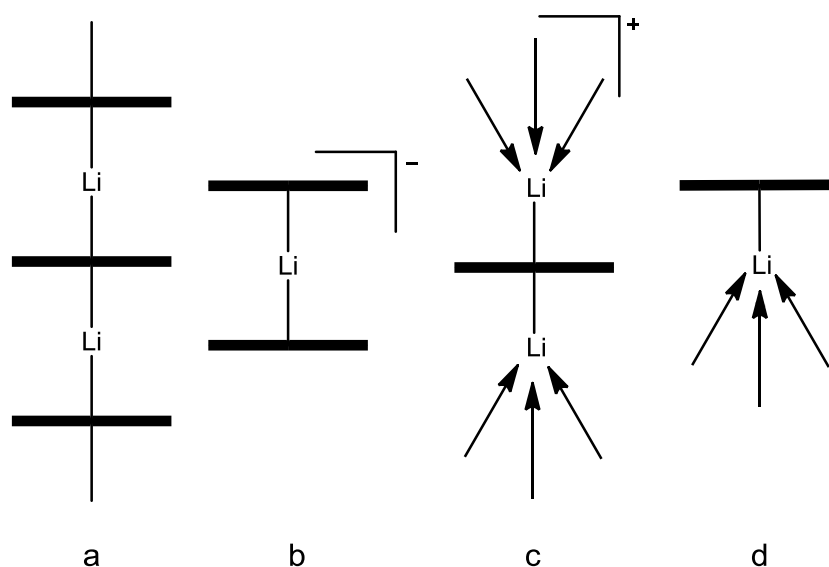
Figure 23: Solvated fragments of polymeric [CpLi]

Salt elimination reactions with titanium and zirconium precursors were attempted but produce either an inextricable mixture of products or highly insoluble materials which could indicate the formation of a polymeric structure.

4.5 Conclusions

New wide-span imine and amine ligands have been synthesised in good yields from readily available precursors. Although reactions between these pro-ligands and first row transition metals salts has proven to be unsuccessful under neutral conditions, under acidic conditions, the ligand is protonated and promotes the formation of the chlorometallates $[H_2L^{AmR}][CoCl_4]$ and $[H_2L^{ImAr}][Zn_4Cl_{10}]$. The latter tetrazincate structure has been observed, for the first time, in a rectangular arrangement.

Further investigation into the use of these ligands has led to the preferential assembly of the trinuclear complexes $[Pd_3Cl_6(L^{ImAr})]$ and $[Pd_3Cl_6(L^{ImR})]$. The rarely observed Pd_3Cl_6 cluster was found to chelate to the imine-nitrogen binding sites of a single ligand. The proximity of these

chelation sites enforced a cradle motif onto the cluster which has not been reported in prior studies.

New wide-span cyclopentadienyl ligands have been synthesised in order to bind a wider variety of metals. Although the solid state structure of [Li_2L^{Cp}] is unclear, its reactivity with transition metals through salt elimination reactions needs to be further investigated, and could lead to the formation sandwich complexes and 2+2 or larger metallo-macrocyles.

4.6 References

[1]   M. Delferro, T. J. Marks, *Chem. Rev.* **2011**, *111*, 2450-2485; R. M. Haak, S. J. Wezenberg, A. W. Kleij, *Chem. Commun.* **2010**, *46*, 2713-2723; H. Dau, C. Limberg, T. Reier, M. Risch, S. Roggan, P. Strasser, *Chem. Cat. Chem.* **2010**, *2*, 724-761.

[2]   N. C. Gianneschi, S. T. Nguyen, C. A. Mirkin, *J. Am. Chem. Soc.* **2005**, *127*, 1644-1645.

[3]   J. P. Collman, R. Boulatov, C. J. Sunderland, L. Fu, *Chem. Rev.* **2003**, *104*, 561-588; R. H. Holm, P. Kennepohl, E. I. Solomon, *Chem. Rev.* **1996**, *96*, 2239-2314; M. J. Wiester, P. A. Ulmann, C. A. Mirkin, *Angew. Chem. Int. Ed.* **2011**, *50*, 114-137.

[4]   G. T. Babcock, M. Wikstrom, *Nature* **1992**, *356*, 301-309.

[5]   N. P. E. Barry, O. Zava, W. Wu, J. Zhao, B. Therrien, *Inorg. Chem. Commun.* **2012**, *18*, 25-28; M. A. Furrer, F. Schmitt, M. Wiederkehr, L. Juillerat-Jeanneret, B. Therrien, *Dalton Trans.* **2012**; N. P. E. Barry, F. Edafe, B. Therrien, *Dalton Trans.* **2011**, *40*, 7172-7180; J. Mattsson, O. Zava, A. K. Renfrew, Y. Sei, K. Yamaguchi, P. J. Dyson, B. Therrien, *Dalton Trans.* **2010**, *39*, 8248-8255.

[6]   C. M. Davis, A. C. Royer, J. B. Vincent, *Inorg. Chem.* **1997**, *36*, 5316-5320.

[7]   A. Earnshaw, B. N. Figgis, J. Lewis, *J. Chem. Soc. A: Inorg., Phys., Theor.* **1966**, 1656-1663.

[8]   T. Glaser, *Chem. Commun.* **2011**, *47*, 116-130; G. Aromí, E. Brechin, *Vol. 122* (Ed.: R. Winpenny), Springer Berlin / Heidelberg, **2006**, pp. 1-67.

[9]   T. Lis, *Acta Crystallogr. Sec. B* **1980**, *36*, 2042-2046.

[10]   R. Inglis, C. J. Milios, L. F. Jones, S. Piligkos, E. K. Brechin, *Chem. Commun.* **2012**, *48*, 181-190; M. Manoli, R. Inglis, M. J. Manos, V. Nastopoulos, W. Wernsdorfer, E. K. Brechin, A. J. Tasiopoulos, *Angew. Chem. Int. Ed.* **2011**, *50*, 4441-4444; G. Karotsis, S. Kennedy, S. J. Teat, C. M. Beavers, D. A. Fowler, J. J. Morales, M. Evangelisti, S. J. Dalgarno, E. K. Brechin, *J. Am. Chem. Soc.* **2010**, *132*, 12983-12990.

[11]   A. L. Gavrilova, B. Bosnich, *Chem. Rev.* **2004**, *104*, 349-384; S. Brooker, *Eur. J. Inorg. Chem.* **2002**, *2002*, 2535-2547; H. L. C. Feltham, S. Brooker,

Coord. Chem. Rev. **2009**, *253*, 1458-1475; P. D. Frischmann, M. J. MacLachlan, *Comments on Inorganic Chemistry* **2008**, *29*, 26-45; J. Vela, L. Zhu, C. J. Flaschenriem, W. W. Brennessel, R. J. Lachicotte, P. L. Holland, *Organometallics* **2007**, *26*, 3416-3423; P. Comba, T. W. Hambley, P. Hilfenhaus, D. T. Richens, *J. Chem. Soc., Dalton Trans.* **1996**, 533-539; P. Comba, A. Fath, T. W. Hambley, D. T. Richens, *Angew. Chem. Int. Ed.* **1995**, *34*, 1883-1885.

[12]   S. Brooker, R. J. Kelly, B. Moubaraki, K. S. Murray, *Chem. Commun.* **1996**, 2579-2580.

[13]   F. Zhang, M. C. Jennings, R. J. Puddephatt, *Organometallics* **2004**, *23*, 1396-1404.

[14]   S. Valiyaveettil, J. F. J. Engbersen, W. Verboom, D. N. Reinhoudt, *Angew. Chem. Int. Ed.* **1993**, *32*, 900-901.

[15]   P. K. Thallapally, G. R. Desiraju, M. Bagieu-Beucher, R. Masse, C. Bourgogne, J.-F. Nicoud, *Chem. Commun.* **2002**, 1052-1053; M. Freytag, P. G. Jones, B. Ahrens, A. K. Fischer, *New J. Chem.* **1999**, *23*, 1137-1139; G. R. Desiraju, R. Parthasarathy, *J. Am. Chem. Soc.* **1989**, *111*, 8725-8726.

[16]   S. L. Price, A. J. Stone, J. Lucas, R. S. Rowland, A. E. Thornley, *J. Am. Chem. Soc.* **1994**, *116*, 4910-4918.

[17]   B. Kuswandi, N. N/a, W. Verboom, D. Reinhoudt, *Sensors* **2006**, *6*, 978-1017; W. A. Quinn, M. A. Saeed, D. R. Powell, M. A. Hossain, *Int. J. Environ. Res. Public Health* **2010**, *7*, 2057-2070; cH. Ihm, S. Yun, H. G. Kim, J. K. Kim, K. S. Kim, *Org. Lett.* **2002**, *4*, 2897-2900.

[18]   E. Corradi, S. V. Meille, M. T. Messina, P. Metrangolo, G. Resnati, *Angew. Chem. Int. Ed.* **2000**, *39*, 1782-1786.

[19]   F. Bottomley, P. D. Boyle, S. Karslioglu, R. C. Thompson, *Organometallics* **1993**, *12*, 4090-4096.

[20]   R. J. Ellis, J. Chartres, K. C. Sole, T. G. Simmance, C. C. Tong, F. J. White, M. Schroder, P. A. Tasker, *Chem. Commun.* **2009**, 583-585.

[21]   F. Bottomley, S. Karslioglu, *J. Chem. Soc., Chem. Commun.* **1991**, 222-223.

[22]   V. R. Pedireddi, D. S. Reddy, B. S. Goud, D. C. Craig, A. D. Rae, G. R. Desiraju, *J. Chem. Soc., Perkin Trans. 2* **1994**, 2353-2360.

[23]   M. A. Hossain, J. A. Liljegren, D. Powell, K. Bowman-James, *Inorg. Chem.* **2004**, *43*, 3751-3755.

[24]   P. M. Maitlis, D. Pollock, M. L. Games, W. J. Pryde, *Can. J. Chem.* **1965**, *43*, 470-478.

[25]   Y. Ohzu, K. Goto, T. Kawashima, *Angew. Chem. Int. Ed.* **2003**, *42*, 5714-5717; Y. Ohzu, K. Goto, H. Sato, T. Kawashima, *J. Organomet. Chem.* **2005**, *690*, 4175-4183.

[26]   B. T. Donovan, R. P. Hughes, P. P. Spara, A. L. Rheingold, *Organometallics* **1995**, *14*, 489-494.

[27]   P. M. Bailey, E. A. Kelley, P. M. Maitlis, *J. Organomet. Chem.* **1978**, *144*, C52-C56; M. Parra-Hake, M. F. Rettig, R. M. Wing, *Organometallics* **1983**, *2*, 1013-1017.

[28]   E. S. Barrett, J. L. Irwin, A. J. Edwards, M. S. Sherburn, *J. Am. Chem. Soc.* **2004**, *126*, 16747-16749; D. A. Makeiff, J. C. Sherman, *J. Am. Chem. Soc.* **2005**, *127*, 12363-12367; R. Hoffmann, J. M. Howell, A. R. Rossi, *J. Am. Chem. Soc.* **1976**, *98*, 2484-2492; W. O. Gillum, R. A. D. Wentworth, R. F.

Childers, *Inorg. Chem.* **1970**, *9*, 1825-1832; R. S. Forgan, J. E. Davidson, S. G. Galbraith, D. K. Henderson, S. Parsons, P. A. Tasker, F. J. White, *Chem. Commun.* **2008**, 4049-4051; fO. D. Fox, T. D. Rolls, M. G. B. Drew, P. D. Beer, *Chem. Commun.* **2001**, 1632-1633.

[29]   X. Liu, R. Warmuth, *J. Am. Chem. Soc.* **2006**, *128*, 14120-14127.

[30]   A. A. Belal, P. Chaudhuri, I. Fallis, L. J. Farrugia, R. Hartung, N. M. MacDonald, B. Nuber, R. D. Peacock, J. Weiss, K. Weighardt, *Inorg. Chem.* **1991**, *30*, 4397-4402; C. Wendelstorf, R. Krämer, *Angew. Chem. Int. Ed.* **1997**, *36*, 2791-2793.

[31]   C. A. Dodds, M.-A. Lehmann, J. F. Ojo, J. Reglinski, M. D. Spicer, *Inorg. Chem.* **2004**, *43*, 4927-4934; P. J. Bailey, M. Lanfranchi, L. Marchiò, S. Parsons, *Inorg. Chem.* **2001**, *40*, 5030-5035; J. Reglinski, M. D. Spicer, M. Garner, A. R. Kennedy, *J. Am. Chem. Soc.* **1999**, *121*, 2317-2318; J. L. Sessler, E. Tomat, V. M. Lynch, *Chem. Commun.* **2006**, 4486-4488.

[32]   P. L. Arnold, N. A. Potter, C. D. Carmichael, A. M. Z. Slawin, P. Roussel, J. B. Love, *Chem. Commun.* **2010**, *46*, 1833-1835; M. Rafizadeh, V. Amani, E. Iravani, B. Neumüller, *Z. Anorg. Allg Chem.* **2005**, *631*, 952-955.

[33]   Y.-Y. Zhang, S.-X. Liu, *Acta Crystallogr. Sec. C* **2009**, *65*, m269-m272.

Chapter 5: Conclusions

Capsular complexes associating metal centres in a highly reactive geometry along with proximate substrate secondary binding sites have been seen to mimic enzymes and their catalytic properties. The formation of capsules through the non-covalent approach is the most efficient in terms of host guest dissociation leading to higher turnover numbers and frequency.

The encapsulation of substrate molecules is paramount to isolate them from the reaction medium and enhance the catalytic activity of the host. H_3L has not only shown a propensity to encapsulate small molecules such as H_2O, but also the ability to encapsulate larger entities, including the stacked six-membered rings $\{Li_6O_6\}$ through the co-operation of two ligand molecules.

The development of secondary substrate binding sites in pyrrole-imine complexes can be achieved by two different methods:

  - tautomerisation into the aza-fulvene

  - protonation of the imine through the addition of acid

Ligand tautomerisation was achieved through the addition of both octahedral and tetrahedral transition metals. The formation of the aza-fulvene isomer was observed on every branch of the ligand upon metallation with Co^{II} whereas only two branches were tautomerised with Zn^{II}. However, the ligand geometry adopted by these two complexes did not lead to the encapsulation of a small molecule in the vicinity of the metal centre but rather to the formation of the mono-metallic multi-ligand complex $[Co(H_3L)_2][Cl]_3$ and multi-metallic multi-ligand complex $[Zn_2(H_2L)_2][Cl]_2$.

Ligand protonation was achieved on a single branch of the tripod through the intrinsic formation of HCl upon addition of MCl_2 (M = Pd or Cu) to H_3L. This resulted in the formation of hangman type ligands with two deprotonated branches of the tripod bound to the metal centre whilst the third arm is pendant. The ligand protonation through the insertion of HCl within the molecule led to the formation of a hydrophobic pocket around the anion. In the case of $[CuCl(H_2L)]$ this also resulted in the full encapsulation of the anion with all three branches of the tripod orientated in the same direction. The replacement of MCl_2 by $M(OAc)_2$ (M = Pd or Cu) led to the formation of similar complexes without any protonation observed. It infers that acetic acid formed during the course of the reaction is not strong enough to protonate H_3L.

The need to form secondary interaction sites upon metallation was avoided with the development of a new tripodal pyrrole-amide ligand (H_6L^2). Reactions with Ti^{iv} resulted in the formation of another hangman complex through the binding of the pyrrolide nitrogens and amide oxygens of two branches of the tripod. The presence of two isopropoxide groups bound to the metal centre prevented potential encapsulation of a substrate molecule between the pendant arm and the metal centre.

The synthesis of new wide-span di-imine, di-amine and *bis*-cyclopentadienyl ligands with a view to form highly ordered complexes such as metallo-cycles and metallo-cryptands was achieved in high yields. Probing of their transition metal chemistry resulted in the formation of cobalt and zinc chlorometallates. Although extraction reactions were attempted, the formation of a third phase early in the investigation limited the results available. The addition of further solubilising groups could in the future

result in good metal extraction as predicted by the formation of the four metal one ligand chlorometallate of zinc. Upon reaction of Pd^{II} with the di-imine ligands, the void between the two chelation sites was bridged by a cluster of three PdCl$_2$ molecules. Although so far the formation of a metallo-cycle with these ligands has not been observed further investigation on the *bis*-Cp ligand needs to be carries out.

In summary, the formation of a substrate binding pocket proximate to a metal centre within H$_3$L is best achieved with square planar or square-planar derived transition metal precursors. Further investigation in this area include the binding of a second metal to the pendant arm to establish a red/ox relationship between the two metals and study the new bimetallic complex's potential towards small molecule activation. New wide-span di-imine and di-amine ligands have been synthesised, but require further development to increase their solubility and metal extraction potential. The metal chemistry of the *bis*-Cp ligand should be further probed with a view to form metallo-cryptands and metallo-cycles.

Chapter 6: Experimental details and characterising data

6.1 General methods and instrumentation

The synthesis of [Li$_3$(L)], [K$_3$(L)], [Ce$_2$(L)$_2$(THF)$_2$], [Ti(O^{i}Pr)$_2$(HL^{Cy})], and [Ti(O^{i}Pr)$_2$(HL^{Me})] were carried out using standard Schlenk procedures or dry box techniques under an atmosphere of dry dinitrogen and using solvents dried by a Vacuum Atmospheres solvent purification assembly. Deuterated C$_6$D$_6$ was dried over potassium, trap to trap vacuum distilled, and freeze-pump-thaw degassed three times prior to use. All other synthetic procedures were carried out using commercial-grade solvent in air. Pyrrole was distilled under reduced pressure prior to use. All other chemicals were used as purchased.

^{1}H NMR spectra were recorded at 298 K, unless otherwise stated on Bruker DPX 250, DPX 360, AVA 400, DMX 500, AVA 500 and AVA 600 spectrometer at operating frequencies of 250.13, 360.13, 399.90, 500.13, 500.12 and 599.81 MHz, respectively. ^{13}C{^{1}H} spectra were recorded on the same spectrometers at operating frequencies of 62.90, 90.55, 100.55, 125.76, 125.76 and 150.82 MHz, respectively. ^{1}H and ^{13}C{^{1}H} spectra were referenced internally to residual protio solvent (^{1}H) or solvent (^{13}C) resonances and are reported relative to tetramethylsilane (δ = 0 ppm) and with coupling constants in Hertz.

Mass spectra were recorded by Mr Alan Taylor of the mass spectrometry service of the University of Edinburgh's School of Chemistry using a Thermo LCQ instrument. Samples were prepared as solutions of MeCN and/or DCM and analysed using electrospray. IR spectra were

recorded on a Perkin Elmer Spectrum 65 FTIR or a JASCO FT/IR-410 spectrometer as solids or KBr disks. UV-Vis spectra were recorded on a Varian Cary 50 scan UV-Visible spectrophotometer. Elemental analyses were carried out by Mr Stephen Boyer at London Metropolitan University.

Cyclic voltamograms were obtained using an Autolab ECO CHEMIE PGSTAT 12 using tetrabutylammonium tetrafluoroborate electrolyte (0.2 M) and complex (1 mM) in dry THF under N_2. A platinum working electrode with a silver wire reference electrode and a platinum foil counter electrode were used for the measurements and values were referenced against ferrocene (Fc/Fc$^+$ E$_{1/2}$ = 0 V).

Single-crystal X-ray diffraction data were recorded on one of four machines:

At 100 K using an Oxford Cryosystems low temperature device attached to an Oxford diffraction SuperNova dual wavelength diffractometer equipped with an Atlas CCD detector and an operating mirror monochromated Cu*Ka* radiation mode (λ = 1.54184 Å).

At 150 K using Oxford Cryosystems low temperature device attached to an Oxford diffraction Eos diffractometer equipped with an Eos detector and operating graphite monochromated Mo*Ka* radiation mode (λ = 0.71073 Å).

At 150 K on a Bruker SMART APEX diffractometer equipped with a CCD area detector using graphite monochromated Mo*Ka* radiation mode (λ = 0.71073 Å).

At 170 K on a Rigaku MM007 diffractometer equipped with a high brilliance Saturn 70 CCD detector using graphite monochromated Mo*Ka* radiation mode (λ = 0.71073 Å).

The structures were solved by direct methods using the WinGX suite of programs[1] and refined using full-matrix least square refinements on |F^2| using SHELXTL-97.[2] Unless otherwise stated, all non hydrogen atoms were placed at calculated position and included as part of a riding model.

The synthesis of 2,2',2''-tripyrrylethane and *tris*(5,5',5''-formyl-2,2',2''-pyrryl)ethane,[3] 1,4-dibromomethyl-2,3,5,6-tetramethylbenzene[4] and 2,3,5,6-tetramethylterephthalaldehyde[5] were carried out as described in the literature.

6.2 Synthetic procedures as described in Chapter 2

6.2.1 Synthesis of H$_3$L
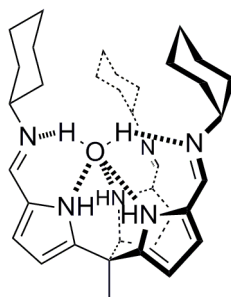
To a mixture of *tris*(5,5',5''-formyl-2,2',2''-pyrryl)ethane (0.48 g, 1.8 mmol) in MeCN (20 mL) was added cyclohexylamine (0.61 g, 6.2 mmol). The mixture was stirred for 16 h during which a colourless precipitate formed which was filtered, washed with MeCN and dried under vacuum to yield 0.89 g, 92 % of H$_3$L as a colourless solid. Single crystals were grown by cooling a saturated MeCN solution. The symmetry-generated structure of H$_3$L.H$_2$O exhibited three-fold rotational disorder of the pyrrole-imine arms from the apical carbon atom C2 and was best refined with anisotropic atomic displacement parameters using a two site 50:50 occupancy protocol. The cyclohexyl carbon were disordered and were refined using a restrained anisotropic model. The hydrogen atoms on the molecule of water were neither located nor placed

geometrically, but were added to the formula; this has resulted in an A-alert in the CIF check.

^{1}H NMR (500 MHz, C$_6$D$_6$): δ_H 8.47 (br. s, 3H, NH), 7.62 (s, 3H, CH imine), 6.26 (d, 3H, $^3J_{HH}$ = 3.57 Hz, pyrrole), 6.02 (d, 3H, $^3J_{HH}$ = 3.57 Hz, pyrrole), 2.84 (tt, 3H, $^3J_{HH}$ = 10.28 Hz, $^3J_{HH}$ = 3.63 Hz, CH cyh), 1.70 (s, 3H, CH$_3$), 1.68 (m, 6H, cyh), 1.62 - 1.50 (m, 12H, cyh), 1.26 - 1.08 (m, 12H, cyh) ppm; ^{13}C{^{1}H} NMR (91 MHz, C$_6$D$_6$): δ_C 149.1, 141.3, 130.6, 128.0, 114.7, 107.9, 68.23, 40.8, 34.7, 25.8, 24.8 ppm; Analysis. Found: C, 75.99, H, 8.89, N, 15.16% C$_{35}$H$_{48}$N$_6$ requires C, 76.05, H, 8.75, N, 15.20 %; ESMS (+ve ion): *m/z* 553.73 ([M+H]$^+$, 100%); IR (KBr): υ 3288 (pyrrole NH), 1639 (C=N) cm^{-1}.

6.2.2 Synthesis of [Li$_3$(L)]
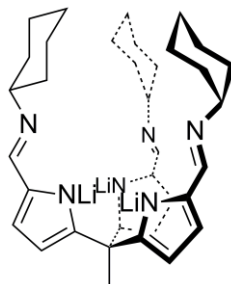
To a solution of H$_3$L (0.11 g, 0.20 mmol) in THF (5 mL), was added a solution of LiN(SiMe$_3$)$_2$ (0.11 g, 0.70 mmol) in THF (5 mL). The mixture was boiled for 16 h under N$_2$ after which the solvents were removed under reduced pressure to afford 0.10 g, 88 % of [Li$_3$(L)] as a colourless powder.

^{1}H NMR (500 MHz, C$_6$D$_6$/THF): δ_H 7.55 (s, 3H, CH imine), 6.85 (d, 3H, $^3J_{HH}$ = 3.68 Hz, pyrrole), 6.66 (d, 3H, $^3J_{HH}$ = 3.68 Hz, pyrrole), 2.78 (s, 3H, CH cyh), 1.62 (s, 3H, CH$_3$), 1.60 (m, 6H, cyh), 1.55 - 1.42 (m, 12H, cyh), 1.15 - 0.86 (m, 12H, cyh) ppm; ^{13}C{^{1}H} NMR (126 MHz, C$_6$D$_6$): δ_C 149.09, 131.03 (q), 127.6, 114.1 (q), 108.7, 69.5, 41.1, 35.7, 30.0 (q), 26.12, 25.2 ppm; IR (nujol): υ No NH present, 1639 (C=N) cm^{-1}.

6.2.3 Crystal formation of [Li$_3$(THF)$_3$(LiOH)$_3$(L)]$_2$

Single crystals were grown by diffusion of hexane into a THF solution of [Li$_3$(L)] at -25 ^{o}C under an atmosphere of N$_2$. The hydrogen atoms H100, H101, H102, located on O4, O5 and O6 respectively, were located on the difference Fourier map and refined with bond length restraints and riding thermal parameters. In this structure, one cyclohexyl group and THF ligand were disordered and were refined with variable two-site occupancies and with isotropic atomic displacement parameters. Also, the THF solvent of crystallisation was disordered and was refined with restrained bond distances and isotropic atomic displacement parameters.

6.2.4 Synthesis of [K$_3$(L)]
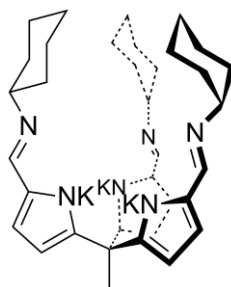
To a solution of H$_3$L (0.20 g, 0.36 mmol) in THF (10 mL), was added a slurry of KH (0.062 g, 1.6 mmol) in THF (5 mL). The mixture was boiled for 16 h under N$_2$ after which the solvent was evaporated under reduced pressure to afford 0.22 g, 90 % of [K$_3$(L)] as a colourless solid.

^{1}H NMR (500MHz, C$_6$D$_6$/THF): δ_H 8.13 (s, 3H, CH imine), 6.53 (d, 3H, $^3J_{HH}$ = 2.78 Hz, pyrrole), 6.15 (d, 3H, $^3J_{HH}$ = 2.78 Hz, pyrrole), 3.08 (m, 3H, CH cyh), 2.10 (m, 9H, CH$_3$ and cyh), 1.76 - 1.48 (m, 24H, cyh) ppm; ^{13}C{^{1}H} NMR (126 MHz, d_5-pyr): δ_C 161.9 (q), 156.4, 135.0, 116.0 (q), 105.7, 69.1, 48.7, 35.9, 31.1 (q), 26.0, 25.6 ppm; IR (nujol): υ No NH present, 1605 (C=N) cm^{-1}.

6.2.5 Synthesis of [Co(H₃L)₂][Cl₃]
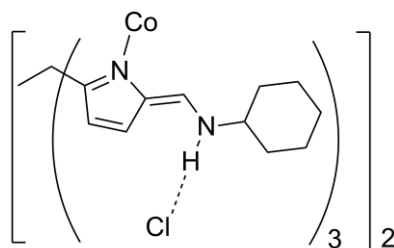
To a solution of H₃L (0.10 g, 0.18 mmol) in EtOH (5 mL), was added a solution of CoCl₂ (0.024 g, 0.19 mmol) in EtOH (10 mL) and a mixture of NaCl (0.011 g, 1.8 mmol) in EtOH (2 mL). The resulting solution was stirred at room temperature for 16 h after which the mixture was filtered. The filtrate was dried under reduced pressure and the residues were washed with EtOAc to afford 0.10 g, 88 % of [Co(H₃L)₂][Cl₃] as a green powder. Single crystals were grown by slow diffusion of Et₂O into a saturated MeOH solution. All three cyclohexyls groups were disordered and were modelled with variable two-site occupancy and anisotropic atomic displacement parameters. The SQUEEZE routine of PLATON[6] was used to evaluate the void space and it was found that 1070.4 Å³ of void space was present in the unit cell, yet this contained only 20 electrons. The primary electron density was found to be within hydrogen-bonding distance to the Cl atoms, so it is likely that it is due to poorly-described water of crystallisation within the void structure. Due to the poor modelling of this electron density, no atoms have been added to the formula.

^{1}H NMR (500 MHz, CD₃OD): δ_H 7.45 (d, 6H, $^3J_{HH}$ = 4.57 Hz, pyrrole), 6.89 (d, 6H, $^3J_{HH}$ = 4.57 Hz, pyrrole), 5.60 (s, 6H, CH imine), 2.62 (m, 12H, CH₃ and CH cyh), 1.87 - 0.67 (m, 60H, cyh) ppm; ^{13}C{^{1}H} NMR (126 MHz, CD₃OD): δ_C 160.4 (q), 152.8, 129.6 (q), 125.0, 111.5, 59.6, 47.0, 32.3, 24.5, 24.2, 17.2 (q) ppm;

Analysis Found: C, 58.71, H, 5.71, N, 12.73 % $C_{70}H_{96}Cl_3CoN_{12}$ requires C, 66.15, H, 7.61, N, 13.23 %; ESMS (+ve ion): *m/z* 1161 ([M+H]$^+$, 100%); ESMS (-ve ion): *m/z* 1159 ([M]$^-$, 15.90 %), 1195 ([M+Cl]$^-$, 76.88 %), 1231 ([M+2Cl]$^-$, 100 %); IR (KBr): υ 3419 (NH), 1636 (C=N) cm^{-1}.

6.2.6 Synthesis of [Zn₂(H₃L)₂][Cl]₂
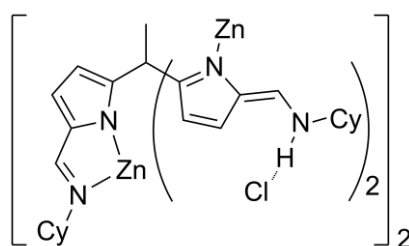
To a solution of H₃L (1.0 g, 1.9 mmol) in EtOH (50 mL), was added NEt₃ (0.38 g, 3.8 mmol) and a solution of ZnCl₂ (0.26 g, 1.9 mmol) in EtOH (10 mL). The resulting solution was stirred at room temperature for 16 h after which the solvents were evaporated under reduced pressure. The residual solids were extracted into CHCl₃ (50 mL), filtered, and the filtrate dried under reduced pressure to afford 0.32 g, 26 % of [Zn₂(H₃L)₂][Cl]₂ as a colourless solid. Single crystals were grown by slow diffusion of Et₂O into a saturated MeOH solution. One cyclohexyl group was disordered and was modelled over two sites with 0.52:0.48 occupancy, bond restraints, and anisotropic atomic displacement parameters. Solvent of crystallisation could not be modelled satisfactorily and the SQUEEZE routine of PLATON[6] was used which found 646.3 Å^3 of void space with 148.5 electrons in the unit cell, which equates to the presence of approximately two molecules of THF per asymmetric unit; the appropriate number of C, H and O atoms were added to the UNIT instruction; this has resulted in an A-alert in the CIF check. The relatively

high residual electron density was located 0.916 Å from Zn1 and is attributed to absorption problems.

^{1}H NMR (400 MHz, CD$_3$OD): δ_H 10.2 (dd, 4H, $^3J_{HH}$ = 15.1 Hz, $^3J_{HH}$ = 3.8 Hz, NH), 8.10 (s, 2H, imine), 7.65 (d, 4H, $^3J_{HH}$ = 4.4 Hz, pyrrole), 6.80 (d, 2H, $^3J_{HH}$ = 3.7, pyrrole), 6.67 (d, 2H, $^3J_{HH}$ = 3.7 Hz, pyrrole), 6.50 (d, 4H, $^3J_{HH}$ = 15.1 Hz, alkene), 5.98 (d, 4H, $^3J_{HH}$ = 3.9 Hz, pyrrole), 3.20 (m, 6H, CH cyh), 2.10 – 0.66 (m, 60H, cyh), 1.94 (s, 6H, CH$_3$) ppm; ^{13}C{^{1}H} NMR (101 MHz, CD$_3$OD): δ_C 160.5, 155.9, 155.0, 149.0, 136.0, 128.1, 124.8, 117.3, 117.1, 109.0, 65.7, 57.3, 45.1, 34.9, 32.6, 31.6, 25.3, 25.1, 24.7, 24.6 ppm; Analysis Found: C, 64.49, H, 7.24, N, 12.72 % C$_{70}$H$_{94}$Cl$_2$N$_{12}$Zn$_2$ requires C, 64.41, H, 7.26, N, 12.88 %; ESMS (+ve ion): *m/z* 617.70 ([M-Zn-ligand]$^+$, 100%), 1233.7 ([M]$^+$, 59.92%); IR (KBr): υ 3419 (NH), 1652 (C=N), 1586 (C=C), 1281 (C-N) cm^{-1}.

6.2.7 Synthesis of [Ce$_2$(L)$_2$(THF)$_2$]
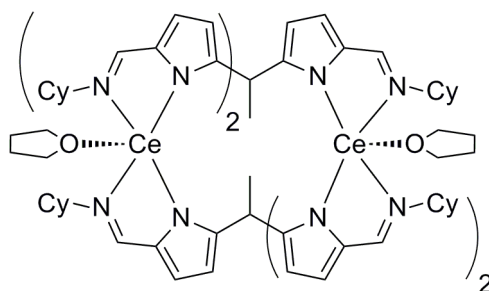
To a cold (0 °C) solution of Ce{N(SiMe$_3$)$_2$}$_3$ (0.11 g, 0.18 mmol) in THF (5 mL), was added a solution of H$_3$L (0.097 g, 0.18 mmol) in THF (20 mL). The mixture was allowed to warm to room temperature and stirred for 8 hours. The solvents were removed under reduced pressure to afford 0.087 g of [Ce$_2$(L)$_2$(THF)$_2$] as a yellow powder. Single crystals were grown by slow diffusion of hexane into a saturated THF solution. One coordination site on the cerium atom was disordered and was modelled as 60/40 occupancy of

THF and H_2O. A second THF molecule was modelled with 40% occupancy and was found to hydrogen-bond to the water molecule. All disordered atoms were modelled with isotropic displacement parameters. Solvent of crystallisation could not be modelled satisfactorily and the SQUEEZE routine of PLATON[6] was used which found 1124 Å ^{3} of void space with 338 electrons in the unit cell, which equates to the presence of approximately two molecules of THF per asymmetric unit; the appropriate number of C, H and O atoms were added to the UNIT instruction. Attempts to repeat the reaction proved fruitless and led to the formation of an inextricable mixture of products. ^{1}H NMR spectra did not show the 2:1 splitting that would be expected for the formation of $[Ce_2(L)_2(THF)_2]$.

6.3 Synthetic procedures as described in Chapter 3

6.3.1 Synthesis of [Pd(HL)]
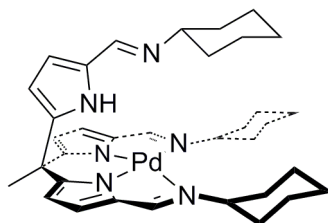
To a mixture of H_3L (0.50 g, 0.91 mmol) in MeCN (10 mL) and NEt_3 (2 mL), was added a solution of $Pd(OAc)_2$ (0.21 g, 0.94 mmol) in MeCN (50 mL). The reaction was stirred for 2 h at room temperature. The precipitate was filtered, washed with MeCN (2 × 10 mL) and dried overnight under high vacuum affording 0.39 g, 62 % of [Pd(HL)] as a yellow solid. Single crystals were obtained by cooling of a saturated solution of MeCN.

^{1}H NMR (400MHz, $CDCl_3$): δ_H 7.59 (s, 1H, imine), 7.57 (s, 2H, imine), 6.65 (d, 2H, $^3J_{HH}$ = 3.4 Hz, pyrrole), 6.60 (d, 1H, $^3J_{HH}$ = 3.9 Hz, pyrrole), 6.16 (d, 2H, $^3J_{HH}$ = 3.4 Hz, pyrrole), 5.89 (d, 1H, $^3J_{HH}$ = 3.9 Hz, pyrrole), 3.24 (m, 2H, CH cyh),

3.23 (m, 1H, CH cyh), 2.06 (s, 3H, CH₃), 2.22 - 1.00 (m, 30H, cyh) ppm; ^{13}C{^{1}H} NMR (126 MHz, CDCl₃): δ_C 156.4 (q), 149.2, 147.5, 142.0 (q), 136.8 (q), 129.8, 116.1 (q), 114.3, 107.7, 106.5, 69.3, 63.2, 46.9 (q), 34.5, 34.1, 31.0, 26.2, 25.8, 25.0; Analysis. Found: C, 63.81, H, 6.93, 12.67 % C₃₅H₄₆N₆Pd requires C, 63.96, H, 7.05, N, 12.79 % ; ESMS (+ve ion): *m/z* 481.29 ([PdL]⁺ loss of free arm, 52 %), 657.36 ([Pd(HL)]⁺, 100 %); IR (KBr): υ 3410 (NH), 1637 (C=N), 1569 (C=C); UV-Vis (CHCl₃, 25 °C): 390 nm (ε =11851 dm³mol⁻¹cm⁻¹), 295 nm (ε = 22734 m³mol⁻¹cm⁻¹)

6.3.2 Synthesis of [Cu(HL)]
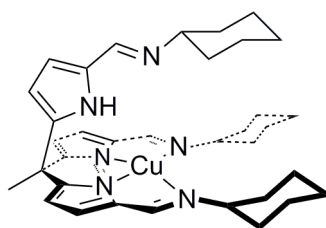
To a suspension of H₃L (1.1 g, 1.9 mmol) in MeCN (50 mL), was added a solution of Cu(OAc)₂ (0.38 g, 1.9 mmol) in MeCN (20 mL). The reaction was stirred at room temperature 2 h after which the solvents were evaporated under reduced pressure. The residual solids were dissolved in THF (10 mL) and precipitated by the addition of hexane (50 mL). The liquors were decanted and the precipitate was washed with hexane (3 × 10 mL) and dried under reduced pressure affording 0.71 g, 60 % of [Cu(HL)] as green solids.

Analysis Found: C, 68.43, H, 7.55, N, 13.68 % C₃₅H₄₆N₆Cu requires C, 68.37, H, 7.46, N, 13.59 %; ESMS (+ve ion): *m/z* 438.29 ([CuL]⁺, loss of protonated arm, 37 %), 614.26 ([M]⁺, 100 %); IR (KBr): υ 3446 (NH), 1653 (C=N), 1576 (C=C) cm⁻¹; UV-Vis (CHCl₃, 25 °C): 280 nm (ε = 64693 dm³mol⁻¹cm⁻¹), 290 nm (ε = 32237 dm³mol⁻¹cm⁻¹), 320 nm (ε = 40570 dm³mol⁻¹cm⁻¹); μ_{eff} (Evan's method) = 2.23 BM.

6.3.3 Synthesis of [Pd(H$_2$L)][Cl]
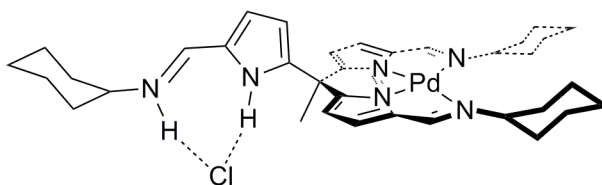
To a mixture of H$_3$L (0.099, 0.18 mmol) in CH$_2$Cl$_2$ (10 mL) and NEt$_3$ (0.70 mL), was added a solution of PdCl$_2$(MeCN)$_2$ (0.052 g, 0.20 mmol) in CH$_2$Cl$_2$ (15 mL). The resulting mixture was stirred at room temperature for 3 h after which the addition of hexane (20 mL) ensured the precipitation of the product which was filtered, washed with hexane (2 × 10 mL) and dried under reduced pressure affording 0.075 g, 60 % of [Pd(H$_2$L)][Cl] product as a yellow powder. Single crystals were grown by slow diffusion of hexane into a saturated CH$_2$Cl$_2$ solution.

^{1}H NMR (400 MHz, CDCl$_3$): δ_H 13.34 (br. s, 1H, pyrrole NH), 12.86 (br. m, 1H, NH), 7.57 (s, 2H, imine), 7.38 (d, 1H, $^3J_{HH}$ = 15.5 Hz, protonated imine), 6.72 (dd, 1H, $^3J_{HH}$ = 4.1 Hz, $^4J_{HH}$ = 2.0 Hz, pyrrole), 6.65 (d, 2H, $^3J_{HH}$ = 3.91 Hz, pyrrole), 6.35 (d, 2H, $^3J_{HH}$ = 3.91 Hz, pyrrole), 5.71 (dd, 1H, $^3J_{HH}$ = 4.1 Hz, $^4J_{HH}$ = 2.0 Hz, pyrrole), 3.42 (m, 1H, CH cyh), 3.23 (m, 2H, CH cyh), 2.31 (s, 3H, CH$_3$), 2.24 - 1.13 (m, 30H, Cyh) ppm; ^{13}C{^{1}H} NMR (126 MHz, CDCl$_3$): δ_C 158.3 (q), 156.5, 147.3, 145.5 (q), 137.1 (q), 129.8, 121.6 (q), 116.4, 113.1, 108.5, 63.2, 61.3, 47.2 (q), 34.1, 32.7, 27.3, 26.2, 26.1, 24.7 ppm; Analysis Found: C, 60.47, H, 6.68, N, 11.92 % C$_{35}$H$_{47}$N$_6$PdCl requires C, 60.60, H, 6.83, N, 12.12 %; ESMS (+ve ion): *m/z* 481.29 ([PdL]$^+$ loss of protonated arm, 19.1 %), 657.27 ([Pd(H$_2$L)]$^+$, 100 %); IR (KBr): υ 3417 (NH), 1658 (C=N), 1568 (C=C) cm^{-1}.

6.3.4 Synthesis of [CuCl(H₂L)]
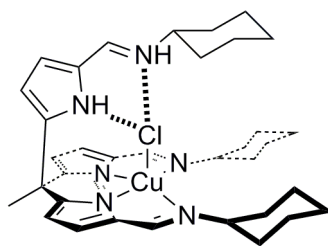
To a mixture of H₃L (0.48 g, 0.87 mmol) in MeOH (50 mL) and NEt₃ (0.48 g, 4.8 mmol), was added a solution of CuCl₂ (0.11 g, 0.82 mmol) in MeOH (20 mL). The resulting solution was stirred for 8 h at room temperature after which it was filtered and solvents were evaporated under reduced pressure to afford 0.37 g, 65 % of [CuCl(H₂L)] as a green powder. Single crystals were grown by slow diffusion of Et₂O into a saturated CHCl₃ solution.

Analysis Found: C, 64.69, H, 7.32, N, 12.84 % $C_{35}H_{47}CuClN_6$ requires C, 64.59, H, 7.28, N, 12.91 %; ESMS (+ve ion): m/z 438.34 ([CuL]⁺ loss of protonated arm, 46 %), 614.17 ([Cu-H₂L]⁺, 100 %), 650.05 ([M+H⁺], 12 %); IR (KBr): υ 3417 (NH), 1660 (C=N), 1581 (C=C) cm⁻¹; UV-Vis (CHCl₃, 25 °C): 314 nm (ε = 28478 dm³mol⁻¹cm⁻¹), 370 nm (ε = 19739 dm³mol⁻¹cm⁻¹). μ_{eff} (Evans' method) = 1.94 BM.

6.3.5 Synthesis of H₃L^CCl3
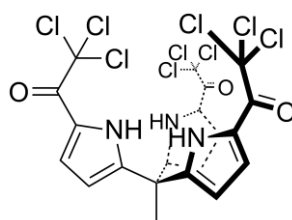
To a degassed solution of trichloroacetyl chloride (12 g, 67 mmol) in Et₂O (10 mL) at 0 °C under N₂, was slowly added a solution of 2,2',2''-tripyrrylethane (3.0 g, 13 mmol) in Et₂O (200 mL). The mixture was allowed to warm to room temperature and stirred for 2 h after which the precipitate was filtered,

washed with Et$_2$O (3 × 25 mL) and dried in air to yield 5.6 g, 65 % of H$_3$L^{CCl3} as a dark pink solid.

^{1}H NMR (250 MHz, CDCl$_3$): δ$_H$ 10.07 (br. s, 3H, NH), 7.37 (dd, 3H, $^3J_{HH}$ = 4.13 Hz, $^4J_{HH}$ = 2.31 Hz, pyrrole), 6.27 (dd, 3H, $^3J_{HH}$ = 4.13 Hz, $^4J_{HH}$ = 2.81 Hz, pyrrole), 2.23 (s, 3H, CH$_3$) ppm; ^{13}C{^{1}H} NMR 96 MHz, CDCl$_3$): δ$_C$ 173.4 (q), 143.5 (q), 123.1, 122.6 (q), 110.8, 94.4 (q), 41.8 (q), 27.7 ppm; Analysis. Found: C, 36.76, H, 1.62, N, 6.26 % C$_{20}$H$_9$Cl$_9$N$_3$O$_3$ requires C, 36.49, H, 1.38, N, 6.38 %; ESMS (+ve ion): *m/z* 659.1 (M$^+$, 100 %); IR (KBr): υ 3331 (pyrrole NH), 1642 (C=O) cm^{-1}

6.3.6 Synthesis of H$_6$L^{Cy}
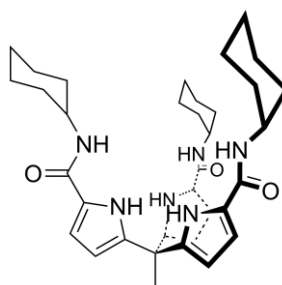
Neat cyclohexylamine (4.5 g, 45 mmol) was added to H$_3$L^{CCl3} (3.0 g, 4.5 mmol) and the resulting solution stirred at room temperature for 16 h. The colourless precipitate was filtered and washed with Et$_2$O (3 × 10 mL) affording 2.6 g, 95 % of H$_6$L^{Cy} as a colourless powder.

^{1}H NMR (360 MHz, d^6-DMSO): δ$_H$ 10.9 (br. s, 3H, pyrrole NH), 7.78 (d, 3H, amido NH), 6.71 (s, 3H, pyrrole), 5.77 (s, 3H, pyrrole), 3.78 (br. s, 3H, CH cyh), 1.84 (s, 3H, CH$_3$), 1.90 - 1.33 (m, 15H, cyh), 1.13 - 0.75 (m, 15H, cyh) ppm; ^{13}C{^{1}H} NMR (96 MHz, d^6-DMSO): δ$_C$ 159.7 (q), 139.7 (q), 126.4 (q), 110.0, 106.9, 47.6, 32.9, 26.7, 25.4, 25.1 ppm; Analysis. Found: C, 69.97, H, 8.05, N, 13.99 % C$_{35}$H$_{48}$N$_6$O$_3$ requires C, 69.91, H, 7.93, N, 13.87 %; ESMS (+ve ion):

m/z 644.8 ([M+2Na]$^+$, 100 %), 600.8 (M$^+$, 45 %); IR (KBr): υ 3436 (amide NH), 3288 (pyrrole NH), 1633 (amide C=O) cm^{-1}.

6.3.7 Synthesis of [Ti(O^{i}Pr)$_2$(HL^{Cy})]
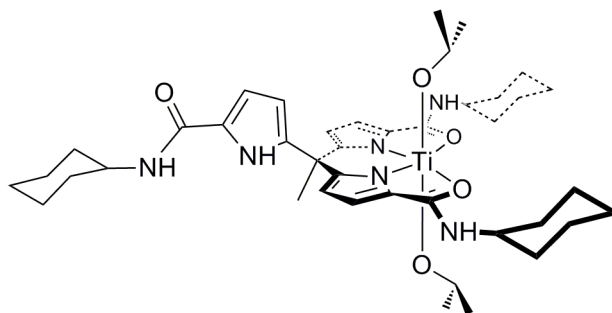
To solution of H$_6$L^{Cy} (0.23 g, 0.38 mmol) in THF (15 mL), was added a solution of Ti(O^{i}Pr)$_4$ (0.12 g, 0.42 mmol) in THF (5 mL) at -20 °C. The mixture was stirred for 2 h and allowed to warm to room temperature after which the solvent was evaporated under reduced pressure to afford 0.18 g, 62 % of [Ti(O^{i}Pr)$_2$(HL^{Cy})] as a pale yellow powder.

^{1}H NMR (360 MHz, CDCl$_3$): δ_H 9.32 (br. s, 1H, NH), 6.65 (d, 2H, $^3J_{HH}$ = 3.67 Hz, pyrrole), 6.42 (d, 2H, $^3J_{HH}$ = 3.67 Hz, pyrrole), 6.36 (d, 1H, $^3J_{HH}$ = 18.1 Hz, amide NH), 5.90 (d, 1H, $^3J_{HH}$ = 7.34 Hz, pyrrole), 5.33 (d, 1H, $^3J_{HH}$ = 7.34 Hz, pyrrole), 5.08 (sep, 1H, $^3J_{HH}$ = 5.79 Hz, CH), 4.95 (sep, 1H, $^3J_{HH}$ = 5.36 Hz, CH), 4.08 (m, 2H, CH cyh), 4.01 (m, 1H, CH cyh), 2.31 (s, 3H, CH$_3$), 1.35 (d, 6H, $^3J_{HH}$ = 5.36 Hz, CH$_3$), 1.20 (d, 6H, $^3J_{HH}$ = 5.79 Hz, CH$_3$), 2.00 - 0.80 (m, 30H, cyh) ppm; ^{13}C{^{1}H} NMR (126 MHz, C$_6$D$_6$/THF): δ_C 164.8, 159.5 (q), 148.4, 143.0 (q), 134.4, 125.7 (q), 109.4 (q), 107.8, 105.4 (q), 105.0, 100.4 (q), 83.7, 71.3, 67.4, 62.6, 60.9, 58.9, 58.5, 56.8, 50.6, 49.2, 47.4, 42.5, 33.5, 29.5 (q), 13.0 ppm; Analysis. Found: C, 64.25, H, 8.02, N, 10.90 %; C$_{41}$H$_{64}$N$_6$O$_5$Ti requires C, 64.05, H, 8.39, N, 10.93 %; IR (KBr): υ 3290 (pyrrole NH), 1591 (C=O free), 1540 (C=Obound) cm^{-1}

6.3.8 Synthesis of H₆L^{Me}
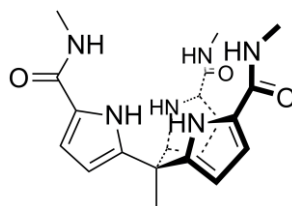
A 40 % solution of methylamine in water (3.5 g, 45 mmol) was added to H$_3$L^{CCl3} (3.0 g, 4.5 mmol). The resulting solution was stirred at room temperature for 2 h after which the precipitate was filtered and washed with Et$_2$O (3 × 10 mL) affording 1.6 g, 89 % of H$_6$L^{Me} as colourless solids.

^{1}H NMR (360 MHz, CD$_3$OD): δ_H 6.44 (d, 3H, $^3J_{HH}$ = 3.42 Hz, pyrrole), 5.77 (br. s, 3H, pyrrole), 2.69 (s, 9H, branch CH$_3$), 1.96 (s, 3H, CH$_3$) ppm; ^{13}C{^{1}H} NMR (91 MHz, CD$_3$OD): δ_C 162.3 (q), 139.9 (q), 124.9 (q), 109.7, 106.2, 40.2 (q), 25.8, 24.4 ppm; Analysis. Found: C, 60.46, H, 5.98, N, 21.07 %; C$_{20}$H$_{24}$N$_6$O$_3$ requires C, 60.59, H, 6.10, N, 21.20 %; ESMS (+ve ion): *m/z* 418.92 ([M+Na]$^+$, 46.62 %), 814.46 ([2M+Na]$^+$, 100 %); IR (KBr): υ 3306 (NH), 1612(C=O), 1538 (C=C) cm^{-1}

6.3.9 Synthesis of [Ti(O^{i}Pr)$_2$(HL^{Me})]
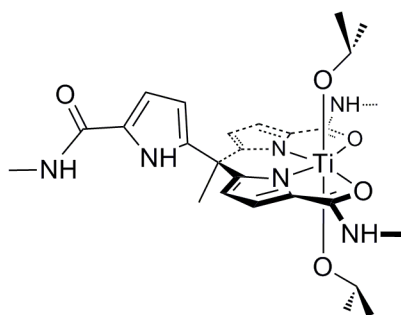
To solution of Ti(O^{i}Pr)$_4$ (0.099 g, 0.35 mmol) in MeCN (5 mL), was added a solution of H$_6$L^{Me} (0.14 g, 0.35 mmol) in THF (15 mL). The reaction was stirred for 2 h at -20 °C upon which a precipitate formed. The solvents were decanted and the crystalline precipitate was washed with hexane (2 × 5 mL)

to afford 0.13 g, 66 % of [Ti(O^{i}Pr)$_2$(HL^{Me})]. Single crystals were obtained by slow cooling a saturated MeCN solution.

^{1}H NMR (250 MHz, CD$_3$CN): δ_H 8.57 (br. s, 1H, NH), 7.07 (br. s, 2H, NH), 6.57 (d, 2H, $^3J_{HH}$ = 3.79 Hz, pyrrole), 6.29 (br. s, 1H, pyrrole NH), 6.25 (dd, 1H, $^3J_{HH}$ = 2.65 Hz, $^4J_{HH}$ = 1.08 Hz, pendant pyrrole), 6.02 (d, 2H, $^3J_{HH}$ = 3.79 Hz, pyrrole), 5.82 (dd, 1H, $^3J_{HH}$ = 2.65 Hz, $^4J_{HH}$ = 1.08 Hz, pendant pyrrole), 4.65 (sep, 1H, $^3J_{HH}$ = 5.91 Hz, CH), 4.53 (sep, 1H, $^3J_{HH}$ = 5.91 Hz, CH), 2.94 (d, 6H, $^3J_{HH}$ = 4.61 Hz, CH$_3$), 2.61 (d, 3H, $^3J_{HH}$ = 4.86 Hz, CH$_3$), 1.97 (s, 3H, CH$_3$), 1.16 (d, 6H, $^3J_{HH}$ = 5.91 Hz, CH$_3$), 1.00 (d, 3H, $^3J_{HH}$ = 5.91 Hz, CH$_3$), 0.87 (d, 3H, $^3J_{HH}$ = 5.91 Hz, CH$_3$) ppm; ^{13}C{^{1}H} NMR (126 MHz, C$_6$D$_6$/MeCN): δ_C 166.0, 161.3 (q), 147.8, 144.4 (q), 134.4, 125.0 (q), 116.6 (q), 110.2, 108.5 (q), 105.9, 104.3 (q), 77.1, 75.9, 67.4, 63.3, 41.8, 40.8 (q), 29.7, 26.0, 25.2 ppm; IR (KBr): υ 3291 (pyrrole NH), 1600 (C=O free), 1558 (C=O bound) cm^{-1}

6.3.10 Anion Binding study of H$_6$L^{Cy}

For each anion studied, a stock solution of set concentration of H$_6$L^{Cy} and anion in CDCl$_3$ was prepared. The required amount of each was added to an NMR tube which was then topped up with CDCl$_3$ so as to keep a constant volume across the samples. Each sample's value is shown in the following tables relative to the required mole ratio required.

Tetrabutylammonium Acetate (TBAOAc)

Concentration of H_6L^{Cy}: 6.11×10^{-3} mol.L^{-1}

Concentration of TBAOAc: 0.270 mol.L^{-1}

Mole fraction		Number of moles		Volume required/L		
Ligand	Anion	Ligand	Anion	Ligand	Anion	Extra Solvent
0.99999	1E-05	4.80E-06	4.80E-11	7.86E-04	1.78E-10	1.44E-05
0.9	0.1	4.32E-06	4.80E-07	7.07E-04	1.78E-06	9.12E-05
0.8	0.2	3.84E-06	9.60E-07	6.28E-04	3.56E-06	1.68E-04
0.7	0.3	3.36E-06	1.44E-06	5.50E-04	5.33E-06	2.45E-04
0.6	0.4	2.88E-06	1.92E-06	4.71E-04	7.11E-06	3.22E-04
0.5	0.5	2.40E-06	2.40E-06	3.93E-04	8.89E-06	3.98E-04
0.4	0.6	1.92E-06	2.88E-06	3.14E-04	1.07E-05	4.75E-04
0.3	0.7	1.44E-06	3.36E-06	2.36E-04	1.24E-05	5.52E-04
0.2	0.8	9.60E-07	3.84E-06	1.57E-04	1.42E-05	6.29E-04
0.1	0.9	4.80E-07	4.32E-06	7.86E-05	1.60E-05	7.05E-04
0.00001	1.00E+00	4.80E-11	4.80E-06	7.86E-09	1.78E-05	7.82E-04

Tetrabutylammonium Fluoride (TBAF)

Concentration of H_6L^{Cy}: 6.11×10^{-3} mol.L^{-1}

Concentration of TBAF: 0.266 mol.L^{-1}

Mole fraction		Number of moles		Volume required/L		
Ligand	Anion	Ligand	Anion	Ligand	Anion	Extra solvent
0.99999	1E-05	4.80E-06	4.80E-11	7.86E-04	1.80E-10	1.44E-05
0.9	0.1	4.32E-06	4.80E-07	7.07E-04	1.80E-06	9.12E-05
0.8	0.2	3.84E-06	9.60E-07	6.28E-04	3.61E-06	1.68E-04
0.7	0.3	3.36E-06	1.44E-06	5.50E-04	5.41E-06	2.45E-04
0.6	0.4	2.88E-06	1.92E-06	4.71E-04	7.22E-06	3.21E-04
0.5	0.5	2.40E-06	2.40E-06	3.93E-04	9.02E-06	3.98E-04
0.4	0.6	1.92E-06	2.88E-06	3.14E-04	1.08E-05	4.75E-04
0.3	0.7	1.44E-06	3.36E-06	2.36E-04	1.26E-05	5.52E-04
0.2	0.8	9.60E-07	3.84E-06	1.57E-04	1.44E-05	6.28E-04
0.1	0.9	4.80E-07	4.32E-06	7.86E-05	1.62E-05	7.05E-04
0.00001	1.00E+00	4.80E-11	4.80E-06	7.86E-09	1.80E-05	7.82E-04

Tetrabutylammonium Chloride (TBACl)

Concentration of H_6L^{Cy}: 6.10×10^{-3} mol.L^{-1}

Concentration of TBACl: 0.272 mol.L^{-1}

Mole fraction		number of moles/mol		Volume/L		
Ligand	Anion	Ligand	Anion	Ligand	Anion	Extra solvent
0.99999	1E-05	4.80E-06	4.80E-11	7.86E-04	1.76E-10	1.44E-05
0.9	0.1	4.32E-06	4.80E-07	7.07E-04	1.76E-06	9.12E-05
0.8	0.2	3.84E-06	9.60E-07	6.28E-04	3.53E-06	1.68E-04
0.7	0.3	3.36E-06	1.44E-06	5.50E-04	5.29E-06	2.45E-04
0.6	0.4	2.88E-06	1.92E-06	4.71E-04	7.06E-06	3.22E-04
0.5	0.5	2.40E-06	2.40E-06	3.93E-04	8.82E-06	3.98E-04
0.4	0.6	1.92E-06	2.88E-06	3.14E-04	1.06E-05	4.75E-04
0.3	0.7	1.44E-06	3.36E-06	2.36E-04	1.24E-05	5.52E-04
0.2	0.8	9.60E-07	3.84E-06	1.57E-04	1.41E-05	6.29E-04
0.1	0.9	4.80E-07	4.32E-06	7.86E-05	1.59E-05	7.06E-04
0.00001	1.00E+00	4.80E-11	4.80E-06	7.86E-09	1.76E-05	7.82E-04

Tetrabutylammonium Bromide (TBABr)

Concentration of H_6L^{Cy}: 6.11×10^{-3} mol.L^{-1}

Concentration of TBABr: 0.217 mol.L^{-1}

Mole fraction		number of moles/mol		Volume/L		
Ligand	Anion	Ligand	Anion	Ligand	Anion	Extra solvent
0.99999	1E-05	4.80E-06	4.80E-11	7.86E-04	2.21E-10	1.44E-05
0.9	0.1	4.32E-06	4.80E-07	7.07E-04	2.21E-06	9.08E-05
0.8	0.2	3.84E-06	9.60E-07	6.28E-04	4.42E-06	1.67E-04
0.7	0.3	3.36E-06	1.44E-06	5.50E-04	6.64E-06	2.43E-04
0.6	0.4	2.88E-06	1.92E-06	4.71E-04	8.85E-06	3.20E-04
0.5	0.5	2.40E-06	2.40E-06	3.93E-04	1.11E-05	3.96E-04
0.4	0.6	1.92E-06	2.88E-06	3.14E-04	1.33E-05	4.72E-04
0.3	0.7	1.44E-06	3.36E-06	2.36E-04	1.55E-05	5.49E-04
0.2	0.8	9.60E-07	3.84E-06	1.57E-04	1.77E-05	6.25E-04
0.1	0.9	4.80E-07	4.32E-06	7.86E-05	1.99E-05	7.02E-04
0.00001	1.00E+00	4.80E-11	4.80E-06	7.86E-09	2.21E-05	7.78E-04

Tetrabutylammonium Iodide (TBAI)

Concentration of H_6L^{Cy}: 5.80×10^{-3} mol.L^{-1}

Concentration of TBAI: 0.263 mol.L^{-1}

Mole fraction		number of moles/mol		Volume/L		
Ligand	Anion	Ligand	Anion	Ligand	Anion	Extra solvent
0.99999	1E-05	4.80E-06	4.80E-11	8.28E-04	1.83E-10	2.76E-05
0.9	0.1	4.32E-06	4.80E-07	7.45E-04	1.83E-06	5.33E-05
0.8	0.2	3.84E-06	9.60E-07	6.62E-04	3.65E-06	1.34E-04
0.7	0.3	3.36E-06	1.44E-06	5.79E-04	5.48E-06	2.15E-04
0.6	0.4	2.88E-06	1.92E-06	4.97E-04	7.30E-06	2.96E-04
0.5	0.5	2.40E-06	2.40E-06	4.14E-04	9.13E-06	3.77E-04
0.4	0.6	1.92E-06	2.88E-06	3.31E-04	1.10E-05	4.58E-04
0.3	0.7	1.44E-06	3.36E-06	2.48E-04	1.28E-05	5.39E-04
0.2	0.8	9.60E-07	3.84E-06	1.66E-04	1.46E-05	6.20E-04
0.1	0.9	4.80E-07	4.32E-06	8.28E-05	1.64E-05	7.01E-04
0.00001	1.00E+00	4.80E-11	4.80E-06	8.28E-09	1.83E-05	7.82E-04

Results

| Mole fraction		δ obs/ppm				
Ligand	Anion	TBAOAc	TBAF	TBACl	TBABr	TBAI
0.99999	1E-05	6.15	6.27	6.24	6.25	6.265
0.9	0.1	6.186	6.29	6.25	6.26	6.271
0.8	0.2	6.247	6.31	6.26	6.28	6.276
0.7	0.3	6.298	6.35	6.27	6.29	6.279
0.6	0.4	6.359	6.4	6.28	6.3	6.286
0.5	0.5	6.42	6.52	6.29	6.32	6.291
0.4	0.6	6.47	6.57	6.3	6.33	6.297
0.3	0.7	6.517	6.59	6.31	6.34	6.303
0.2	0.8	6.517	6.6	6.33	6.35	6.324
0.1	0.9	6.517	6.6	6.38	6.39	6.345
0.00001	1.00E+00	6.517	6.6	6.38	6.39	6.345

6.4 Synthetic procedures as described in chapter 4

6.4.1 Synthesis of L^{ImAr}
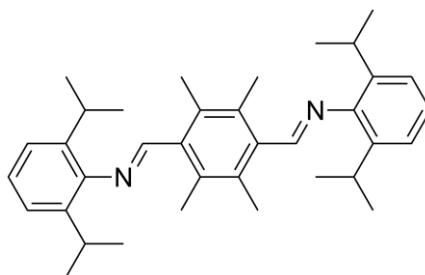
To solution of 2,3,5,6-tetramethylterephthalaldehyde (2.0 g, 11 mmol) in MeCN (50 mL), was added diisopropylaniline (3.7 g, 22 mmol). Trifluoroacetic acid (1 mL) was added to the solution dropwise. The mixture was stirred for 1 h at room temperature after which it was neutralised using KOH (aq). The resulting yellow precipitate was filtered and washed with MeCN (3 × 10 mL) and dried under vacuum to afford 4.8 g, 86 % of L^{ImAr} as a yellow powder. Single crystals were grown by cooling of a saturated MeCN solution.

^{1}H NMR (400 MHz, CDCl$_3$): δ_H 8.67 (s, 2H, imine CH), 7.27 – 7.15 (m, 6H, aromatic), 3.18 (sep, $^3J_{HH}$ = 6.81 Hz, 4H, isopropyl CH), 2.55 (s, 12H, CH$_3$), 1.25 (d, $^3J_{HH}$ = 6.81 Hz, 24H, CH$_3$) ppm; ^{13}C{^{1}H} NMR (126 MHz, CDCl$_3$): δ_C 164.6, 149.6 (q), 137.9 (q), 135.8 (q), 134.6 (q), 124.4, 123.3, 28.0, 24.0, 16.8 ppm; Analysis Found: C, 84.76, H, 9.57, N, 5.47 %, C$_{36}$H$_{48}$N$_2$ requires C, 84.98, H, 9.51, N, 5.51 %; ESMS (+ve ion): *m/z* 509.22([M+H]$^+$, 100 %); IR (ATR): υ 1630 (C=N), 1588 (C=C) cm^{-1}.

6.4.2 Synthesis of L^{AmAr}
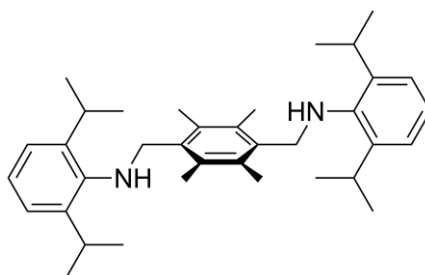
Method 1: To a mixture of 1,4-dibromomethyl-2,3,5,6-tetramethylbenzene (5.6 g, 18 mmol) in MeCN (150 mL) was added NEt$_3$ (5 mL) followed by 2,6-diisopropylaniline (8.0 g, 45 mmol). The mixture was boiled for 8 h, after which the solvents were evaporated under reduced pressure. The residues were dissolved in water, extracted into CH$_2$Cl$_2$ that was then evaporated to dryness. The crude colourless solids were recrystallised from hot MeCN to afford 4.8 g, 53 % of L^{AmAr} as colourless microcrystals. Single crystals were grown by slow cooling of a saturated solution of MeCN. The amine hydrogens in L^{AmAr} were located from the difference Fourier map and refined with riding thermal parameters and bond distance restraints.

Method 2: To a solution of L^{ImAr} (0.10 g, 0.19 mmol) in THF (5 mL) was added a solution of NaBH$_4$ (0.079 g, 2.1 mmol) in MeOH (5 mL). The mixture was stirred vigorously for 2 h, after which the solvents were evaporated under reduced pressure and the residues taken up in water (10 mL) and extracted with CH$_2$Cl$_2$. The organic layer was dried over MgSO$_4$, and the solvents evaporated under reduced pressure to yield a colourless crude solid that was recrystallised from MeCN to afford 0.021 g, 20 % of L^{AmAr} as a colourless solid.

^{1}H NMR (400 MHz, CDCl$_3$): δ_H 7.16 – 7.05 (m, 6H, aromatics), 4.22 (s, 4H, CH$_2$), 3.30 (sep, 4H, CH), 3.07 (br. s, 2H, NH), 2.35 (s, 12H, CH$_3$), 1.25 (d, 24H, CH$_3$) ppm; ^{13}C{^{1}H} NMR (126 MHz, CDCl$_3$): δ_C 144.2 (q), 141.7 (q), 136.2 (q),

133.5 (q), 123.8, 123.3, 50.8, 28.1, 24.4, 16.9 ppm; Analysis. Found: C, 84.46, H, 10.13, N, 5.51 % $C_{36}H_{52}N_2$ requires C, 84.32, H, 10.22, N, 5.46 %; ESMS (+ve ion): *m/z* 1022.69 ([2M-3H$^+$], 71 %), 513.18 ([M+H]$^+$, 69 %), 336.23 ([M-CH amine]$^+$, 100 %); IR (KBr): υ 3400 (NH), 1442 (C-N) cm^{-1}.

6.4.3 Synthesis of L^{ImR}
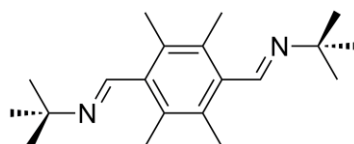
To a solution of 2,3,5,6-tetramethylterephthalaldehyde (4.3 g, 23 mmol) in MeCN (100 mL) was added tert-butylamine (4.1 g, 56 mmol). Trifluoroacetic acid (0.5 mL) was added dropwise and the mixture was stirred for 1 h at room temperature after which it was neutralised with KOH (aq). The resulting colourless precipitate was filtered, washed with MeCN (3 × 10 mL), and dried under vacuum to afford 4.9 g, 70 % of the L^{ImR}.

^{1}H NMR (400 MHz, CDCl$_3$): δ_H 8.55 (s, 2H, CH imine), 2.17 (s, 12H, CH$_3$), 1.38 (s, 18H, ^{t}Bu) ppm; ^{13}C{^{1}H} NMR (500 MHz, CDCl$_3$): δ_C 158.1, 136.8 (q), 131.7 (q), 58.2 (q), 29.7, 16.3 ppm; Analysis. Found: C, 80.03, H, 10.57, N, 9.05 %; $C_{20}H_{32}N_2$ requires C, 79.94, H, 10.73, N, 9.32 %; ESMS (+ve ion): *m/z* 301.09 ([M]$^+$, 100 %), 245.10 ([M-^{t}Bu]$^+$, 14.5 %); IR (ATR): υ 1651 (C=N) cm^{-1}.

6.4.4 Synthesis of L^{AmR}
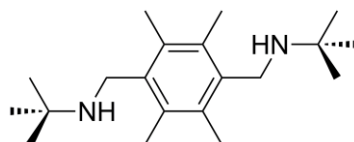
Method 1: To a solution of L^{ImR} (2.5 g, 8.2 mmol) in MeOH (40 mL) was added NaBH$_4$ (1.6 g, 41 mmol). The resulting solution was stirred for 2 h at room temperature after which the solvent was evaporated under reduced pressure. The residues were extracted into a mixture of CH$_2$Cl$_2$ (10 mL) and

water (10 mL) and the organic phase dried over MgSO₄. The solvents were evaporated under reduced pressure to afford 2.3 g, 92 % of L^{AmR} as a colourless solid.

Method 2: A mixture of *tert*-butylamine (0.062 g, 8.5 mmol) and 1,4-dibromomethyl-2,3,5,6-tetramethylbenzene (0.10 g, 0.31 mmol) was heated to reflux for 8 h. The resulting precipitate was isolated by suction filtration and dried under vacuum to afford 0.038 mg, 40 % L^{AmR} as a colourless solid.

^{1}H NMR (400 MHz, CDCl₃): δ$_H$ 3.73 (s, 4H, CH₂), 2.31 (s, 12H, CH₃), 1.22 (s, 18H, ^{t}Bu) ppm; ^{13}C{^{1}H} NMR (126 MHz, CDCl₃): δ$_C$ 135.8 (q), 133.2 (q), 50.5 (q), 41.6, 29.1, 15.1 ppm; Analysis. Found: C, 78.91, H, 12.00, N, 9.24 %; C₂₀H₃₆N₂ requires C, 78.88, H, 11.92, N, 9.20 %; ESMS (+ve ion): *m/z* 304.97 ([M]⁺, 100%), 232.05 ([M-^{t}Bu-N]⁺, 44.1 %); IR (KBr): υ 3334 (NH), 1473 (C-C), 1228 (CN) cm^{-1}.
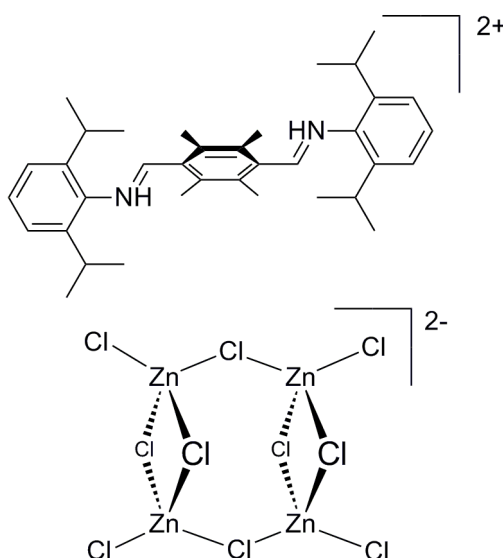
6.4.5 Synthesis of [CoCl₄][L^{AmR}]
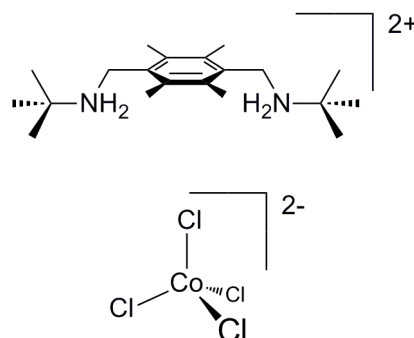
To a solution of L^{AmR} (0.10 g, 0.33 mmol) in Et₂O (10 mL) was added a solution of concentrated (aqueous) HCl (0.024 g, 0.66 mmol) in Et₂O (2 mL). The resulting solution was stirred for 30 min after which a suspension of CoCl₂ (0.043 g, 0.33 mmol) in Et₂O (5 mL) was added. The resulting mixture was stirred at room temperature for 1 h after which the resulting precipitate was filtered under reduced pressure and washed with Et₂O (3 × 5mL) to afford 0.138 g, 63 % of [H₂L^{AmR}][CoCl₄] as blue solids.

Single crystals were obtained by the addition of L^{AmR} and $CoCl_2$ to a solution of bench $CDCl_3$. The ammonium hydrogen atoms were located from the difference Fourier map and refined with riding thermal parameters and bond distance restraints.

Analysis. Found: C, 47.45, H, 7.58, N, 5.37 % $C_{20}H_{36}Cl_4CoN_2$ requires C, 47.54, H, 7.18, N, 5.54 %; IR (KBr): υ 3419 (NH), 1635 (C-C aromatic), 1593 (CN) cm^{-1}.

6.4.6 Synthesis of $[Zn_4Cl_{10}][H_2L^{ImAr}]$

To a solution of L^{ImAr} (0.14 g, 0.20 mmol) in Et_2O (10 mL), was added a solution of concentrated (aqueous) HCl (0.014 g, 0.40 mmol) in Et_2O (2 mL). The resulting solution was stirred for 30 min after which a solution of $ZnCl_2$ (0.11 g, 0.78 mmol) in Et_2O (5 mL) was added. The mixture was stirred at room temperature for 1 h and the resulting precipitate filtered under reduced pressure and washed with Et_2O (3 × 5 mL) to afford 0.14 g, 63 % of $[Zn_4Cl_{10}][H_2L^{ImAr}]$ as a colourless solid. Single crystals were grown by addition of L^{ImAr} and $ZnCl_2$ to a solution of bench $CDCl_3$. The iminium hydrogens were located in the difference Fourier map and refined with riding thermal parameters and bond distance restraints.

Analysis. Found: C, 38.46, H, 4.52, N, 2.31 % $C_{36}H_{50}Cl_{10}N_2Zn_4$ requires C, 38.37, H, 4.47, N, 2.49 %; IR (KBr): υ 3587 (NH), 1653 (C=N), 1608 (C=C) cm^{-1}

6.4.7 Synthesis of [(Pd$_3$Cl$_6$)L^{ImAr}]
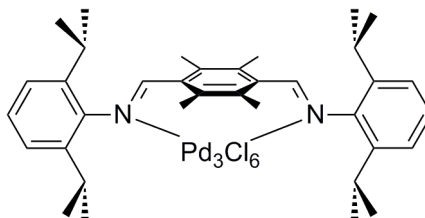
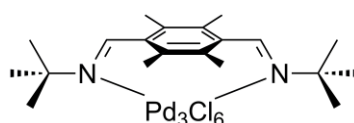

To a solution of L^{ImAr} (0.10 g, 0.19 mmol) in CH$_2$Cl$_2$ (5 mL), was added a solution of PdCl$_2$(MeCN)$_2$ (0.15 g, 0.59 mmol) in CH$_2$Cl$_2$ (15 mL). The mixture was stirred for 3 h at room temperature, after which the precipitate was filtered, washed with hexane (3 × 5 mL) and dried under vacuum to afford 0.14 g, 70 % of [(Pd$_3$Cl$_6$)L^{ImAr}] as a red solid. Single crystals were grown by cooling of a saturated solution of CH$_2$Cl$_2$. The structure suffers from whole molecule disorder with an occupancy ratio of 0.89:0.11. Within the minor component the Pd atoms were refined freely and isotropically, the Cl positional parameters were refined, but a common isotropic displacement parameter fixed at 0.06 Å^2. Both molecules were restrained to be geometrically similar. Within the major component, only Pd and Cl atoms were refined anisotropically. Allowing the light atoms to refine with anisotropic displacement parameters (adps) reduced R1 only modestly, but led to a number of atoms adopting physically unreasonable adps. This is probably a consequence of the whole-molecule disorder.

^{1}H NMR (500 MHz, CDCl$_3$): δ_H 8.38 (s, 2H, imine CH), 7.50 – 7.25 (m, 6H, aromatic), 3.56 (sep, $^3J_{HH}$ = 6.97 Hz, 2H, isopropyl CH), 3.75 (s, 6H, aryl CH$_3$), 3.49 (sep, $^3J_{HH}$ = 6.97 Hz, 2H, isopropyl CH), 2.09 (s, 6H, aryl CH$_3$), 1.85 (d, $^3J_{HH}$ = 6.97 Hz, 6H, CH$_3$), 1.48 (d, $^3J_{HH}$ = 6.97 Hz, 6H, CH$_3$), 1.25 (d, $^3J_{HH}$ = 6.97 Hz, 6H, CH$_3$), 1.23 (d, $^3J_{HH}$ = 6.97 Hz, 6H, CH$_3$) ppm; ^{13}C{^{1}H} NMR (126 MHz,

CDCl₃): δ$_C$ 180.5, 145.5 (q), 141.7 (q), 141.5 (q), 137.4 (q), 135.7 (q), 133.8 (q), 129.2, 125.3, 124.7, 29.1, 28.6, 26.1, 25.2, 24.4, 23.7, 20.9, 17.0 ppm; Analysis. Found: C, 41.39, H, 4.58, N, 2.54 %, $C_{36}H_{48}Cl_6N_2Pd_3$ requires C, 41.55, H, 4.65, N, 2.69 %; ESMS (+ve ion): *m/z* 507.49 ([ligand-H⁺], 91.76 %), 613.21 ([ligand + Pd]⁺, 27 %) 717.17 ([ligand + 2Pd]⁺, 82.43 %), 757.15 ([ligand + Pd₂Cl]⁺, 79.99 %), 860.96 ([ligand + Pd₂Cl₄]⁺, 100 %); IR (ATR): υ 1608 (C=N), 1590 (C=C) cm⁻¹; UV-Vis (CHCl₃, 25 °C): 431 nm (ε = 2711 dm³mol⁻¹cm⁻¹).

## 6.4.8 Synthesis of [(Pd₃Cl₆)L^{ImR}]

To a solution of PdCl₂(MeCN)₂ (0.26 g, 0.99 mmol) in CH₂Cl₂ (15 mL) was slowly added to a solution of L^{ImR} (0.12 g, 0.33 mmol) in CH₂Cl₂ (5 mL). The mixture was stirred for 3 h at room temperature, after which the resulting precipitate was filtered, washed with hexane (3 × 5 mL), and dried under vacuum to afford 0.21 g, 77% of [Pd₃Cl₆(L^{ImR})] as red solids. Single crystals were grown by slow cooling a saturated solution of CH₂Cl₂. In the structure, one tertiary butyl group had three-fold rotational disorder and was modelled over two sites with 0.66:0.34 occupancy and anisotropic atomic displacement parameters.

¹H NMR (400MHz, CDCl₃): δ$_H$ 8.45 (s, 2H, CH imine), 2.94 (s, 6H, CH₃), 1.90 (s, 6H, CH₃), 1.86 (s, 18H, ᵗBu) ppm; ¹³C{¹H} NMR (126 MHz, CDCl₃): δ$_C$ 176.8, 136.4 (q), 134.3 (q), 132.2 (q), 68.0 (q), 32.5, 20.5, 17.2 ppm; Analysis. Found: C, 29.01, H, 3.71, N, 3.26 % $C_{20}H_{32}Cl_6N_2Pd_3$ requires C, 28.86, H, 3.87, N, 3.37 %; ESMS (+ve ion): *m/z* 299.28 ([L-2H⁺], 100 %), 549.04 ([L+2Pd+Cl]⁺, 81.38 %),

682.01 ([L+Pd$_3$Cl$_5$]$^+$, 72.90 %); IR (ATR): υ 1628 (C=N) cm^{-1}; UV-Vis (CHCl$_3$, 25 °C): 310 nm (ε = 5422 dm^{3}mol^{-1}cm^{-1}).

6.4.9 Synthesis of H$_2$L^{Cp}
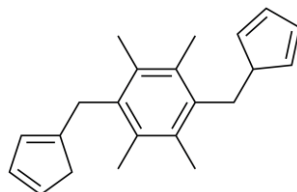
All manipulations were carried out under an atmosphere of dry nitrogen. To a solution of 1,4-dibromomethyl-2,3,5,6-tetramethylbenzene (4.5 g, 14 mmol) in THF (30 mL) was slowly added a solution of NaCp (3.1 g, 35 mmol) in THF (30 mL) at 0 °C. The resulting mixture was stirred at room temperature for 2 h after which the mixture was filtered. Hexanes (100 mL) were added to the filtrate and the precipitate filtered and dried under reduced pressure affording 3.8 g, 93 % of H$_2$L^{Cp} as a colourless powder.

^{1}H NMR (500 MHz, C$_6$D$_6$): δ$_H$ 6.55 – 5.69 (m, 10H, Cp), 3.72 (m, 2H, CH Cp), 2.73 (m, 4H, CH$_2$), 2.20 (s, 12H, CH$_3$) ppm; Analysis. Found: C, 90.99, H, 9.12 %; C$_{22}$H$_{26}$ requires C, 90.98, H, 9.02 %; IR (KBr): υ 1610 (C=C), 1434 (CH$_2$ bend).

6.4.10 Synthesis of [Li$_2$L^{Cp}]
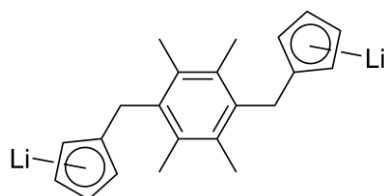
To a solution of H$_2$L^{Cp} (0.11 g, 0.38 mmol) in C$_6$H$_6$ (10 mL), was added a solution of Li(N(SiMe$_3$)$_2$) (0.14 g, 0.84 mmol) in C$_6$H$_6$ (10 mL). The resulting mixture was stirred at room temperature for 8 h after which the precipitate

was filtered and washed with C_6H_6 (2 × 10 mL) affording 0.10 g, 95 % of [Li$_2$L^{Cp}] as a colourless powder.

^{1}H NMR (400 MHz, C_6D_6/THF): δ_H 5.42 (m, 4H, Cp), 5.36 (m, 4H, Cp), 3.77 (s, 4H, CH$_2$), 2.19 (s, 12H, CH$_3$) ppm; ^{13}C{^{1}H} NMR (101 MHz, C_6D_6/THF): δ_C 137.7 (q), 131.0 (q), 117.6 (q), 102.7, 101.2, 31.1, 16.5 ppm.

6.5 References

[1]   L. J. Farrugia, *J. Appl. Crystallogr.* **1999**, *32*, 837-838.
[2]   G. M. Sheldrick, *Acta Cryst.* **2008**, *A64*, 112-122.
[3]   P. D. Beer, A. G. Cheetham, M. G. B. Drew, O. D. Fox, E. J. Hayes, T. D. Rolls, *Dalton Trans.* **2003**, 603-611.
[4]   A. W. Van der Made, R. H. Van der Made, *J. Org. Chem.* **1993**, *58*, 1262-1263.
[5]   Y.-T. Chan, X. Li, M. Soler, J.-L. Wang, C. Wesdemiotis, G. R. Newkome, *J. Am. Chem. Soc.* **2009**, *131*, 16395-16397.
[6]   A. L. Speck, PLATON, a multipurpose crystallographic tool, Utrecht University, Utrecht, The Netherlands, **2001**.